Rational Synthesis of Nanoparticle-MWCNT Hybrid Nanostructures through Non-Covalent Interactions with Organic Polymers

A thesis submitted for the degree of

Doctor of Philosophy in Materials



Pablo Quijano Velasco

Lincoln College, University of Oxford

Trinity 2021

Dedicated to my parents Luis y María

for their love and support

Declaration

This thesis is submitted for the degree of Doctor of Philosophy in Materials at the University of Oxford. No part of this thesis has been accepted or is currently being submitted for any degree, diploma, certificate or other qualification in this University or elsewhere. I certify that the work presented in this thesis is my own, except where indicated.

Abstract

The synthesis of hybrid nanostructures comprised by CNTs and nanoparticles is a promising field of research due to their potential applications in catalysis, energy storage, energy generation and biomedical technologies. However, the field lacks of synthetic guidelines for the rational design of hybrid nanostructures. This Thesis aims to stablish synthetic guidelines that consider the forces involved during the synthesis of iron oxide nanoparticle-CNT hybrids where polymers are used to mediate the interactions between the nanomaterials.

The functionalisation of MWCNTs with polystyrene is studied as the first level of hierarchy representing the polymer-MWCNT interactions. Non-covalent methods were found the most effective way to create polystyrene functionalised MWCNTs. It was found that the solvent used during the functionalisation was the parameter that had a higher effect in the amount of polystyrene found in the MWCNTs. The surface energy solubility parameter theories were proposed as a predictive synthetic model for the design of polymer functionalised MWCNTs. The predictions of the model were compared with the amount of polystyrene found in the functionalised MWCNTs synthesised in different solvents, finding good agreement between the predictions and the experimental evidence.

The next level of nanostructural hierarchy was addressed by studying the synthesis of polystyrene coated iron oxide nanoparticle-CNT hybrids. The solvent was found to play a key factor in the amount of polystyrene coated iron oxide nanoparticles found in the hybrid structures. The surface energy based solubility parameter theory was used to understand the amount of iron oxide nanoparticles found in the hybrids synthesised in different solvents, showing a better agreement with the experimental results than other parameters previously highlighted in the literature.

The results and ideas proposed in this Thesis will contribute to the future development of the rational synthesis of nanoparticle-CNT hybrid structures.

Acknowledgements

The development of this project would not have been possible without a large number of people who contributed to my professional and personal development. First, I would like to thank my supervisors Professor Nicole Grobert and Professor Kyriakos Porfyrakis, for their guidance and for having my back through this long period. I would like to thank Dr. Vikram Karde and Dr. Jerry Heng for agreeing in collaborating with me, their time, experiments and lessons on the measurement of surface properties of solid materials. I would thank and acknowledge Yumiko Ito for being an excellent Summer Student and performing key experiments with me. In addition, I want to give my gratitude to Dr. Panos Dallas and Dr. Puiki Leung for incorporating me into their own research projects.

I would like to thank the members of the Lincoln MCR for the good memories forged during my time in Oxford. First, I would like to thank Dr. Lewis Arthurton for the good days in the EC house and for not killing me by setting the house on fire (although he was close in many occasions). I want to thank Michael Nixon, Simon Faulkner and Laura Simmons for making Deep Hall feel like a second home to me where I could go and rant about the disappointing Arsenal performance of the week. Finally, I want to thank Jasha Trumpf for being like a brother to me during this time and reminding me to keep the self-actualisation on the latest version for each day.

I would also like to thank my colleagues from the Nanomaterials by Design and Nanocarbon research groups. I learned a great deal from each one of them and I am grateful for their welcoming behaviour and scientific insights. I want in particular to thank Ilija Rasovic, Ceren Zor, Dillon McGurty, Eoin O'Sullivan, John Ballentine, Pierre Romain, Jesus Acapulco and Dominique Piché for the great memories and their friendship. Also a big shout to Dr. Albert Xiao another brother I made during this period, with whom I obtained important insights while sitting in front of the

barbecue fumes.

I would like to thank my brother Juan for keeping family just a few miles distance from me. For my brothers Francisco and Bernardo, and my sister Monica for their support from distance that I could feel every single day. For my nieces and nephew for being source of joy and inspiration for me to be the best I can. Finally, to my parents ”Luis y Maria” who are my biggest supporters and the best role models I could have ever asked for.

Publications and Presentations

The work presented in this thesis has been included in the following journal article and manuscript in preparation:

Chapter 3

P. Quijano Velasco, K. Porfyrakis and N. Grobert, *The application of the surface energy based solubility parameter theory for the rational design of polymer-functionalized MWCNTs*, Phys. Chem. Chem. Phys., 2019, 21, 5331–5334.

Chapter 4, 5

P. Quijano Velasco, V. Karde, Y. Ito, J. Heng, K. Porfyrakis and N. Grobert, *Rational synthesis of polymer coated inorganic nanoparticles-MWCNT hybrids via solvophobic effects*. In preparation

In addition, the results presented in this thesis have been presented in the following scientific conferences:

P., Quijano Velasco, P., Porfyrakis P., Grobert N. (2020). *Improving Functionalization of MWCNTs through Non-Covalent Interactions with Organic Molecules*. Materials Research Society Fall & Spring virtual meeting.

P., Quijano Velasco, P., Porfyrakis P., Grobert N. (2019). *The application of the surface energy based solubility parameter theories for the rational design of polymer-functionalised MWCNTs*. Royal Society of Chemistry 14th International Conference on Materials Chemistry, Birmingham, UK.

Contents

1 Introduction **1**

1.1 Carbon nanotubes 3

1.1.1 Carbon nanotubes structure 3

1.1.2 Carbon nanotubes physical properties 6

1.1.3 Carbon nanotube chemistry 9

1.2 Bottom-up assembly of nanostructures based on carbon nanotubes (CNTs) 16

1.3 Thesis Outline 18

2 Methods **20**

2.1 Synthesis and characterisation of polystyrene 20

2.1.1 Atom transfer radical polymerisation 20

2.1.2 Nuclear magnetic resonance spectroscopy 22

2.1.3 Matrix-assisted Laser Desorption/Ionisation time-of-flight mass spectrometry 24

2.1.4 Gel permeation chromatography 25

2.2 Characterisation of MWCNTs, polystyrene functionalised MWCNTs and IONP-MWCNT hybrids 26

2.2.1 Fourier Transform Infrared Spectroscopy 26

2.2.2 X-ray photoelectron spectroscopy (XPS) 27

2.2.3 Raman spectroscopy 29

2.2.4 Thermogravimetric analysis 31
2.2.5 Inverse gas chromatography 32
2.2.6 Transmission electron microscopy 33
2.3 Synthesis and characterisation of IONPs 35
2.3.1 Nanoparticle synthesis by thermal decomposition of inorganic precursors 35
2.3.2 Powder X-ray diffraction 37
2.3.3 Dynamic light scattering 37

3 Functionalisation of MWCNTs with polystyrene through covalent and non-covalent methodologies 39

3.1 Intoduction 39
3.1.1 Non-covalent functionalisation 40
3.1.2 Covalent functionalisation 45
3.2 Materials and methods 52
3.2.1 Chemicals 52
3.2.2 Characterization 53
3.2.3 Synthesis of polystyrene 54
3.2.4 Synthesis polystyrene with an azide end-group 56
3.2.5 Synthesis of polystyrene with an aldehyde end-group 56
3.2.6 Nitrene cycloaddition of PS-N_3 with MWCNTs 56
3.2.7 Prato reaction of PS-Al with MWCNTs 57
3.2.8 Non-covalent functionalisation of MWCNTs with polystyrene 57
3.2.9 Synthesis of polystyrene with a pyrene end-group 58
3.3 Results and discussion 59
3.3.1 Covalent functionalisation of MWCNTs 59
3.3.2 Non-covalent functionalisation of MWCNTs 69

3.3.3 Effect of other parameters in the non-covalent functionalisation of MWCNTs . . . 74
3.4 Conclusions . . . 79

4 Solubility parameter theories as predictive models of polystyrene functionalisation of MWCNTs in different solvent media 82

4.1 Intoduction . . . 82
4.1.1 Solubility Parameter Theories . . . 84
4.2 Materials and methods . . . 92
4.2.1 Chemicals . . . 92
4.2.2 Characterization . . . 93
4.2.3 IGC analysis of 10nmMWCNTs . . . 93
4.2.4 Calculation of the HSP of 10nmMWCNTs . . . 93
4.2.5 Calculation of surface energy of the 10nmMWCNTs through IGC analysis . . . 95
4.2.6 Calculation of SEBSP . . . 97
4.3 Results and discussion . . . 98
4.3.1 HSP and surface energy determination of 10nmMWCNTs with IGC . . . 98
4.3.2 Application of Surface Energy Based Solubility Parameter theory for the non-covalent polymer functionalisation of MWCNTs . . . 102
4.4 Conclusions . . . 106

5 Synthesis of IONP-MWCNT hybrids 109

5.1 Intoduction . . . 109
5.1.1 Synthesis of nanoparticle-CNT hybrids . . . 111
5.1.2 Synthesis of ex-situ inorganic nanoparticle-carbon nanotube hybrids . . . 111

5.1.3 Ex-situ synthesis of nanoparticle-CNT hybrids through non-covalent interactions . . . 115
5.2 Materials and Methods . . . 120
5.2.1 Chemicals . . . 120
5.2.2 Characterisation . . . 120
5.2.3 Synthesis of polystyrene ligands . . . 121
5.2.4 Synthesis of iron oxide nanoparticles . . . 122
5.2.5 Oleylamine ligand exchange to polystyrene ligand . . . 123
5.2.6 Synthesis of IONP-MWCNT hybrids . . . 123
5.2.7 Study of overall concentration of IONP and MWCNTs for the synthesis of IONP-MWCNTs hybrids . . . 124
5.2.8 Study of concentration of iron oxide nanoparticle for the synthesis of IONP-MWCNTs hybrids . . . 124
5.2.9 PSIONP area coverage analysis of PSION-50nmMWCNT hybrids . . . 125
5.3 Results and discussion . . . 126
5.3.1 Synthesis of nanoparticles and ligand exchange . . . 126
5.3.2 Functionalisation of MWCNTs with IONPs . . . 134
5.3.3 SEBSP for nanoparticle functionalisation . . . 141
5.3.4 Effect of the concentration of starting solutions in the PSIONP-10nmMWCNT hybrid . . . 145
5.3.5 Effect of the MWCNT diameter on the morphology of PSIONP-MWCNT hybrids . . . 151
5.4 Conclusions . . . 157

6 Summary, Conclusions and Outlook 160

Bibliography 166

A List of Common Abbreviations **179**

B List of Common Symbols **182**

C Supplementary Characterisation Data **183**

Chapter 1

Introduction

A core principle in Materials Science is that the properties of a substance are defined by both their chemical composition and the structure it presents at different length scales. In this way if one is interested in designing a material that displays a set of particular properties, one requires control of both the chemical composition and its structure at different scales. This concept is the foundation for what is now known as the "bottom-up" synthesis of materials, which aims to fabricate materials by controlling their structure from the atomic to the microscopic length scale. The concept behind the bottom up fabrication of materials was famously popularised in 1959 by Richard Feyman's lecture called "There's plenty of room at the bottom", there he argued that advances in fabrication techniques would eventually allow for the manipulation of single atoms leading to the design of materials with atomic precision. Until that point the synthesis and processing of materials into specific atomic and microstructures was well understood, but the synthesis and structural control of materials with a length scale between the atomic and micronsized structures was still missing. During the last three decades of the 20^{th} century advances in characterisation techniques and material synthesis have opened the doors for the development of the science at the nanoscale, the missing link between atoms and

microstructures.

Nanomaterials and nanostructures are the core subject of study for the nanoscale science. A nanomaterial is defined as a material with one or more external or internal dimensions on the scale between 1 to 100 nm. Nanomaterials are classified depending on how many of its dimensions are found in the nanoscale. According to this classification zero-dimensional (0D) nanomaterials present all their dimensions in the nanoscale, one-dimensional (1D) nanomaterials present one of their dimensions outside of the nanoscale and two-dimensional (2D) nanomaterials present two dimensions outside of the nanoscale. A nanostructure on the other hand is simply defined as a material that presents an internal or surface structure at the nanoscale. Besides having a length scale that links the atomic and the microscale, nanomaterials present two main characteristics that make them unique. First, nanomaterials present a large surface area to size ratio that creates a large amount of high energy surface atoms that can interact with their environment. Second, nanomaterials present unique physical properties that are dependent on their size due to the small crystalline domains of these materials and quantum confinement effects.

In recent years, the application of a diverse range of 0D, 1D and 2D nanomaterials have shown great success in the fields of electronics [1, 2] and energy storage [3, 4], and have been highlighted as promising materials for structural materials [5, 6] and medicine [7, 8]. Moreover, there is still plenty of room to study the application of these nanomaterials as new building blocks for the bottom up synthesis of complex structures. The use of 1D and 2D nanomaterials as templates to fabricate nanostructures from a bottom-up approach is a promising case since one of their dimensions already has microscale length. A potential nanomaterial to be used as a template for the bottom up fabrication of nanostructures are carbon nanotubes (CNTs), which are the 1D nanomaterial of the family of carbon allotropes. CNTs present a nanoscaled diameter with a microscaled length, which provides them with a high aspect ratio and a large surface area. More importantly, CNTs are able

to interact with molecules through covalent and non-covalent interactions providing means to introduce functional groups that can engage in the intermolecular forces required to create complex nanostructures. The central topic of this thesis is to study the interactions of CNTs with polymers, with the aim to increase our understanding of the functionalisaiton of CNTs and how can this be exploited to create hierarchical nanostrucutres with nanoparticles from a bottom up approach. The following section of this introductory chapter will describe the structure of CNTs and highlight what properties make them an interesting material for the development of new nanostructures.

1.1 Carbon nanotubes

1.1.1 Carbon nanotubes structure

The atomic structure of a CNT is similar to graphene consisting in a single layer of carbon atoms arranged in a hexagonal lattice with predominantly sp^2 hybridised C-C bonds. In contrast to the planar structure found in graphene, the monatomic thin carbon layer is wrapped around an axis forming a hollow tubular structure as displayed in Figure 1.1. The tubular ends of the CNT structure are capped by a hemisphere that consists of a combination of carbon pentagons and hexagons that can be observed in Figure 1.1A. The deviation from a planar arrangement to a curved structure is caused by a small degree of sp^3 hybridisation in the C-C double bonds [9]. The curvature of CNTs creates an additional feature on their structure called helicity, which is related to the way that the carbon sheet is folded into the tubular arrangement. The helicity of CNTs is defined by the chiral vector C (n,m), and each vector corresponds to a CNT with a particular bonding structure and diameter [10]. In an analogous manner to graphene and graphite, CNTs can be formed by layered structures where the sheets of carbon atoms are folded around

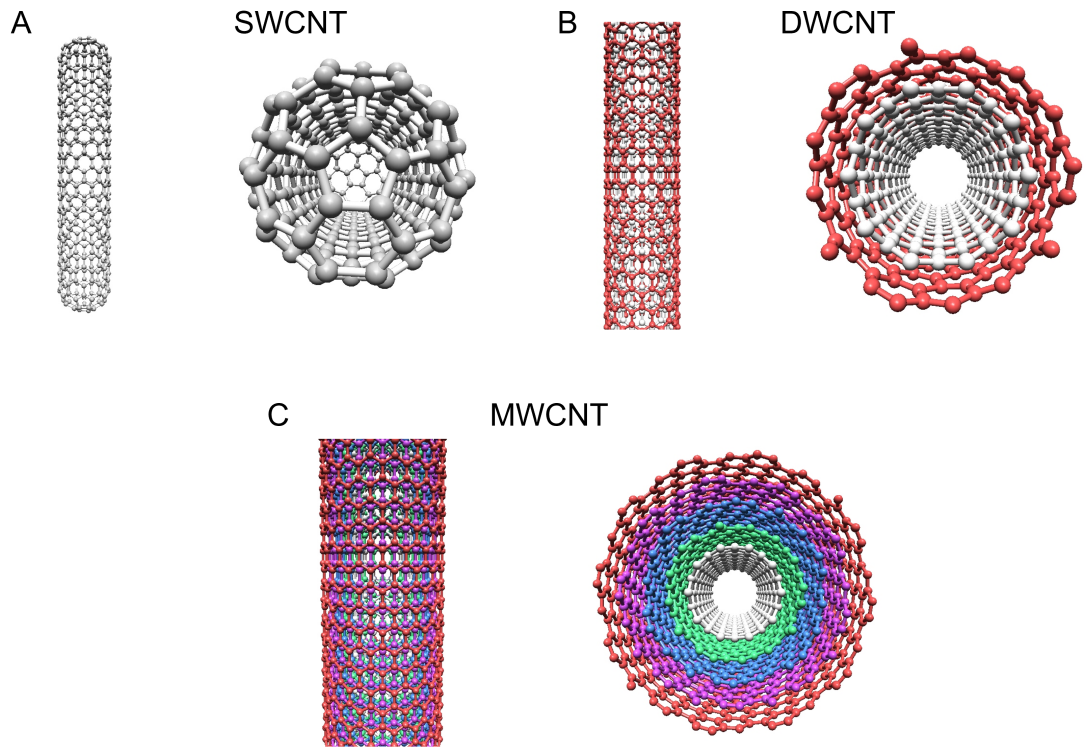


Figure 1.1: *Schemes of (A) SWCNT sidewall and end-cap structure, (B) DWCNT sidewall structure and cross-section and (C) MWCNT sidewall structure and cross-section.*

each other creating concentrically arranged tubes. Depending on the number of walls CNTs are classified as single-wall carbon nanotubes (SWCNTs), double-wall carbon nanotubes (DWCNTs) or multi-wall carbon nanotubes (MWCNTs) as shown in Figure 1.1.

CNTs as any other material present different types of defects throughout their structure that have impact in their physical properties. In general, I propose to group CNT defects in three main categories that are exemplified in Figure 1.2. First, topological defects that arise due to the occurrence of five and seven membered carbon rings in the hexagonal lattice. The presence of pentagons and heptagons leads to a reorganization in the bonding angles of the crystal lattice causing respectively concave and convex curvatures in the structure of the CNTs [11]. These defects can occur isolated or in pair combinations, having additive effect in the overall curvature of the CNTs as depicted in Figure 1.2A. Second, hybridization defects are caused due

to the presence of fully sp^3 hybridized carbon bonds as shown in Figure 1.2B, these defects can be induced by the chemical treatment of CNTs as it will be discussed later. Finally, traditional crystallographic defects related to discontinuities in the crystalline structure such as vacancies, interstitials and dislocations are also found in CNTs. An example of a vacancy crystallographic defect is depicted in Figure 1.2C.

The most important factor influencing the defect density of CNTs is the technique used for their synthesis, which can be classified in two main methods arc/laser evaporation and chemical vapor deposition (CVD) [9]. Briefly, the former technique consists in the electric arching or high temperature laser irradiation on metal-doped graphite rods. This methodology generally secures the synthesis of high quality SWCNTs and MWCNTs, with a low concentration of defects [9]. The second method involves the catalytic growth of CNTs from metal nanoparticles through CVD techniques. Depending of the methodology different carbon sources have been used ranging from gases with low molecular weight (*i.e.* CH_4) [12] to organic solvents [13]. Interestingly SWCNTs and MWCNTs growth by CVD present different degrees of defect densities, the former presenting qualities comparable to arc/laser evaporation techniques while MWCNTs present a high degree of defect density [9].

CNTs are not found as discrete materials and after synthesis they form aggregates or bundles between each other, which have widths that can be observed in the

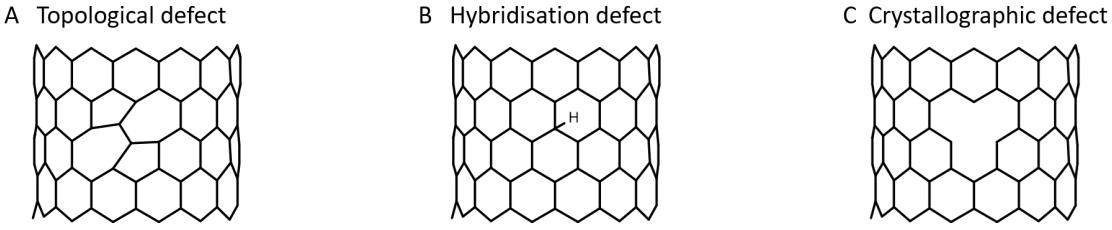


Figure 1.2: *(A) Scheme of a heptagon-pentagon pair in a SWCNT that exemplifies a topological defect. The overall curvature of the tube is not affected in this case. (B) Scheme of SWCNT with a hybridisation defect represented by an sp^3 carbon bonded with a hydrogen atom in the lattice. (C) Scheme of a SWCNT presenting a vacancy that exemplifies a crystallographic defect. For reasons of clarity the double bonds in all of the schemes were omitted.*

microscale and macroscale [9]. The formation of these bundles is driven by the large surface area of the CNTs, which causes their aggregation to minimise their surface energy. The bundles are strongly held together through Van der Waals interactions that require to be broken for the manipulation of isolated CNTs [14]. This behaviour has two important implications, first the physical properties observed for CNTs at the nanoscale will differ from their macroscopic behaviour. Second, the high surface energy and strong interaction between CNTs within the bundles makes them difficult to disperse and impossible to dissolve in any solvent [15]. This behaviour has important impact on the ability to process and manipulate CNTs into nanostructures that can exploit the outstanding physical properties of CNTs. The next two sections are focused in the physical and chemical properties of CNTs, expanding the discussion on the implications of CNT microstructure in their properties and the importance of nanostructuring.

1.1.2 Carbon nanotubes physical properties

Bearing in mind the strong C-C bonds and the hyper-conjugated crystalline structure of CNTs is not surprising that this material displays outstanding mechanical, electrical and thermal properties. A summary of some experimental and theoretical physical properties of CNTs is presented in Table 1.1. Since the physical properties of CNTs are closely related to their crystal structure, the introduction of defects results in a reduced mechanical, electrical and thermal performance. Another caveat is that these properties have been calculated and measured for isolated CNTs, it should be expected that the macroscopic properties measured of CNTs will be lower for all of the categories.

CNTs display a peculiar band structure due to the disparity in the number of allowed electronic states between the circumferential and the axial direction [9]. The helicity of SWCNTs has a significant impact on their electronic band structure and depending on the chiral vectors CNTs can either behave as metallic or

semiconducting materials [24]. On the other hand, MWCNTs are normally considered as metallic conductors [25] although metallic and semiconducting behaviour for MWCNTs have been experimentally observed [26]. A further consequence of the limitation in the allowed electronic states of CNTs is that they show an electron conduction in quantised electron states [9]. This behaviour is normally referred to as quantum wires and has two important repercussions on the conductivities of CNTs. First, the electron transport along CNTs can present a ballistic behaviour (*i.e.* the electrons do not loose energy due to scattering) and second the electrical resistance in CNTs does not increase with length [27]. These properties grant CNTs the ability to conduct large amounts of current with minimal loss due to heating. The presence of hybridization and crystallographic defects have a disruptive impact and can even impair the electron conduction at high defect densities [28, 29].

Heat conduction in CNTs occurs by coupled C-C vibrations throughout the 1-D lattice, causing long phonon mean pathways and similarly to the electric transport a quantized behaviour has been theorized (*i.e.* thermal conduction through the CNT is independent of tube length) [30]. The density of defects, in particular those related to the deviation in the crystal structure can have a significant effect on the thermal conductivity of the CNT [31]. To put this into context, the effect of defects in the thermal properties of SWCNT have been simulated by Sevik *et al.* [32] where they established that even low defect concentrations (*e.g.* 0.5%) can induce the saturation of the thermal conductivity to 160 W $m^{-1}K^{-1}$, an order of magnitude

Table 1.1: *Summary of reported electrical, thermal and mechanical properties of CNTs.*

Property	Theoretical	SWCNTs	MWCNTs
Quantum conductance	Yes [16]	Yes [17]	Yes [18]
Thermal conductivity [W/m·K]	6600 [9]	3500 [19]	3000 [20]
Young's modulus [TPa]	1.26 [21]	1.2 [22]	0.87 [23]

below their theoretical value.

In addition, CNTs present exceptional mechanical properties granted by the strength of the sp^2 C-C bonds, and have been considered as the ultimate high-modulus low-density fibrous materials [21]. Once again, the mechanical properties of CNTs are closely related to the amount of defects present in their structure, and simulations of SWCNTs under axial tension predict that the presence of defects induces the cleavage of the C-C bonds during fracture [21]. Thus, the presence of defect sites in the CNT structure will have an important contribution to the CNTs tensile strengths.

The remarkable physical properties of CNTs have been highlighted for their potential application in semiconductor, electronic and structural materials. In addition to their physical properties, their large aspect ratio make them promising templates for nanostructured materials. However, one of the main causes that has delayed the wide spread application of CNTs is the fact that the bundled configuration presented by CNTs in the microscale has a detrimental impact in their properties. For example the mechanical failure of SWCNT bundles observed in the macroscale is an order of magnitude smaller than for isolated SWCNTs since the failure mechanism results from the disruption of the Van der Waals forces interacting between tubes [33]. In addition, the formation of bundles create boundary resistance between the CNTs for thermal conduction affecting the efficiency of phonon transport [34]. This effect is largely increased when the bundles are not aligned in a particular axis. Finally, the electrical properties of CNTs suffer less of a direct impact due to their agglomeration into bundles, although CNT inter-junctions within bundles can increase the resistance of the material [2].

The strong dependence of CNT properties on their microstructural conformation highlights the importance of processing the CNTs into desired microstrucutres. However, the strong bundling between CNTs and high aspect ratio makes this materials difficult to process through wet chemical methods. To overcome these limitations

the chemical functionalisation of CNTs can be exploited to break the bundling of tubes and to enhance their dispersion in solvents. In addition, the chemical functionalisation of CNTs can provide the means to create nanostructures where CNTs are coupled with other nanomaterials that exhibit complementary magnetic, chemical and optical properties. The following section will revise the versatile chemical behaviour of CNTs provides the means for them to interact with other nanomaterials that could lead to the emergence of cooperative and synergistic properties. Exploiting this interactions is the foundation of this Thesis.

1.1.3 Carbon nanotube chemistry

A feature that makes CNTs a promising material for the bottom-up synthesis of nanostructures is their ability to undergo chemical functionalisation on their surface through covalent and non-covalent interactions with organic molecules. Chemical functionalisation can be used to incorporate functional moieties with the ability to interact with a wide range of materials through intermolecular interactions. The ability of CNTs to interact with organic molecules can be described in terms of their electronic structure, which can be regarded either as a highly π-conjugated bulky ligand for non-covalent functionalisation or as a polyaromatic structure presenting electron deficient alkene bonds for covalent functionalisation [35]. Both methods have been widely used to increase the poor solubility of CNTs in both organic and aqueous media, and to tune or add chemical properties to their structure.

Covalent functionalisation involves the formation of a new covalent bond bridging between the carbons atoms of the CNTs and other organic molecules. The major driving force for this type of reactions is the relaxation of the angle strain in the carbon bonds of CNTs due to the transition from sp^2 to a sp^3 C-C bonds [36]. Because of this change in the hybridization, the reactivity of CNTs is closely related to their curvature and CNTs with small diameters should present enhanced chemical reactivity [37]. Another important factor in the chemistry of CNTs is thought to

be the presence of topological defects, since the presence of heptagon and pentagon rings modifies the local curvature of CNTs [38, 39].

Covalent functionalisation is normally categorized in defect-site chemistry and sidewall functionalisation. The former technique involves introducing hybridization defects into the structure of CNTs, which present a higher chemical reactivity and thus can be exploited in further chemical transformation. The most common method to introduce defects involves the oxidation of CNTs through wet chemical methods. Treatment with oxidizing acids, such as nitric ($HNO_{3(aq)}$) and sulphuric ($H_2SO_{4(aq)}$) acids at low temperatures (*i.e.* below 50 °C) is a common technique to purify CNTs from carbonaceous contaminants and residual catalysts particles. During these procedures, new hybridization defects are induced in the carbon lattice, creating a wide variety of chemical functionalities such as ethers, epoxides, hydroxyl and ketones [11]. The extent of oxidation can be enhanced by increasing the reaction time and temperature [40], using sonication during the reaction [41], or adding additional oxidizing agents (*i.e.* $KMnO_4$, OsO_4, H_2O_2) [42, 41, 43]. With these treatments, the rupture of C-C bonds on the sidewalls of the tubes can be achieved by the introduction of carboxyl moieties. The introduced carboxyl functional groups can be used for standard carboxyl organic reactions, allowing for the introduction a wide range of chemical functionalities as summarised in Figure 1.3.

Sidewall functionalisation consists of the direct introduction of organic molecules through reactions that exploit the inherit chemical bonding of CNTs. The sp^2 carbon network of CNTs chemically behaves as an electron deficient alkene, making this material susceptible to reactions such as radical additions [44, 45], carbene [46] and nitrene cycloadditions [47], and 1,3-dipolar cycloadditions [38, 48, 49, 50, 51]. In contrast to defect-site chemistry where through oxidation procedures a wide range of chemical functionalities are introduced, sidewall functionalisation procedures exclusively modifies the surface chemistry of the CNTs with a specific molecule as exemplified in Figure 1.4. In addition to a larger control during the functionalisa-

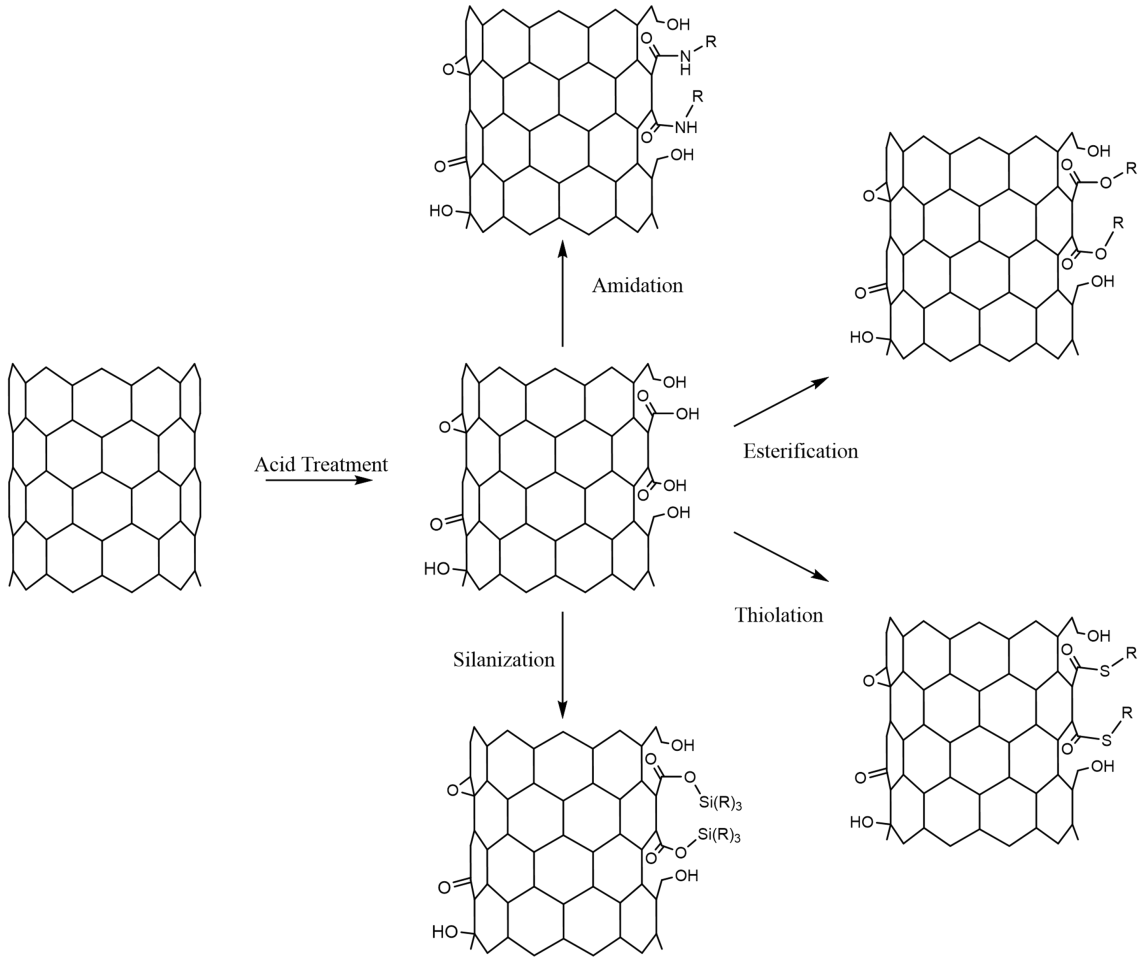


Figure 1.3: *Scheme of the oxidation of CNTs through acid treatment and further functionalisation through defect-site chemistry. Acid treatment of CNTs can be used to create oxygen rich functioanlities such as hydroxyl, epoxide and carboxylic acid groups. The latter can be exploited through organic chemistry to attach further functionalities through amidation, estrification, thoilation or silizanisation reactions. For reasons of clarity the double bonds and carbon-hydrogen bonds on the CNT structure have been omitted.*

tion, the properties of the CNTs are less affected through sidewall functionalisation since it introduces a smaller degree of hybridization defects in the CNT structure.

Non-covalent functionalisation results from the interaction of the CNTs conjugated surface with other chemical species, via Van der Waals forces and the so-called π-π interactions [52]. This approach allows the introduction of polymers and small organic molecules onto the CNT structure without affecting the sp^2 network, thus having only minor impacts in their physical properties [36]. Van der Waals interactions between aliphatic chains and CNTs have low binding strengths and weakly

interact with CNTs in organic solvents [36]. These weak interactions are mostly used to stabilize CNT dispersions in polar media with amphiphilic molecules. For example, common surfactants such as sodium dodecyl sulphonate and sodium dodecyl benzyl sulphonate are widely use to create CNTs in aqueous solvents [53]. The interaction between the CNTs and surfactants arise due to the high energy interphase found between the CNTs and the aqueous media, which leads to the aggregation of the aliphatic chains of the surfactant into the surface of the tube [53]. The interaction between small organic molecules and CNTs also depends on

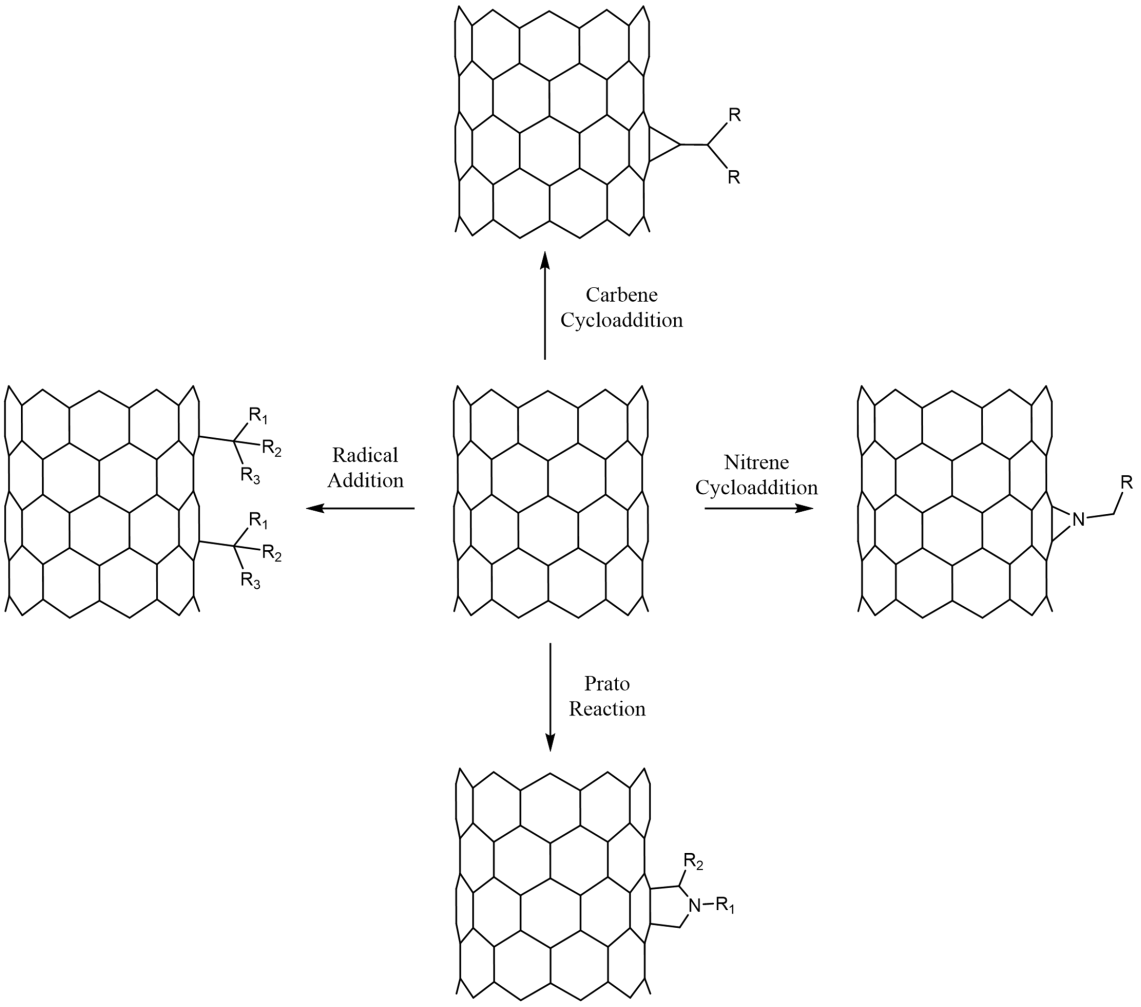


Figure 1.4: *Scheme of different side-wall functionalisation reactions that have been reported for CNTs. It can be observed that in contrast to defect functionalisation where a whole plethora of oxygen rich functional groups are incorporated, side-wall functionalisation procedures only incorporate the functional group introduced by the specific reaction. All double carbon bonds in the CNT structure and carbon-hydrogen bonds are omitted for reasons of simplicity.*

the functional groups held by the molecules. Amines and other nitrogen containing compounds have been used to stabilize dispersions of CNTs in aqueous and organic solvents [54]. The favourable interaction between amines and CNTs is also observed in the relatively high affinity of pristine CNTs for solvents such as N-methyl-2-pyrrolidone (NMP) and dimethylformamide (DMF) [55]. The interaction is thought to occur via a weak transfer of electron density from the nitrogen atoms to the surface of the CNTs [55, 54]. This hypothesis is supported by the correlation between the increase in the basicity of the amines and their capability of creating CNTs dispersions [55].

Polymers can also interact via non-covalent interactions with the surface of CNTs. For example, vinyl polymers such as polyvinylpyrrolidone and polystyrene sulphonate are known to disperse SWCNTs in aqueous media [56]. The interactions involved in this particular case are thought to be driven by the hydrophobicity of the CNTs and a weak π-CH interaction between the SWCNTs and the backbone of the polymers [56]. In similar fashion to surfactants, amphiphilic block copolymers have been used to stabilize CNTs dispersions.

Poly-aromatic molecules can bind strongly with the surface of CNTs [25], among these porphyrins and pyrenes have been widely used to create stable SWCNT solutions [57, 58] and form supramolecular assemblies from the surface of SWCNTs [59]. These interactions are commonly referred to as π-π stacking interactions, but a more intricate interaction is responsible for this behaviour. For these systems, the quenching in the fluorescence of poly-aromatic molecules is observed [60, 61], suggesting a charge transfer from the organic molecule to the CNT [60, 61, 62]. This type of donor/acceptor interactions is thought to present a contribution of electrostatic interactions and π-orbital mixing, which accounts for the strong contact between these aromatic molecules and CNTs [63]. In the field, these interactions are normally regarded as specific and irreversible [57], although it has been demonstrated that the solvent can play an important role in the stability of the donor/acceptor interactions

in simple poly-aromatic molecules [63]. Further studies on the nature of these systems could prove key to optimize the functionalization of CNTs by donor/acceptor interactions.

A similar behaviour is observed with poly-aromatic and other π-conjugated polymers. Enhanced solubility of MWCNTs has been observed when block copolymers containing a pyrene section [62] or even just in polymers with a single pyrene unit [64]. On the other hand, conductive polymers are known to interact closely with the surface of CNTs. For example, when both SWCNTs or MWCNTs interact with the polythiophene based P3HT-block-polysytrene, the NMR and UV-vis absorption spectrum seem to indicate that the interaction of the block-copolymer is through the conductive polymer rather than the polystyrene block [65].

In the last three decades considerable progress has been achieved in the field of functionalisation of CNTs and a large number of articles are published every year where the functionalisation of CNTs is used for the processing of CNTs or for the incorporation of particular properties for a specific application. However, major challenges are still present in the field. First, the functionalisation of CNTs is difficult to characterise, in particular for MWCNTs where multiple indirect methods have to be used to provide evidence of functionalisation. Second, the fact that both organic molecules and polymers can interact with CNTs through non-specific Van der Waals interactions indicates that even when covalent functionalisation procedures are implemented a certain degree of non-covalent interactions between the CNT and the molecule should also be expected. Furthermore, the lack of direct evidence for covalent functionalisation adds further challenges to understanding what kind of interactions are occurring between the organic molecules and the CNTs. The following example of a study by Qin *et al.* [66] illustrates this point. In their study they reported the synthesis of SWCNTs functionalised via a nitrene cycloaddition with a polystyrene molecule. The direct evidence of this functionalisation would be the characterisation of a N-C bond formed between the polystyrene chains and

the SWCNTs. However, the characterisation provided to support the functionalisation was the increase in defect sites in the SWCNTs. This data only demonstrated changes in the SWCNT structure and did not provide information of a N-C bond formation. Since the increase in defect sites could have been attributed to the high temperature ultra-sonication used during the reaction procedure [67, 68, 69] this evidence is not sufficient to attribute the incorporation of polystyrene molecules via covalent functionalisation and the influence of non-covalent interactions cannot be ruled out. In general, reports in the field of CNT chemistry do not evaluate the non-covalent interactions against the covalent interactions that might be taking place in their studies. Improving the characterisation and exploring how molecules interact with CNTs after the functionalisation procedure is key to finding theories that can be used to increase the efficiency of chemical functionalisation of CNTs.

Finally, there are still gaps in the literature of the functionalisation of CNTs with organic molecules. In particular regarding how non-covalent interactions occur between organic molecules and CNTs. Most reports do not use empirical data to understand how the interactions are occurring between organic molecules and CNTs. This causes most reports to use simple hypothesis derived from the chemical structure of the molecule involved in the functionalisation to determine the nature of the interaction between the CNT and molecule. In addition, there is a knowledge gap regarding the effect that various parameters used during functionalisation procedures have on the interactions between CNTs and organic molecules. Understanding the whole picture of interactions that occur during functionalisation procedures is required to create a consistent theory that can be applied for the rational design of functionalised CNTs.

Even after decades of research more studies are required to address the fundamentals of the functionalisation of CNTs with organic molecules, and it will be prerequisite for the bottom-up design of nanostructures based on CNTs. Addressing these limitations is the starting point of Chapter 3, where covalent and non-covalent

methodologies for the functionalisation of MWCNT with polystyrene are compared. Although this piece of work is focused mainly on non-covalent and covalent side-wall functionalisation of MWCNTs with polymers, I believe that the results and hypothesis proposed in this thesis will have an impact in other forms of MWCNT functionalisation.

1.2 Bottom-up assembly of nanostructures based on CNTs

From the perspective of the bottom-up assembly of nanostructures after the molecule-nanomaterial interaction the next length scale of organisation involves the interactions between different types of nanomaterials. Currently there are two main approaches for the fabrication of nanostructures that involve two or more distinct nanomaterials. The first approach involves the direct manipulation of nanomaterials using scanning probes to obtain the desired nanostructure. While these methodologies provide accurate spatial control over the composition of the nanostructure they pose several challenges for their use in mass production, making this approach difficult to apply for their commercial application [70]. A second approach is via self-assembly techniques that rely on the physicochemical interaction between the nanomaterials to control the composition of the nanostructure. This approach could provide highly scalable methodologies for the bottom-up fabrication of nanostructures [70]. The ability of CNTs to be functionalised with organic molecules is a desirable attribute for the bottom-up self-assembly of nanomaterials, since it allows for the introduction of a wide variety of chemical functionalities that can provide the basis for the interactions to create structures involving different nanomaterials.

In this Thesis I focus on the assembly of MWCNTs and inorganic nanoparticles via the self-assembly approach. This system is a particularly interesting starting point for the fabrication of new nanostructures from a bottom up approach. De-

pending on their chemical composition inorganic nanoparticles present magnetic, optical and catalytic properties that when paired with the mechanical, thermal and electrical properties of CNTs can be used in a wide range of applications. From a structural perspective, the one-dimensional structure of CNTs provide a microscaled template for the organisation of nanoparticles into a larger scale. In addition, colloidal nanoparticles are normally stabilised by organic molecules that can be used to potentially functionalise the surface of CNTs.

Inorganic nanoparticle-CNT hybrid structures have attracted interest from the scientific community in the last two decades for their potential utility in a broad range of applications. The advantages of coupling inorganic nanoparticles with CNTs can be exemplified with the use of transition metal oxide nanoparticles coupled with CNTs for energy storage applications such as Li-ion batteries. Transition metal oxides present excellent electrochemical properties to be used as high capacity electrodes but present poor electrical conductivity, which hinders their performance in Li-ion batteries [71]. The incorporation of CNTs as a conductive additive can provide low resistance pathways for the conduction of the electrons exchanged during the electrochemical reaction [72]. In comparison to other conductive additives, CNTs present nanoscaled dimensions that are similar to the ones presented by the inorganic nanoparticles. This gives CNTs a dimensional advantage to other conductive additives by presenting larger surface interactions between the electrochemically active material and the CNTs, while limiting the excess volume and mass incorporated by the CNTs. Other applications in the field of chemical sensors [73], biomedicine [74] and energy generation [75] can be found in the literature. A key feature for the successful performance of these hybrid structures is a close contact between the materials, understanding how the interactions between inorganic nanoparticles and CNTs can be optimised is required to unlock the full capabilities of these structures.

In comparison to the chemical functionalisation of CNTs, the synthesis of hybrid structures fabricated from inorganic nanoparticles and CNTs can be considered the

next step of hierarchy for the bottom-up assembly of nanostructures. When organic molecules are used to mediate the interactions between CNTs and nanoparticles it should be expected that the same parameters that are involved in the functionalisation of CNTs with organic molecules should apply for the synthesis of the hybrid nanostructures. Understanding if the same principles that dictate the chemistry of the interactions between CNTs and organic molecules can be translated to other nanomaterials is required for the efficient fabrications of hybrid nanostructures. In Chapter 3 and 5 we focus on the development of theories and models of functionalisation of CNTs with organic molecules that are consistent with the synthesis of nanostructures that incorporate both nanoparticles and CNTs. I hope that the research presented in this thesis will aid to unlock the full potential of these hybrid structures.

1.3 Thesis Outline

The aim of this thesis is to advance our knowledge in the bottom-up fabrication of nanostructures from a self-assembly approach. In this line of thought I focus on studying the interactions between MWNCTs, organic polymers and inorganic nanoparticles at the polymer-MWCNT and nanoparticle-MWCNT length scale. Chapter 1 has served as an introduction to CNTs, which is the 1-D nanomaterial that will act as the template material for the fabrication of nanostructures in this thesis. Chapter 2 will introduce the main synthetic and characterisation methods that were used throughout the experiments presented in these studies. Chapter 3 focuses on the smaller length scale, the interactions between MWCNTs and organic polymers. The studies discussed in Chapter 3 compare covalent and non-covalent methodologies to functionalise MWNCTs with polystyrene molecules. The purpose of this comparative study is to tackle some of the problems regarding the functionalisation of CNTs described in Section 1.1.3 and to determine the most effective way

to obtain polystyrene functionalised MWCNTs. In addition, I discuss the effect of other parameters such as the MWCNT diameter and the solvent media have in the degree of polystyrene functionalisation of MWCNTs.

In Chapter 4 I study the role of the solvent media in the non-covalent functionalisation of MWCNTs with polystyrene. The main objective is to propose a model that incorporates a broader set of interactions between the different chemicals used during the functionalisation of CNTs in comparison to previous research. The Chapter focuses on how the surface energy difference between the solvent and the MWCNTs can be used to understand the difference in the degree of functionalisation observed when the solvent medium is changed. For this purpose I focus in measuring the surface energy and solubility parameters of MWCNTs. In this chapter I propose the application of the solubility parameter theories as a model to predict the degree of polystyrene functionalisation depending on the solvent media.

Finally, Chapter 5 studies the interactions between iron oxide nanoparticles (IONPs) and MWCNTs as a case study of the subsequent length scale for nanomaterial assembly. In this chapter I explore the impact of different parameters such as the organic ligands mediating the interactions between the MWCNTs and IONPS, the diameter of the MWCNTs and the solvent. According to the results presented in Chapter 4, I hypothesise that the mechanism of functionalisation of IONPs with MWCNTs is also controlled by the difference of surface energy between MWCNTs and solvent media. The next Chapter of thesis will make a summary of the background theory for the characterisation and synthetic methods used during the experiments reported in this work.

Chapter 2

Methods

The methods for the synthesis and characterisation of the materials produced in this thesis encompass various fields of research such as CNT science, nanoparticle science and polymer science. In this chapter I present an overview of the different methodologies used throughout this thesis. The methods are classified depending on their relevance for each of the materials used throughout the thesis, although in some instances the techniques were used in more than one of the materials systems. After the conclusion of this methods overview the following chapters will discuss the bulk of the experimental results produced in this thesis.

2.1 Synthesis and characterisation of polystyrene

2.1.1 Atom transfer radical polymerisation

Atom transfer radical polymerisation (ATRP) is a free radical polymerisation technique used for the synthesis of polymers with low polydisperisty due to the control in the concentration of growing polymer chains achieved through the reaction. The mechanism of ATRP is depicted in Figure 2.1. In summary, a alkyl halide initiator is first reacted with a low-oxidation state metal complex. For this study,

2-(4-bromomethyl)phenylpropionicacid was used as initiator molecule, and bis(2,2'-bipyridine) copper (I) bromide complex is used as the catalyst. This reaction creates a radical that initiates the polymerization reaction by reacting with the desired vinyl monomer (styrene in the present study). The propagation of the polymerisation is mediated by the action of the metal catalyst by two processes. First the transfer of the halide to the radical chain and reduction of the metal catalyst to its starting oxidation state, which causes the deactivation of the polymerisation reaction. Second, the reactivation of the polymer chains into radicals by the subsequent oxidation of the metal catalyst as in the initiation state. The equilibrium constant of the deactivation process (k_d) is larger than the activation reaction (k_a), producing a low concentration of growing radical polymer chains. This deactivation effect reduces the number of termination coupling reactions and allows for the step-by-step growth of polymer chains, thus creating polymers with controlled molecular weight and low polydispersity. Finally the termination of the reaction is facilitated by introducing air into the reaction causing the oxidation of the metal catalyst and the deactivation of the growing polymer chains [76].

An advantage of ATRP is that allows for the control of end-group functionalities in two different ways. First, the vast number of alkyl halides that can be used during the polymerisation reactions allows for the control of the functional groups in the first molecule of the polymer chain. Second, the pendent bromide group obtained when the reaction is terminated allows for subsequent post-synthetic modifications by a large number of substitution reactions [76]. In Chapter 3 ATRP is used to synthesise polystyrene with low polydispersity, which is then post-synthetically functionalised with various chemical groups for the covalent and non-covalent functionalisation of MWCNTs. While in Chapter 5 we exploit the carboxyl group found in the initiator of the polymerisation reaction to attach polystyrene chains to the surface of iron oxide nanoparticles.

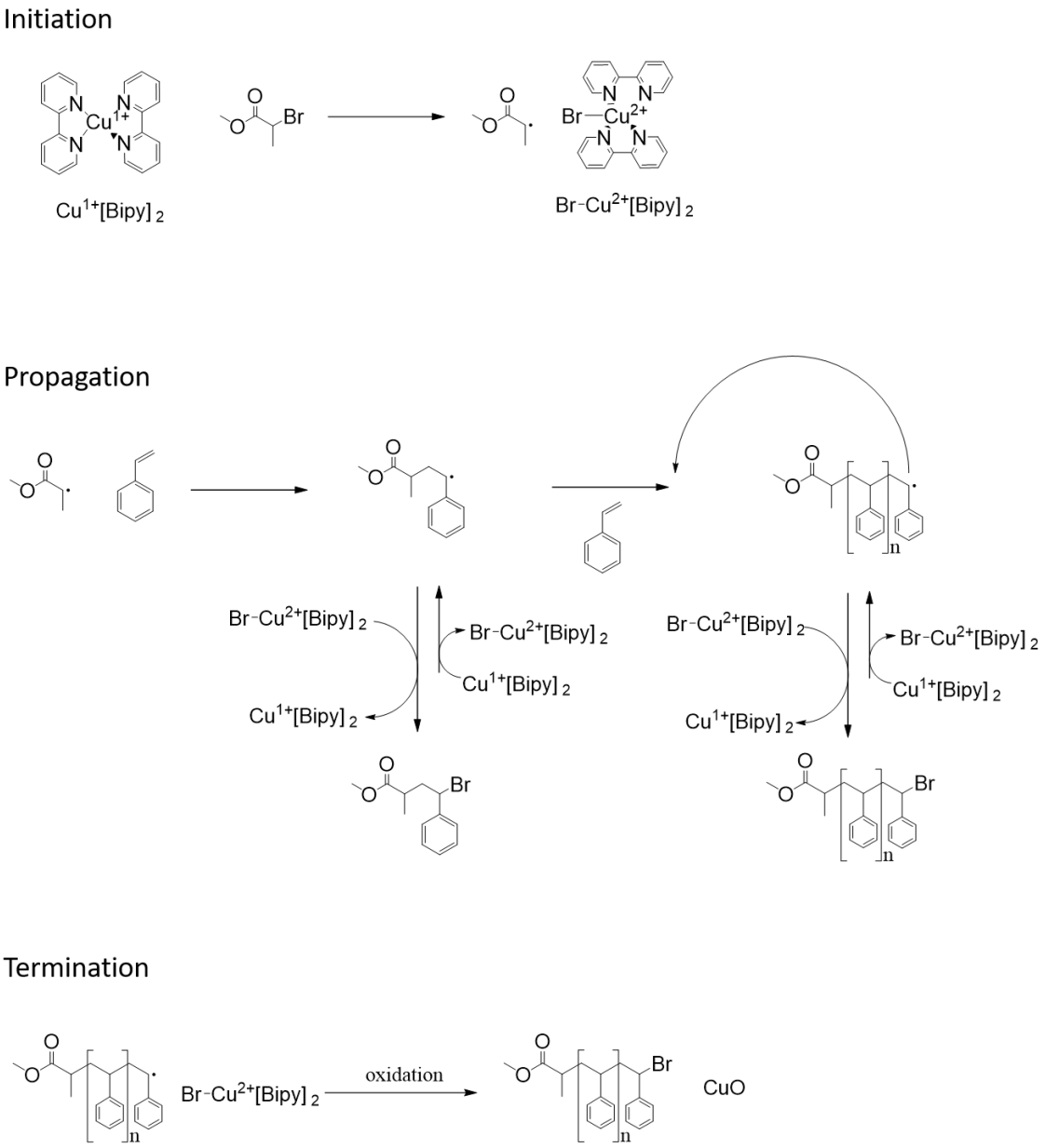


Figure 2.1: *Example of an ATRP synthesis of polystyrene. First in the initiation stage the initiator molecule reacts with the copper catalyst. During the propagation stage the catalyst controls the rate of the reaction maintaining a low concentration of living radicals in solution. Finally the termination step involves the irreversible oxidation of the catalyst causing the reaction to finish.*

2.1.2 Nuclear magnetic resonance spectroscopy

Solution based nuclear magnetic resonance (NMR) is a standard characterisation procedure for molecular materials, in particular carbon based molecules such as polymers. NMR spectroscopy is based on the transition of an atomic nuclei into an excited state by the absorption of radio electromagnetic radiation. Many nuclei

present a nuclear magnetic moment with degenerate energy levels that depend on the spin angular momentum of the nuclei. In the presence of a magnetic field the energy levels lose degeneracy since the spin angular momentum of the nuclei can point in the same or opposite direction of the magnetic field. The energy gap between the split energy levels corresponds to the radio frequency range of the electromagnetic spectrum, thus the nuclei can be excited by the absorption of radio frequency into an excited state. The value of the energy gap will depend of the size of the magnetic moment of the nucleus, the strength of the magnetic field and the chemical environment of the nuclei since the magnetic fields of surrounding electrons will contribute to the magnetic field acting on an adjacent nucleus. In this way NMR spectroscopy can measure a spectra where the transitions can be used to identify the present nuclei and their bonding environment [77].

In an NMR spectrometer a constant value of radio waves is used to excite the nuclei into the higher energy state, while the strength of the magnetic field is varied. NMR spectrum is plotted using the concept of chemical shift, that is based on the observation that different nuclei will be in resonance with the radio wave at different magnetic field strengths. In this way the value for the absorption to the excited state is measured in the ppm difference in the magnetic field strength required for the transition in comparison to a specific nuclei used as a standard[77]. In particular proton NMR (^{1}H NMR) is relevant for this study, in this case the nuclei that is examined is ^{1}H that is commonly present in most organic molecules. The electronic density present in the atoms directly adjacent to the carbon atom bonding to a particular ^{1}H, will affect the strength of the perceived magnetic field by the ^{1}H. In turn, the perceived magnetic field by the ^{1}H will affect the magnitude of the spin transition energy gap for the ^{1}H. The transition of the ^{1}H in tetramethyl silane (TMS) is used as a reference value which is set at 0 ppm. As more electronegative atoms than silicon are adjacent to the atom where the ^{1}H is bonded, their NMR peaks will appear at higher chemical shift values. Each organic functional group

tends to affect the chemical shift of a ^{1}H NMR spectrum within a short range of values. In this way the chemical shifts of each ^{1}H observed in NMR spectroscopy can be used to elucidate the composition and structure of organic molecules. In Chapter 3 ^{1}H NMR spectroscopy is used to characterise the synthesis of polystyrene molecules and their further chemical transformation into polystyrene molecules with various chemical functionalities.

2.1.3 Matrix-assisted Laser Desorption/Ionisation time-of-flight mass spectrometry

Matrix-assisted Laser Desorption/Ionisation (MALDI) mass spectrometry is one of the most popular methods for the molecular weight and chemical characterisation of high molecular weight organic and biomolecules. For MALDI mass spectrometry the a small amount of the molecule to be analysed is first crystallised with another organic molecule that acts as a matrix. This mass spectrometry technique produces the ionisation of the desired analyte by the interaction of an ultra-violet laser with the co-crystallised organic matrix, producing single charged species that are then accelerated by the action of an electric field. The time that each ionised molecule take to reach the detector depends on the charge to mass ratio, with heavier molecules with the same charge reaching the detector in longer times. In this way the ionised molecules can be separated and the spectrum of the molecules with different mass present in the sample can be obtained [78].

The process of desorption and subsequent ionisation of the molecules in MALDI spectrometry is not fully understood, involving primary events in the solid state and secondary events in the gaseous form. In some cases metal ions are required to be incorporated into the matrix to induce charged adducts with the desorbed molecules. However, the experimental success of MALDI to analyse high molecular weight molecules has established it as one of the main methods for the precise

determination of the molecular mass of a population of polymer chains [78]. The main advantage observed for MALDI is that it is a soft ionisation technique where the molecules being analysed present usually a single charge and the fragmentation of the analysed molecule is rarely observed. This can be observed in Figure 2.2 where a polystyrene sample was characterised through MALDI mass spectrometry. In Chapter 3 MALDI mass spectrometry is used to analyse the composition of polystyrene molecules and their molecular weights.

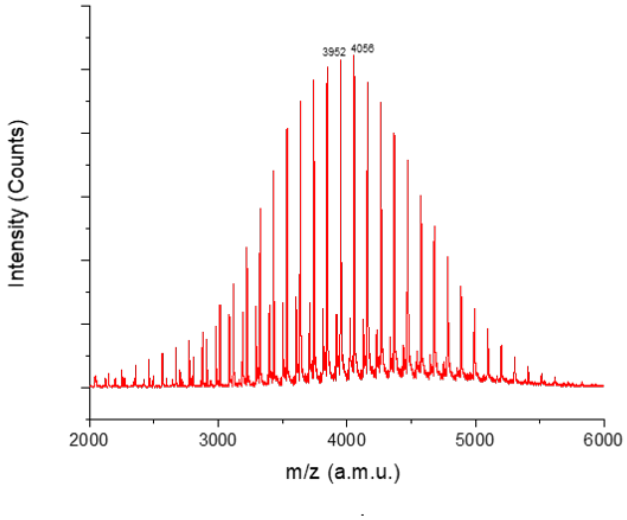


Figure 2.2: *Example of a mass spectrometry measurement of a polystyrene sample. Each peak represents the molecular weight of a polystyrene chain. Polystyrene molecules with a narrow molecular weight distribution is expected since polymerization reactions produce a distribution of polymer molecules. The difference between each peak represents the molecular weight of a monomer unit.*

2.1.4 Gel permeation chromatography

Gel permeation chromatography (GPC) is a size exclusion chromatographic technique where the stationary phase is made of porous polymer beads and the mobile phase are organic solvents. The separation principle for the solute molecules in this chromatographic technique is the diffusion of the solute molecules within the stationary phase pores. Each molecule will have an specific retention time that depends on their size, where larger molecules are eluted quicker and thus have shorter

retention times since their ability to permeate through the pores is smaller that of smaller molecules. This technique is widely used to analyse the size distribution of molecular weights of polymers and the quantitative determination of their molecular weight by calibration standards. Three main parameters are determined in this thesis by GPC. First is the number average molecular weight of polymer chains (M_n) which is defined as the total weight of polymer dived by the number of polymer chains. Second, is the weight average molecular weight (M_w) which considers that larger and smaller polymer chains will have a different contribution to the number of molecules per mass. M_w provides information of the molecular weight that the average polymer chain would have. Finally, the molar mass polydispersity that is defined as (M_w/M_n) that gives information of how broad a population of polymer chains is, the closer to 1 the narrower the dispersity of molecular weights [79]. In Chapter 3 GPC is used to determine the molecular weight of polystyrene.

2.2 Characterisation of MWCNTs, polystyrene functionalised MWCNTs and IONP-MWCNT hybrids

2.2.1 Fourier Transform Infrared Spectroscopy

Infrared spectroscopy is a characterisation method based on the ability of molecules to absorb electromagnetic radiation in the infrared region into excited vibrational states. For a molecule to be able to absorb infrared electromagnetic radiation it requires a change on the dipole moment within the molecule after the absorption of the electromagnetic radiation. The energy required for the transition into an excited state relates to the mass of the elements involved in the chemical bond and the energy of the bond between both atoms. In this way, the observation of infrared

absorption with different energies provides structural information of the chemical bonds observed in the material [80].

Fourier transform infrared spectroscopy (FTIR) is a specific technique to obtain the infrared absorption spectrum of a material that consists of shinning a source of a broad band infrared light into the sample. Through a configuration of static and dynamic mirrors specific wavelengths are transmitted or blocked through interference into the sample, allowing the collection of a spectrum of absorption at each specific infrared wavelength [80]. Different sampling methods can be used to obtain the infrared spectrum of a material, two methods with particular interest for this work are transmission-FTIR and attenuated total reflection (ATR) FTIR. Transmission-FTIR consists of measuring the total transmitted infrared radiation through a sample, in this case the wavelengths that are not transmitted are due to the absorption by the sample. This method is preferred for powder samples that are normally combined with potassium bromide using a mortar and pestle to decrease the diameter of large particles, which cause reflection and poor infrared spectrum. This is the most common method used for the analysis of functionalised CNT samples. Transmission-FTIR is used in Chapter 3 to demonstrate the non-covalent functionalisation of MWCNTs with polystyrene. ATR uses a the reflection of the infrared radiation through a prism with a large refractive index to probe the sample. The advantage of ATR-FTIR relevant for this work is the ability of casting solutions into the ATR crystal facilitating the sample preparation procedure. ATR-FTIR is used in Chapter 5 is used to characterise the ligand exchange of iron oxide nanoparticles.

2.2.2 X-ray photoelectron spectroscopy (XPS)

X-ray photoelectron spectroscopy (XPS) is a technique used to study the elemental composition of the surfaces of materials. The technique consists of the photoelectric emission of core electrons of the elements present in the sample, caused by

the absorption of X-ray electromagnetic radiation. Since each electron has a quantised ionization energy that is determined by their atomic electron configuration and bonding environment. In this way, XPS can be used to probe the chemical composition of a material. In XPS an X-ray source supplies high energy photons that cause the ionisation of the electron while the rest of the photon energy is transferred as kinetic energy to the ionised electrons. The kinetic energy of ionized electrons is the value measured in XPS, since a monochromatic beam of X-rays is used the kinetic energy value of the emitted electrons will correspond to a spectrum that is characteristic for each element present in the sample. This technique is highly surface sensitive with a probing depth of approximately 10 nm [81].

The value of the kinetic energy measured of the emitted core electron will depend of the X-ray source, element and bonding environment of the atom. In this way an element will present a particular peak that presents contributions depending on their bonding environment. More quantitative information about the composition of the bonding environment of the elements in the sample can be obtained through deconvolution of the elemental peak by fitting theoretical curves that account for the contribution of each bonding environment [81]. For the analysis of CNT structure the emission of electrons from the carbon 1s orbital (C1s) is commonly used to assess the ratio between sp^2 and sp^3 carbon atoms in the sample. In Figure 2.3 the result of the deconvolution analysis of the C1s spectrum of MWCNTs is presented, as it can be seen the contribution of each peak to the area below the curve of the spectrum can be used to understand the different chemical environments of the carbon atoms. In Chapter 3 XPS is used to characterise the functionalisation of MWCNTs with polystyrene.

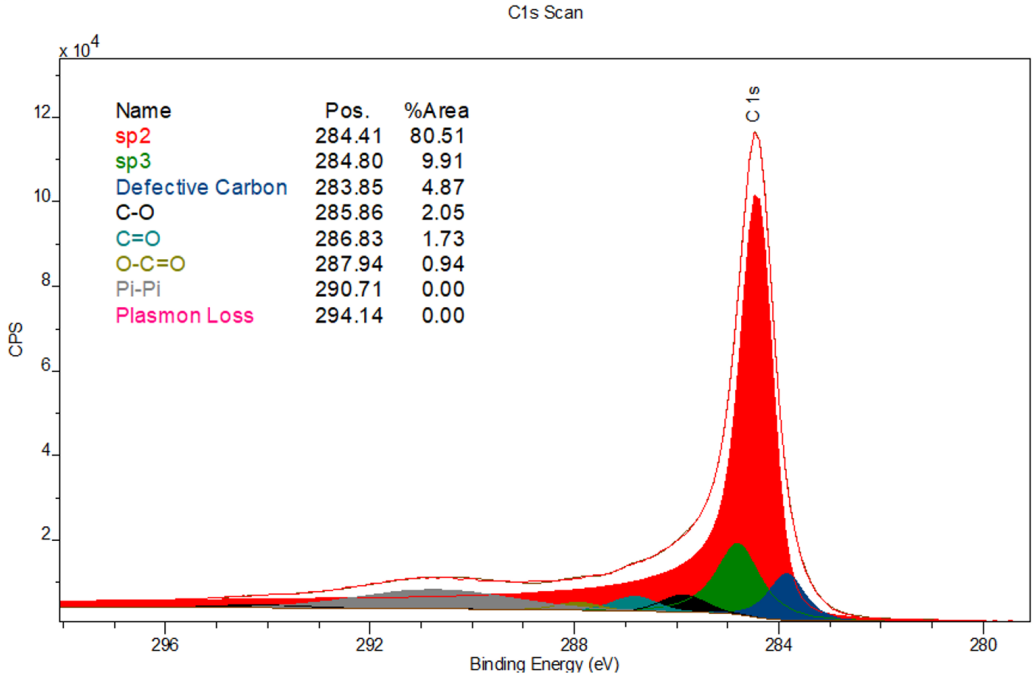


Figure 2.3: *Example of an XPS spectrum of the emission of C1s electrons in MWCNTs. The spectrum has been fitted with curves that represent the emission of electrons by carbon atoms with different bonding environment. The analysis allows the comparison of the area underneath each curve to compare ratios of carbon atoms with different bonding environments present in the material.*

2.2.3 Raman spectroscopy

Raman spectroscopy is based on the principle of inelastic scattering (Raman scattering) of light caused by the partial transfer of electromagnetic energy to the vibrational modes of the material. During Raman scattering a partial transfer of energy from a photon to the sample occurs, causing a change on the material vibrational state and the emission of a photon with an energy value that has shifted by a value equal to the energy of the vibrational state energy change in the material. In general, Raman spectroscopy measures the energy loss of photons or Raman shift, due to the excitation of a sample into a higher vibrational state. Similarly to IR spectroscopy, the energy value of this vibrational state is defined by the chemical structure of the sample, thus information of the bond structure of a material can be obtained. In contrast to IR spectroscopy, Raman scattering can occur even when

no overall dipole change is observed for the excited vibrational state, thus providing information about bond vibrations that cannot be observed by IR spectroscopy [82]. For this reason Raman spectroscopy has been a useful tool to study monoelemental materials such as CNTs where the transition to different vibrational modes is not accompanied with a change in the dipole moment within the electronic structure in the material.

The Raman spectrum of MWCNTs presents two characteristic peaks that provide important information about the bonding structure of the material (Figure 2.4). The first peak observed approximately at 1300 cm^{-1} is referred to as the defect-induced peak or D-peak, and is caused due to vibrations of structural defects that break the symmetry of the theoretical sp^2 carbon lattice of the MWCNTs [83]. The second feature observed around 1500-1600 cm^{-1} is the graphite-like peak or G-peak, this peak is related to a stretching mode observed for a perfect sp^2 carbon lattice [83]. The intensity ratio between the D-peak and G-peak (I_D/I_G) is commonly used as a parameter to assess the amount of defects present in a MWCNT, where a large ratio indicates a large proportion of defects present in the sample. The I_D/I_G is commonly used to evaluate the covalent functionalisation of MWCNTs since an increase in the value of the ratio is expected due to the disruption of the sp^2 by the introduction of sp^3 hybridized carbon atoms during functionalisation [84]. In Chapter 3 Raman spectroscopy is used to characterise the functionalisation of CNTs with polystyrene and to evaluate the formation of covalent bonds between polystyrene and MWCNTs.

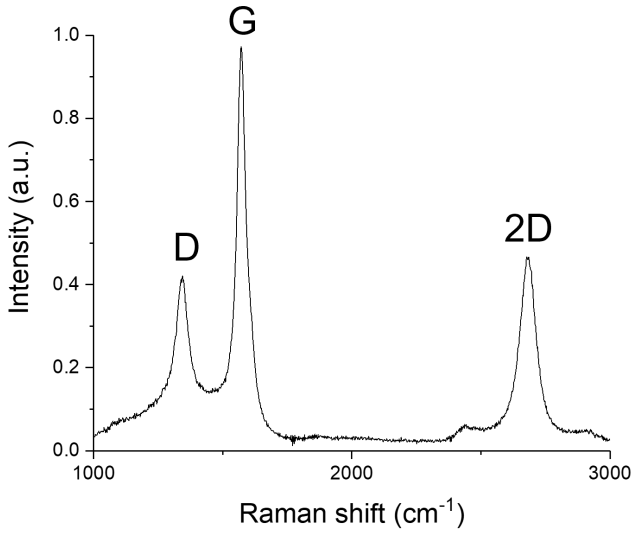


Figure 2.4: *Example of a Raman spectrum of a sample of MWCNTs. The features corresponding to the D, G and 2D peak are labelled correspondingly.*

2.2.4 Thermogravimetric analysis

Thermogravimetric analysis (TGA) is a thermal analysis technique that measures the mass change of a sample as a function of temperature. In this way TGA provides information when a chemical reaction that involves a mass change occurs. TGA equipment consists of a microbalance within a furnace, the microbalance and furnace are isolated from the open environment and a gas flow is normally kept constant within the furnace. The microbalance is used to hold a crucible where the sample to be analysed is contained, while the furnace is used to heat the sample to particular temperature. A dynamic scan is used when the temperature of the sample is require to change over time, while a isothermal scan is used when the sample needs to be held to a constant temperature over time. Figure 2.5 shows a sample that has been characterised through an isothermal and dynamic scan. Figure 2.5A shows the change of mass in the sample against the temperature of the sample, while Figure 2.5B shows the TGA curve of the same sample plotted against time. The first weight loss observed in Figure 2.5A represents a weight loss that occurred during an isothermal scan. Since the weight loss occurred at a constant temperature the

weight loss profile is very sharp. This weight loss is equivalent to the first weight loss observed in the TGA profile displayed in Figure 2.5B. In contrast with Figure 2.5A the weight of the sample continuously decreases along the x-axis, which causes the TGA curve to display a less abrupt weight loss. The second weight loss observed in Figure 2.5A&B was obtained through a dynamic scan, it can be observed that in this case both profiles have the same shape.

In addition to the control in temperature profiles, the atmosphere of the furnace can be controlled through the nature of gas used during the TGA experiment. In this Thesis the oxidation processes caused by reaction with oxygen were analysed by using an air atmosphere while the decomposition of organic molecules through non-oxidative processes were analysed in a nitrogen atmosphere [85]. In Chapter 3 and 5 TGA is used to analyse the composition of polystyrene functionalised MWCNTs and IONP functionalised MWNCTs, providing information of the degree of functionalisation in the MWCNTs structures.

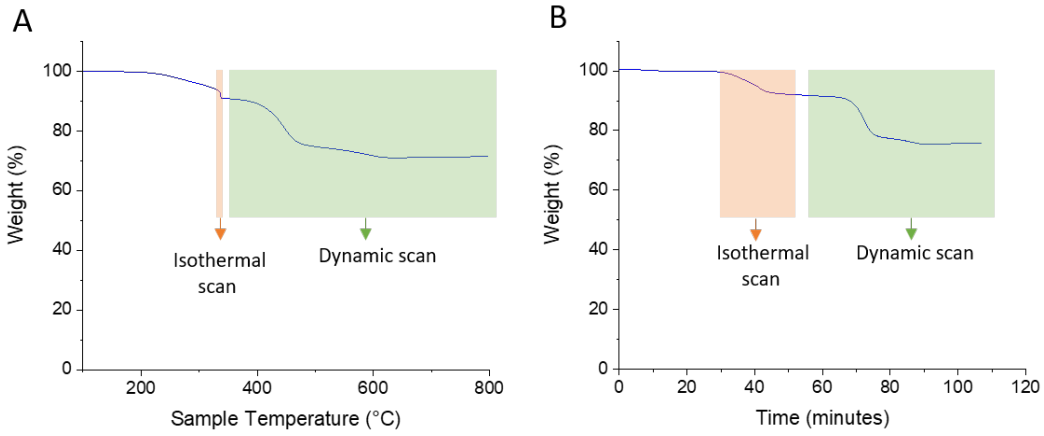


Figure 2.5: *Example of TGA curves of a sample of a iron oxide nanoparticle-MWCNT hybrid. Both curves represent the same experiment but in A) the weight change is plotted against the temperature of the sample, while B) shows the weight change plotted against time.*

2.2.5 Inverse gas chromatography

Inverse gas chromatography (IGC) is a powerful technique to study the thermo-

dynamic surface properties of materials. It fundamentally consists of a stationary phase packed in a column and a gas/vapour mobile phase. The main difference with other chromatographic techniques is that the sample of interest is the stationary phase. The mobile phase also referred to as probe molecules, consists of a gas or vapours of a volatile substance that is introduced to the column by a carrier gas. For the determination of the thermodynamic parameters of the stationary phase the probe molecules are normally introduced at very low concentrations to avoid intermolecular interactions between the probe molecules, for this reason it is referred to as infinite dilution. The parameter measured by an IGC is the retention time of the probe molecules in the column, which provides indirect information of the probe-sample surface interactions. Although retention time is the parameter directly measured by the IGC, the specific retention volume is normally the parameter used for the calculation of the thermodynamic parameters of the studied sample. The specific retention volume can be obtained from:

$$V_g = \frac{jF(t_r - t_m)T}{273.2m} \tag{2.1}$$

Where F is the flow of the carrier gas, t_r is the retention time of the probe, t_m the void retention time measured for a non-interacting probe, T is the temperature of the column, m the mass of the sample acting as a stationary phase, and j is the James-Martin factor that corrects the effects for pressure drop and packing density of the stationary phase [86].

In Chapter 4, IGC is used to determine the surface energy and Hansen solubility parameters of MWCNTs.

2.2.6 Transmission electron microscopy

In transmission electron microscopy (TEM) a set of electromagnetic lenses are used to focus a high energy electron beam into a sample. This is a high resolution tech-

nique allowing imaging with a point resolution in the sub-nanometer scale making it a powerful characterisation technique for nanostructured materials. The imaging occurs when the electron beam is transmitted through the sample causing scattering events, which produce a beam that contains a projection of the sample that can be recorded into an image. Since the electron beam is transmitted through the whole structure of the material, bulk information of the structure of the material is obtained. The scattering events of electrons create different contrast through the sample that increases with thickness of the sample (thickness contrast), density and the atomic number of the elements present in the sample (mass contrast). In addition, the wavelength of the electron beam is small enough to be diffracted by the crystal structure of the sample, allowing imaging of crystal planes due to the contrast created by the interference of the diffracted electron beam (diffraction contrast) [87]. Figure 2.6 exemplifies these three type of contrast observed in TEM micrographs. In Chapter 5 TEM is used to image IONPs and MWCNTs-IONP hybrids, exploiting the mass-thickness contrast to study the structure of these materials.

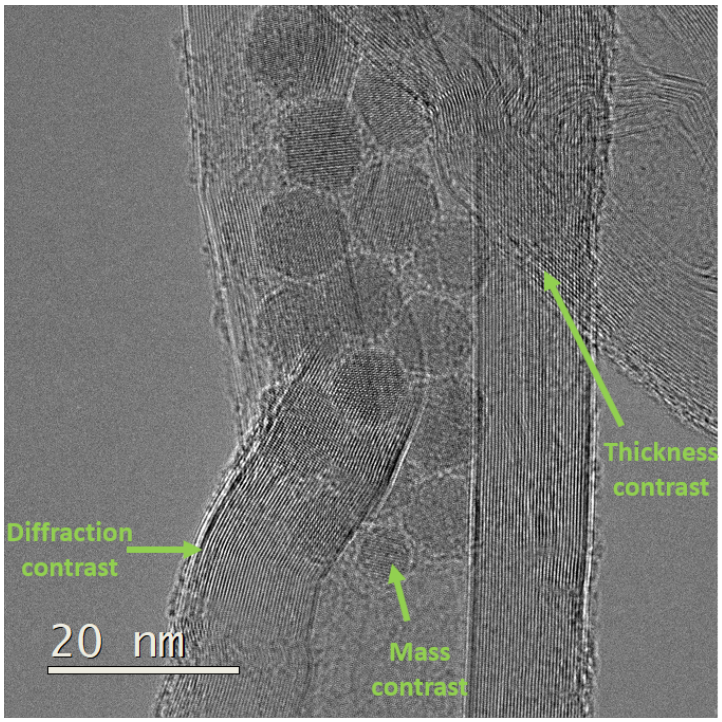


Figure 2.6: *TEM micrograph of a hybrid structure containing MWCNTs and iron oxide nanoparticles. Different type of contrast can be observed in the image. Thickness contrast is observed in the area where two MWCNTs overlap. Mass contrast is observed in the darker features observed for iron oxide nanoparticles in comparison to MWNCTs. Diffraction contrast can be observed in lattice fringes produced by the parallel crystal planes of the MWCNT walls.*

2.3 Synthesis and characterisation of IONPs

2.3.1 Nanoparticle synthesis by thermal decomposition of inorganic precursors

Thermal decomposition of inorganic precursors is a widely used method for the synthesis of nanoparticles, which consists of the nucleation of inorganic crystals through the thermal decomposition of organometallic compounds in solution at high temperatures (100-300 °C). These syntheses require high boiling point solvents and organic molecules that can act as surfactants. In brief the synthesis mechanism consists of the decomposition at elevated temperatures of metal precursors into an inorganic phase that remains in solution in a metastable state. The metastable state is preferred to the more stable solid phase due to the high surface energy

interface between the solvent and the solid nuclei. As the thermal decomposition continues the metastable phase reaches a concentration that allows the formation of solid nanocrystal that have a critical radius where the volume of the inorganic clusters is such that the free energy of particle precipitation is larger than the energy penalty created by the solid-liquid interphase. At this point the inorganic clusters quickly nucleate into an insoluble solid crystal phase. As the precursor continues to decompose the particles continue to grow aided by the stabilisation of surfactants that sterically hinder their aggregation. Due to the quick nucleation process and the surfactant regulated growth, the resulting nanoparticles present monodisperse diameters with a small size distribution [88]. In addition, the surfactant passivating layer can be post-synthetically substituted for a wide range of molecules allowing for the control of the surface chemistry of the nanoparticles.

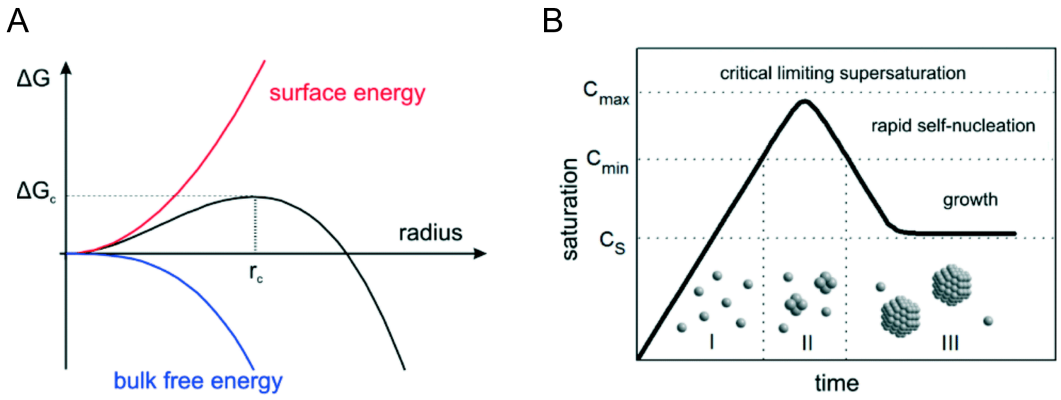


Figure 2.7: *A) Change of free energy dependence on surface energy and bulk free energy. It can be observed that after a critical radius the change in free energy is negative. B) Mechanism of nucleation and growth during thermal decomposition of nanoparticles. At a critical supersaturation concentration the quick nucleation of small nuclei with a critical radius is triggered, followed by the growth of the nanoparticles controlled by the surfactant molecules. Reproduced from Ref. [89] with permission from the Royal Society of Chemistry*

2.3.2 Powder X-ray diffraction

X-ray diffraction is a technique used to determine the crystal structure of a material obtained through the analysis of the diffraction of X-ray electromagnetic radiation that is produced by the spacings of the crystal planes of the material. The diffracted X-rays will constructively interfere when Bragg's Law condition is met, which states that the product of two times the sine of the X-ray incident angle (θ) times the crystal plane spacing (d) are equal to an integer multiple (n) of the wavelength of the X-rays (λ), otherwise the X-ray destructively interfere:

$$n\lambda = 2dsin(\theta) \tag{2.2}$$

The interference of the X-rays by the crystal spacings of the material leads to the formation of a interference or diffraction pattern that is characteristic of the crystal structure presented by the analysed material. Powder X-ray diffraction (PXRD) is used for the analysis of polycrystalline samples that can be considered as a population of randomly arranged single crystals. In this way a significant number of each possible plane orientation will meet Brags Law's requirements and thus PXRD records all the possible crystal plane diffractions that can be observed for the sample [90]. Finally, the diffraction patterns of the sample can be compared with patterns obtained from standard references or theoretical predictions to determine their crystal structure. In Chapter 5 PXRD is used to determine the crystal structure of iron oxide nanoparticles.

2.3.3 Dynamic light scattering

Dynamic light scattering (DLS) is a technique used to measure the size of particles in solution. In DLS a laser is used to illuminate a sample containing particles that cause the scattering of light in all directions due to the laser interactions with the

particles. The scattered light will interfere constructively and destructively, creating an interference pattern that is recorded. Due to Brownian motion of the particles in solution the intensity of the interference pattern will fluctuate over time. The rate of intensity fluctuation of the interference pattern depends on the speed that the particles are moving in the liquid medium, which in turn is associated to the size of the particles. The Stoke-Einstein equation relates the size of a particle to their speed, predicting that smaller particles have higher speeds than large particles in the same conditions. In this way, DLS records the intensity fluctuation of the interference pattern and by using a correlation function calculates the size distribution of the particles in the solution. The diameter of the particles measured through DLS is called te hydrodynamic diameter, since it incorporates information about the solvation shell surrounding the particle in solution [91]. In Chapter 5 DLS is used to measure the hydrodynamic diameter of IONPs coated with two different ligands to prove the stability of particles in solution and providing information about the nature of the ligands coating the nanoparticle cores.

Chapter 3

Functionalisation of MWCNTs with polystyrene through covalent and non-covalent methodologies

3.1 Intoduction

The ability of polymers to stabilise dispersions of CNTs while incorporating chemical functionalities into their surface makes polymer functionalisation a very promising path for the bottom up synthesis of nanostructures based on CNTs. The stabilisation of dispersions would aid the processability of the material while the incorporation of chemical groups on the surface of CNTs can provide the basis for robust chemical interactions with other materials. In order to improve the bottom-up assembly of hierarchical nanostructures based on MWCNTs that are mediated through the interactions with organic polymers it is key to understand which are the most efficient methodologies to promote MWCNT-polymer interactions. In this Chapter I tackle the comparison between covalent and non-covalent polymer-MWCNTs interaction as a first step to elucidate which approach is more efficient for the polymer function-

alisation of MWCNTs. Specifically in this Chapter I explore the functionalisation of MWCNTs with polystyrene (PS) through covalent and non-covalent methodologies. For this purpose I synthesised three types of polystyrene molecules, two of these molecules presented reactive groups in their structure for their application for either Prato or nitrene cycloaddition reactions with MWCNTs. A third polystyrene molecule that did not present functional groups capable of covalent reactions with MWCNTs was used as a control to compare the efficiency of the functionalisation between the covalent reactions and a system that could only interact through non-covalent forces with MWCNTs. The characterisation of the functionalised MWCNTs show that the efficiency between covalent and non-covalent methods are comparable, and strongly suggest that even when the covalent methodologies are attempted the main forces involved in the functionalisation are non-covalent interactions between the polymers and MWCNTs. Moreover, these studies show that the solvent medium has an important impact in the amount of polystyrene functionalisation of MWCNTs through non-covalent interactions. Finally I discuss how other parameters such as polymer concentration and how functional groups capable of strong $\pi - \pi$ interactions may affect the efficiency of non-covalent functionalisation of MWCNTs.

Before discussing my results herein I introduce the methodologies that have been used for the polymer functionalisation of CNTs through non-covalent and covalent interactions.

3.1.1 Non-covalent functionalisation

Non-covalent functionalisation occurs when CNTs and polymers interact through non-covalent means such as Van der Waals, hydrogen bonding and ionic forces. The principal characteristic of non-covalent functionalisation is that there is no formation of a chemical bond between the CNT and the polymer molecule. Since non-covalent functionalisation procedures do not change the bonding environment of CNTs it allows the outstanding physical properties of CNTs to be maintained, while the

properties of the organic molecules are incorporated into the system [45]. The functionalisation of CNTs through non-covalent forces with polymers have been reported for hydrophobic polymers [92], hydrophlic polymers [56], conjugated polymers [93], bio-polymers [94] and block copolymers [95]. The fact that a wide range of polymers with completely different chemical properties can functionalise CNTs through non-covalent forces makes the non-covalent functionalisation between polymers and CNTs a universal phenomenon that should be expected for every polymer and CNT mixed in a solvent [92].

In a seminal study, O'Connell *et al.* [56] proposed the mechanism for the non-covalent polymer functionalisation of SWCNTs by studying the functionalisation of SWCNT with polystyrene sulfonate and polyvinyl pyrrolidone in water. The authors argued that the surface functionalisation of SWCNTs with the water-soluble polymers reduced the unfavourable hydrophobic interactions between the CNTs and water, and it was the reduction of this high energy interphase that acted as the driving force for the functionalisation. This method of functionalisation is commonly referred to as "polymer wrapping" since the polymer is believed to wrap around the surface of the CNTs (Figure 3.1). Other studies have provided evidence for the argument that hydro or solvophobic effects are the driving force of polymer wrapping. For example, Meuer and Braun [64] reported the observation of a larger degree of functionalisation for SWCNTs with poly(diethylene glycol methyl ether methacrylate) in water was possible compared to tetrahydrofuran. They attributed the different degree of functionalisation to the hydrophobic nature of the CNT surface.

Non-covalent functionalisation of CNTs via polymer wrapping is commonly used to create stable dispersions of CNTs in aqueous and organic solvents. When the polymer wraps around the surface of the CNTs they cause the stabilisation of CNT dispersions through steric mechanisms and by disrupting the CNT-CNT interactions [56]. The final conformation of the polymers on the surface of the CNTs is believed to

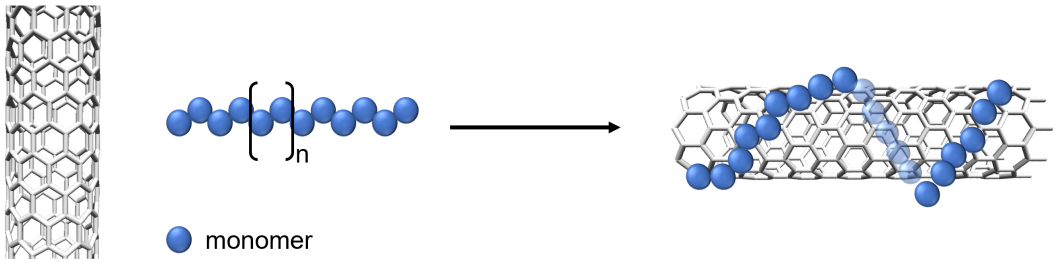


Figure 3.1: *Scheme representing non-covalent polymer functionalisation of CNTs via the polymer wrapping mechanism. The polymer molecules represented by the blue sphere chains coat or wrap around the surface of the CNTs when mixed in a solvent. In addition, the polymer chains induce the stabilisation of CNT dispersions via steric mechanisms.*

depend on the nature of the chemical composition and the flexibility of the polymer backbones [96, 97]. In addition, research on the stabilisation of 2D nanomaterials via polymer functionalisation has suggested that the conformation of the polymer chains on the surface of these nanomaterials will depend on the balance of the polymer-nanomaterial and the polymer-solvent interactions [98]. Finally, other geometrical considerations must be taken into account particularly regarding the size of the polymer chains relative to the circumference of the CNTs. If the circumference of the CNTs is larger than the length of a polymer chain it would be impossible for the polymer to wrap around the surface of the CNT, in this case the polymer would only be coating a section of the surface of the CNT and not wrapping around its circumference.

Although the hypothesis proposed by O'Connel *et al.* highlights the importance of the solvent-CNT interactions during the non-covalent functionalisation of CNTs with polymers, most efforts to optimize polymer-CNT interactions have instead focused on studying how the chemical structure of polymers impact the intermolecular forces involved during the functionalisation. Regarding the chemical composition of polymers it has been established that CNTs can have favourable interactions via π-π interactions with highly conjugated functional groups (*e.g.* pyrenes [57], porphyrins

[45, 35]) and π-conjugated polymers [62]. However, assessing the intermolecular interactions between CNTs and polymers that do not present highly conjugated functional groups is more challenging. In many cases there are different reports that propose contrasting means of interaction for the same polymer. A good example is the case of polystyrene where it has been proposed that the interactions between CNTs and the polymer chains occur via CH-π interactions between the polymer backbone and the sp^2 lattice of the CNTs [92], while others argue that the functionalisation is driven by $\pi - \pi$ interactions between the benzene polystyrene rings and the surface of the CNTs [99, 100, 101].

Predicting the intermolecular interactions between polymers and CNTs is a difficult task, and little attention has been placed to other forces involved in the functionalisation of CNTs with polymers such as the impact of the solvent medium. The mechanism proposed by O'Connell *et al.* [56] implies that the difference in the degree of polymer functionalisation of the CNTs is dependent on the interactions of the solvents with the surface of the CNTs. In this way, it would be expected that the amount of polymer functionalisation (*i.e.* the number of chains functionalising a CNT) will increase when the interactions between the CNTs and the solvent are not energetically favourable. In this Chapter I explore the effect of the solvent medium on the functionalisation of MWCNTs with polystyrene, demonstrating that by selecting an appropriate solvent the amount of polymer functionalising the MWCNTs can considerably increase.

In addition to polymer wrapping, other non-covalent mechanisms of functionalisation have been prosed in the literature. In particular, it has been reported that certain polymers can be designed so a portion of the polymer interacts preferentially with the CNT surface. This can be achieved by adding pendent pyrene or porphyrine molecules at the end of the polymer molecule as depicted in Figure 3.2. This molecules are believed to interact through π-π and charge transfer interactions with the surface of the CNTs. Bahun *et al.* [102] studied the interaction

between SWCNTs and a polystyrene block copolymer where one of the monomers presented a pyrene pendent functional group. The addition of a pyrene group in one of the blocks of the copolymer increased the dispersability of the CNTs in various organic solvents. The authors suggested that the copolymer section containing the pyrene groups had a preferential binding on the surface of the CNTs. This caused the outward extension of the other copolymer section, which helped to stabilise the dispersions more efficiently. In another study, Meuer *et al.* [103] demonstrated that even incorporating a single pyrene pending group at one of the ends of the PMMA chain produced an enhanced dispersability of MWCNTs in organic solvents.

Most studies that deal with the non-covalent functionalisation of CNTs with polymers aim to improve the dispersion of CNTs in solvents. For this reason the main experimental evidence for the effectiveness of the functionalisation are the stability and concentration of the resulting functionalised CNT dispersions. To measure the concentration of functionalised CNTs in dispersions UV-vis is the most common technique. However, the concentration of CNT dispersion is not a direct measurement of the amount of polymer interacting with the CNT surface. In fact,

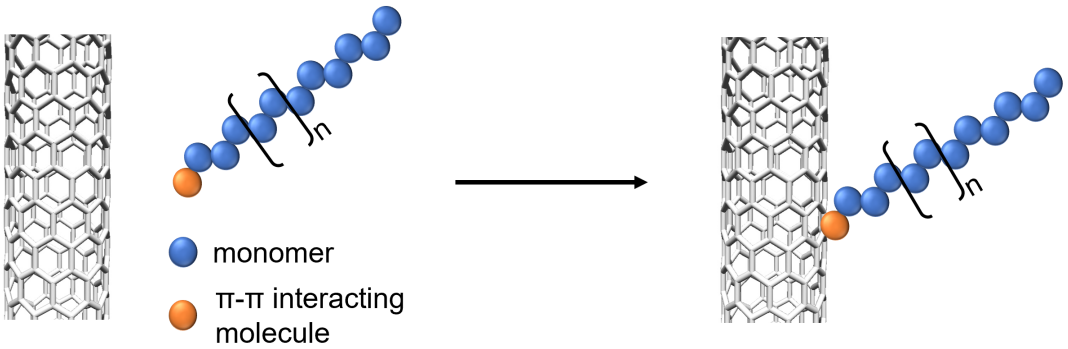


Figure 3.2: *Non-covalent functionalisation with polymers presenting a portion of the polymer that can interact preferentially with the CNT surface (e.g. charge transfer and π-π interactions). In this case it is believed that instead of a polymer wrapping around the CNT axis, a section of the polymer preferentially binds with the surface of the CNTs. This in turn allows the polymer chain to extend outwards the surface of the CNT, providing a higher degree of steric stabilisation of the CNT dispersions.*

this would be a measurement of the ability of the polymer to stabilise the CNT dispersion. The lack of quantitative evidence for the functionalisation of CNTs makes it difficult to understand how non-covalent interactions between polymers and CNTs can be improved. In this study I relied on TGA characterisation to provide quantitative data providing a more accurate assessment of the degree of the polymer functionalisation of CNTs since the composition of the polymer present in the sample can be accurately measured through this characterisation method.

The main disadvantage that has been highlighted for the non-covalent functionalisation of CNTs with polymers is that the forces involved during the functionalisation are subject to reversibility [56]. The reversibility of non-covalent interaction arise from their relatively weak forces in comparison to a chemical bond. For this reason many studies favour a functionalisation approach where a chemical bond between the polymer molecules and the surface of CNTs is formed, which is the topic covered in the next section.

3.1.2 Covalent functionalisation

Covalent functionalisation of CNTs with polymers involves the formation of a direct chemical bond between the polymer molecules and the CNTs. Covalent functionalisation procedures can be categorised into “graft to” and “graft from” procedures[62]. “Graft to” procedures consist of the reaction between a CNT and a previously synthesised polymer. The functionalisation can occur as a one-step synthesis by a direct reaction between a pristine CNT and a polymer molecule, or by multi-step procedure where the CNTs are first functionalised with reactive organic molecules that can in turn react with a polymer molecule (Figure 3.3A). On the other hand, ”graft from” procedures consist in performing a polymerisation reaction directly from the surface of the CNTs. In contrast to “graft to”procedures, CNTs need to be functionalised previously with molecules that can act as an initiator for the polymerisation reaction (Figure 3.3B). Both methods have been reported to be successful methodologies to

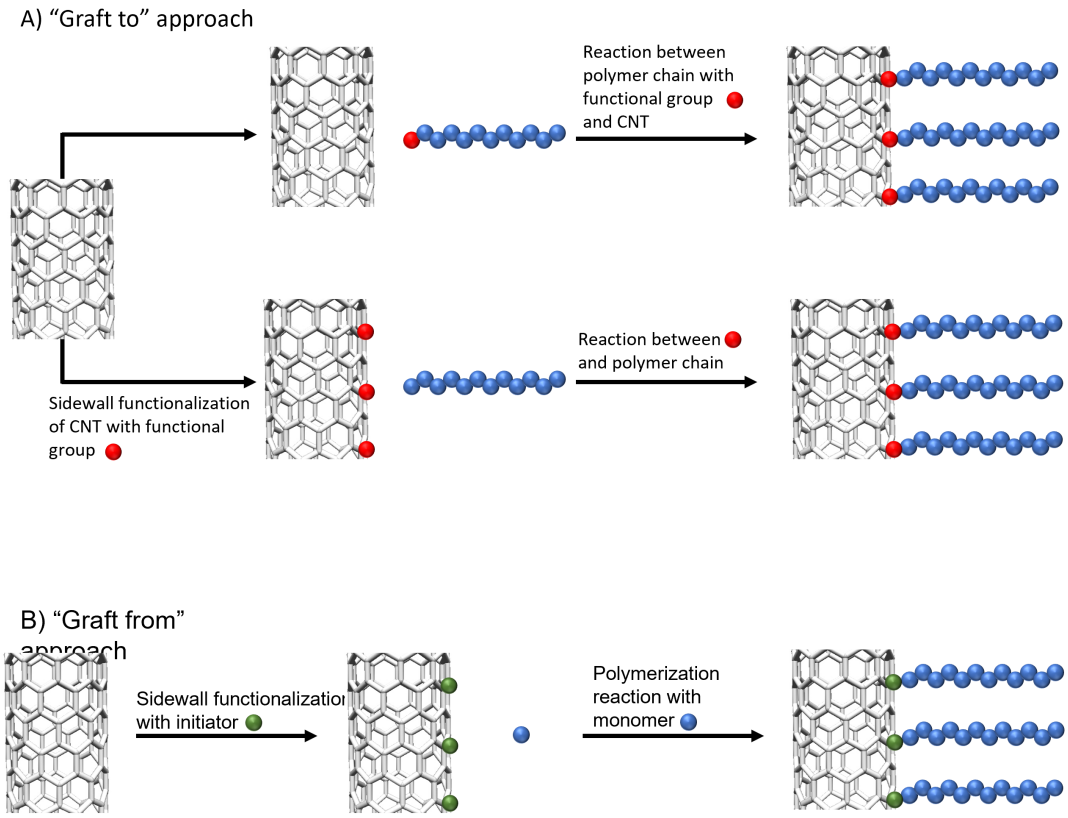


Figure 3.3: *Overview of the different approaches for the covalent functionalisation of CNTs with polymers. A) Overview of “graft from” methods. The functionalisation can be performed through one step or multi-step methodologies to create bonds between the CNT side-walls and the polymer chains. B) Overview of “graft to” methods. In contrast to “graft from”,“graft to” procedures require a first functionalisation step to incorporate initiators for the polymerisation reaction.*

functionalise CNTs [45].

In this study we focus on “graft to” methodologies for the covalent functionalisation of MWCNTs. “Graft to” methodologies have the advantage of decoupling the functionalisation reaction with CNTs from the polymer synthesis allowing control of the polymer molecular weight, polydispersity and composition prior to the functionalisation reaction [45]. In contrast, “graft from” procedures present synthetic complications since the growth of the surface initiated polymers are difficult to follow and control. In addition, the evaluation of the molecular size and polydispersity of the polymer becomes more complicated since the bonds between the polymer molecules and CNTs have to be cleaved off before being subjected to stan-

dard polymer characterisation procedures [66]. Finally, the objective of this study is to compare non-covalent and covalent interactions between polymers and MWCNTs to evaluate the efficiency of these two distinct methods. "Graft from" functionalisation does not involve the direct interaction between MWCNTs and polymers, since the polymer is synthesised from the surface of MWCNTs making this approach unsuitable for the objective of this study.

Most reports of "graft to" functionalisation of MWCNTs involve multi-step reactions that start with the incorporation of chemically reactive carboxylic acid functional groups in the CNT surface through oxidation reactions. The carboxylic acid functional groups can be then used to graft polymer chains to the surface of the CNTs [104, 105]. This method although effective is rather inconvenient since it involves several functionalisation steps and provides little control in the chemical composition of the CNTs due to the introduction of other non-carboxylic oxygen rich functional groups during the oxidation step. In addition, the introduction of oxygen rich functional groups has a detrimental impact on the physical properties of the CNTs [106, 107]. Finally, the chemistry related to the transformation of the carboxylic acid groups on the CNT surface can be considered as carboxylic organic chemistry since the reactions used are not targeting the chemical properties inherent to the CNT structure. In this Chapter we focus on the non-covalent and covalent methods relevant to the chemistry of pristine MWCNTs, for these reasons functionalisation methodologies that involve oxidation procedures are not further discussed.

Higher control of the functionalisation of CNTs can be obtained using reactions that occur directly on the sp^2 surface of pristine CNTs instead of reacting with carboxylic groups introduced through oxidation. In this Chapter I explore the Prato and the nitrene cycloaddition reactions which exploit the inherit chemistry of CNTs. Experimentally the Prato reaction consists of a one-step reaction where CNTs are mixed with an aldehyde and an α-aminoacid as shown in Figure 3.4. The aldehyde

and aminoacid react to create an azomethine ylide, a highly reactive molecule that in turn reacts in a [3+2] cycloaddition with the sp^2 lattice of the CNT. The Prato reaction has been successfully used to introduce initiator molecules in various reports [108, 109, 110] for their use in "graft from" procedures.

The [2+1] nitrene cycloaddition of an organic azide is another reaction that has been reported to introduce initiator molecules on the surface of MWCNTs [111]. This reaction consists of the thermal decomposition of an organic azide in the presence of CNTs. The azide decomposes to a highly reactive nitrene intermediate which undergoes a cycloaddition reaction with the sp^2 lattice of the CNT as displayed in Figure 3.5. The great advantage of this reaction lies on the simplicity of the reaction since it only involves the initiator molecule that is being introduced.

A handful of studies have reported the direct functionalisation of CNTs through "graft to" procedures, which include cycloaddition reactions [66], radical additions [112] and nucleophilic additions of negatively charged polymers reduced with organo-

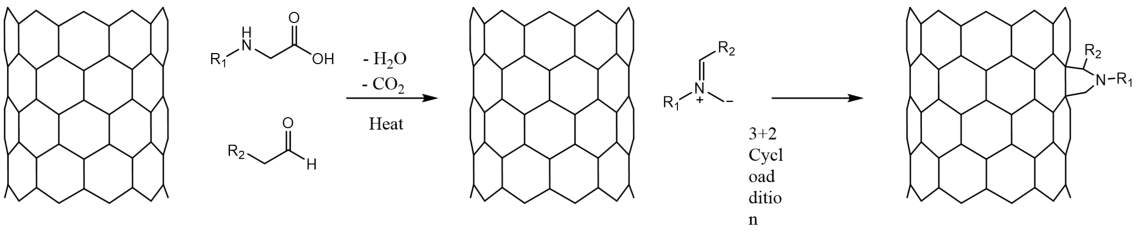


Figure 3.4: *Scheme depicting the mechanism for the Prato reaction. First, an aldehyde containing molecule reacts with an α-aminoacid to form an azomethine ylide. In a second step, the azometine ylide reacts trough a cycloaddition reaction with the surface of the CNT. For reasons of clarity the double bonds of the CNTs have been omitted.*

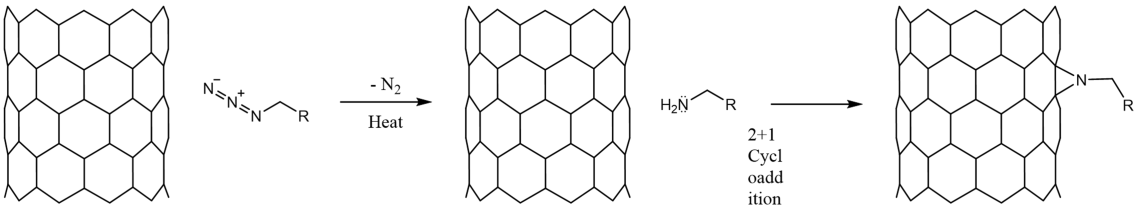


Figure 3.5: *Scheme depicting the nitrene cycloaddition reaction. First, an organic azide thermally decomposes to form a nitrene. In the second step, the nitrene performs a cycloaddition reaction on the surface of the CNT. For reasons of clarity the double bonds of the CNTs have been omitted.*

lithium compounds [113]. In particular the [2+1] nitrene cycloaddition of an organic azide has received wide interest since azide containing polymers are easily synthesised. Qin *et al.* [66] reported the synthesis of polystyrene functionalised SWCNTs by the [2+1] cycloaddition of nitrenes. In a straight forward protocol they reported that the decomposition of polystyrene molecules with azide end groups could be used to functionalise SWCNTs. Raman and FTIR spectroscopy were used to provide indirect evidence of the covalent functionalisation of the products of the reaction. However, no control experiments were provided to eliminate the possible contributions of non-covalent forces to the functionalisation. In contrast to "graft from", "graft to" procedures that use the Prato reaction has not been reported.

Regarding the methodology of polymer synthesis, controlled radical polymerisation methods such as atom transfer radical polymerisation (ATRP), reversible addition-fragmentation chain-transfer (RAFT) and nitroxide mediated radical polymerisation have been the most commonly used synthetic methods for the covalent functionalisation of CNTs with polymers [114]. The advantage of these controlled radical polymerisation methods lies in their ability to control the first and last molecule (end groups) of the polymer molecules. For instance, the first molecule of the polymer chain is determined by the initiator of the polymerisation reaction. By selecting a molecule with specific functional groups that can also be used to functionalise the CNT surface provides an excellent initiator candidate for "graft from procedures". In addition, the control of the initiator molecule, the terminal molecule of the polymer can also be controlled. For example, an ATRP reaction produces polymers with a bromine group that can be easily substituted to incorporate functionalities to the polymer chains required for "graft to" procedures. In this work ATRP was used for the synthesis of polystyrene that incorporates functional groups that could be used for the covalent functionalisation of MWCNTs.

A gap in the literature regarding the covalent functionalisation of CNTs with polymers is what role non-covalent forces have during covalent functionalisation

procedures, which is specially important for "graft to" methods. Since non-covalent interactions between polymers and CNTs is a phenomenon observed for the full spectrum of polymers, we would expect that this interactions are also present when covalent functionalisation is attempted. A potential way to evaluate the role of non-covalent interactions during covalent functionalisation methodologies is by using control experiments where non reactive polymer chains are mixed with CNTs. The TGA of the products would provide information of the difference in composition when covalent and non-covalent functionalisations procedures are used. This practice is not normally used in studies dealing with CNT functionalisation in the literature and is central for the results presented in this Chapter, where control experiments are used to compare the efficiency of covalent functionalisation reactions.

A major challenge in the covalent functionalisation of CNTs is the characterisation of the products of the reactions. Currently there are no known methods that can directly characterise the formation of a chemical bond between the CNT and an organic molecule. For this reason a combination of TGA, Raman spectroscopy, FTIR and XPS spectroscopy are the main techniques used for the characterisation of covalently functionalised CNTs. Raman spectroscopy provides information of the ratio between sp^2 and defective sp^3 carbons in the CNT lattice, which is generally assessed by measuring the D to G peak ratio observed in the Raman spectra. When the ratio increases it can be taken as an indication that the reaction was successful due to the disturbance of the sp^2 lattice of the CNT caused by the formation of sp^3 bonds with the introduced molecule. However, it is important to consider that a chemical reaction might not be the only cause for the introduction of defects into the CNT structure since common procedures used during functionalisation methodologies such as ultrasonication are known to incorporate defects into the CNTs [67, 68, 69].

TGA is normally used to evaluate the overall weight composition of a sample. Most organic molecules and polymers such as polysytrene, can be selectively decom-

posed under N_2 atmosphere leaving the CNT structure intact. TGA can be used to measure the amount of polymer that has been introduced into the CNT structure by selectively decomposing the organic molecules in the sample. Knowing the weight composition of polymer in the sample enables the comparison of the effectiveness of a functionalisation procedure. However, the observed presence of polymers or molecules through TGA does not provide direct evidence for the formation of a direct chemical link.

Other spectroscopic procedures such as FTIR and XPS can be used as a way to characterise the presence of organic molecules that are bonding with CNTs. FTIR can provide information of the vibration of the bonds present in the sample, if the typical absorption peak for the covalent bond formed between the CNT and organic molecule is found it can be taken as an evidence for the functionalisation of the CNTs. However, this is not a simple task since FTIR spectrum will include the vibrations of both CNTs and the organic molecule introduced, making it difficult to discern between the peaks that can be attributed to the organic molecule and the peaks that can be attributed to the CNT. For this reason the evidence that FTIR spectroscopy provides is mostly to confirm the presence of the introduced organic molecule. On the other hand XPS can provide detailed information of the elemental composition of the surface of the functionalised CNTs. Peak fitting can be used to analyse the bonding environment for each element and can provide evidence for new bond formation. The biggest challenge with XPS relies in the fact that the position of the peaks of the different bonding environments of the elements in the sample tend to be close to each other. For this reason the conclusions derive from peak fitting have to be taken with caution.

In this chapter we use a combination of Raman spectroscopy, FTIR, TGA and XPS to characterise the products of polystyrene functionalised MWNCTs by covalent and non-covalent methods. A thorough characterisation of the materials allows for the comparison of the efficiency between both methodologies. However, the

results of the characterisation presented in this study demonstrates that it is difficult to find conclusive evidence for the formation of chemical bonds using only these characterisation methods. Which highlights the importance of performing control experiments to determine the nature of the interactions between the polymers and the CNTs.

The next section describes the characterisation and experimental methods used during for this study.

3.2 Materials and methods

In the following section I outline the details of the matrials, synthetic and characterisation methods used during the experiments performed for this Chapter.

3.2.1 Chemicals

Tetrahydrofuran (THF) (HPLC grade $\geq$ 99.9%), styrene (containing 4-tertbutyl catechol > 99%), 2,2-bipyridine (99%), 2-(4-bromomethyl)phenylpropionic acid (96%) and copper (I) bromide (99.999% trace metal basis) used for the synthesis of polystyrene by atom transfer polymerisation procedure were purchased from Sigma-Aldrich.

The solvents used for the functionalisation experiments were purchased from the following providers. Dichloromethane (DCM) ($\geq$ 99.98%), DMF (HPLC grade $\geq$ 99.99%) and toluene (HPLC grade $\geq$ 99.99%) were purchased from Fischer Scientific. NMP (HPLC grade $\geq$ 99%) and acetone (Analytical Grade $\geq$ 99%) were purchased from Sigma-Aldrich. Orto-dichlorobenzene (o-DCB) (Reagent grade $\geq$ 99%) was purchased from Honeywell. Two different samples of MWCNTs were used for this study. The NC700 MWCNTs (10nmMWCNTs) were purchased from Nanocyl with an average diameter of 10 $\pm$ 2 nm. The aerosol assisted chemical vapor deposition MWCNTs (50nmMWCNTs) with an average diameter of 53 $\pm$ 25 nm were synthesised in house following following a procedure reported previously in the literature

[115].

DCTB (trans-2-[3-(4-tert-butylphenyl)-2-methyl-2-propenylidene]malononitrile, 98%) and silver trifluoroacetate (98%) used for MALDI-TOF characterization were purchased from Sigma Aldrich and used as received.

Deuterated chloroform (99.8% deuterium) was purchased and used as received from Sigma-Aldrich.

Potassium bromide Uvasol® for infra red spectroscopy was used to prepare the samples for FTIR.

3.2.2 Characterization

Solution nuclear magnetic resonance (NMR) spectra were recorded at 298 K on a 400 MHz Bruker AVANCE III HD. The samples were prepared using deuterated chloroform.

MALDI-TOF mass spectrometry for the molecular weight characterization was recorded on a Bruker Microflex LT spectrometer. Following a previous report [116] the samples were prepared using a polymer solution with a concentration of 2 mg/mL in THF, a 0.6 M solution of DCTB in THF and 0.06 M solution of silver trifluoracetate in THF. The silver trifluoroacetate was added to promote the ionization of the polymer. For the analysis 10 µL of each solution were mixed in a vial, afterwards 0.5 µL of the mixture was drop casted in the MALDI-TOF target.

Themogravimetric analysis was performed under nitrogen atmosphere in a Perkin Elmer Diamond TG/DTA6300 using a heating rate of 10 °C/minute. Approximately 5 mg of sample were used for each experiment.

Gel permeation chromatography (GPC) data was obtained using a Shimadzu LC-20AD instrument with HPLC grade THF as the eluent flowing at 1.0 mL/min at 30 °C and calibrated using near monodisperse polystyrene standards.

Transmission Electron Microscopy images were recorded on a JEOL 3000F TEM microscope operating with an accelerating voltage of 300 kV. The samples were

prepared by drop casting MWCNTs dispersions in acetone onto lacey-carbon copper grids.

FTIR spectroscopy data was acquired in a Varian Excalibur FTS 3500 FTIR spectrometer using solid samples in transmission mode. The samples were prepared by mixing with a mortar and pestle 0.1 mg of MWCNTs in 100 mg of KBr. The powders were compressed into pellets using a Graseby Specac hydraulic press to a pressure equivalent to 7 tons.

Raman spectroscopy was performed in a JY Horiba LabRAM ARAMIS confocal Raman microscope using a 532 nm laser. The samples were prepared by drop casting dispersions of MWCNTs in aluminium stubs. For each sample five different positions of the sample were recorded, each of them comprised of five independent measurements.

For XPS analysis the spectrum were acquired using a Thermo Scientific K-Alpha XPS instrument equipped with a microfocussed monochromated Al X-ray source. The source was operated at 12 keV and a 400 micron spot size was used. The analyser operates at a constant analyser energy (CAE) 200 eV for survey scans and 50 eV for detailed scans. Charge neutralization was applied using a combined low energy / ion flood source. The data acquisition and analysis were performed with Thermo Scientifics Avantage software. Peak fitting (Lorentzian / Gaussian (L/G) 30%) was applied following removal of a Smart background. Normalised atomic percentages were determined from peak areas of the elemental main peaks detected on the survey scan following background subtraction and application of Thermo sensitivity factors.

3.2.3 Synthesis of polystyrene

The methodology for the ATRP synthesised polystyrene (PS-Br) was based on a procedure reported previously [117]. In a typical experiment, 2-(4-bromomethyl)phenylpropionic acid (1.05 g, 4.34 mmol), copper (I) bromide (0.62 g, 4.34 mmol), and 2,2-

bipyridine (1.35 g, 8.68 mmol) were added to a three-necked round bottom flask. The flask was fitted with a septum and the solid powders were flushed in vacuum and purged with argon on a Schlenck line, the evacuation procedure was repeated three times. Afterwards, DMF (3.5 mL) were added and the mixture was flushed in vacuum and purged with argon on a Schlenck line, the evacuation procedure was repeated three times. Under a nitrogen flow, deoxyganated styrene (20 mL) was added with a syringe to the reaction vessel and it was placed in an oil bath at 110 °C for 3 hours. Afterwards, the reaction mixture was stopped and diluted in THF (200 mL). The mixture was vacuum filtered through a short neutral alumina column to remove the solid catalyst particles, the mixture was concentrated under vacuum and precipitated in methanol twice. The polymer was separated by vacuum filtration obtaining a light blue powder. ^{1}H NMR was consistent with the expected polystyrene spectrum and MALDI-TOF mass spectrometry showed that the difference of the molecular mass between peaks is equal to 104 g/mol consistent with the expected mass of styrene monomers. ^{1}H NMR (450 MHz, $CDCl_3$): δ 7.10-6.50 ppm (broad, aromatic H), 4.5-4.2 (broad, CH_2-Br) 2.5-1.1 ppm (broad, CH+CH_2). For the complete NMR spectrum refer to Figure C.1 in Appendix C. The polymer number average molecular weight (M_n = 3333 g/mol) and weight average molecular weight (M_w = 3609) were determined by GPC. The degree of polymerisation expected for the synthesised polystyrene is approximately 33 repeat units based on the M_w. The length of a fully extended polystyrene molecule is estimated to be on average 10 nm in length. This value was obtained by calculating the length of the carbon bonds forming the backbone of a polystyrene molecule with 33 repeat units according to this formula:

$$polymer\ length = 2Nl \tag{3.1}$$

Where N represents the degree of polymerisation and l is the length of a C-C

bond, which is equal to 0.154 nm. The degree of polymerisation is multiplied by a factor of two since polystyrene monomers have two C-C bonds in their backbone.

3.2.4 Synthesis polystyrene with an azide end-group

The methodology for the synthesis of polystyrene with an azide end group (PS-N_3) was based on a method reported previously [66]. Briefly, polystyrene synthesised by ATRP (500 mg, 0.15 mmol, 1 eq.) and sodium azide (34 mg, 0.525 mmol, 3.5 eq.) were measured and transferred into a round bottom glass. Afterwards DMF (2 mL) was added and the reactions was left stirring for 12 h at 25 °C. Afterwards, methanol (12 mL) was added to precipitate the product. The product was vacuum filtered an washed thoroughly with methanol and deionised water (DI water). The products were vacuum dried and analysed by ^{1}H NMR (450 MHz, $CDCl_3$): δ 7.10-6.50 ppm (broad, aromatic H), 2.5-1.1 ppm (broad, CH+CH_2), 3.87 (singlet, CH_2-N_3). For the complete NMR spectrum refer to Figure C.2 in Appendix C.

3.2.5 Synthesis of polystyrene with an aldehyde end-group

The synthesis of polystyrene with an aldehyde end-group (PS-Al) consisted of mixing 4-hydroxybenzaldehyde (73 mg, 0.6 mmol, 4 eq.) and potassium carbonate (500mg, excess) and DMF (5 mL) in around bottom flask. After stirring the mixture for 1 h, PS synthesised by ATRP (500 mg, 0.15 mmol, 1 eq.) was added. The mixture was left stirring at 80 °C for 24 h. The mixture was filtered through alumina to remove the excess of potassium carbonate. The product was precipitated with methanol, filtered and washed with methanol. The product was characterised by by ^{1}H NMR (450MHz, $CDCl_3$): δ 7.10-6.50 ppm (broad, aromatic H), 2.5-1.1 ppm (broad, CH+CH_2), 9.7 ppm (s, CH=O), 7.55 ppm (broad, aromatic aldehyde). For the complete NMR spectrum refer to Figure C.3 in Appendix C.

3.2.6 Nitrene cycloaddition of PS-N_3 with MWCNTs

In a typical experiment MWCNTs (10 mg) (10nmMWCNTs or 50nmMWCNTs) and PS-N_3 (100 mg) were dissolved in DMF or o-DCB (10 mL). The mixture was sonicated for 1 hours and degassed by 3 cycles of vacuum/Ar. The mixture was then heated to 130 °C for 120 h. The mixture was cooled down to room temperature and diluted with solvent (100 mL). Afterwards the mixture was vacuum filtered and washed 3 times with solvent (10 ml). Afterwards, the solid filtrate was re-dispersed in solvent (10 ml) and ultrasonicated for 15 minutes, filtered and washed 3 times with solvent (10 ml). This procedure was repeated a total of three times. The liquid phase obtained after each of the washing steps was evaporated under vacuum and the residue was used for NMR analysis.

3.2.7 Prato reaction of PS-Al with MWCNTs

In a typical experiment MWCNTs (10 mg) (10nmMWCNTs or 50nmMWCNTs), (4-methoxybenzyl)glycine (38 mg) and PS-Al (100 mg) were dissolved in DMF (10 mL). The mixture was ultrasonicated for 1 hours and degassed by 3 cycles of vacuum/Ar. The mixture was then heated to 130 °C for 120 h. The mixture was cooled down to room temperature and diluted with solvent (100 mL). Afterwards the mixture was vacuum filtered and washed 3 times with DMF (10 ml). Afterwards, the solid filtrate was re-dispersed in DMF (10 ml) and ultrasonicated for 15 minutes, filtered and washed 3 times with DMF (10 ml). This procedure was repeated a total of three times. The liquid phase obtained after each of the washing steps was evaporated under vacuum and the residue was used for NMR analysis.

3.2.8 Non-covalent functionalisation of MWCNTs with polystyrene

In a typical procedure for the non-covalent polymer-functionalisation of MWCNTs with PS consisted in mixing 10nmMWCNTs (20 mg) and polystyrene (200 mg) (Mn = 3333 mol) in either acetone, DCM, toluene, DMF, o-DCB or NMP (20 mL). The mixture was ultrasonicated for 1 hour. Afterwards, the mixture was vacuum filtered and washed 3 times with solvent (10 mL). The solid filtrate was re-dispersed in solvent (20 mL) and ultrasonicated for 15 minutes, filtered and washed 3 times with solvent (10 mL). This procedure was repeated a total of three times. The liquid phase obtained after each of the washing steps was evaporated under vacuum and the residue was used for NMR analysis.

3.2.9 Synthesis of polystyrene with a pyrene end-group

In typical experiment for the synthesis of polystyrene with a pyrene end-group (PS-Py) PS-N_3 (200 mg, 0.0572 mmol, 1 eq.) were mixed with 1-ethynylpyrene (14 mg, 0.0572 mmol, 1 eq.), copper (I) bromide (4.9 mg, 0.0286 mmol, 0.5 eq.) were measured and transferred to a 25 mL round bottom flask. The flask was fitted with a septum and the solid powders were flushed in vacuum and purged with argon on a Schlenck line, the evacuation procedure was repeated three times. In a separate vial DMF (3 mL) and PMDETA (12 μL) were mixed and flushed in vacuum and purged with argon on a Schlenck line, the evacuation procedure was repeated three times. The liquid mixture was transferred to the round bottom flask using a Ar purged syringe and the mixture was left under Ar atmosphere stirring for 24 h. Afterwards, the mixture was diluted in THF (50 mL) and the mixture was filtered through a short neutral alumina column to remove the catalyst particles. The liquid phase was concentrated in a rotary evaporator. The product was diluted in THF (10 mL) and the polymer was precipitated by the addition of methanol. The polymer was

isolated by vacuum filtering and characterised by ^{1}H NMR. ^{1}H NMR (450 MHz, $CDCl_3$): δ 7.1-6.5 ppm (broad, benzene aromatic H), 4.5-4.2 (duplet, CH_2-Br) 2.5-1.1 ppm (broad, CH+CH2), 7.9-8.5 ppm (broad, pyrene aromatic H), 5.2 (broad, CH-N). For the complete NMR spectrum refer to Figure C.4 in Appendix C.

3.3 Results and discussion

3.3.1 Covalent functionalisation of MWCNTs

Covalent functionalisation of MWCNTs was attempted via Prato and nitrene cycloaddition reactions. For each reaction, the end groups of the polystyrene molecules were functionalised with chemical groups that could react with MWCNTs either by adding an azide group (PS-N_3) for a nitrene cycloaddition reaction or an aldehyde (PS-Al) for the Prato reaction. The functional polymers were characterized with NMR spectroscopy, which corroborated a successful attachment of the functional groups (see Section 3.2). Afterwards, the functionalised polystyrene was used for the functionalisation of 10nmMWCNTs with a 10 $\pm$ 2 nm diameter. The functionalisation for both reactions was performed using the same methodologies, solvents and temperatures. Parallel to each reaction a control experiment was performed where unreactive polystyrene molecules (PS-Br) was used instead of the functionalised polystyrene molecules. The purpose of the control was to compare the efficiency of a non-covalent method of functionalisation with the products of the covalent functionalisation reactions.

Each product from the reaction and control experiments was characterised by FTIR, XPS and Raman spectroscopy to confirm the presence of polystyrene in the sample. The FTIR spectra of the products, polystyrene and 10nmMWCNTs is presented in Figure 3.6. Two regions of the spectra are highlighted to confirm the presence of PS in the samples. The region found between 3150-2750 cm^{-1} that cor-

responds to the C-H bond stretch is highlighted in yellow, which can be clearly observed in the spectrum of PS as two asymmetric peaks. Similarly, the products of the functionalisation experiments all present one or two weak peaks in that same region. In contrast, the spectrum of 10nmMWCNTs present no signal in this region. The second region of interest is between 1500-600 cm^{-1} that is normally referred to as the fingerprint region of a molecule. For PS we can see several peaks of different intensities in this region. On the other hand, the products of the functionalisation experiments present lower transmittance in this region when compared to the 10nmMWCNT spectrum. Although the peaks are not strong enough to be fully resolved it can be inferred that the decrease of transmittance in this region is due to the presence of PS. These evidence suggests the presence of PS in the products of the functionalisation experiments but it does not provides evidence confirming that a direct bond has been made between the PS chains and the surface of the 10nmMWCNTs. Alternatively, the formation of C-N bonds could be used as evidence of functionalisation since both Prato and nitrene cycloaddition reactions involve the presence of C-N bonds(see Figure 3.4 and 3.5). However, the bands are found below 1400 cm^{-1}, which is not well resolved in the spectra of the products of the functionalisation experiments.

In addition, XPS analysis was used to support the FTIR characterisation. By analysing the C 1s and N 1s XPS spectrum we can obtain information regarding the difference of bonding environments observed for the surface atoms of the pristine 10nmMWNCTs and the products of the functionalisation reactions. The peak fitting of the C 1s section of the XPS spectrum was preformed according to a previous report by Blume *et al.* [118]. In Figure 3.7A an example of the peak fitting is presented, as it can be observed these methodologies enable the estimation of the contribution of the different bonding environments observed for the carbon atoms in the sample. We would expect to observe an increase of the sp^3 hybridised C atoms in the products of the functionalisation reaction in comparison to 10nmMWCNTs

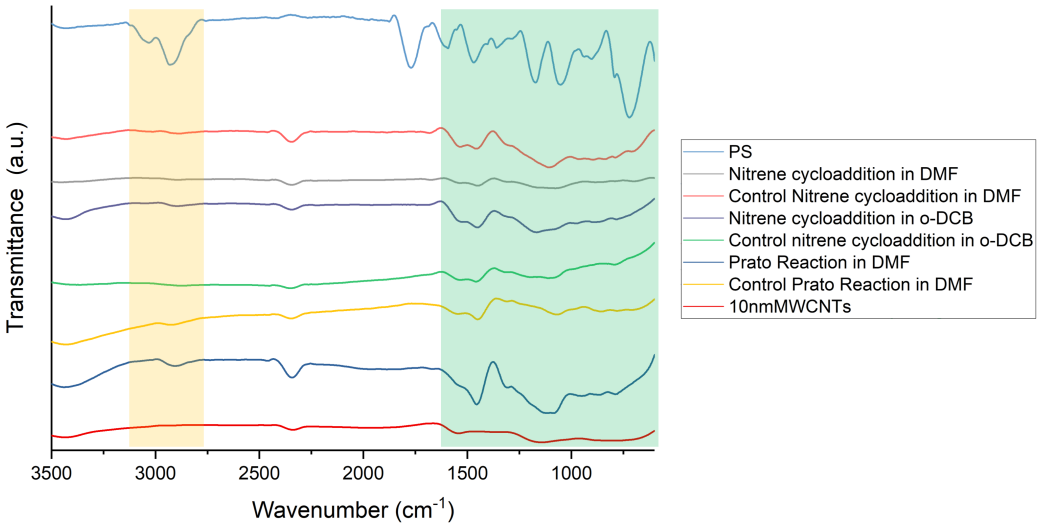


Figure 3.6: *FTIR spectra of polystyrene, functionalisation products and 10nmMWNCTs. Two sections of the spectra are highlighted: in yellow C-H stretch and in green the fingerprint region of polystyrene.The C-H stretch and PS fingerprint region is observed for PS, control and reactions of the functionalisation experiments; while is not observed in the 10nmMWCNTs spectrum.*

due to the sp^3 carbon atoms present in the polystyrene back chain. On the other hand, the fitting of the N 1s peak was performed according a previous report by Zorn *et al* [119] that used the N 1s section of the XPS spectrum to characterise the products of a nitrene cycloaddition reaction with graphene. In this study they attributed two peaks relevant to the products of their reactions in the N 1s region. The first one around 400 eV which was attributed to an amine N-H environment and the second around 402 eV attributed to the N-C bonding environment as displayed in Figure 3.7. However, it is important to note that the latter peak was still observed in samples where the reaction procedure was performed in the absence of graphene although with lower intensity.

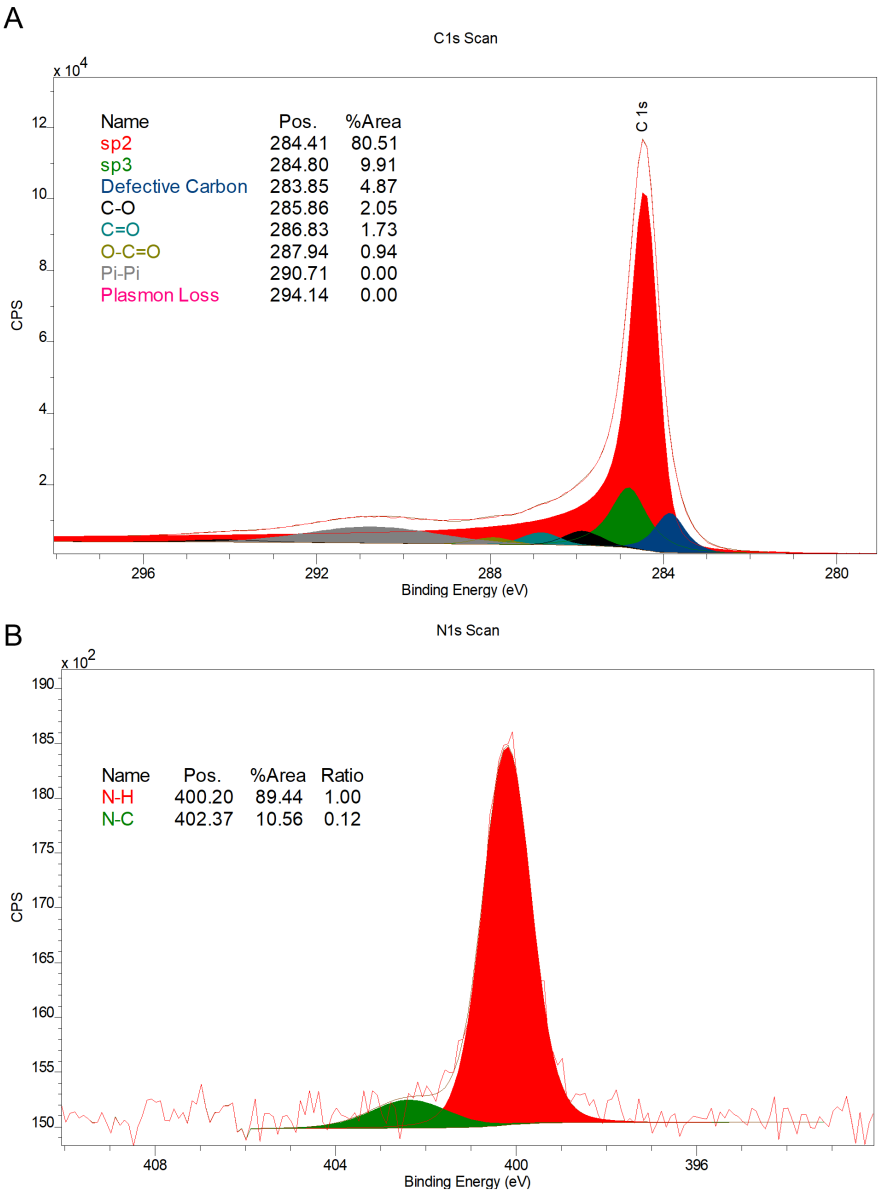


Figure 3.7: *A) XPS C 1s spectrum of 10nmMWCNTs B) XPS N 1s of 10nmMWNCTs functionalised with PS through the nitrene cycloaddition reaction in o-DCB.*

In Table 3.1 the summary of the XPS analysis of all the samples is presented. The first observation to note is that the contribution to the C 1s peak of carbon atoms with an sp^3 hybridisation increased for all samples after the functionalisation experiments. This data substantiates the evidence provided by FTIR characterisation that polystyrene chains are indeed functionalising the surface of the 10nmMWCNTs. Second, it was found that the presence of N atoms in the samples only occurred in

Table 3.1: *Summary of the characterisation of PS functionalised 10nmMWCNTs through covalent methodologies.*

Sample	PS wt% content [%]	C content [%]	sp^3 C content [%]	O content [%]	N content [%]	N-C/N-H ratio
10nmMWCNTs	-	98.39	9.91	1.61	0	-
Nitrene cycloaddition reaction in o-DCB	6.89	94.84	18.70	4.13	1.02	0.12
Nitrene cycloaddition control in o-DCB	8.82	98.10	15.07	1.90	0	-
Nitrene cycloaddition reaction in DMF	13.03	98.67	21.36	1.02	0.31	0.24
Nitrene cycloaddition control in DMF	15.40	99.14	21.52	0.86	0	-
Prato reaction in DMF	12.08	97.01	17.25	2.54	0.45	0.10
Prato control in DMF	12.19	96.05	17.00	3.95	0	-

the experiments where a reaction was performed. This is consistent with the fact that the reactants for both Prato and the nitrene cycloaddition reaction present nitrogen atoms in their structure. On the other hand, the control experiments presented no nitrogen peaks in their individual XPS spectra. When the N 1s peak of each reaction experiment was fitted with the N-H and N-C contributions, the N-H peak was found to be ten to four times larger. This suggests that the reactions are not occurring very efficiently and little to no formation of N-C bonds is observed. As mentioned previously in the report of Zorn *et al.* [119] the presence of the N-C peak was observed even when the decomposition of the azide was performed without graphene. Moreover, Zorn *et al.* reported a ratio of N-H/N-C between one and two, which is smaller than what observed in this experiments [119]. Thus, further evidence is required to assert that a direct bond between the 10nmMWCNTs and polystyrene is being formed.

The products of the reactions and the control experiments were analysed by Raman spectroscopy. The Raman spectrum of the functionalisation experiments and the pristine 10nmMWCNTs are presented in Figure 3.8, it can be observed that the spectra show no visible change between the pristine 10nmMWCNTs, control and reaction experiments. The values of the D/G ratios of all samples were calculated to be 1.4, suggesting that defects in the crystalline structure of the 10nmMWCNTs are not being introduced during the functionalisation experiments.

The data obtained through FTIR, XPS and Raman spectroscopy gave inconclusive evidence for the formation of covalent bonds between the polymer chains and the 10nmMWNCTs. For this reason TGA was performed on the products of the reactions and control experiments to evaluate the amount of polymer present in the samples after the functionalisation procedure. TGA was performed under a N_2 atmosphere to selectively decompose the polystyrene molecules present in the sample since polystyrene presents a decomposition temperature of 415 °C under N_2 atmosphere while the 10nmMWCNTs remain intact. As it can be observed in Fig-

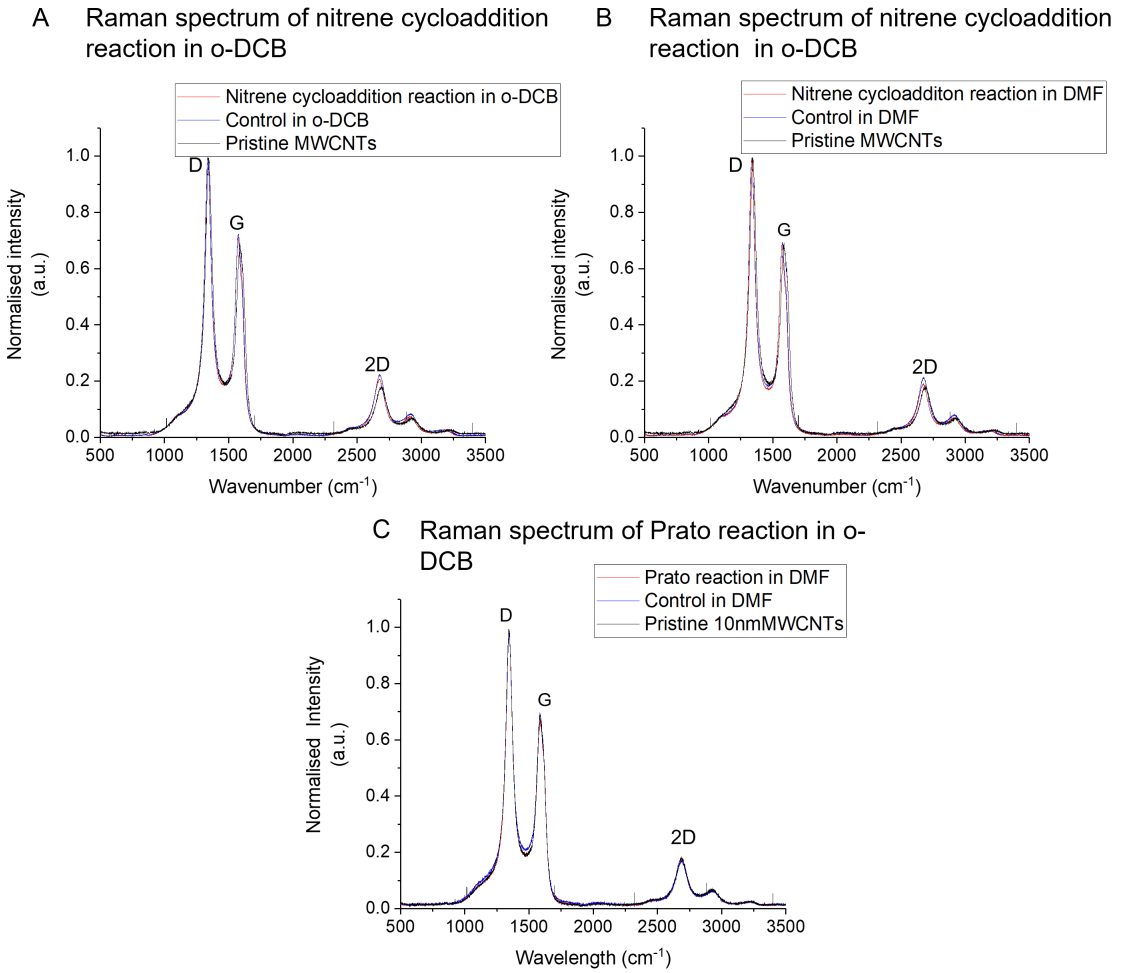


Figure 3.8: *Raman spectra of (A) experiments related to nitrene cycloaddition of PS-N_3 with 10nmMWCNTs in o-DCB. (B) Experiments related to nitrene cycloaddition of PS-N_3 with 10nmMWCNTs in DMF. (C) Experiments related to the Prato reaction of PS-Al with 10nmMWCNTs in DMF. The spectra of the reaction and control experiments present the same D/G ratio as the pristine 10nmMWCNTs for all cases.*

ure 3.9A, the amount of polystyrene in the sample can be obtained by measuring the weightloss observed in the TGA curve and thus the value of this weightloss was used to determine the degree of polystyrene functionalisation by weight percentage (wt%) in the sample. If there are significant differences in the composition between the control and the reaction experiments then further conclusions can be done to assess if the interactions between the 10nmMWCNTs and the polystyrene molecules occur through the formation of covalent bonds or through non-covalent interactions.

In Figure 3.9B the degree of polystyrene functionalisation for each experiment is

displayed, it can be observed that the amount of polystyrene present in the sample was similar for both the Prato and nitrene cycloaddition reactions. This observation suggests that the efficiency of the reaction between the two different methodologies is comparable. This is an unexpected result since it would be expected that different reactions would present different yields. Specially considering that the nitrene cycloaddition reaction has been established as a more reactive functionalisation methodology for SWCNTs in comparison to the Prato reaction [120]. The observation of a comparable degree of functionalisation between both reactions suggests that a similar mechanism of interaction is causing the polystyrene functionalisation of the MWCNTs, which could be attributed to non-covalent interactions between the polystyrene chains and the MWCNTs.

In addition, when the composition of polystyrene from the control experiments is compared to the composition observed for the reaction products, a very similar result was observed for both Prato and nitrene cycloaddition reaction. The observation that the unreactive PS-Br molecules are functionalising the MWCNTs at a similar degree in comparison to PS-N_3 and PS-Al, substantiates the hypothesis that

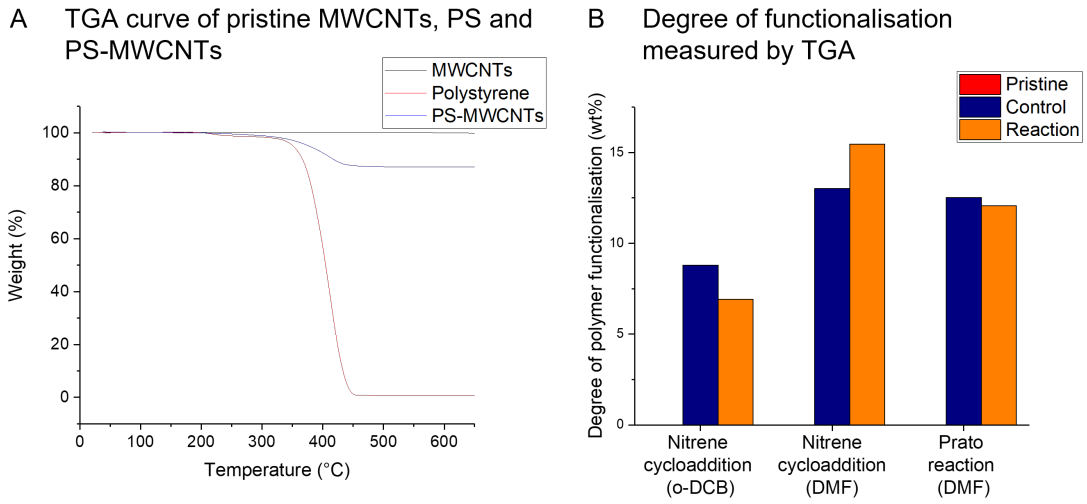


Figure 3.9: *(A) Example of TGA curves used to calculate the degree of polymer functionalisation of PS functionalised 10nmMWCNTs. (B) Percentage of polystyrene present in the sample for Prato and nitrene cycloaddition reactions. Comparable degrees of functionalisation were observed for both reactions when DMF was used. The degree of functionalisation of the nitrene cycloaddition varied when the solvent changed from DMF to o-DCB.*

the interactions between the polystyrene and 10nmMWCNTs do not occur via the formation of covalent bonds but through non-covalent interactions. For the case of the nitrene cycloaddition in DMF the reaction product presented slightly higher polystyrene weight percentage in comparison to the control product. The opposite behaviour was observed for the Prato reaction in DMF. Is important to note that these sets of experiments were only performed once, which makes difficult to understand why there are small differences observed for the functionalisation between reaction and control experiments. It would be expected that if the experiments were repeated in triplicate there would be a range of polystyrene composition observed in the products of the experiments due to random variation inherit to experimental procedures and measurements. This variations could explain the small differences in polystyrene composition observed for reaction and control experiments.

The effect that the solvent media has in the degree of polystyrene functionalisation of MWCNTs was studied to further explore parameters that might have an impact in the reactions. Thus, the solvent was changed from o-DCB to DMF for the nitrene cycloaddition reaction. The polystyrene composition in the experiments performed in o-DCB was considerably lower in comparison to DMF (Figure 3.9B). This results demonstrated that changing the solvent media had a more considerable impact than the reaction procedure used during the functionalisation methodology. Similarly to the previous experiments, the degree of functionalisation observed for the control experiment was comparable to the amount of polystyrene observed in the reaction product. Solvents are known to have an important impact in the performance of organic reactions, but observing similar behaviour for both reaction and control is unexpected. This result supports the claim that the forces that dictate the interactions between polystyrene and MWNCTs in both the control and reaction experiments are the same. Thus, it can be concluded that the interactions are not of a covalent nature and more likely due to non-covalent forces.

A possible explanation to the similar degrees of functionalisation observed for

the control and the functionalisation experiments is that the degree of covalent and non-covalent functionalisation are similar using 10nmMWCNTs with their specific diameter. To understand if the reactivity of the MWCNTs can have an influence on the amount of polystyrene observed for the control and functionalisation experiments, the functionalisation of MWCNTs synthesised through aerosol assisted chemical vapour deposition (50nmMWCNTs) that present a larger diameter of 53 $\pm$25 nm was performed. The reactivity of CNTs is strongly dependent on their diameters, small diameter tubes present a higher strain in the sp^2 carbon lattice making them more reactive [45]. Thus, observing a smaller degree of polystyrene functionalisation through covalent methods in larger diameter MWCNTs could provide evidence for a different mechanism of functionalisation between the control and reaction experiments. However, the characterisation presented in Figure 3.10 for 50nmMWCNTs shows a similar behaviour to what it was observed for 10nmMWNCTs. The control and reaction experiment resulted in similar degrees of polymer composition and D/G ratio, and the same conclusion can be made from the polystyrene composition of the samples obtained through TGA characterisation. The fact that increasing the diameter of the MWCNTs does not decrease the amount of polystyrene found in the reaction experiments in comparison to the controls, strongly suggests that the functionalisation occurs through non-covalent interactions between the MWCNTs and polystyrene molecules. In addition, it offers evidence against the hypothesis that the degree of covalent and non-covalent functionalisation are similar for 10nmMWCNTs since it would be unlikely that the same behaviour should be observed for the 50nmMWCNTs.

Due to the challenging nature of the characterisation of funcitonalised MWCNTs is difficult to assert without doubt if there are direct chemical links between the polystyrene molecules and MWCNTs for the methodologies where covalent functionalisation was attempted. However, the previous results demonstrated that for the two samples of MWCNTs used in this study the efficiency of non-covalent func-

tionalisation with polystyrene is comparable to what was observed for the covalent approaches. In addition, the characterisation of the products in the reaction and control experiments strongly suggest that is more likely that non-covalent forces are driving the functionalisation for all the methods explored in this experiments. Since non-covalent methods are simpler for the synthesis of polystyrene functionalised MWCNTs than covalent methods, I decided to further explore the parameters that could be used to increase the efficiency of this type of functionalisation.

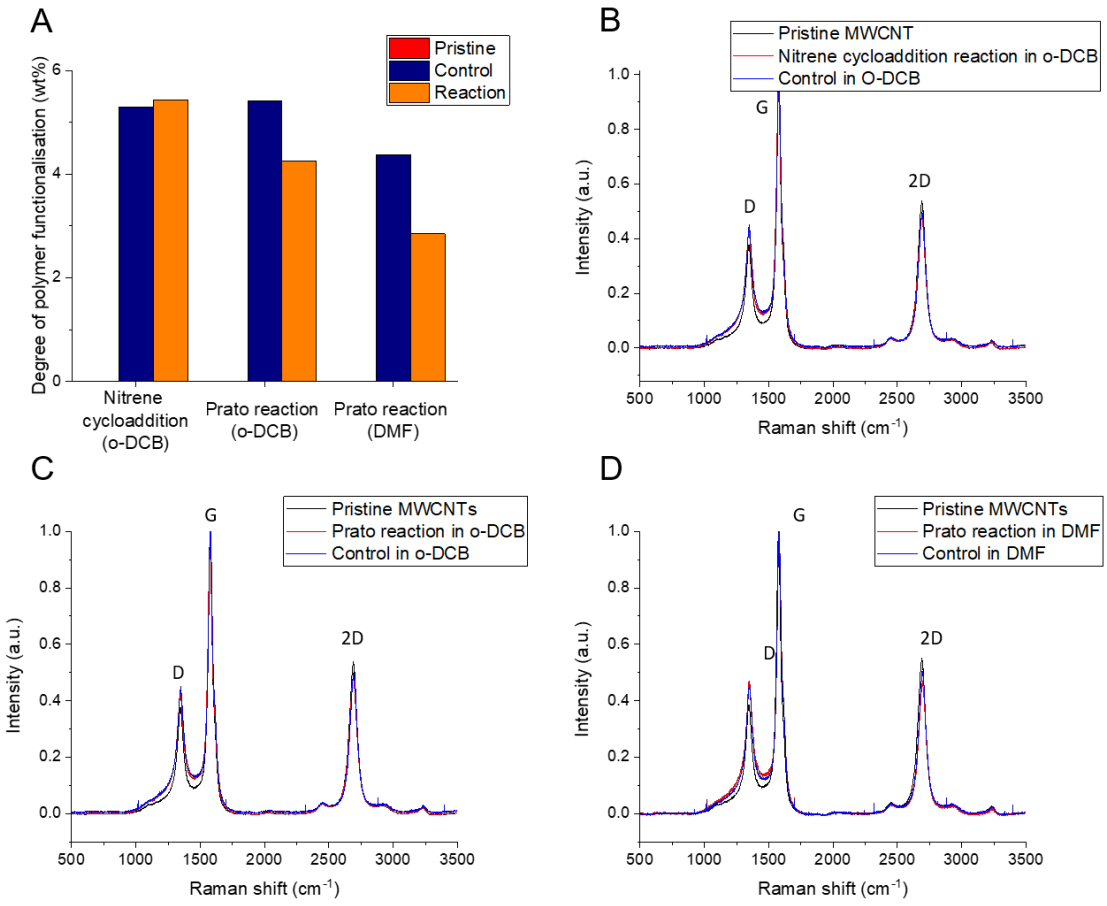


Figure 3.10: *Characterisation of the functionalisation experiments of 50nmMWCNTs. A) Summary of the TGA characterisation of the PS-50nmMWCNTs. B-D) Raman spectra of pristine AACVD-MWCNTs, control experiments, B) PS-Nitrene-50nmMWCNTs in o-DCB, C) PS-Prato-50nmMWCNTs in o-DCB and D)PS-Prato-50nmMWCNTs in DMF.*

3.3.2 Non-covalent functionalisation of MWCNTs

To further investigate the role that the solvent has on the degree of non-covalent functionalisation of MWCNTs with polystyrene, a set of non-covalent functionalisation experiments was performed using PS-Br and 10nmMWCNTs in six different solvent media. The six selected solvents covered the whole range between good solvents to bad solvents for both for MWCNTs dispersions and polystyrene solutions (Table 3.2). Here I use the term good solvent for MWCNTs as solvents that are known to create dispersions with high concentration and long stability over time. While bad solvents for MWCNTs are those where the formation of long term stable dispersions have not been reported. The term good solvent for polymer solutions refers to solvents where the solvent-polymer interaction is more favourable than the monomer-monomer interaction. The term bad solvent for polymer solutions on the other hand refers to solvents where monomer-monomer interactions are more favourable than the solvent-polymer interaction. The products were analysed by TGA, XPS and FTIR to characterise the presence of polystyrene for each functionalisation. In addition, the washes performed during the functionalisation methodology (see Section 3.2.8) were recovered and analysed by NMR to evaluate if after the washing procedures there was still polystyrene being removed from the sample.

Figure 3.11 presents the NMR spectrum from the filtrates after each step of washing through the functionalisation procedure where acetone was used as the solvent medium. It can be observed that the signal corresponding to the aromatic hydrogen atoms of the polystyrene molecule decreases subsequently after each washing procedure until it is not observable either in the third or fourth wash. This behaviour was observed for all the functionalisation experiments performed during this study (see Figure C.5 in Appendix C). Taking into account that polystyrene is highly soluble in all the solvents used during the study we can be confident that the washing procedure

is removing all the free polystyrene from the sample. Moreover, we can be certain that the remaining polymer molecules are bound to the surface of 10nmMWCNTs by non-covalent interactions displaying a large degree of irreversibility.

The summary of the TGA analysis of the samples is presented in Table 3.2. The results show that the solvent medium used during the functionalisation had a strong impact on the amount of polystyrene observed in the sample, where each solvent presented a characteristic degree of functionalisation. The impact of the solvent was considerable to the extent that a three-fold increase in the polymer composition was observed when the solvent medium was changed from o-DCB to acetone. Furthermore, the three solvents in which the 10nmMWCNTs presented the lowest degree of polymer functionalisation (DMF, NMP, o-DCB) have been widely regarded as good solvents for the dispersion of CNTs [121, 122]. The fact that

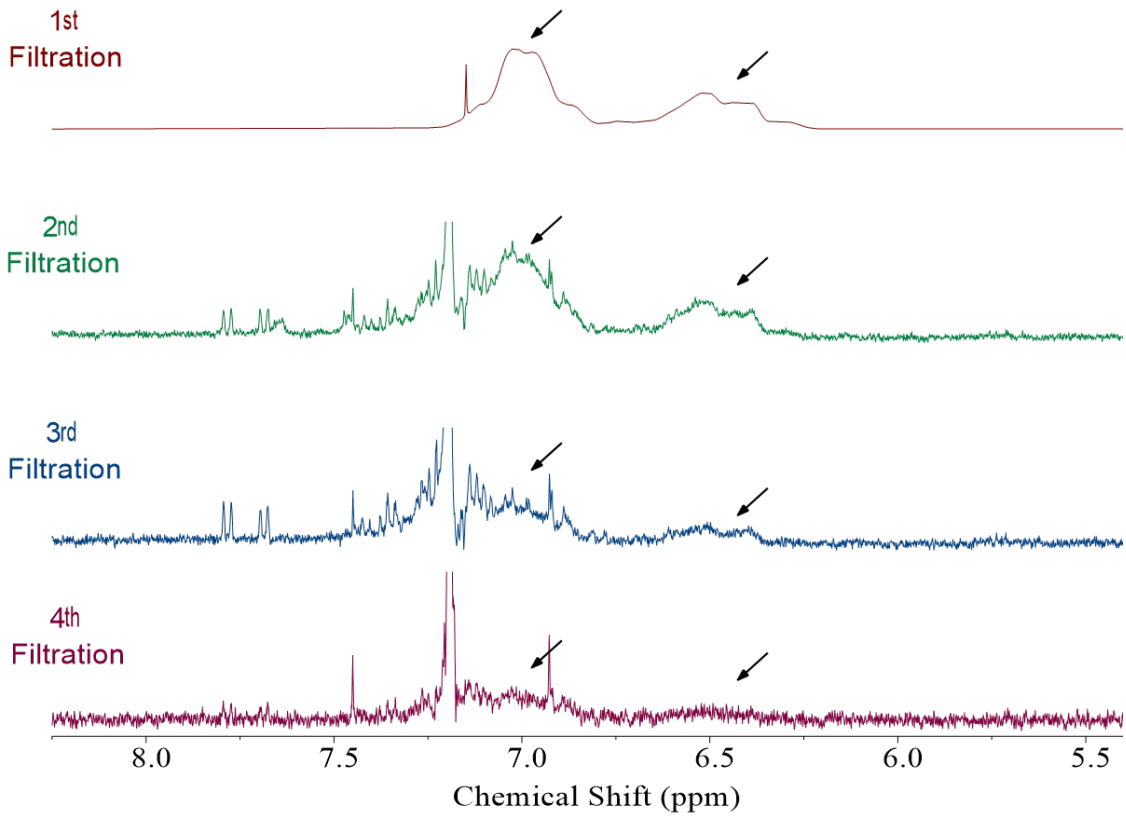


Figure 3.11: *NMR spectra of the filtrates after each washing step of the functionalisation procedure. This spectrum was taken from a sample where acetone was used as the solvent. The arrows point to the position of polystyrene aromatic protons. No polymer can be clearly observed after the fourth redispersion.*

solvents known to be good for the dispersion of CNTs presented the lowest degree of polymer functionalisation is consistent with O'Connell *et al.* [56] hypothesis, since the thermodynamic driving force for the polymer functionalisation would depend on the interactions between the MWCNTs and the solvents. According with this hypothesis as the interactions between a solvent and a CNT are more favourable the smaller degree of functionalisation would be expected.

XPS and FTIR analysis was used to characterise the presence of polystyrene in the sample. Figure 3.12 presents the FTIR spectrum of the different PS functionalised 10nmMWCNTs samples and pristine 10nmMWCNTs. The presence of hydrocarbon chains in the functionalised samples is confirmed by the observation of the C-H stretching modes around 2971 cm^{-1} and 2863 cm^{-1} that do not appear in the pristine 10nmMWCNTs spectrum as highlighted in yellow in Figure 3.12. In addition, it can be observed that the spectrum of the PS functionalised 10nmMWCNTs present decreased transmittance in the fingerprint region of PS. XPS was used to further confirm the claim of the presence of polystyrene molecules in the functionalised 10nmMWCNTs samples. The C 1s peak was deconvoluted to obtain information of the bonding environment of the carbon atoms present in the PS functionalised 10nmMWCNTs samples similarly to what was presented in Section 3.3.1 (see Figure C.7 in Appendix C for the XPS spectrum of samples synthesised in each solvent). The C1s peak of the pristine 10nmMWCNTs presented a 9.9% sp^3

Table 3.2: *Summary of the characterisation of PS functionalised MWCNTs through non-covalent interactions.*

Solvent	PS solubility	MWCNT solubility	PS weight content [%]	XPS sp^3 C content [%]
o-DCB	Good [123]	Good [121]	5.3 ± 1.0	22.4
NMP	Good [123]	Good [121]	8.6 ± 2.9	24.0
DMF	Bad [124]	Good [121]	10.0 ± 0.2	33.1
DCM	Good [123]	Bad [15]	11.1 ± 1.4	33.9
Toluene	Good [123]	Bad [121]	11.7 ± 1.2	34.05
Acetone	Bad [123]	Bad [121]	15.9 ± 0.5	39.0

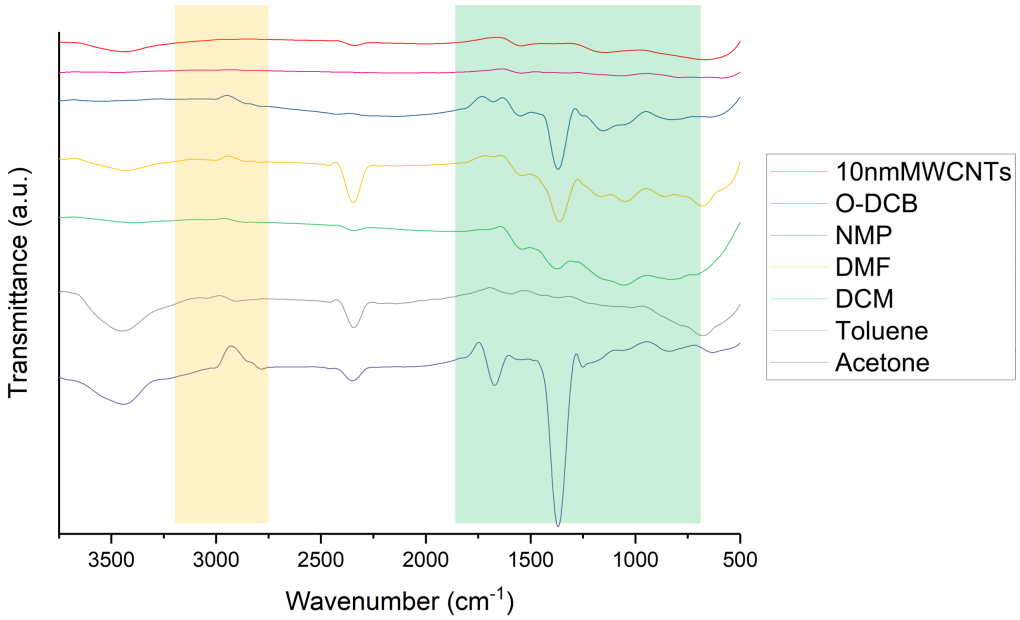


Figure 3.12: *Plot of FTIR spectrum of non-covalent PS functionalised 10nmMWCNTs, the peaks corresponding to the stretching of the CH bond is observed in the window between 2800-3000 cm^{cm-1}. The intensity of the peak increases with the increase in the degree of functionalisation while the pristine MWCNTs do not present a peak.*

carbon hybridization. In contrast, all samples of PS functionalised 10nmMWCNTs presented a higher percentage of sp^3 carbon bonding as it can be observed in in Table 3.2, where the percentage of sp^3 carbon in the C 1s peak of the XPS spectra of all the samples is presented. These results show that the contribution of sp^3 carbon to PS functionalised 10nmMWCNTs is higher in the samples prepared in solvents where a higher degree of polymer functionalisation was observed. This observation confirms the claim that the weightloss observed in the TGA is in fact the decomposition of the polystyrene in the sample.

In addition, the results presented in Table 3.2 support the hypothesis that the interactions between the MWCNTs and the solvent have a major impact in the degree of functionalisation than the interactions between the polymer and the solvent. If the latter was true, solvents that present favourable interactions with polystyrene (*i.e.* good solvents) such as o-DCB, toluene and DCM would be expected to decrease

the degree of polymer functionalisation of the MWCNTs due to the competition with the solubilisation of the polymer chains. This effect is only observed for o-DCB, furthermore DMF is the third solvent with the lowest degree of functionalisation and is considered a poor solvent for polystyrene. The contradictory results between what would be expected from good solvents and bad solvents exemplified in this study supports the hypothesis that the interactions between the MWCNTs and the solvent have a major impact in the degree of functionalisation than the interactions between the polymer and the solvent.

The solvent dependent functionalisation of the 10nmMWNCTs with polystyrene is consistent with the polymer wrapping mechanism proposed by O'Connel *et al.* [56]. However, it is not expected that the polystyrene molecules in our system will be wrapping around the surface of the 10nmMWCNTs. This claim is justified when we consider that the degree of polymerisation of the polystyrene molecules used in this study was approximately 33 repeat units, which correlates to a 10 nm length of a fully stretched polystyrene chain. This length is a third shorter than the 31 nm circumference of the 10nmMWCNTs, thus is not geometrically possible to have polystyrene chains wrapping around the surface of the 10nmMWCNTs. In addition, we are not considering the impact that the solvent might have in the final conformation of the polymer or if the polymer might be found as a coiled or random walk on the surface of the 10nmMWCNTs, which would lead to a head to tail polymer length significantly smaller than our 10 nm estimation. For this reason the conformation of the polystyrene chains would be more accurately described as polystyrene molecules coating sections of the surface of the 10nmMWCNTs. Previous research has proposed that polymer coating and polymer wrapping should be considered analogous phenomenon that is universal for any polymer system mixed with CNTs in solution, which is supported by my experimental results [92].

3.3.3 Effect of other parameters in the non-covalent functionalisation of MWCNTs

The degree of polymer functionalisation of MWCNTs could be affected by the polymer concentration. If the functionalisation of MWCNTs is thought of as a chemical equilibrium, a higher concentration of free polymer in solution would shift the equilibrium causing an increase in the number of polymer chains coating the MWCNTs and thus increasing the degree of functionalisation. On the other hand, the increase in the concentration of polymer could also decrease the degree of polymer functionalisation of the MWCNTs by not allowing the MWCNTs to form a stable dispersion and thus decreasing the surface of MWCNTs exposed to polymer chains. This is a well-accepted behaviour of colloidal dispersions stabilised by polymer chains that is normally referred to as destabilization through depletion forces. The destabilization of colloidal dispersions via depletion forces occurs due to the difference of osmotic pressure between two closely spaced particles and the bulk of the solution. When the free polymer concentration is high enough to overcome the repulsion forces between particles the colloids aggregate. Previous reports have demonstrated that the dispersion of MWCNTs functionalised via non-covalent interactions with polymers can be destabilised by depletion forces [64].

To understand the role that the polymer concentration has in the polystyrene functionalisation of MWCNTs and to study if there are depletion forces in our experiments, I varied the ratio of the mass of 10nmMWCNTs to polymer (10nmMWCNTs:polymer) used for the non-covalent functionalisation of 10nmMWNCTs with polystyrene using acetone as the solvent medium. Based on the results presented in Section 3.3.2 the following 10nmMWCNTs to polystyrene ratios were used: 1:10, 1:1 and 1:0.33. This ratios are all in excess in comparison to the weight ratio of 10nmMWCNTs to polymer of 1:0.2 observed in the TGA characterisation of polystyrene functionalised MWCNTs in acetone reported in Section 3.3.2, which

could be considered as a the maximum PS composition that could be observed since the experiment was performed in a large polystyrene excess in comparison to 10nmMWCNTs. To characterise the difference in the degree of functionalisation TGA analysis of the samples was performed. Figure 3.13 demonstrates that the degree of polymer functionalisation is dependent on the starting concentration of the polymer and as the polymer concentration increases the degree of functionalisation increases. This observation is in agreement with the proposal that the functionalisation of MWCNTs is part of a chemical equilibrium where the higher concentration of polymer shifts the equilibrium towards polymer coating the surface of the MWCNTs. In addition, it demonstrates that the experiments were not performed in the depletion regime since it would be expected that the degree of functionalisation would decrease with higher polymer concentration.

Previous literature have demonstrated that the degree of functionalisation of MWCNTs can be optimised by the incorporation of chemical functional groups that

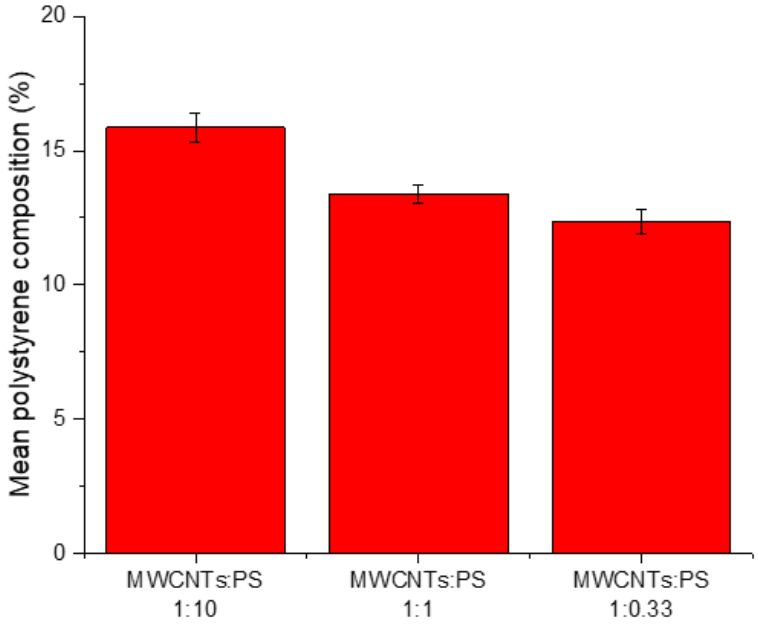


Figure 3.13: *Polystyrene composition of functionalised MWCNTs at different MWCNTs:PS ratios.*

can interact through π-π interactions such as pyrene groups [103, 102]. The addition of pyrene end groups to polymers have also been reported to improve the dispersions of polymer stabilised CNTs. It is hypothesised that the interaction of pyrene end groups with the surface of CNTs is favoured in comparison to the polymer wrapping by the whole polystyrene chain, thus allowing the polymer chains to extend out of the CNTs and enhancing the steric stabilization of the CNT in dispersion [103]. Following this train of thought, the ability of pyrene groups to improve the stability of CNT dispersions could also be used to enhance the degree of functionalisation of the MWCNTs with polymers. Moreover, the addition of pyrene groups into the polymer structure could enhance the interactions between the polymers chains and the MWCNTs. This in turn could potentially provide a means of functionalisation that is driven mainly by the pyrene-CNT interactions and thus would present less dependency on the solvent media.

For this purpose, polystyrene molecules with pyrene end-groups were synthesised (PS-Py). The synthesis of PS-Py is represented in Figure 3.14, the first step involved the substitution of the pendant Br group with an azide, followed by a second step where an azide click reaction with 1-ethynyl pyrene was performed to obtain a polystyrene chain with a pyrene end group.The products were characterised

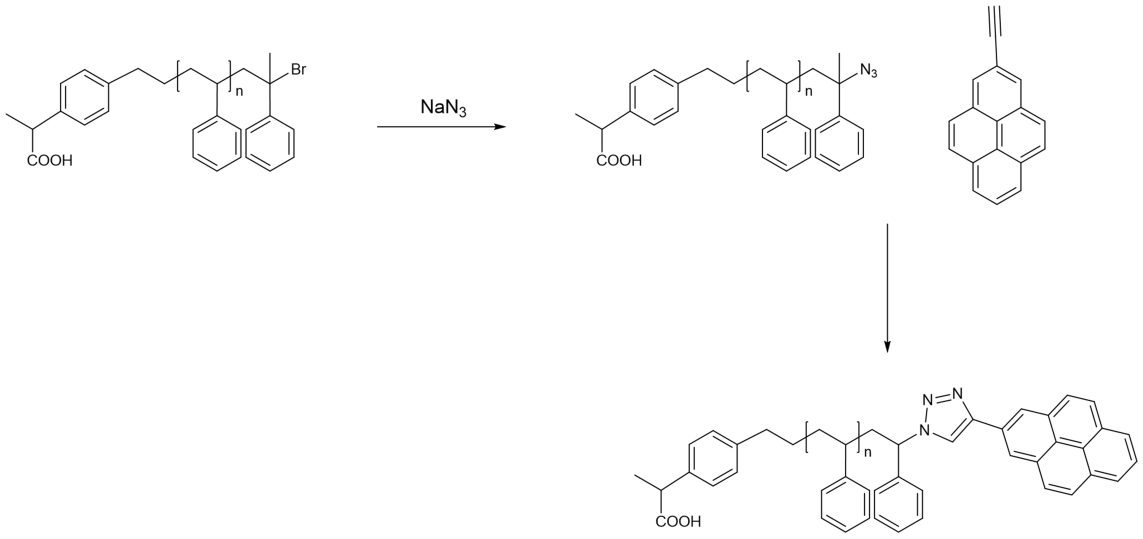


Figure 3.14: *Synthesis route for PS-Py.*

by mass spectrometry and NMR, corroborating the success of the reaction. Afterwards, non-covalent functionalisation of MWCNTs with PS-Py was carried out in acetone and DCM at a 1:1 polymer to MWCNT weight ratio. The products were then analysed by TGA to observe if there was a improvement of the degree of functionalisation. Figure 3.15 shows that incorporating a pyrene functionality increases the degree of polymer functionalisation by 2.6% in acetone. Thus the incorporation of a pyrene group increases the degree of functionalisation by a small margin. When the functionalisation experiment was performed in DCM, a decrease in the degree of functionalisation of 2.4% was observed. In comparison, the decrease of polymer functionalisation with PS-Br between acetone and DCM was 4.9%. This result demonstrates that the solvent media still has an effect on the degree of functionalisation of MWCNT with PS-Py molecules. However, the strength of the effect is smaller in comparison to PS-Br, which suggests that the incorporation of pyrene end groups has a favourable effect in the interactions of polymer chains with the surface of CNTs.

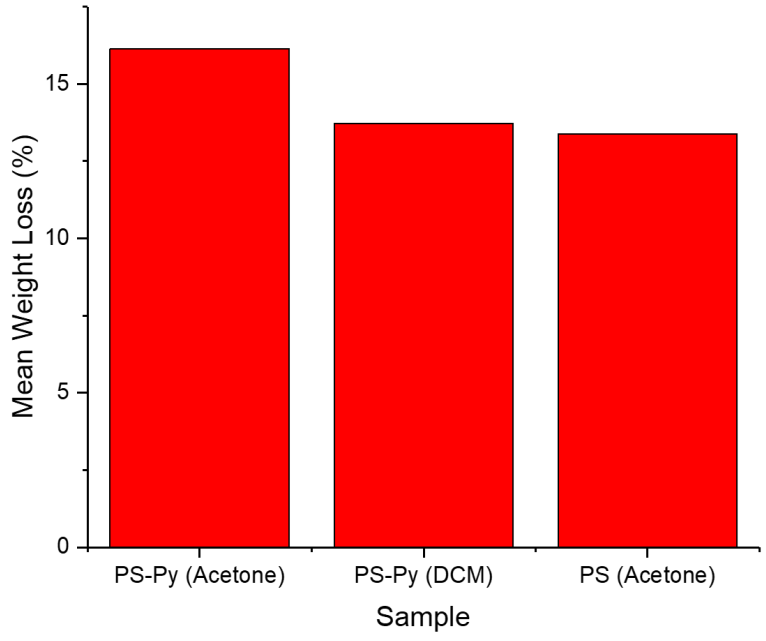


Figure 3.15: *Polystyrene composition of functionalised MWCNTs with PS-Py.*

3.4 Conclusions

The aim of this chapter was to explore the polymer functionalisation of MWCNTs via covalent and non-covalent methodologies. In this context, two different covalent functionalisation reactions were tested using functionalised polystyrene molecules, and were compared to control experiments with polymers that would not react covalently with the MWCNTs surface. The products of the functionalisation experiments were characterised by several spectroscopic methods that confirmed the incorporation of polystyrene in the MWCNT samples but provided inconclusive information regarding the formation of direct chemical bonds between the polystyrene chains and the surface of the MWCNTs. An important contribution of this study was the demonstration of the usefulness of performing control experiments parallel to the reactions since the TGA analysis of the reaction and control experiments were found to be the most compelling evidence to understand the nature of the interactions between the polystyrene chains and the surface of MWCNTs.

The TGA data showed that the degree of functionalisation of the products of the Prato and nitrene cycloaddition reactions were comparable. Moreover, the reactions and control experiments presented a similar degree of functionalisation suggesting that the polymer-MWCNTs interactions arose through non-covalent forces. When the solvent media used during the functionalisation methodology was changed there was a significant difference in the degree of functionalisation indicating that the solvent played a crucial role in the interactions between PS and MWCNTs. This observation was consistent with the hypothesis proposed by O'Connel *et al.* for the mechanism of polymer wrapping of CNTs through non-covalent forces. This observation further supported the claim that non-covalent interactions were likely to be the major forces observed during the functionalisation procedures and there was no evidence for covalent functionalisation in the products from the Prato and nitrene cycloaddition procedures.

In line with these observations I concluded that covalent and non-covalent approaches were just as efficient for the functionalisation with polystyrene of the MWCNTs samples used in this study. I strongly believe that even when covalent functionalisation is attempted, non-covalent forces between the polymer chains and MWCNTs are the main interaction taking place during the functionalisation. It is important to remark that this conclusion might change for different samples of CNTs since their reactivity is closely linked to their diameter. Nonetheless, the results reported in this Chapter highlight that non-covalent forces between CNTs and polymers should be taken in consideration when direct "graft to" functionalisation methodologies are used. In addition, for these MWCNTs samples I conclude that non-covalent functionalisation is the best path to exploit polymer-MWCNT interactions for the bottom-up synthesis of nanostructures.

Further study supported the primary role of solvents in the non-covalent functionalisation of MWCNTs with polymers. Non-covalent functionalisation of MWCNTs was performed with six different solvents that are known to have favourable and unfavourable interactions with polystyrene and MWCNTS. The TGA and XPS characterisation demonstrated that the solvent-MWCNTs interactions strongly influence the degree of non-covalent functionalisation with polystyrene. In addition, the degree of non-covalent functionalisation increased a 3-fold from functionalisations done in o-DCB to acetone, thus demonstrating through quantitative characterisation a methodology to control the degree of PS functionalisation of MWCNTs. This study highlights for the first time the importance of the solvent medium to maximise polymer-MWCNT interactions, I believe that choosing the appropriate solvent can have important implications for the rational synthesis of nanostructures based on MWCNTs.

Finally, the study of other parameters such as polymer concentration and the use of pyrene functionalised polymers showed a small impact in the optimization of the functionalisation procedure. The variation of polymer concentration suggested

that the non-covalent functionalisation results from a quasi irreversible equilibrium between the free polymer in solution and the polymer coating the surface of the MWCNTs. This result highlights the robustness of the polymer-MWCNT interaction through non-covalent forces, which can provide adequate stability for the synthesis of nanostructures. Finally, adding pyrene end groups demonstrated a small increase in the degree of functionalisation, which still displayed a dependency in the solvent used during the functionalisation. However, I consider that the small increase in the degree of functionalisation is not large enough to invest the effort of synthesising the PS-Py molecule to improve the degree of functionalisation of MWCNTs.

These basic studies have contributed to expand our understanding of polymer functionalisation of MWCNTs. In particular, we demonstrated that the degree of PS non-covalent functionalisation of MWCNTs is highly sensitive to the solvent media. Understanding how the degree of polymer functionalisation of MWCNTs is affected by the interactions between the solvent molecules and MWCNTs could potentially be used to predict the effectiveness of non-covalent functionalisation of MWCNTs in different solvents, which would have important implications for the design of nanostructures based on MWCNT-polymer interactions. The following Chapter focuses on the study of the surface interactions between solvents and MWCNTs, where we propose the application of the Solubility Parameter theory as a qualitative predictive model for the non-covalent functionalisation of MWCNTs with polymers in different solvent media.

Chapter 4

Solubility parameter theories as predictive models of polystyrene functionalisation of MWCNTs in different solvent media

4.1 Intoduction

In Chapter 3 a study of the functionalisation of MWCNTs with polystyrene via covalent and non-covalent methodologies was presented. Based on the results of this study I concluded that non-covalent interactions were the most efficient of the methods used during the study for the functionalisation of MWCNTs with polystyrene. In addition, it was demonstrated that the solvent medium had a considerable impact on the degree of non-covalent functionalisation of MWCNTs with polystyrene. Exploiting the impact of the solvent medium on the degree of polymer functionalisation could be useful for the synthesis of nanostructures based on polymer-MWCNTs interactions. However, predictive models are required to select the appropriate me-

dia that maximises the polymer-MWCNT interactions. In this Chapter I propose the application of surface energy based solubility parameter theories as models to predict the degree of polystyrene functionalisation of MWCNTs in different solvents, making this study the first time that a predictive model for the non-covalent functionalisation of MWCNTs with polymers has been proposed.

I decided to apply the surface energy based solubility parameter theories for the prediction of the degree of polystyrene functionalisation of MWCNTs due to the fact that the dependency of the solvent medium on the degree of functionalisation is consistent with the mechanism proposed by O'Connell *et al.* [56] for polymer wrapping. This mechanism states that the degree of polymer functionalisation of CNTs is thermodynamically driven by the CNT interactions with the solvent media and implies that the polymer functionalisation will increase when the interactions between the CNTs and the solvent are not thermodynamically favourable. Thus the quality of the CNT-solvent interactions should be proportional to the degree of polymer functionalisation of MWCNTs in a particular solvent. So far the solubility parameter theories have been the most successful models to estimate the solvent-CNT interactions and have been used to select organic solvents that can efficiently stabilize CNT dispersions [15, 125, 126, 127], making it an ideal model to be applied for the polymer functionalisation of CNTs.

For the purpose of applying the surface energy based solubility parameter theory (SEBSP) to predict the degree of polystyrene functionalisation of MWCNTs, the surface energy and Hansen solubility parameter (HSP) of 10nmMWNCTs were measured with inverse gas chromatography (IGC) in collaboration with Dr. Vikram Karde from Imperial College London. The measured surface properties of the 10nmMWCNTs were found to be consistent with the values that have been reported previously in the literature [128]. The Hansen and Hildebrand SEBSP were used to estimate the solvent-10nmMWCNT interactions for the six solvents used in Chapter 3 for the non-covalent functionalisation of MWCNTs. Our hypothesis pre-

dicted that the degree of polystyrene functionalisation should increase for solvents where the solvent-10nmMWCNTs interaction was less favourable. When compared with the TGA values of polystyrene content the solvents that were predicted by both the Hildebrand and Hansen SEBSP theory to present unfavourable interactions with MWCNTs presented the highest degree of polystyrene functionalisation, while the opposite trend was observed for the solvents that were predicted to have more favourable interactions with MWCNTs. Finally, it was established that the Hansen SEBSP provided the most accurate prediction of the degree of polystyrene functionalisation of MWCNTs in the solvents used for this study.

The next section introduces the concepts of related to the solubility parameter theories, highlighting their application in CNT science.

4.1.1 Solubility Parameter Theories

The solubility parameter theories attempt to determine if a particular solute is soluble in a certain solvent. Thermodynamically the solubility of solute in a solvent depends on the value of the free energy of mixing (ΔG_{mix}), which involves an enthalpic (ΔH_{mix}) and an entropic (ΔS_{mix}) contribution as follows:

$$\Delta G_{\mathrm{mix}} = \Delta H_{\mathrm{mix}} - T\Delta S_{\mathrm{mix}} \tag{4.1}$$

According to thermodynamics it is expected that a solute is soluble in a particular solvent when the ΔG_{mix} is negative or in other words when $\Delta H_{mix}<\Delta S_{mix}$. The ΔS_{mix} arises from the increase of disorder achieved by mixing the solute and solvent, it presents most often a positive value and tends to be the thermodynamic drive for solubilisation. On the other hand, the ΔH_{mix} is related to the intermolecular forces acting between the solvent and solute molecules, it indicates the strength of their interactions and it can be either positive or negative. When the ΔH_{mix} is minimised the solute-solvent intermolecular interactions are considered to be more favourable

and the condition of $\Delta H_{mix}<\Delta S_{mix}$ is met, making the solute more likely to be soluble in a particular solvent. The solubility parameter theories attempt to calculate the ΔH_{mix} between a solute and a solvent to predict their ability to form a solution. The success of the solubility parameter theories is due to the simplicity of the model to provide qualitative guidelines of the interactions of solutes and different solvents.

As it was first proposed, the Hildebrand solubility parameter theory is based on the definition of the enthalpy of mixing by Hilderbrand-Scratchard:

$$\Delta H_{\mathrm{mix}} = \phi_a \phi_b (\delta_a - \delta_b)^2 \tag{4.2}$$

Where ϕ_i represents the volume fraction and δ_i is the Hildebrand solubility parameter of the solute or solvent. Hildebrand defined the solubility parameter of a substance as the square root of the cohesive energy ($E_{C,i}$) of the substance divided by its molar volume (V_o):

$$\delta_i = \sqrt{\frac{E_{C,i}}{V_{o,i}}} \tag{4.3}$$

According to Hildebrand the enthalpic interactions between a solute and a solvent is minimized when the cohesive energy densities of the solute and solvent are similar [129].

The Hildebrand solubility parameter was found to be a good approximation for the prediction of the solubility of non-polar organic molecules in non-polar organic solvents [129]. However, it fails to predict the solubility of molecules presenting permanent dipoles and of molecules that interact through electron exchange mechanisms (e.g. hydrogen bonding) [129]. To address this problem, Charles Hansen proposed that the cohesive energy densities of a molecule arise from the sum of different intermolecular forces. Under this premise, Hansen broke down the cohesive energy in three contributions: Dispersive ($E_{C,D}$), Polar ($E_{C,P}$) and Hydrogen Bonding ($E_{C,H}$) (later referred as electron exchange) [129], redefining the cohesive energy

density ($E_{C,Total}$) of a substance as:

$$E_{C,Total} = E_{C,D} + E_{C,P} + E_{C,H} \tag{4.4}$$

Hansen also defined a solubility parameter for each of the energy density contributions, which are now known as the Hansen solubility parameters (HSP):

$$\delta_{i=D,P,H} = \sqrt{\frac{E_{C,i}}{V_{o,i}}} \tag{4.5}$$

If the HSP of two substances are plotted in a 3-dimensional space, the distance between each point will correlate with the difference between their cohesive energies. Hansen proposes to calculate this distance parameter (R_a) as follows:

$$R_a = \sqrt{4(\delta_{D,A} - \delta_{D,B})^{1/2} + (\delta_{P,A} - \delta_{P,B})^{1/2} + (\delta_{H,A} - \delta_{H,B})^{1/2}} \tag{4.6}$$

In this way, as the R_a decreases a more favourable interaction between the solute and solvent is expected. Hansen observed that by introducing a factor of four multiplying the dispersive contribution a more accurate value was obtained. The physical interpretation of this factor is still in debate [15], although Hansen speculates that it has to do with the fact that dispersive forces do not have directional restrictions while polar and electron exchange interactions do [129].

In addition, Hansen introduced the concept of a solubility sphere presenting a radius that is particular for each molecule (R_o). This solubility sphere is obtained experimentally by measuring the distances between the solute and a range of solvents where the substance is soluble and insoluble. Finally, R_o is determined where the number of good solvents inside the volume of the sphere is maximized and the number of non-solvents is minimized [129]. This R_o can be used to predict the solubility of substance in a certain solvent by dividing the R_a distance with the R_o radius. If $R_a/R_o < 1$ the solvent is predicted to solubilize the substance, on the

other hand if $R_a/R_o > 1$ the substance is predicted to be insoluble in the solvent.

While there are theoretical models for the calculation of the HSP of small organic molecules from physical constants, the determination of the HSP of polymers and other materials is mostly done by empirical methods [129]. The most used methodology is called the "sphere technique" that consists of testing the solubility of the substance with unknown HSP in a wide range of solvents with well-known HSP. This information is then plotted in a 3-dimensional space and a solubility sphere is constructed where the surface of the sphere is located where the maximum of good solvents are inside of the sphere and the minimum outside. The centre of this sphere is then taken as the HSP of the substance [129].

Detriche *et al.* [127, 126] were the first to estimate the HSP of CNTs using the "sphere technique" by evaluating SWCNT, DWCNTs and MWCNTs dispersions in different solvents. They reported that the HSP of SWCNTs and DWCNTs presented small variation, and they observed that graphitisation treatments for all type of CNTs (i.e. treating the CNTs at 2000 °C in Ar) had a small impact on the HSP values of the CNTs. In addition, they also found that for all of the CNTs there were a large number of solvents where HSP theory failed to explain the behaviour of the solutions.

In a second attempt to estimate the HSP values of SWCNTs Bergin *et al.* [15] made an in depth study to evaluate the physical characteristics presented by solvents that could create stable CNT dispersions. In this case, the HSP values for the SWCNTs were obtained by calculating the concentration weighted average of the δ_i of the solvents that successfully dispersed SWCNTs. The authors argued that this method to calculate the HSP was superior to the "sphere technique", since they are centring the HSP sphere in relation to the best solvents for the CNT dispersion instead of the boundary solvents. Although they were able to demonstrate solvents with unprecedented dispersability for SWCNTs, they still observed many non-solvents that presented an R_a similar to what it was observed for good solvents.

In the same study, Bergin *et al.* [15] explored the nature between the interactions of CNTs and solvents, concluding that the surface energy was a more suitable parameter in comparison to cohesive energies to evaluate these interactions. This argument was based on the observation that most of the successful solvents presented a surface tension of approximate 40 mJ/m^2. Based on this findings the authors proposed that a better model would be obtained if the calculation of the solubility parameters were defined by the surface energy instead of the cohesive energy of solvents and CNTs, calling this model the surface energy based solubility parameter theory (SEBSP). They proposed to calculate the ΔH_{mix} according to the Hildebrand definition as follows:

$$\Delta H_{\text{mix}} = \left(\sqrt{E_{S,a}} - \sqrt{E_{S,b}}\right)^2 \tag{4.7}$$

Where $E_{S,i}$ is the surface energy of the solute and solvent.

In addition, Bergin *et al.* [15] propose that the surface energy of the solvents and solutes can be separated into contributions of dispersive, polar and hydrogen bonding forces in analogy to the HSP theory. Thus, Bergin defines the surface energy ($E_{S,Total}$) of a substance as:

$$E_{\text{S,Total}} = E_{\text{S,D}} + E_{\text{S,P}} + E_{\text{S,H}} \tag{4.8}$$

With each contribution to the surface energy having a solubility parameter associated defined as:

$$\partial_i = \sqrt{E_{\text{S,i}}} \tag{4.9}$$

To obtain the values of the SEBSP of the solvents Bergin *et al.* used the equations previously proposed by Beerbower [130] and Koenhen *et al.* [131]:

$$E_{\text{S,i}} = \frac{\alpha_i \delta_i^2}{\alpha_D \delta_D^2 + \alpha_P \delta_P^2 + \alpha_H \delta_H^2} E_{\text{S,Total}} \tag{4.10}$$

Where α_i are empirical constants that are equal to $\alpha_D = 1$ and $\alpha_{\text{P,H}} = 0.63212$. In

addition, $E_{S,Total}$ of the solvents was calculated using the following equation:

$$E_{\mathrm{S,Total}} = \gamma + T\Delta S_s \tag{4.11}$$

Where γ is the surface tension of the solvent and ΔS_s is equal to 0.1 mJ m^{-2} K^{-1} and it is constant for any organic solvent [132].

Analogous to Hansen, they used the notion of the R_a distance to estimate the ΔH_{mix} between CNTs and solvents using the following equation:

$$R_a = \sqrt{(\partial_{\mathrm{D,A}} - \partial_{\mathrm{D,B}})^{1/2} + (\partial_{\mathrm{P,A}} - \partial_{\mathrm{P,B}})^{1/2} + (\partial_{\mathrm{H,A}} - \partial_{\mathrm{H,B}})^{1/2}} \tag{4.12}$$

When the authors plotted the R_a of each solvent against the concentration obtained from the dispersions, they found a better fit in comparison to what they had obtained with the HSP parameters. However, just as the SEBSP was also unsuccessfully to explain the ability of many of the solvents to disperse SWCNTs.

Finally, Bergin *et al.*[15] noted that the best solvents for the dispersion of SWCNTs are solvents that present atoms with non-bonding electron pairs (e.g. amides) and argues that one of the causes that may account for the observed inconsistencies of the SEBSP theory is the role that electron exchange interactions may play during the dispersion of CNTs [15]. The shortcomings of HSP theory to model electron exchange interaction have been widely reported in the literature [133] since it does not make a difference between molecules that act mainly as donors, acceptors or both.

In addition, it is important to note that the HSP theory and thus the SEBSP theory are based in the solubility of organic molecules in organic solvents. However, Bergin *et al.* could not demonstrate that SWCNTs were solubilized in the rigorous thermodynamic definition (i.e. $\Delta G_{mix} < 0$), or if the mixture was a metastable dispersion. This suggests that even if certain solvents with well-defined HSP pa-

rameters are very successful in the dispersion of CNTs, it does not necessarily mean that the HSP parameters of the solvent and the CNTs are similar. This observation raises questions in the accuracy of the method used by Bergin *et al.* to calculate the HSP parameters of SWCNTs used for this study. This claim is supported by the recent reports from Hardy and Bock [134], where they did a computational simulation of the dispersion of [10,10] SWCNTs in six different solvents and compared it with the experimental data from Bergin *et al.* Their results predicted that these mixtures are in fact metastable dispersion and that not only good cohesive forces between the CNTs and solvents have an impact on the quality of the dispersion, but also conformational interactions between the solvent molecules in the first layer of solvation [134]. This observation highlights that to characterise the HSP of non-soluble materials such as CNTs it is required a characterisation method that does not rely in the solubility of the material in solvents.

Other characterisation methods have been used to characterise the HSP of CNTs. In particular, inverse gas chromatography (IGC) has proven to be a powerful technique to characterise the surface properties of solid materials since it calculates the values from enthalpies of adsoprtion of a wide range of solvents. The fact that the calculation of the HSP parameters is obtained directly from the thermodynamic interactions between the analyte and solvents makes this methodology more accurate than Hansen and Bergin methods. Lim *et al.* [125] used IGC to characterise the HSP parameters of MWCNTs and evaluated the concentration of CNT dispersions in a wide range of solutions. Using the HSP obtained from IGC they found a strong linear correlation between the R_a distance and the concentration of CNTs, which is presented in Figure 4.1. Interestingly in their study they found two separate linear trends one encompassing good solvents for CNT dispersions known to have electron exchange interactions with graphitic carbons such as N-methylpyrrolidone and ortho-dicholorobenzene. The second trend included solvents that are not considered to be good for CNT dispersions and do not participate in electron exchange

interactions with CNTs.

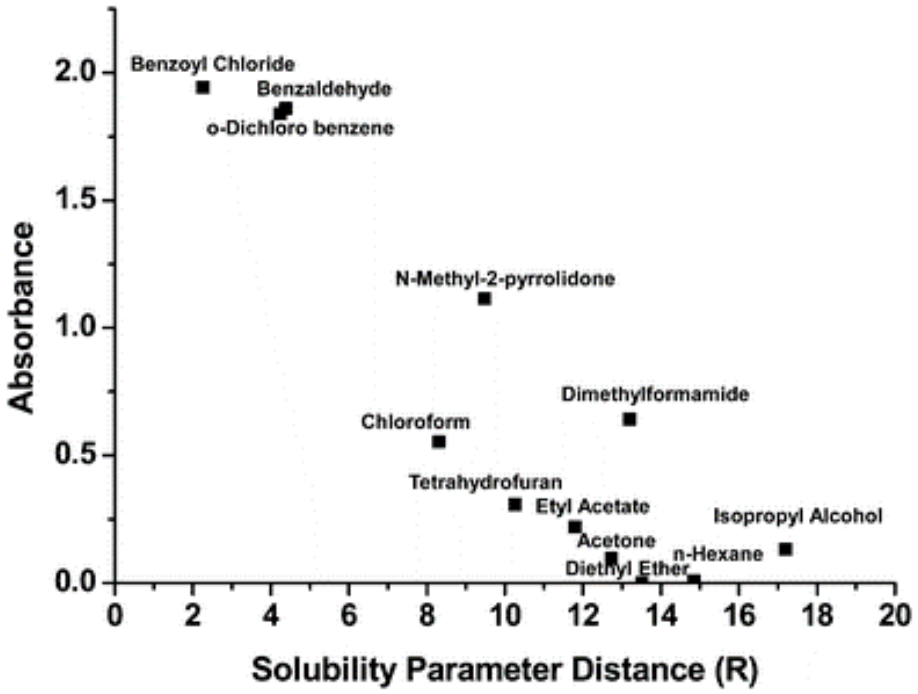


Figure 4.1: *Plot of absorbance of MWCNT dispersions in different solvents against the solvent-MWCNT R_a distance as reported by Lim et al. Two different linear trends are observed. Adapted from reference* [125] *with permission of the Royal Society of Chemistry.*

The reports of Detriche, Bergin and Lim highlight the applicability of the solubility parameter theories to evaluate the CNT-solvent enthalpic interactions. In all cases the purpose of their study was to show the application of the solubility parameter theories for the selection of solvents to be used to prepare CNT dispersions. These studies presented mixed results since the solubility parameter theories were not able to account for why solvents with solubility parameters similar to the ones measured for the CNTs were not able to make dispersions with a high CNT concentration. This observation should not be discouraging for the purpose of using the solubility parameter theories to evaluate CNT-solvent interactions since the metastable dispersion of CNTs require more than just favourable enthalpic interactions as it was demonstrated by Hardy *et al.* [134]. In this way, the application of the solubility parameter theories to evaluate the solvent-CNT interactions could prove to be a useful tool for other purposes than the preparation of CNT dispersions.

One of these potential applications is for the non-covalent functionalisation of CNTs with polymers. If the mechanism for polymer wrapping proposed by O'Connel *et al.* is accurate then the evaluation of the solvent-CNT interactions using the solubility parameters theories should be able to provide a prediction of the degree of polymer functionalisation of CNTs with a particular polymer in different solvents.

The present study is the first time that the solubility parameter theories have been used as a model to predict the degree of functionalisation of CNTs with a polymer. To achieve this we characterised the surface energy and solubility parameters of 10nmMWCNTs using the IGC technique performed according to Lim *et al.* Then the solubility parameter difference according to Hildebrand and Hansen were calculated, and compared with the TGA characterisation obtained from the functionalisation experiments. In the following section we summarise the characterisation methods and calculations used for the determination of the SEBSP of 10nmMWNCTs and solvents.

4.2 Materials and methods

4.2.1 Chemicals

For the IGC characterisation of 10nmMWNCTs the following solvents were used. n-Octane (anhydrous $\geq$ 99%), n-heptane (HPLC grade $\geq$ 99%), n-hexane (HPLC grade $\geq$ 99.5%), ethanol (puriss. p.a., ACS reagent, absolute alcohol), ethyl acetate (HPLC grade $\geq$ 99.7%), acetonitrile (HPLC grade $\geq$ 99.9%) and dichloromethane (HPLC grade $\geq$ 99.8%) were purchased from Sigma Aldrich. Toluene (99.5%, AnalaR NORMAPU™ACS, Reag. Ph. Eur.) was obtained from VWR chemicals.

4.2.2 Characterization

The IGC surface analysis of 10nmMWCNTs was performed using an inverse gas chromatography surface analyser (IGC SEA) manufactured by Surface Measurement Systems (SMS).

4.2.3 IGC analysis of 10nmMWCNTs

For the analysis 10nmMWCNTs (approximately 10 mg) sample were packed into a silanised glass column (internal diameter of 3 mm) and closed with a silanised glass wool on both ends. The sample was packed by mechanical tapping using a jolting voltameter (SMS) to remove voids in the sample. The packed column was placed in an oven to condition for analysis at a 0% relative humidity for 2 hours under helium flow. The IGC measurements were performed in a range of temperature from 50-110 °C at 0% relative humidity. Helium was used as carrier gas at a flow rate of 12 mL/min. Methane was used as a reference gas to determine the dead volume. The analysis was performed at an infinite dilution region using octane, heptane and hexane to determine the dispersive surface energy interactions of 10nmMWCNTs. To evaluate the polar and hydrogen bonding interactions ethyl acetate, dichloromethane, toluene and acetonitrile was employed.

4.2.4 Calculation of the HSP of 10nmMWCNTs

The calculation of the HSP parameters with the data obtained from IGC analysis was performed according to Lim *et al.* [125]. The enthalpy of adsorption (ΔH_{ads}) of a solvent probe can be obtained by measuring in IGC the retention volume (V_g) of the solvent a different temperatures. The (ΔH_{ads}) for the probe is then calculated by obtaining the slope of the following linear relationship between retention volume (V_g) and the inverse of temperature (T):

$$lnV_g = -\frac{\Delta H_{\text{ads}}}{RT} + C \tag{4.13}$$

The V_g of eight solvent probes where obtained from IGC analysis described in Section 4.2.3 at temperatures ranging from 50-100 °C to calculate the ΔH_{ads} of each solvent on 10nmMWCNTs. The ΔH_{ads} was then used to obtain the HSP of 10nmMWCNTs by applying a multilinear regression on the following equation:

$$-\Delta H_{\text{ads}} = -\Delta E_{\text{ads}} = V_i(\delta_d^i\delta_d^j + \delta_p^i\delta_p^j + \delta_h^i\delta_h^j) \tag{4.14}$$

Where V_i is the molar volume of the solvent molecules, ${\delta^{\text{solvent}}}_{\text{d,p,h}}$ are the corresponding HSP of the solvent probes and ${\delta^{\text{10nmMWCNTs}}}_{\text{d,p,h}}$ are the HSP of 10nmMWCNTs. The values for ${\delta^{\text{solvent}}}_{\text{d,p,h}}$ and the V_i of the solvents are known quantities. The values for ΔH_{ads} have been obtained through IGC. This linear equation presents 3 unknown values that correspond to the ${\delta^{\text{10nmMWCNTs}}}_{\text{d,p,h}}$ of the MWCNTs. A multilinear regression analysis is a methodology used to obtain the values of the coefficients where a linear relationship is found between a dependent variable (y) and multiple independent variables (x) as follows:

$$y = B_0 + B_1x_1 + B_2x_2 + B_3x_3 + ... + B_kx_k + \epsilon \tag{4.15}$$

Where B_i are constant coefficients, B_o is the intercept and ϵ are the residuals. When Equation 4.15 is compared with Equation 4.14, the y dependent variable corresponds to $-\Delta H_{\text{ads}}$ and the x dependent variable would be the product of the molar volume of the solvent probe and their corresponding HSP values (eg. ${V_i\delta_{(\text{d,p,h})}}^{\text{Solvent}}$), and the coefficients ($B_{1,2,3}$) obtained from the multiple linear regression analysis would correspond to ${\delta^{\text{10nmMWCNTs}}}_{\text{d,p,h}}$. Thus, by doing a multilinear regression analysis using the software Microsoft Excel we obtained the values of the HSP of 10nmMWCNTs.

4.2.5 Calculation of surface energy of the 10nmMWCNTs through IGC analysis

The calculation of the dispersive and polar surface energy of a solid probe can be obtained with IGC by the calculation of the free energy of adsorption (ΔG_{ads}) of different solvent probes according to the following equation:

$$\Delta G_{\text{ads}} = RTlnV_g \tag{4.16}$$

Where R is the ideal gas constant, T is the temperature of the column and V_g is the special retention volume of the solvent probe.

The calculation of the dispersive surface energy of 10nmMWCNTs was performed through the Dorris-Gray method [135]. This method calculates the dispersive surface energy (γ^d) of a solid analyte from the value of the free Gibbs energy of adsorption of a CH_2 group on the surface of the analyte. The calculation of the ΔG_{CH_2} is obtained from the V_g measurement of multiple linear alkane solvent probes. For the present study hexane, heptane and octane were used as the alkane probes during the IGC analysis. The ΔG_{CH_2} is then obtained from the slope of the following linear equation:

$$RTlnV_g = \Delta G_{CH_2} N_C \tag{4.17}$$

Where N_C is the number of carbons in the alkane probes. Finally, the value of the γ^d of the solid analyte can be obtained from the following equation:

$$\gamma^d = \frac{{\Delta G_{CH_2}}^2}{4\gamma_{CH_2}(a_{CH_2}N_a)^2} \tag{4.18}$$

Where a_{CH_2} is the cross sectional area of a CH_2 which is equal to 0.06 nm^2 and N_a is Avogadro's number.

For the calculation of the polar surface energy (γ^p) of 10 nmMWCNTs the Schultz

method was applied [136]. This method calculates the polar surface energy of the solid analyte (γ^p) from the calculation of the polar free energy of adsorption (ΔG^P) of a monopolar acidic probe (in this case DCM) and a monopolar basic probe (in this study ethyl acetate). The ΔG^P of both probes can be obtained from the following equation:

$$\Delta G^P = \Delta G_{\text{ads}} - \Delta G^D \tag{4.19}$$

Where ΔG^D is the dispersive free energy of adsorption. While ΔG_{ads} can be directly obtained from the IGC data using Equation 4.16, ΔG^D has to be calculated indirectly. For this calculation it is first required to obtain an equation that can predict the ΔG^D of any molecule, this can be obtained from a linear regression of a plot of the ΔG_{ads} of molecule probes that can only interact through dispersive molecules (i.e. linear alkanes) against the product of their surface area per probe molecule (a) times the square root of their dispersive surface energy (γ^d). The linear regression obtained is the following:

$$\Delta G^D = c + ba(\gamma^d)^{1/2} \tag{4.20}$$

In this case the values of the y intercept (c) and the slope (b) were obtained from a linear regression of the values of the ΔG_{ads} for hexane, heptane and octane. The ΔG^D for DCM (ΔG^P_{DCM}) and ethyl acetate (ΔG^P_{EA}) are then calculated by substituting their corresponding surface area and dispersive surface energy values.

With the ΔG^P values of DCM and ethyl acetate calculated, the acidic (γ_s^+) and basic (γ_s^-) parameter of the surface energy of the 10nmMWCNTs can be obtained from the following equation:

$$\gamma^-_{10nmMWCNTs} = \left(\frac{\Delta G^P_{DCM}}{2N_A a_{DCM}}\right)^2 \left(\frac{1}{\gamma^+_{DCM}}\right) \tag{4.21}$$

and

$$\gamma^{+}_{10nmMWCNTs} = \left(\frac{\Delta G^{P}_{EA}}{2N_A a_{EA}}\right)^2 \left(\frac{1}{\gamma^{-}_{EA}}\right) \tag{4.22}$$

The γ^p value of the 10nmMWCNTs can then be calculated by the following equation:

$$\gamma^{P}_{10nmMWCNTs} = 2(\gamma^{+}_{10nmMWCNTs}\gamma^{-}_{10nmMWCNTs})^{1/2} \tag{4.23}$$

Finally the total surface energy of MWCNTs can be obtained from:

$$\gamma_{10nmMWCNTs} = \gamma^{P}_{10nmMWCNTs} + \gamma^{D}_{10nmMWCNTs} \tag{4.24}$$

4.2.6 Calculation of SEBSP

The calculation of the HSP surface energy based solubility parameters was performed according to the methodology proposed by Bergin *et al.* [15]. In summary, the value of ∂_i for each solvent and 10nmMWCNTs was calculated using Equation 4.10 and Equation 4.11. In addition to the calculation of the SEBSP of 10nmMWCNTs from the IGC characterisation, the solubility parameter values reported by Lim *et al.* [125] for MWCNT were also used to calculate the ∂_i. The summary of the values is reported in Table 4.1

Table 4.1: *HSP, surface tension, surface energy and SEBSP of the solvents used during this study.* [a] *Values taken from: Hansen Solubility Parameters: A User's Handbook* [129]. [b] *Values taken from: Lim et al.* [125]. [c] *Values taken from: Thermophysical Properties of Chemicals and Hydrocarbons* [137]. [d] *Values taken from: Menzel et al.* [128].

Substance	δ_D ($MPa^{1/2}$)	δ_P ($MPa^{1/2}$)	δ_H ($MPa^{1/2}$)	γ (mJ/m^2)	$E_{S,Total}$ (mJ/m^2)	∂_D ($mJ^{1/2}/m$)	∂_P ($mJ^{1/2}/m$)	∂_H ($mJ^{1/2}/m$)
o-DCB	19.2[a]	6.3[a]	3.3[a]	35.55[c]	64.85	7.9	2.0	1.1
NMP	18[a]	12.3[a]	7.2[a]	42.51[c]	71.81	7.1	3.9	2.3
DMF	17.3[a]	13.7[a]	11.3[a]	34.43[c]	63.73	6.2	3.9	3.2
DCM	18.2[a]	6.3[a]	6.1[a]	27.84[c]	57.14	7.1	1.9	1.9
Toluene	18[a]	1.4[a]	2.0[a]	27.93[c]	57.23	7.5	0.5	0.7
Acetone	15.5[a]	10.4[a]	7.0[a]	23.04[c]	52.34	6.1	3.2	2.2
MWCNTs	21.3[b]	6.8[b]	3.2[b]	-	114[d]	10.3	2.6	1.2
Lim *et al.* 10nmMWCNTs	20.5	6.7	7.2	-	119.1	10.2	2.7	2.9

4.3 Results and discussion

4.3.1 HSP and surface energy determination of 10nmMWCNTs with IGC

The first step for the calculation of the HSP of the 10nmMWCNTs was to obtain the ΔH_{ads} of the solvent probes according to Equation 4.13. The ΔH_{ads} was obtained from the slope of the linear function between the $\ln V_g$ against the inverse of temperature. In Figure 4.2 the linear plots for the solvent probes is presented and the summary of the values of the ΔH_{ads} is presented in Table 4.2. It can be observed that the probes that presented a higher affinity were non-polar solvents such as alkanes and toluene. This is consistent with the fact that MWCNTs are considered a material with a non-polar structure. Polar solvents with the capability to accept hydrogen bonds such as acetonitrile, ethanol and ethyl acetate presented a mid range interaction. Finally, dichloromethane presented the smallest ΔH_{ads}. Dichloromethane is a solvent with a dipolar moment that is not a good hydrogen bond acceptor [138]. The fact that polar solvents that are hydrogen bonding acceptors had a high ΔH_{ads} with the surface of 10nmMWCNTs suggest that the defects present in this MWNCTs have oxygen groups such as carboxylic acids that could act as hydrogen bond donors.

The ΔH_{ads} values obtained from the IGC analysis were used to obtain the HSP

Table 4.2: *Values of the enthalpy of adsorption obtained for each solvent probe.*

Solvent	Slope of linear regression	ΔH_{ads} [kJ/mol]	V_i [cm^3/mol]	δ_t [$MPa^{1/2}$]	δ_d [$MPa^{1/2}$]	δ_p [$MPa^{1/2}$]	δ_h [$MPa^{1/2}$]
Acetonitrile	3554	-29.6	52.7	24.4	15.3	18.0	6.1
Dichloromethane	1450	-12.1	64.4	20.2	18.2	6.3	6.1
Ethanol	4386	-36.5	58.5	26.5	15.8	8.8	19.4
Ethyl Acetate	3987	-33.2	98.6	18.2	15.8	5.3	7.2
Heptane	5680	-47.2	146.9	15.3	15.3	0	0
Hexane	4669	-38.8	131.4	14.9	14.9	0	0
Octane	6508	-54.1	163.4	15.5	15.5	0	0
Toluene	4813	-40.0	106.5	18.2	18	1.4	2

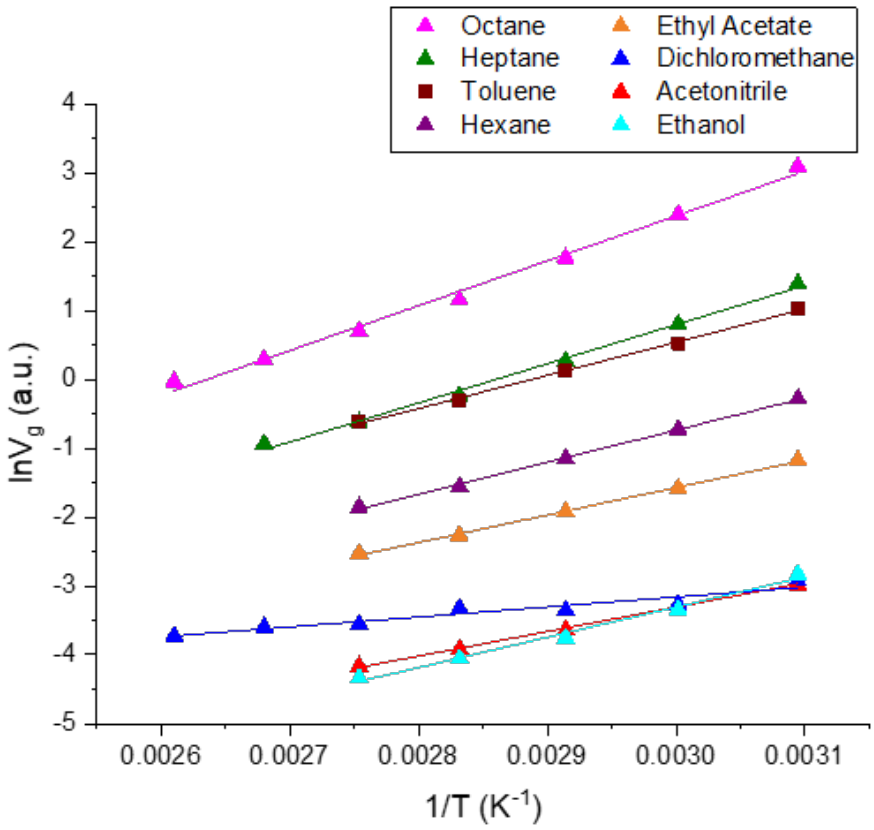


Figure 4.2: *Determination of the ΔH_{ads} of 10nmMWCNTs with IGC. The slope of the linear regressions is used to calculate the ΔH_{ads} according to Equation 4.13.*

parameters of 10nmMWCNTs by performing a multiple linear regression according to Equation 4.14. Two different methods where used to estimate the HSP parameters of 10nmMWCNTs and the results are presented in Table 4.3. In Method 1, we used the data directly obtained from IGC for the multiple linear regression analysis. As it can be observed in Table 4.3 the results largely differ from what was obtained in previous reports. In particular it is important to notice that the prediction given by the multiple linear regression has a y-intercept with a magnitude close to the experimental data. It can be seen from Equation 4.14 that an ΔH_{ads} equal to zero would be expected if the solvent probe presented a δ equal to 0. The observation of a large value for the y-intercept is not consistent with the theory since it would imply that a substance with δ equal to zero would still cause a change in the ΔH_{ads}.

For Method 2, I added a hypothetical data point where a substance with δ equal to zero would present a ΔH_{ads} also equal to zero to correct for the observation of a

large y-intercept. The result is presented in Table 4.3, it can be seen that the Method 2 to calculate the HSP parameters of the 10nmMWCNTs resulted in values closer to the values reported previously for MWCNTs by Lim *et al.* The 10nmMWCNTs used for this study presented a larger δ_h in comparison to those reported by Lim *et al.*, this difference can be explained by noting that the XPS analysis of the MWCNTs showed a 1.61% content of oxygen atoms while the sample used by Lim *et al.* presented 0.7% oxygen [125]. On the other hand, the δh obtained through Method 1 is much larger than what was observed previously for MWCNTs and does not correlate as closely with the oxygen content determined by XPS characterisation of the 10nmMWCNT sample, providing further support for including the hypothetical corrective point. Moreover, the value of the y-intercept was considerably closer to zero and the R^2 value of the linear regression was closer to 1, indicating that a higher degree of linear relationship is observed in comparison to the values obtained through Method 1. For these reasons the HSP values obtained through Method 2 were used for the calculation of the SEBSP of 10nmMWCNTs.

The determination of the dispersive surface energy of 10nmMWCNTs was obtained through IGC analysis according to the Doris-Grey method. The dispersive surface energy was obtained at various temperatures, which are presented in Figure 4.3A. It can be observed that the dispersive contribution to the surface energy showed an inverse linear relationship with temperature, which suggests that the dispersive interactions between the probe molecules and the 10nmMWCNTs are disrupted by the thermal energy of the system. The polar contribution of surface

Table 4.3: *Comparison of the HSP parameters of 10nmMWCNTs obtained by Method 1, Method 2 and reported from Lim et al.*

Sample	Method	δ_d [$MPa^{1/2}$]	δ_p [$MPa^{1/2}$]	δ_h [$MPa^{1/2}$]	y-Intercept [kJ/mol]	R^2	Ref
10nmMWCNTs	1	29.4	19.1	11.3	21.7	0.6657	This work
10nmMWCNTs	2	20.5	6.7	7.2	-1.6	0.8231	This work
Hanos MWCNT CM-250	1	21.3	6.8	3.2			[125]

energy was calculated through the Schultz method for different temperatures, which are presented in Figure 4.3. In contrast to the dispersive surface energy, the polar contribution did not vary significantly with temperature. This observation suggests that in the range of temperatures used for the IGC characterisation the polar interactions between the probe molecules and the 10nmMWCNTs were not disturbed by the increase in the thermal energy of the system while the dispersive interactions are. This contrasting behaviour for the dispersive and polar surface energy values in function of temperature is consistent with the fact that polar forces are more robust than dispersive forces. To put into context the energy of Van der Waals interactions between small organic molecules are between 2-4 kJ/mol while polar interactions are between 4-13 kJ/mol [139]. On the other hand, for the range of temperatures used during this study the average thermal energy of a molecule in ideal conditions is between 4.1-4.7 kJ/mol, which is smaller than the value expected for small organic molecule polar interactions but of the same order of magnitude as dispersive interactions.

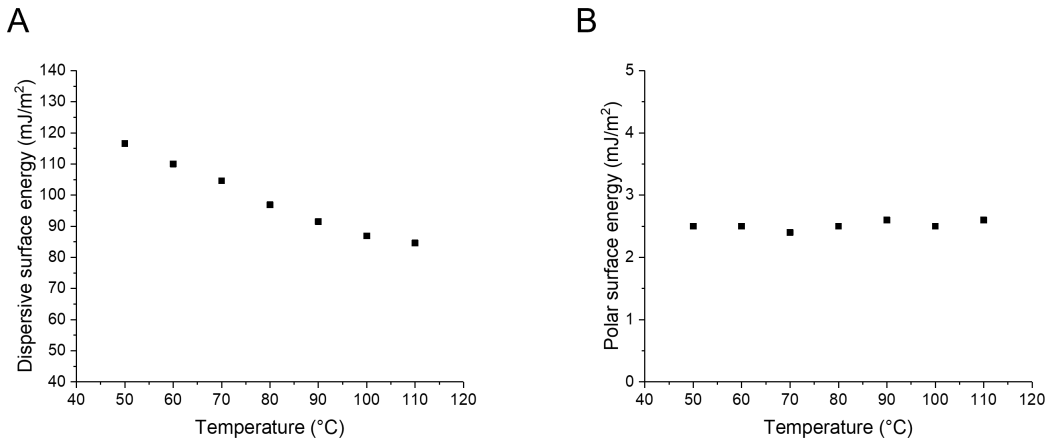


Figure 4.3: *Plot of the A) dispersive surface energy and B) polar surface energy of 10nmMWCNT at different temperatures.*

4.3.2 Application of Surface Energy Based Solubility Parameter theory for the non-covalent polymer functionalisation of MWCNTs

The mechanism for the non-covalent functionalisation proposed by O'Connel *et al.* establishes that the driving force for the non-covalent functionalisation MWCNTs with polymers is caused by the unfavourable energy interaction between the solvent and the surface of the MWCNTs. The hypothesis proposed by O'Connel *et al.* is consistent with the observed dependence in the degree of PS functionalisation on the solvent media that was presented in Chapter 3. Thus, I proposed that estimating the energy in the interface between a solvent and a MWCNT could be used to predict the degree of PS functionalisation of 10nmMWCNTs. To calculate the energy of the interactions between the solvent medium and MWCNT, the SEBSP proposed by Bergin *et al* was applied [15]. This model was chosen because of its simplicity and due to the previous reports where it was used to predict the enthalpy of interaction between solvents and graphitic carbons to generate stable dispersions.

First, the Hildebrand SEBSP difference between the MWCNTs and each solvent was calculated using Equation 4.7 and this value was plotted against the degree of polymer functionalisation. The larger the Hildebrand SEBSP difference between the MWCNTs and the solvent indicates that the ΔH_{mix} between them is less favourable and thus a larger degree of functionalisation would be expected. Figure 4.4A shows a rough trend where NMP, o-DCB and DMF present both the lower degree of functionalisation as well as the lowest Hildebrand SEBSP difference. On the other hand, toluene, DCM and acetone presented the largest degree of functionalisation and SEBSP difference. However, closer inspection reveals the limitations of the model to make a precise prediction between the solvents. For example, according to the Hildebrand model the degree of functionalisation of o-DCB should be higher in comparison to the one observed in NMP. Nonetheless, the opposite trend is observed

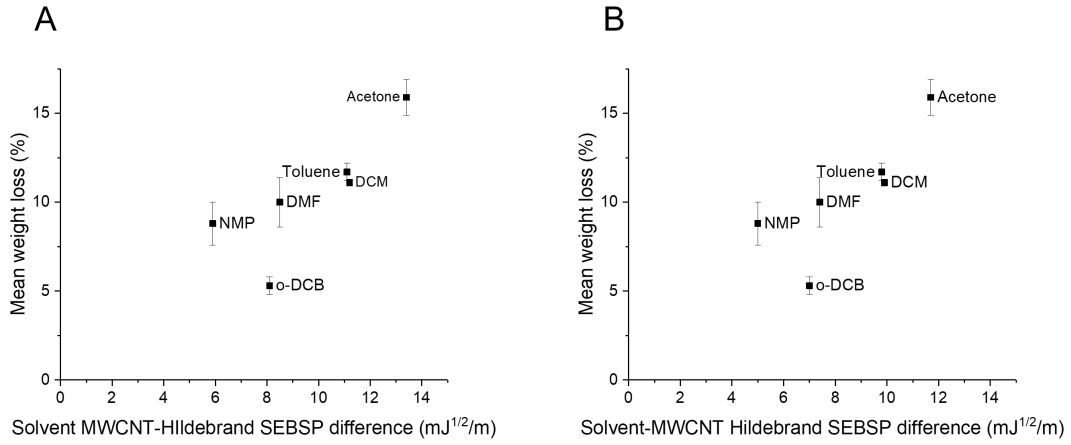


Figure 4.4: *Plots of the Hildebrand SEBSP difference between the solvents and 10nmMWCNTs against the mean polymer weightloss measured by TGA. A) The Hildebrand SEBSP difference was calculated using the presented experimental IGC data for 10nmMWNCTs B) The Hildebrand SEBSP difference was calculated using surface energy reported by Menzel et al.* [128].

in the experiments. The same observation can be made for toluene and DCM, showing the limited predictive power of this model.

The limitation of the Hildebrand SEBSP theory to explain the differences between the surface energy difference and the degree of polymer functionalisation might be due to the fact that the interactions between solvents and solutes arise through different intermolecular forces. Although the surface energy of a material will be related to the intermolecular forces taking place at their surface, the strength of these interactions are different depending if polar, dispersive or electron exchange interactions are occurring. A possible way to obtain a more accurate prediction of the degree functionalisation is by using the Hansen SEBSP theory. This theory proposes to divide the surface energy of a substance in three contributions related to polar, dispersive and electron exchange interactions, providing the basis to have a more accurate prediction.

The Hansen SEBSP of 10nmMWCNTs and solvents where obtained following the method proposed by Bergin *et al.* [15] (see Section 4.2.6 and Table 4.4). The Hansen SEBSP distance was calculated and the summary is presented in Table 4.5. In Figure 4.5A the plot of the SEBSP distance between each solvent and 10nmMWCNTs

Table 4.4: *HSP values for MWCNTs reported by Lim et al. and this work.*

Sample	∂_{Total} [$\text{mJ}^{1/2}/\text{m}$]	∂_{D} [$\text{mJ}^{1/2}/\text{m}$]	∂_{P} [$\text{mJ}^{1/2}/\text{m}$]	∂_{H} [$\text{mJ}^{1/2}/\text{m}$]
10nmMWCNTs	10.9	10.2	2.6	2.8
Lim MWCNTs	10.7	10.2	2.6	1.2

against the amount of polystyrene found in the products is presented. The overall trend demonstrates that as the distance between the solvent and 10nmMWCNTs increases the larger amount of polystyrene functionalisation is observed. This observation is consistent with our hypothesis that as the solvent-MWCNT interactions are less favourable a larger degree of polystyrene is expected to functionalise the MWCNT surface. It can be observed that only the results obtained for DCM and DMF strongly deviate from linearity. In addition, the trend obtained from the application of the Hansen SEBSP displays a more linear behaviour in comparison to the one obtained with the Hildebrand SEBSP distance (Figure 4.4A) . This observation can be attributed to the more precise prediction that can be obtained using the Hansen SEBSP theory.

Previous to the writing of this Thesis our research group had reported that the SEBSP theories could be used as a guideline to predict the degree of polymer functionalisation of MWCNTs [140]. In the publication the HSP that were used to calculate the Hansen and Hildebrand SEBSP distance between 10nmMWCNTs

Table 4.5: *Summary of the degree of polystyrene functionalisation of 10nmMWCNTs in the six different solvents used in the study, and the SEBSP distance between solvents and 10nmMWCNTs.*

Solvent	PS weight loss [%]	Solvent-MWCNT Hildebrand SEBSP difference [$\text{mJ}^{1/2}/\text{m}$]	Solvent-MWCNT Hansen SEBSP difference [$\text{mJ}^{1/2}/\text{m}$]
o-DCB	5.3±0.5	8.1	2.2
NMP	8.8±1.2	5.9	3.1
DMF	10±1.4	8.5	4.2
DCM	11.1±0.2	11.2	3.0
Toluene	11.7±0.5	11.1	3.3
Acetone	15.9±1.0	13.4	4.1

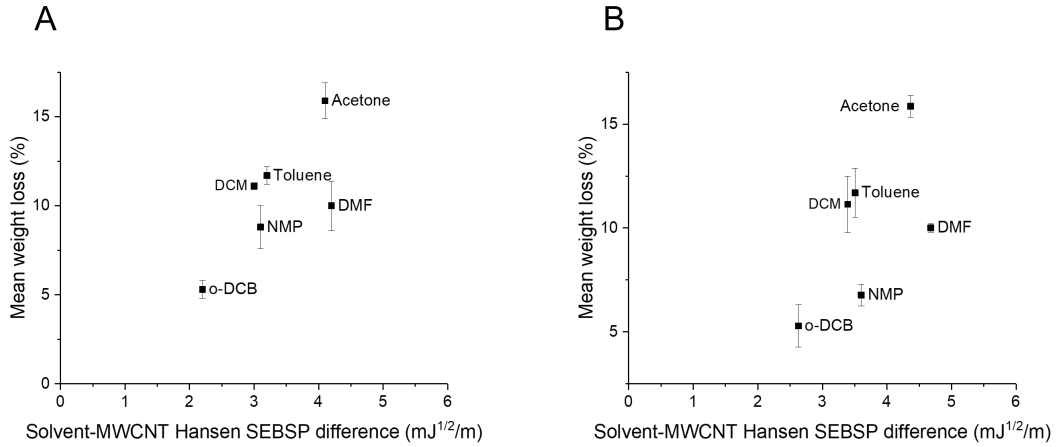


Figure 4.5: *Plots of the Hansen SEBSP difference between the solvents and 10nmMWCNTs against the mean polymer weightloss measured by TGA. A) The Hansen SEBSP difference was calculated using the experimental IGC data for 10nmMWCNTs B) The Hansen SEBSP difference was calculated using HSP values obtained by Lim et al.*[125].

and solvents were taken from the values reported by Lim *et al.* [125]. However, is important to note that the synthesis of the MWCNTs used in the study by Lim *et al.* was different from the synthesis used for the 10nmMWCNTs. The chemical and structural composition of MWCNTs will depend on the methods used during their synthesis, and the values of the HSP parameters of MWCNTs will vary depending on their structure and chemical functionalisation [127, 126]. In Figure 4.4B and 4.5B we present the plots Hildebrand and Hansen SEBSP distance against the degree of polymer functionalisation observed for different solvents that were published in our original report. It can be observed that in the case of the Hildebrand distance the trend follows the same shape, this is because the Hildebrand difference only depends on the surface energy of the MWCNTs and solvents. In this way as long as the surface energy measured for the 10nmMWCNTs sample was larger than the surface energy of the solvents the trend would have had the same shape regardless. In addition, the surface energy used from previous results for the calculation of the Hildebrand SEBSP it was very close to what obtained through IGC analysis of the 10nmMWCNTs.

On the other hand, the Hansen SEBSP distance obtained after measuring the

HSP of the 10nmMWCNTs presents important differences in comparison to the values obtained from our previous report. This differences are better observed when Figure 4.5A and B are compared. In the publication we argued that when the Hansen SEBSP was used to model the degree of polystyrene functionalisation of 10nmMWCNTs there was two different trends observed. The first trend contained DCM, toluene and acetone, while the second trend encompassed o-DCB, NMP and DMF. This claim was inspired by the results published by Lim *et al.* [125]. In their study, the HSP theory was applied to predict the ability of different solvents to disperse MWCNTs. Their results also presented two distinct trends as seen in Figure 4.1. In our article I hypothesized that the observation of two trends in Lim *et al.* and in our experiments could be explained due to the limitations of the HSP parameter theory to model electron exchange interactions accurately. The SEBSP distance presented by o-DCB, NMP and DMF seemed to be overestimated by the model. These solvents have been reported to have electron exchange interactions with graphitic materials such as graphene [141], which would have supported our claims. However, when the HSP of 10nmMWCNTs were measured a single trend was observed. This suggests that characterising the surface properties of the specific MWCNTs used during functionalisation is key to obtaining the closest predictions with the SEBSP theory.

4.4 Conclusions

The objective of this Chapter was to evaluate the capacity of the Surface Energy Based Solubility Parameter Theory as a model for the prediction of the degree of polystyrene functionalisation of MWCNTs. The values obtained from the SEBSP theories of solvent-MWCNT interactions were found to have a linear relationship with the values obtained from TGA for the degree of polymer functionalisation of 10nmMWCNTs with polystyrene. Between the Hildebrand and the Hansen SEBSP

theory, the latter was found to provide a more accurate representation of the differences in the degree of polystyrene functionalisation of MWCNTs in different solvent media. I concluded that the Hansen SEBSP theory is more successful in predicting the polymer functionalisation in comparison to the Hildebrand theory due to the separation of the surface energy of the solvent and 10nmMWCNTs into three different intermolecular contributions. The SEBSP estimate of the solvent-MWCNT interactions was compared to the values obtained from the HSP values for MWCNT reported previously in the literature. I found that a better prediction of the degree of polystyrene functionalisation is obtained when the specific values of 10nmMWCNTs that were measured during study were used, instead of the values reported previously in the literature. This highlights the importance of measuring the surface properties specific to the material used during the functionalisation procedure. In addition to these findings the results presented in this chapter also had an important contribution to the processing of IGC data for the calculation of the HSP of MWCNTs. In particular, I found that applying a correction for the y-intercept provided a better fit for the HSP of 10nmMWCNTs when the multilinear regression analysis was used on the retention data obtained from the IGC analysis.

Finally, these results empirically confirm the solvent role in the non-covalent functionalisation of CNTs with polymers as was first proposed by O'Connel *et al.* Moreover, the fact that the solubility parameter theories can explain the differences in the degree of functionalisation provides further validation for the application of the solubility parameter theory to evaluate the enthalpy of interaction between organic solvents and MWCNT. The role of the solvent medium in the interactions of polymers and MWCNTs could be expected regardless of the material system used. In this way, if a nanomaterial that is coated with a polymer is to be dispersed with MWNCTs in different organic solvents we should expect to see a difference in the degree of functionalisation of the MWCNT with the nanomaterial depending on the solvent used during the synthesis. Therefore, the principles and models discussed in

this chapter should be relevant for a system involving two nanomaterials and could be applied for the bottom-up synthesis of nanostructures where polymers mediate the interactions between CNTs and other nanomaterials. The following Chapter tackles this next level of nanostructural hierarchy, where the functionalisation of MWCNTs with iron oxide nanoparticles coated with polystyrene is discussed.

Chapter 5

Synthesis of IONP-MWCNT hybrids

5.1 Intoduction

Studying the parameters affecting the functionalisation of MWCNTs with polymers has been the main topic discussed throughout the previous experimental chapters. In Chapter 3 the use of non-covalent methods were found to be more suitable for the synthesis of nanostructures than covalent methods, due to their similar yield of functionalisation and increased simplicity. In Chapter 4 the SEBSP theory was applied as a model to predict the degree of non-covalent functionalisation of MWCNTs with polystyrene in different solvents, demonstrating that the Hansen SEBSP was a good predictor for the amount of functionalisation of 10nmMWCNTs with polystyrene. From the perspective of the bottom-up synthesis of nanostructures mediated by polymer interactions these studies are placed at the molecular level of hierarchy. In this Chapter the focus is shifted towards the next level of nanostructural hierarchy, where I explore the synthesis of hybrid nanostructures composed of iron oxide nanoparticles (IONPs) coated with organic molecules and MWCNTs. In this case,

the organic molecules coating the IONPs will mediate the non-covalent interactions between both nanomaterials. For this purpose oleylamine coated iron oxide nanoparticles (OAIONPs) were synthesised through a methodology previously reported by our research group [142]. Afterwards, a ligand exchange procedure was developed to exchange the surface oleylamine (OA) ligands for polystyrene molecules, thus obtaining polystyrene coated iron oxide nanoparticles (PSIONPs). Based on the knowledge obtained from the previous Chapters, the synthesis of IONP-10nmMWCNT hybrids was performed through a non-covalent methodology using OAIONPs and PSIONPs. The effect that the solvent had on the amount of IONPs found in the hybrids was evaluated and compared with the predictions made by the Hansen SEBSP theory. My results demonstrate that the composition of PSIONP-10nmMWCNT hybrids are in good agreement with the Hansen SEBSP theory. In addition to the effect of the solvent media, the effect that the relative concentrations of PSIONPs to MWNCTs have on the morphology of the hybrids was also explored. The experimental data suggests that nanoparticles tend to progressively accumulate forming aggregates between MWCNT bundles. Finally, a series of experiments evaluated the effect that the diameter of MWCNTs has on the morphology of PSIONP-MWCNT hybrids, demonstrating that MWCNT with large diameters present a higher surface coverage.

Before exploring the results obtained in these studies I present an introductory section that serves as an overview of the synthesis methods that are currently used to fabricate nanoparticle-CNT hybrids, with a particular focus on the synthesis of hybrids where the CNTs and nanoparticles are interacting through non-covalent forces. In addition, the studies that focus on the mechanisms of interaction between nanoparticles and CNTs will be highlighted for later comparisons with the results obtained from my experimental work.

5.1.1 Synthesis of nanoparticle-CNT hybrids

The synthesis of nanoparticle-CNT hybrids can be divided in two main categories: *in-situ* and *ex-situ* synthesis. *In-situ* synthesis is used when nanoparticles are synthesised in the presence of CNTs, which act as templates for the nucleation of nanoparticles in their surface as presented in Figure 5.1A. On the other hand, in *ex-situ* synthesis the nanoparticles are first synthesised and in a second step they are assembled with CNTs through wet chemical methods as depicted in Figure 5.1B. In general, the *ex-situ* approach allows a higher degree of control in the surface chemistry, size and morphology of the nanoparticles [143]. In this Chapter I will focus on the *ex-situ* methodologies for the synthesis of nanoparticle-CNT hybrids since the objective of this project is to study the parameters that affect the synthesis nanostructures based on polymer-nanomaterial interactions. For this purpose the *ex-situ* methodology is more suitable since it allows one to tailor the surface chemical composition of the nanoparticles prior to the synthesis of the nanoparticle-CNT hybrid. The rest of this introductory section will present an overview of the *ex-situ* synthesis of nanoparticle-CNT hybrids, stressing the different forces that are known to influence these interactions.

5.1.2 Synthesis of ex-situ inorganic nanoparticle-carbon nanotube hybrids

The main advantage of the *ex-situ* synthesis of nanoparticle-CNT hybrids is that through this method it is possible to decouple the synthesis of nanoparticles from the synthesis of the nanoparticle-CNT hybrid. For this reason *ex-situ* synthesis offers a higher degree of control on the means of interaction between the nanoparticles and CNTs, which is a requisite for the bottom-up synthesis of nanostructures based on polymer-nanomaterial interactions. From the wide variety of colloidal methodologies for the synthesis of nanoparticles, thermal decomposition of metal precursors in the

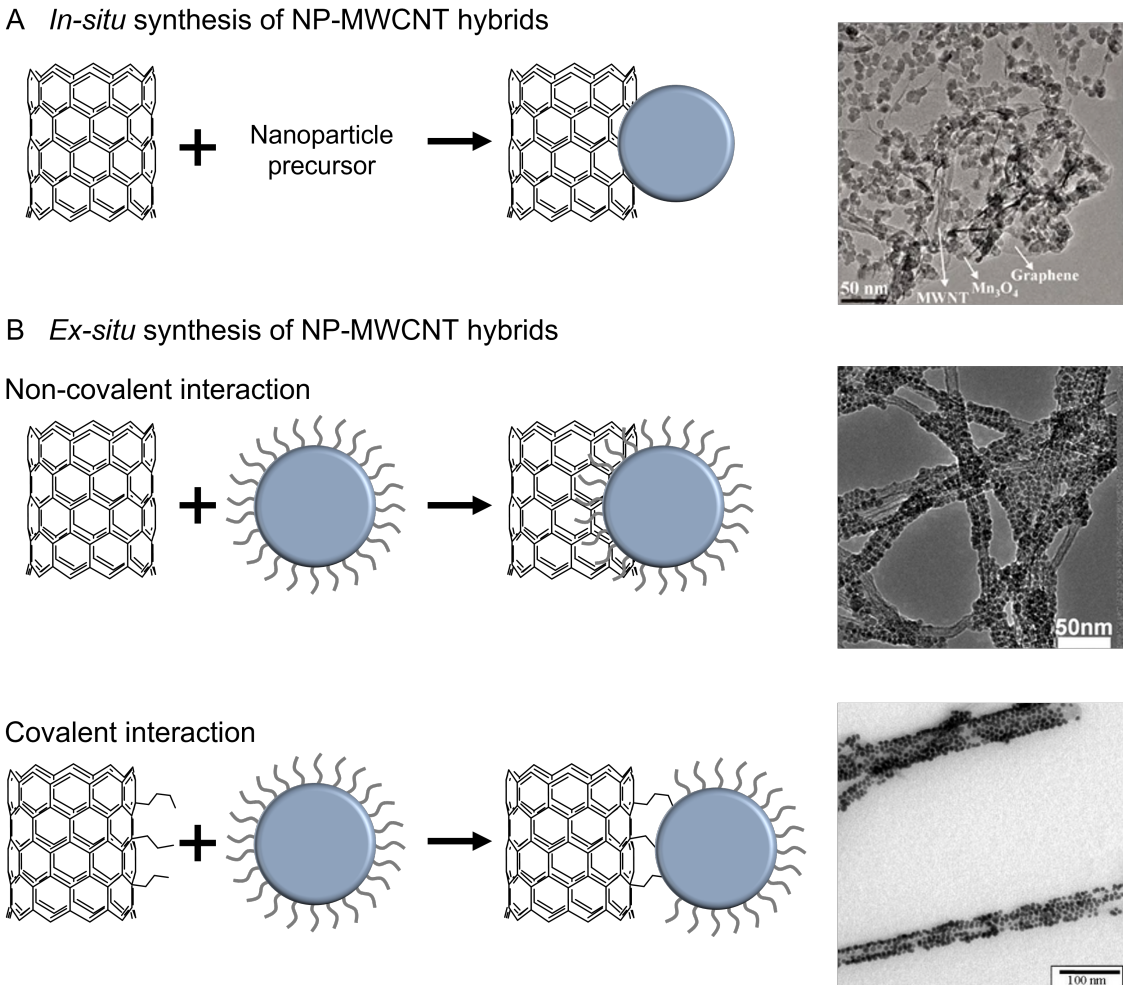


Figure 5.1: *Scheme representing the A) in-situ and B) ex-situ synthesis of nanoparticle-MWCNT hybrids. It can be noted that a higher degree of control in the nanoparticle shape and size distribution is obtained in in-situ methods in comparison to ex-situ methods. Adapted from Ref.[144] with permission from The Royal Society of Chemistry. Adapted with permission from Xianglong Li, Yi Jia, and Anyuan Cao ACS Nano 2010 4 (1), 506-512[145], ©2010, American Chemical Society. Adapted by permission from: Springer Nature, Nano Research, "Engineering manganese oxide/nanocarbon hybrid materials for oxygen reduction electrocatalysis" Feng, Ju et al.* [146] *©2012.*

presence of surfactants offers the highest degree of control in size, morphology and chemical composition of colloidal nanoparticles [88]. In addition, the surfactant passivating layer can be post-synthetically substituted for a wide range of molecules allowing for the control of the surface chemistry of the nanoparticles.

The second step for the *ex-situ* synthesis of nanoparticle-CNT hybrids consists of assembling the nanoparticles and CNTs by modulating their interactions through physical or chemical interactions. In general this step can be classified into covalent

or non-covalent methodologies depending on the nature of the interactions linking the nanoparticle to the surface of the CNT as depicted in Figure 5.1B. In the covalent approach the CNTs have to be modified with chemical functionalities that can either interact directly with the core of the nanoparticle by substituting the ligands stabilising the surface of the particle, or by adding a functional group capable of creating a covalent bond between the CNT surface and the ligands coating the nanoparticles. On the other hand, non-covalent methodologies rely in electrostatic and dispersive forces to create a weaker intermolecular interaction between the surface of the CNTs and the nanoparticle ligands or their core.

It is important to note that non-covalent interactions between the nanoparticles and CNTs will also be present when covalent methodologies are used [147]. However, it is understood that in the covalent approach the contribution that directs the functionalisation will be the formation of a chemical bond between the nanoparticle and CNT. It is difficult to compare the effectiveness between covalent and non-covalent methodologies due to the fact that in covalent methodologies the CNTs and nanoparticles are also subjected to non-covalent interactions between them. However, certain differences can be observed between the two approaches. First, the use of a covalent methodology will inevitably lead to a disruption of the properties of the CNTs due to the introduction of chemical functionalities into the sp^2 lattice of the CNTs [107]. Thus, non-covalent methodologies should be preferred when affecting the properties of the CNTs is detrimental for the application of the nanoparticle-CNT hybrid.

Secondly, covalent methodologies can provide a stronger interaction between the CNTs and nanoparticles with a higher degree of irreversibility. Experimental and theoretical evidence has shown that covalent methodologies create a chemical bond between CNTs and nanoparticles that is energetically stronger than non-covalent forces, thus providing a robust interaction that presents higher stability [147]. In general, evidence for the higher degree of irreversibility of the interaction between

nanoparticles and CNTs studies is based on the observation that the nanoparticle-CNT hybrid will not decouple after washing or sonication procedures [148, 149, 3]. However, non-covalent forces can create an interaction that is stable through washing and sonication procedures in a similar fashion to what it was observed for MWCNTs and PS in Chapter 3 [147].

Finally, covalent methodologies are based on interactions between CNTs and nanoparticles localised in sections of the CNT surface that have been chemically modified. This non-homogenous interaction through the CNT surface arises due to the fact that the chemical functionalities used to link the nanoparticles with the CNTs will be more likely localised in defect points, which will not have necessarily a homogeneous distribution in the CNT structure [143]. Thus, covalent methodologies can lead to the fabrication of nanoparticle-CNT hybrids that present an uneven interaction of the nanoparticles through the surface of the CNTs. This observation has been demonstrated previously through microscopic analysis of nanoparticle-CNT hybrids prepared via the oxidation of CNTs by different methods[150] and by protecting the CNT sidewall to oxidation creating hybrids where the caps show a striking difference in coverage in comparison to the bulk of the CNTs [151]. On the other hand, non-covalent approaches tend to be more continuous along the CNT surface when the chemical structure of the CNT has not been modified prior to the synthesis of the nanoparticle-CNT hybrid [152]. The reason behind this is that the surface physical and chemical properties will be on average constant along the CNT. The effectiveness of covalent and non-covalent methods will depend on the specific procedure of synthesis of the nanoparticle-CNT hybrid. However, it has been experimentally demonstrated that both methods can potentially present a similar degree of coverage of the CNT surface with nanoparticles [147].

Covalent and non-covalent approaches should be used depending on the end application of the nanoparticle-CNT hybrid. The ex-situ synthesis through covalent interactions has dominated the literature, mainly due to the fact that covalent

methods present a stronger interaction between the nanoparticle and the CNT. On the other hand, non-covalent approaches offer a more straight forward approach for the design of nanoparticle-CNT hybrids and have a smaller impact in the inherit properties of the CNTs. The literature on this topic shows that both non-covalent and covalent methodologies are suitable for the bottom up synthesis of hierarchical nanostructures based on CNTs and nanoparticles. However, the topic that has been discussed through this Thesis is the use of polymers as molecules to modulate the interactions between MWCNTs and other materials to create hierarchical nanostructures. As concluded in Chapter 3 non-covalent methodologies proved to be more efficient in comparison to the covalent methods used during the study. For this reason I will be focussing on the ex-situ synthesis of nanoparticle-CNT hybrids through non-covalent interactions mediated by polymers or other organic molecules. I believe that understanding the non-covalent interactions between CNTs and nanoparticles is key for the progress of ex-situ synthesis of this materials, and it would have an impact for both non-covalent and covalent approaches. For an in-depth discussion of ex-situ synthesis of nanoparticle-CNT hybrids through covalent methods the reader is referred to the following reviews [148, 143].

5.1.3 Ex-situ synthesis of nanoparticle-CNT hybrids through non-covalent interactions

In general, the forces that direct the formation of nanoparticle-CNT hybrids through non-covalent interactions have been classified as electrostatic [153], hydrogen bond [154], $\pi - \pi$ [152, 155], Van der Waals [147], solvophobic [156] and charge transfer interactions [157]. This classification has been established by different authors depending on the chemical structures that are believed to drive the functionalisation of the CNT surface with nanoparticles. The arguments given in most reports are based on the logical reasoning of the authors and normally provide limited or no

evidence to support their claims. Although these hypothesis should not be undervalued, the whole range of interactions involved between the CNTs and nanoparticles should be consider to understand the driving forces involved during the synthesis of nanoparticle-CNT hybrids.

In a seminal study Sainsbury *et al.* [147] proposed a model to calculate the interaction energy between nanoparticles and MWCNTs for the *ex-situ* synthesis of gold nanoparticle-MWCNT (AuNP-MWCNT) hybrids. In their model they proposed that the energy of the non-covalent interaction between AuNPs and CNTs would be equal to the sum of the attractive Van der Waals and charge transfer interactions, and the repulsive osmotic, elastic and non-elastic interactions. By modelling the value of the interaction energy in terms of nanoparticle-MWCNT distance they proposed a model to calculate the interaction energy profiles between MWCNTs and nanoparticles that was dependent on their chemical surface composition (Figure 5.2B). For their model, Sainsbury *et al.* hypothesised that the interactions between MWCNTs and nanoparticles took the form of a reversible equilibrium where the nanoparticles could attach and detach from the MWCNT surface (Figure 5.2C). The strength of the interaction energy between the AuNPs and MWCNTs determined the degree of reversibility of the interaction, since the interaction profiles that had deeper energy wells would create AuNP-MWCNT hybrids where the detachment of AuNPs from the surface of the MWCNTs had a larger energy barrier to overcome. In this way, the value of the interaction energy between nanoparticle and MWCNT at the minima of the profile could be used to calculate a theoretical surface coverage, based on the probability for the nanoparticle to overcome the energy barrier of interaction.

In the same study, Sainsbury *et al.* [147] tested the predictions of their theoretical models by studying the degree of coverage of AuNPs observed for synthesised AuNP-MWCNT hybrids. For the synthesis of the AuNP-MWCNT hybrids they used tetraoctylammonium bromide (TOAB) coated AuNPs in combination with pristine

MWCNTs, or alkyl-modified MWCNTs with molecules with different lengths as depicted in Figure 5.2A. The theoretical predictions of the degree of coverage of TOAB coated AuNPs at the surface of MWNCTs predicted a 80% or higher surface coverage for pristine nanotubes and alkyl-modified MWCNTs with alkyl chains with 4 or less carbons, a quick decrease to approximately 50% in the theoretical surface coverage for alkyl-modified MWCNTs with alkyl chains with 5 carbon atoms, and a less than 10% surface coverage for alkyl-modified MWCNTs with alkyl chains with

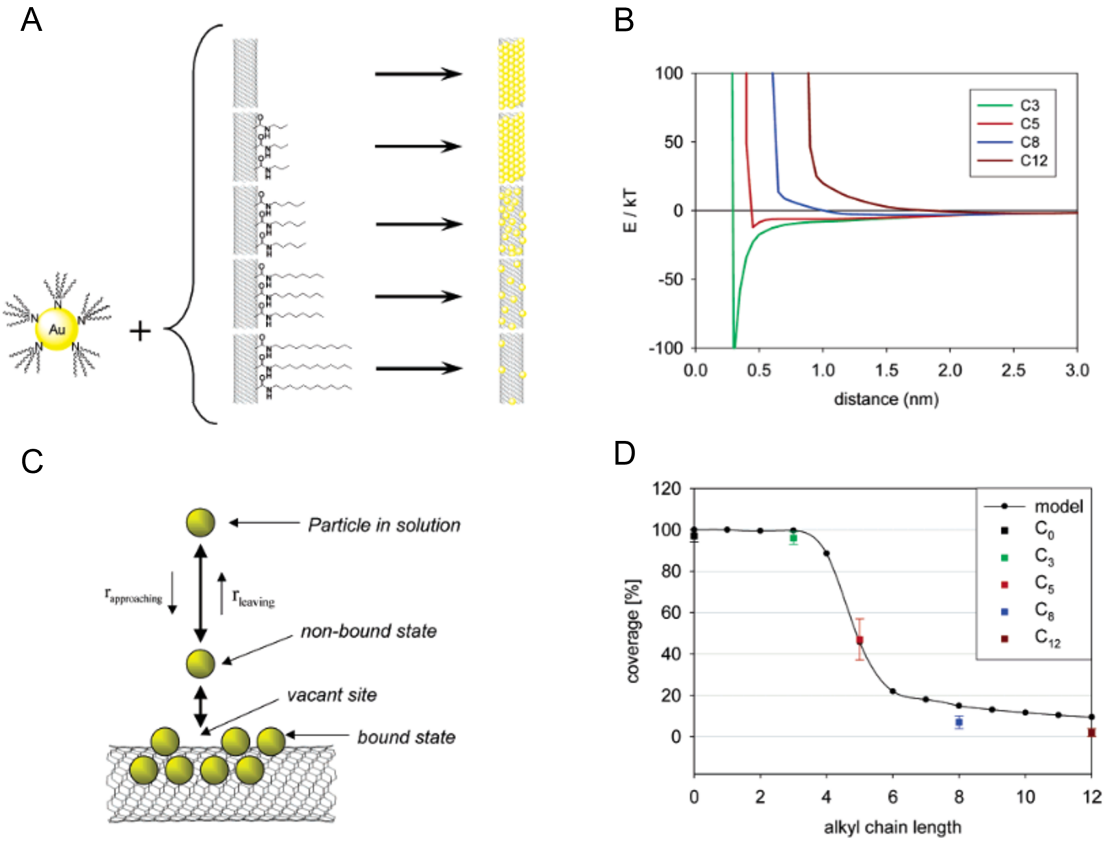


Figure 5.2: *Summary of findings by Sainsbury et al. A) Scheme representing the experiments where MWNCTs functionalised with alkyl chains of different lengths were used to modulate the interactions of MWCNTs with AuNPs. B) Plot of the interaction energy between MWCNTs and AuNPs at different distances. The energy minima shifts to more positive values when longer alkyl chains are present. C) Scheme representing the equilibria between unbound and bound AuNPs during synthesis. D) Comparison of the percentage coverage of AuNPs on MWNCTs from the theoretical model and the experimental values of AuNP-MWCNT with different alkyl chains. Adapted with permission from: Copyright Toby Sainsbury et al.,The Journal of Physical Chemistry B, 2005 109 (34), 16310-16325[147], ©(2005), American Chemical Society*

8 or more carbon atoms. As it can be observed in (Figure 5.2D) the experimental results where in very close proximity to their experimental predictions. This evidence showed that the Van der Waals and charge transfer interactions between MWCNTs and AuNPs decreased rapidly when the distance between the nanoparticle and MWCNT increased. Thus, longer alkyl chains on the surface of the MWCNTs caused an increase of the distance of interaction between the AuNPs and the surface of the MWCNT, thus decreasing their attractive interactions.

The research carried by Sainsbury *et al.* demonstrated the predictive capability of evaluating the interactions between nanoparticles and CNTs for the synthesis of nanoparticle-CNT hybrids. However, the study only focused on the interactions between the nanomaterials and did not consider other thermodynamic implications that can have an impact in the free energy of the system such as the solvent used during the synthesis of the hybrids. Rance and Khlobystov [158] reported that solvents do have an impact on the synthesis of AuNP-MWNCT hybrids. In their study, dodecanethiol coated Au nanoparticles (DDT-AuNPs) were used to synthesise AuNP-MWCNT hybrids in different organic solvents. In their study they explained that both MWCNTs and DDT-AuNPs are known to have negative surface charges creating an inherent electrostatic repulsion. They argued that the attractive Van der Waals and solvophobic forces between the nanoparticles and MWCNTs had to overcome the electrostatic repulsion inherit to their surface charge, and thus manipulating the strength of this repulsion could provide control in the degree of nanoparticle functionalisation of MWCNTs. The authors saw that the amount of AuNPs attached to the surface of the MWCNTs decreased exponentially with the increase of the dielectric constant of the solvents. They rationalised this observation by considering the effect of the nanoparticle capacitance in the media. They argued that if the DDT-AuNPs were considered as isolated charged spheres located within two dielectric layers (ligand and solvent) it would be expected that an increase in the dielectric constant of the solvent would result in an increase in the localised charge

on the surface of the nanoparticles. An increase in the localised negative charge on the surface of the AuNPs nanoparticles would increase the repulsive electrostatic interaction between the negative charged nanoparticles and MWCNTs, thus the amount of particles interacting with the surface of the MWCNTs would be expected to decrease.

Other important parameters have been established to have an effect on the degree of functionalisation of CNTs with nanoparticles for the synthesis of nanoparticle-CNT hybrids. In particular, the diameter of the nanoparticle and CNT has been demonstrated to have a considerable impact on the degree of nanoparticle functionalisation of CNTs. Rance et al. [159] studied the impact on the functionalisation of MWCNT with citrate stabilised AuNPs (Cit-AuNPs) when the nanoparticle diameter, MWCNT diameter and length was varied. Their results showed that the property that had a larger impact was the MWCNT diameter, where MWCNTs with larger diameters displaying a higher affinity for the Cit-AuNPs. They argued that the observation of an increase in the degree of functionalisation as the diameter of the MWCNT became larger was due to the higher polarisability of the electronic structure of the MWCNT. This in turn would lead to stronger Van der Waals interactions between the nanomaterials.

More research is required to unlock the full potential of the bottom-up synthesis of nanoparticle-CNT hybrids. The results presented in Chapter 3 demonstrated the importance of the solvent role in the degree of polymer functionalisation of MWCNTs due to the solvophobic interactions between the MWCNTs and the solvent media. Herein we present a similar analysis for the synthesis of IONP-MWCNT hybrids. First we will detail the synthesis and characterisation of OA coated IONPs (OAIONPs) and the ligand exchange to obtain PSIONPs. Afterwards we will discuss the impact that the ligand and the solvent has on the degree of functionalisation of MWCNTs with IONPs. My results are discussed and compared with the findings of Sainsbury and Rance. Finally I will study how the morphology of the PSIONP-

MWCNT hybrids is affected by varying the diameter of the MWCNTs and the concentrations of starting materials during synthesis.

5.2 Materials and Methods

5.2.1 Chemicals

Iron (III) acetylacetonate ($\geq$ 99.9% trace metals basis), oleylamine (technical grade 70%), Ethanol (puriss.), tetrahydrofuran (HPLC grade $\geq$ 99.9%), dichloromethane (DCM,$\geq$ 99.98%) and toluene (HPLC grade $\geq$ 99.99%) used for the nanoparticle synthesis, ligand exchange and nanoparticle functionalisation of 10nmMWCNTs were purchased from Sigma Aldrich.

The 10nnMWCNTs were obtained from Nanocyl (NC7000) and the 50nmMWCNTs were synthesised in-house via AACVD [115].

For details of chemicals used for the synthesis of the polystyrene ligand (PS) see Section 3.2.1.

5.2.2 Characterisation

Powder X-ray diffraction was acquired with a Rigaku Miniflex diffractometer equipped with a Cu k-alpha X-ray source.

Transmission electron microscopy images were recorded on a JEOL 3000F TEM microscope operating in an accelerating voltage of 300 or 200 kV. The samples were prepared by drop casting dispersions in organic solvents onto lacey-carbon or carbon thin-film copper grids.

FTIR spectroscopy data was acquired in a Varian Excalibur FTS 3500 FTIR spectrometer using attenuated total reflection (ATR) mode. The samples were dropped cast from concentrated solutions in different organic solvents into the ATR window of the spectrometer. The spectrum of the samples was acquired after the

volatile organic solvents had evaporated.

Themogravimetric analysis was performed under air and nitrogen atmosphere in a Perkin Elmer Diamond TG/DTA6300. Approximately 5 mg of sample was used for each experiment. For the analysis of the IONP-MWCNTs composites in air the samples were preheated from room temperature to 100 °C, where they were held in an isothermal scan for 10 minutes to remove water from the sample pan. The sample was heated at a rate of 10 °C/minute to 340 °C, where it was held in a isothermal scan for 20 minutes. Finally, the sample was heated to 800 °C at a rate of 10 °C/minute. For the analysis of nanoparticles and IONP-MWCNTs in nitrogen atmosphere, the samples were preheated from room temperature to 100 °C, where they where held in an isothermal scan for 10 minutes to remove water from the sample pan. Finally, the samples were heated at a rate of 10 °C/minute to 800 °C.

Ultraviolet-visible spectroscopy was performed in a Varian Cary 5000. The measurement of the samples were performed in quartz cuvettes.

Dynamic light scattering (DLS) characterisation was performed in a Malvern Panalytical Zetasizer Nano ZS equipped with a He-NE green laser with a wavelength of 633 nm. The analysis of the samples was performed in quartz cuvettes. Previous to the DLS analysis the solutions were characterised in UV-vis to measure the absorption of each solution at 633 nm.

5.2.3 Synthesis of polystyrene ligands

For the synthesis and characterisation of the polystyrene with a carboxylic acid pendent group ligand refer to Section 3.2.3. The molecular weight for the polystyrene molecules used in all experiments presented in this chapter was $M_n = 2459$ and $M_w = 2630$ determined by GPC. The degree of polymerisation expected for the synthesised polystyrene is approximately 24 repeat units based on the M_w. The length of a fully extended polystyrene molecule is estimated to be on average 7.4 nm in length. The root-mean-squared head to tail distance estimated for this polystyrene molecules is

3.4 nm according to the following equation:

$$R_o = (2N)^{1/2} C_\infty^{1/2} l \tag{5.1}$$

Where N represents the degree of polymerisation, C_∞ is the characteristic ratio of the polymer and l is the length of a C-C bond, which are equal to 10.8 and 0.154 nm respectively. The degree of polymerisation is multiplied by a factor of two since polystyrene monomers have two C-C bonds in their backbone.

5.2.4 Synthesis of iron oxide nanoparticles

The synthesis of iron oxide nanoparticles was conducted according to previously published methodologies [142, 160]. In a typical experiment iron (III) acetylacetonate (1 g, 3 mmol, 1 eq.) and oleylamine (30 mL) were measured an transferred to a 100mL three-necked round bottom flask fitted with an immersion-type thermocouple. The flask was connected to a Schlenk line and the thermocouple was connected to a proportional-integral-derivative (PID)-controlled heating mantle and the flask sealed with a ground-glass stopper. The mixture was evacuated under vacuum and flushed with nitrogen a total of three times. The mixture was heated under vacuum to 100 °C, the temperature was held for 30 minutes to remove any moisture from the reaction mixture. Afterwards, the mixture was heated to 300 °C and the temperature was held for 1 hour. Afterwards the reaction mixture was cooled to room temperature and ethanol (50 mL of) was added. The mixture was transferred into 3 separate centrifuge tubes and the mixture was centrifuged at 4250 rpm for 10 minutes resulting in the separation of a clear supernatant and a black pellet in the bottom of the tubes. Afterwards, the clear supernatant was discarded, ethanol (10 mL) was added to each tube and the solid pellets were sonicated for 5 minutes. The mixture was centrifuged at 4250 rpm for 5 minutes, the clear supernatant was discarded and the nanoparticles were solubilised in an organic solvent.

5.2.5 Oleylamine ligand exchange to polystyrene ligand

In a typical experiment PS in toluene (5 mL of a 5 mg/mL solution), OAIONPs (1mL of 25 mg/mL solution) and toluene (4 mL) were mixed and left stirring at room temperature for 24 hours. The mixture was transferred to a centrifuge tube and precipitated by adding ethanol causing the aggregation of the nanoparticles. The mixture was centrifuged for 10 minutes at 4025 rpm, the supernatant was discarded and the solid pellet of OAIONPs was redispersed in toluene (500 μL). To wash the unbind polystyrene from the sample, the nanoparticles were washed by adding ethanol (500 μL), followed by centrifugation at for 10 minutes at 4025 rpm. The supernatant was discarded and the solid pellet of OAIONPs was redispersed in toluene (500 μL) and washed using the same procedure for a total of five repetitions. Finally, the nanoparticles were dried using a nitrogen air gun and dispersed in a desired organic solvent (DCM, THF or toluene).

5.2.6 Synthesis of IONP-MWCNT hybrids

In a typical experiment for the non-covalent nanoparticle-functionalisation of MWCNTs with iron oxide nanoparticles consisted in mixing 10nm-MWCNT (5 mg), IONP solution (1 mL) in an organic solvent (DCM, Toluene or THF) with a concentration approximately 25 mg/mL and the corresponding solvent toluene, DCM or THF (4 mL). The mixture was ultrasonicated for 1 hour. Afterwards the mixture was vacuum filtered and washed 3 times with solvent (10 mL). The solid filtrate was redispersed in solvent (20 mL) and ultrasonicated for 15 minutes, filtered and washed 3 times with solvent (10 mL). This procedure was repeated three times in total.

5.2.7 Study of overall concentration of IONP and MWCNTs for the synthesis of IONP-MWCNTs hybrids

For the study of the overall concentration of IONP and MWCNTs for the synthesis of IONP-MWCNTs composites the weight ratio between IONPs and MWCNTS was kept to a 1:1 ratio. For a typical experiment 4 dispersions with a concentration 0.2 mg/mL, 0.1 mg/mL, 0.05 mg/mL and 0.025 mg/mL of MWCNTs (50nm-MWCNTs or 10nm-MWCNTs) and IONP (OA-IONP and PS-IONP) in THF were prepared. In a vial a MWCNTs dispersion (500 μL) was left under sonication for 5 minutes. Afterwards, IONPs solution (500 μL) was added drop-wise and left under ultra-sonication for 5 minutes. The solid was collected at the bottom of the vial with a magnet. The supernatant was removed and THF (1000 μL) was added.

5.2.8 Study of concentration of iron oxide nanoparticle for the synthesis of IONP-MWCNTs hybrids

For the study of the concentration of IONPs for the synthesis of IONP-MWCNTs composites the weight ratio between IONPs and MWCNTS was varied from a 0.33:1, 1:1 and 3:1 ratios. For a typical experiment 3 dispersions with a concentration 0.017 mg/mL, 0.05 mg/mL and 0.15 mg/mL of IONP (OA-IONP and PS-IONP) and a dispersion with concentration of 0.05 mg/mL of MWCNTs (50nm-MWCNTs or 10nm-MWCNTs) in THF were prepared. In a vial a MWCNTs dispersion (500 μL) was left under sonication for 5 minutes. Afterwards, IONPs solution (500 μL) was added drop-wise and left under sonication for 5 minutes. The solid was collected at the bottom of the vial with a magnet. The supernatant was removed and THF (1000 μL) was added.

5.2.9 PSIONP area coverage analysis of PSION-50nmMWCNT hybrids

ImageJ was used to process the TEM images of PSIONP-50nmMWCNT hybrids to calculate the are coverage of PSIONP on the surface of 50nmMWCNTs. The analysis consisted in removing the pixels occupied by PSIONPs on the surface of 50nmMWCNTs. Sections of 50nmMWCNTs with 200nm of length where selected for each measurement. Afterwards the area fraction of PSIONPs was calculated by measuring the area fraction of deleted pixels from the analysed section of 50nmMWCNTs in the image. For each sample 20-30 sections of MWCNTs were used for the analysis. An example of a processed image can be found in Appendix C C.8.

5.3 Results and discussion

5.3.1 Synthesis of nanoparticles and ligand exchange

Iron oxide nanoparticles (IONPs) where synthesised via the thermal decomposition of iron (III) acetylacetonate ($Fe(Acac)_3$) in oleylamine (OA) based on a method reported previously within our research group [142]. The reaction consists of the decomposition of $Fe(Acac)_3$ at temperatures above 180 °C into iron oxide nuclei. The growth of the iron oxide nuclei to IONPs is modulated by the attachment of OA molecules to their surface through coordination bonds with the iron ions. Finally, when the growth stage is finished the product is OA coated IONPs (OAIONPs) with a small size distribution. The OA coating acts as a surfactant that avoids the aggregation of particles by providing steric stabilisation. In addition, the OA layer also determines the surface chemistry of the particles allowing for the dispersion of the IONPs in a wide variety of non-polar organic solvents. The concentration of $Fe(Acac)_3$ precursor to OA has been demonstrated to modulate the final size of the nanoparticles [142], with the conditions used in this study the nanoparticles presented an average size of 7.7±1.8 nm. The synthesised OAIONPs were dispersed in THF, toluene and DCM. The TEM micrographs and size distribution of the particles are presented in Figure 5.3. As it can be observed after synthesis the particles were well dispersed in all solvents, not showing signs of aggregation. In addition, the size distribution of the particles in all solvents was similar.

The crystal phase composition of the nanoparticles was characterised by powder X-ray diffraction (PXRD). In Figure 5.4 the PXRD diffractogram of the OAIONPs is presented, the pattern and intensity of the peaks is consistent with the iron oxide spinel ferrite structure. Iron oxide presents two different crystal phases with a spinel ferrite structure known as maghemite (Fe_2O_3) and magnetite (Fe_3O_4). The difference between these crystal phases is found in the oxidation states of the iron

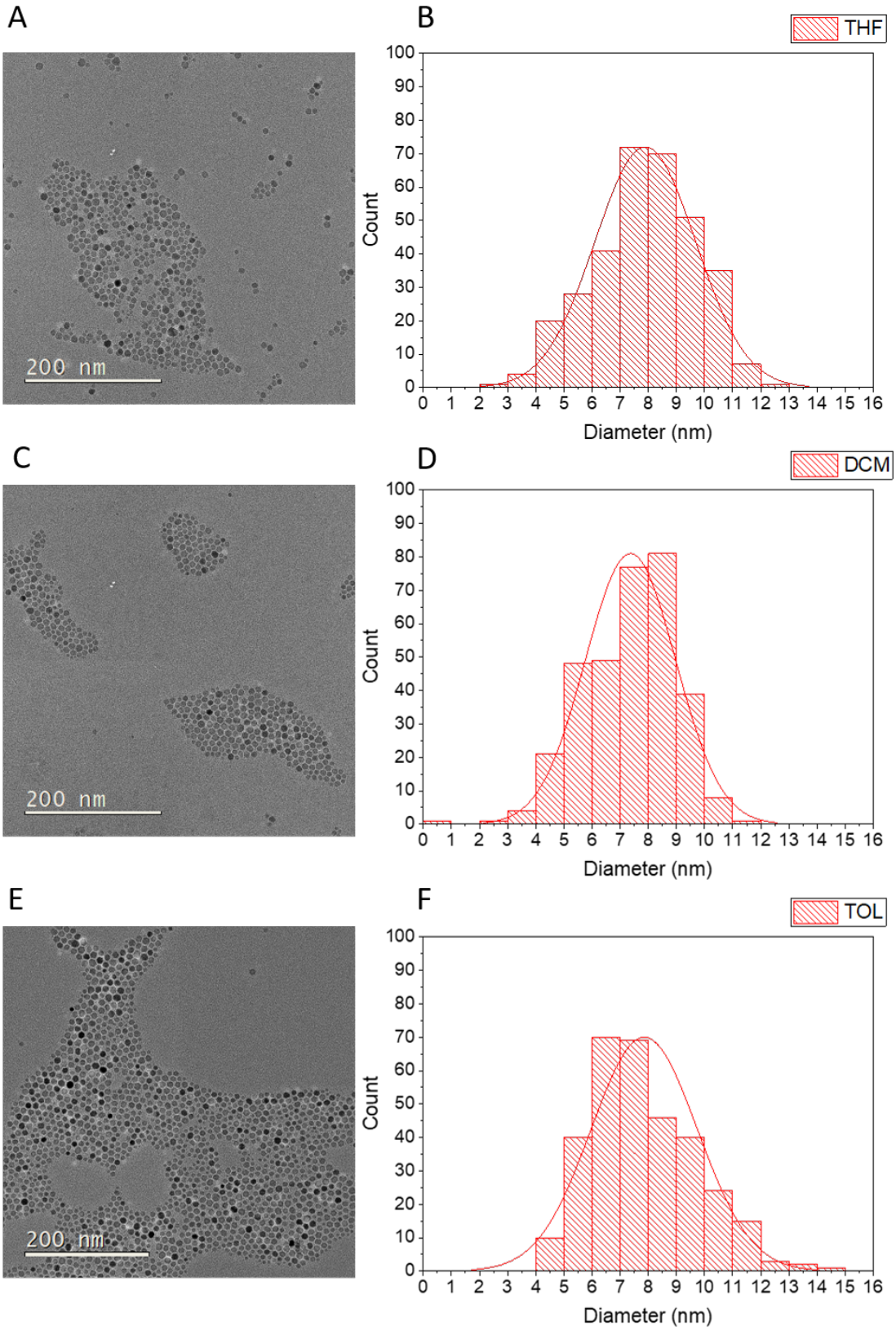


Figure 5.3: *TEM micrographs and size distribution histograms of OAIONPs from A-B) solution in THF, C-D) solution in DCM and E-F) solution in toluene.*

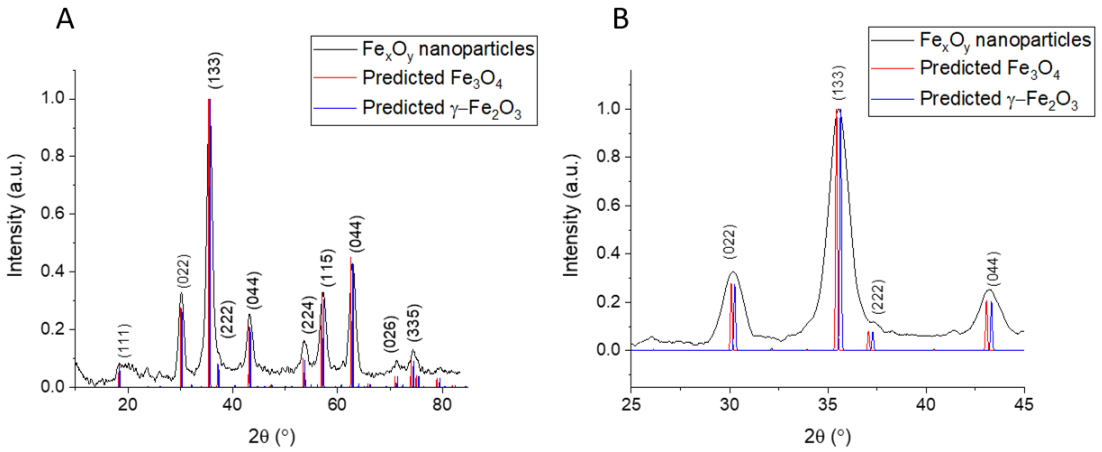


Figure 5.4: *A)PXRD diffractogram of OAIONPS consistent with spinel ferrite crystal structure B)Magnification of the position of the diffraction peaks in relation to the theoretical positions from maghemite and magnetite phase.*

ions, in maghemite the iron ions are present in an oxidation state of Fe^{3+} while in magnetite the iron ions are present as Fe^{2+} and Fe^{3+}. In Figure 5.4B a magnification of the PXRD diffractogram of the OAIONPs is presented, when compared with the theoretical crystal structure of maghemite and magnetite it can be observed that the peaks of the diffractogram are found in between the theoretical angles expected for both crystal phases. Thus, we can conclude that the nanoparticles present a mixed spinel ferrite crystal structure of maghemite and magnetite [161].

The OAIONPs were studied in DLS to understand their behaviour in solution. While the measurement of nanoparticle size with TEM provides information of the diameter of the nanoparticle inorganic core, DLS measures the hydrodynamic diameter of the particles that includes the length of the surfactant layer coating the IONPs [162]. As it can be observed in Figure 5.7, DLS analysis showed a single distribution of particles in all solvents suggesting that the OAIONPs were forming stable dispersions with no observable aggregation of the particles. The hydrodynamic diameter of the particles for all solvents where of similar size ranging in average from 9.7-10.6 nm. Using the diameter obtained from TEM measurements and the hydrodynamic diameter obtained from DLS we calculated the surfactant height (h) of the particles. The height of the surfactant layer for OAIONPs ranged from 2.0-2.9 nm, suggesting

that the OA is indeed coating the nanoparticles in solution and providing effective steric stabilisation to the particles. The length of a oleylamine molecule ranges between 1.5-1.7 nm, the fact that the oleylamine height observed for the average OAIONP was larger than the length of an oleylamine molecule strongly suggests that the ligand sphere coating the nanoparticles is likely to be larger than a single oleylamine layer.

To attach PS chains into the surface of the IONPs, the particles were subjected to a ligand exchange procedure where the OA coating of the OAIONPs was exchanged for PS ligands to render PS coated IONPS (PSIONPs). The procedure involved mixing the OAIONPs with PS molecules synthesised via ATRP that presented carboxylic acid end groups, the weakly bound OA was displaced by the PS molecules thanks to a more thermodynamically robust coordination bond between the carboxylate end group and the iron ions at the surface of the particle [163]. The ligand exchange was performed in toluene and redispersed in either THF, DCM or toluene. Figure 5.5 shows the TEM micrographs and size distributions of the IONPs after the ligand exchange procedure. It can be seen that after the ligand exchange the particles did not form agglomerates, presenting a similar morphology and size distribution.

FTIR analysis before and after the ligand exchange procedure demonstrates the successful displacement of OA ligands with PS. In Figure 5.6 it can be observed that the FTIR spectrum significantly changed after the ligand exchange for the samples regardless the solvent where the OAIONPs were dispersed. This is more clearly observed in Figure 5.6B,D&F, where it can be observed that after the ligand exchange procedure there is the presence of characteristic polystyrene signals such as the C-H aromatic stretch peaks in the range between 3000-3100 cm^{-1}, three aromatic C=C stretch in the range between 1450-1600 $cm^{-}1$, and the C-H aromatic out-of-plane bending peaks in the range between 675-900 cm^{-1} (for a full discussion in the FTIR spectra of oleylamine and PS see Appendix C Figure C.9).

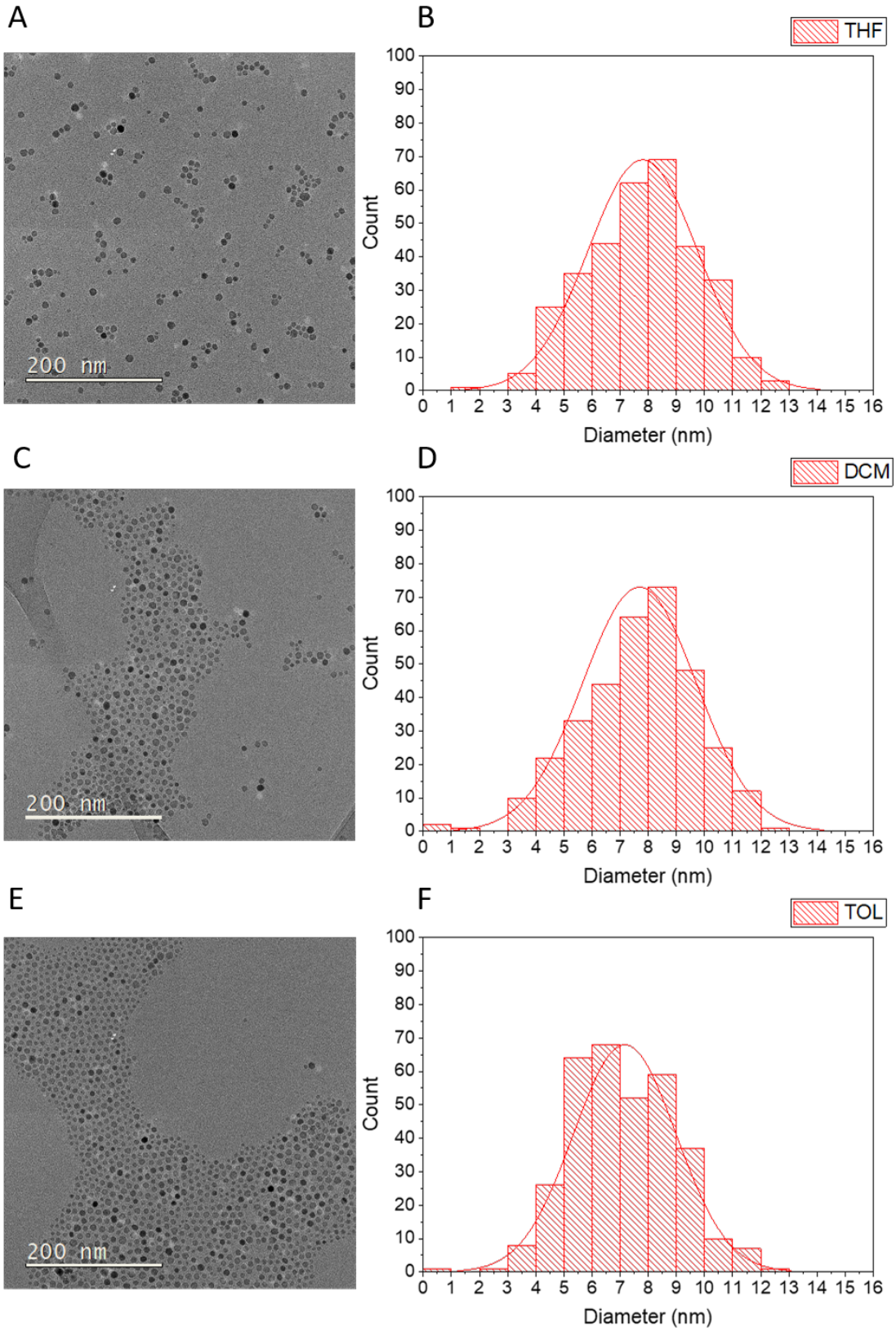


Figure 5.5: *TEM micrographs and size distribution histograms of PSIONPs from A-B) solution in THF, C-D) solution in DCM and E-F) solution in toluene.*

In addition, DLS analysis was performed on the PSIONPs after the ligand exchange to study the changes in the solvation layer of the nanoparticles (Figure 5.7). DLS demonstrated the increase of 2-3 nm of the hydrodynamic diameter in all cases suggesting that larger molecules are coating the IONPs. The height of the surfactant layer after ligand exchange was between 5.2-5.5 nm for the PSIONPs, more than twice as large in comparison to the height observed for OAIONPs. When compared with the approximate 7.4 nm length expected for a fully stretched polystyrene molecule, the height of the polystyrene ligands on the surface of the IONPs is smaller. On the other hand, the height of the polystyrene ligands is larger than the approximate 3.5 nm root-mean-squared head to tail distance of these polystyrene molecules. This suggests that the conformation of the polystyrene ligand is partially stretched. This observations are consistent with previous research that demonstrated that polymer brushes grafted from nanoparticles surfaces present a conformation where the polymer chains are stretched normal to the surface of the nanoparticle and then transition into a coiled conformation as the chains extend into the solution [164].

In addition to spectroscopic evidence supporting the ligand exchange from OAIONPs to PSIONPs, the success of the ligand exchange was also demonstrated by the change in the solubility of the IONPs in different solvents. The steric stabilisation of nanoparticles depends on the interactions between the surfactant coating and the solvent media. Unfavourable high energy interactions between solvents and the surfactants will cause the aggregation of nanoparticles to minimise the free energy of the system. Figure 5.8 presents a photograph of the dispersions of OAIONPs and PSIONPs in different organic solvents showing that OAIONPs formed stable dispersions in hexane, cyclohexane, acetone and DMF while PSIONPs did not. The stability of polymer coated particles strongly depends on the conformation of the polymer chains in solution, a stable dispersion is expected when good solvents are used that allow for the polymer chains to adopt an extended conformation. On the other hand, the aggregation of particles is expected for bad solvents where the

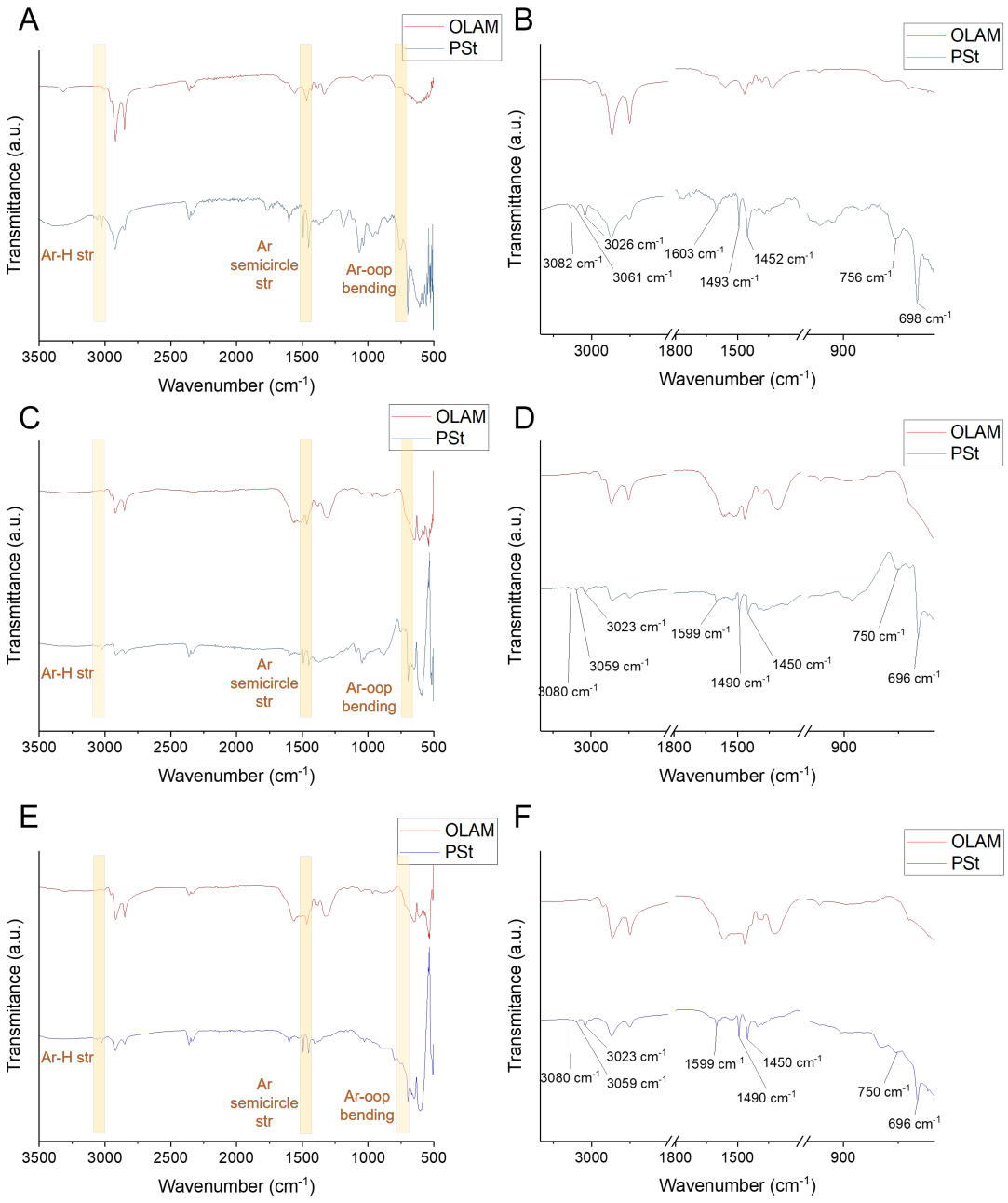


Figure 5.6: *FTIR spectra of OAIONPs and PSIONPs in A-B) THF, C-D)DCM and E-F) toluene.*

solubilised polymer chains are contracted [165]. After the ligand exchange from OA to PS the solubility behaviour of the PSIONPs was consistent with the predictions expected for polymer stabilised particles where good solvents for PS (e.g. THF, DCM, toluene, o-DCB, NMP) create stable nanoparticle dispersions while bad solvents (e.g. DMF, cyclohexane, acetone) and solvents where polystyrene is insoluble (ethanol, hexane) do not disperse the nanoparticles. In contrast, OAIONPs are soluble in all tested solvents except ethanol.

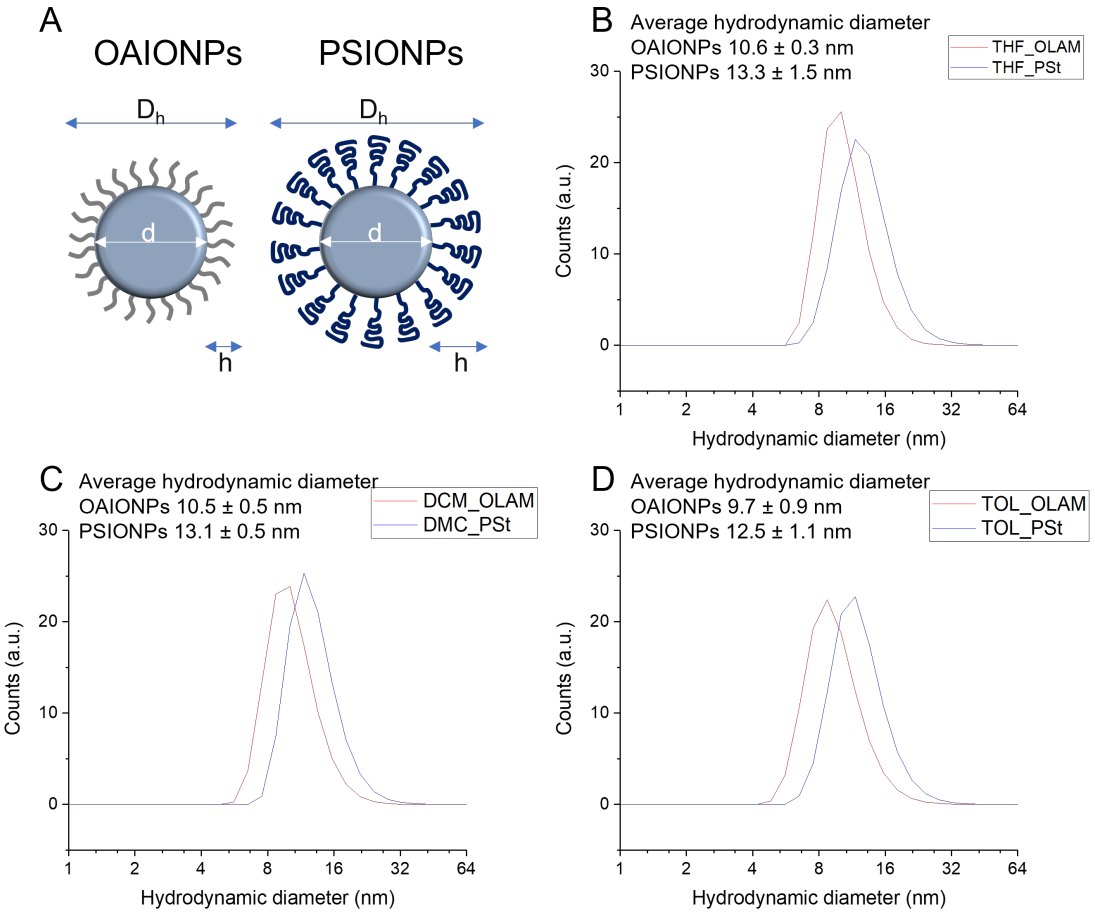


Figure 5.7: *A) Scheme representing the lengths of the core nanoparticle diameter and hydrodynamic diameter of OAIONPs and PSIONPs containing a single layer of surfactant molecules. It can be observed that the hydrodynamic diameter of PSIONPs is expected to be larger due to the longer length or ligand height observed for the polystyrene ligands. The DLS measurement of number mean hydrodynamic diameter of OAIONPs and PSIONPs in B) THF, B) DCM and C) toluene. After the ligand exchange for all solvents the hydrodynamic diameter of the PSIONPs were larger in comparison to the OAIONPs, suggesting that larger molecules are coating the surface of the IONPs.*

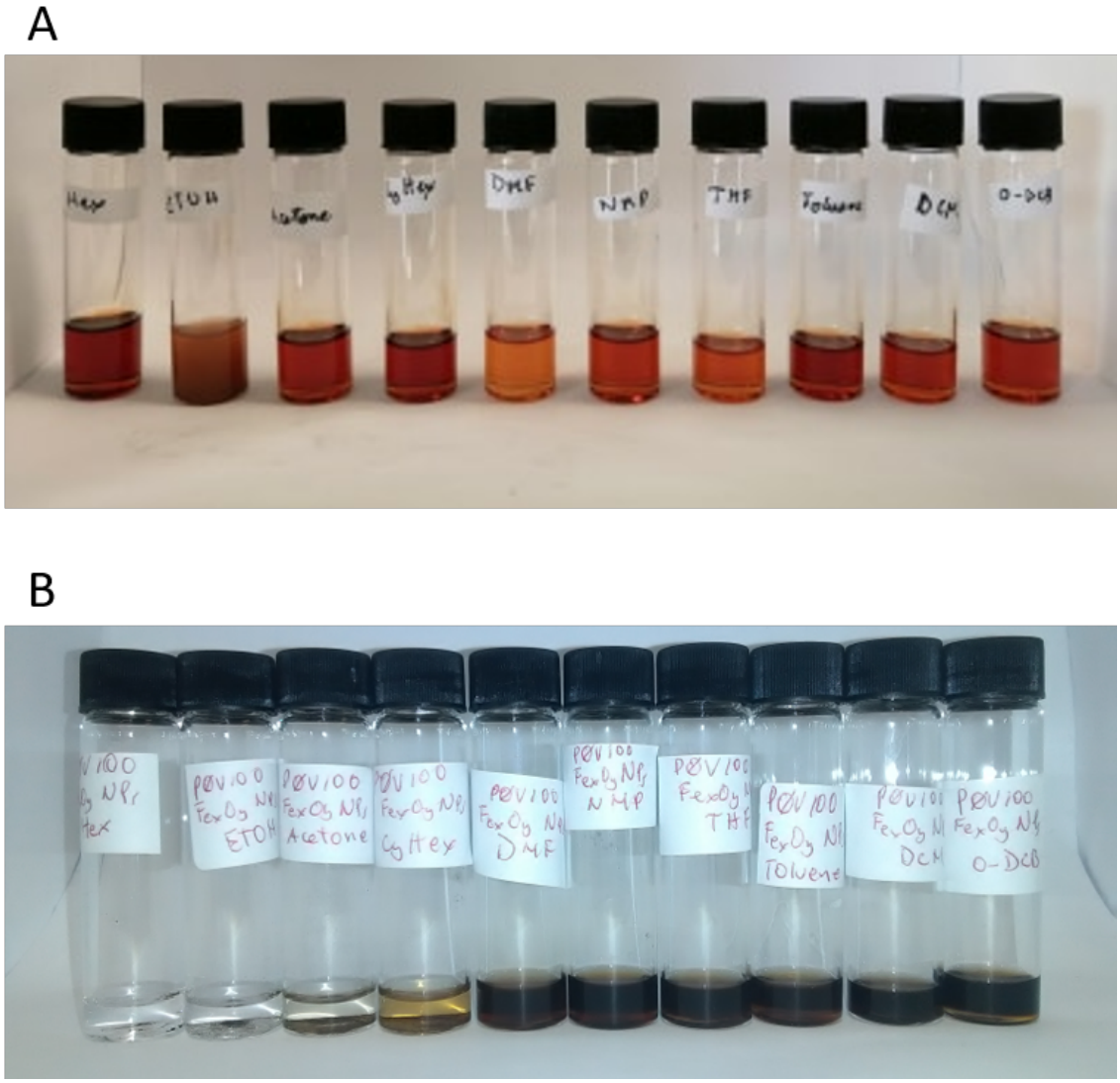


Figure 5.8: *A) Picture displaying dispersions of OAIONPs (left to right) in hexane, ethanol, acetone, cyclohexane, DMF, NMP, THF, toluene, DCM, o-DCB. The differences in colour of the samples are due to variations in the concentration of the solutions. B) Picture displaying dispersions of PSIONPs (left to right) in hexane, ethanol, acetone, cyclohexane, DMF, NMP, THF, toluene, DCM, o-DCB.*

5.3.2 Functionalisation of MWCNTs with IONPs

The functionalisation of MWCNTs with IONPs was performed by mixing under ultrasonication a mixture of IONPs (OAIONPs or PSIONPs) and 10nmMWCNTs in a 5:1 weight ratio in THF, toluene or dichloromethane. The IONP-MWCNT hybrids were filtered, redispersed in the same solvent used during the functionalisation and ultrasonicated. This washing procedure was repeated three times. After the third

wash the characteristic amber colour of IONPs in the liquid phase separated by filtration disappeared completely, suggesting that most free IONPs had been washed away from the solid phase. The IONP-MWCNT hybrids where dried and analysed in TGA to obtain the composition of the samples.

First I performed TGA on the nanoparticle samples to determine the conditions to obtain the composition of ligands, nanoparticles and MWCNTs in the hybrids. Figure 5.9A and B shows the TGA temperature profiles under air and nitrogen atmosphere of OAIONPs and OAIONP-10nmMWCNT hybrids. For OAIONPs, the TGA curve under air atmosphere presents a large weight-loss between 200-500 °C of approximately 60% that can be attributed to the oxidation of the organic ligands to carbon dioxide. In contrast under nitrogen atmosphere two different weight-losses are observed. The first weight-loss of approximately 33% is observed at temperatures bellow 500 °C. This weight-loss has been reported previously to be linked to the partial decomposition of the OA ligands into smaller hydrocarbons and the formation of graphitic carbon catalysed by the presence of iron oxide nanoparticles [166]. A second 25% weight-loss it is observed at temperatures between 600-700 °C, resulting in a final weight percentage comparable to the analysis in air. Thus, the second weight-loss could be attributed to the redox reaction between graphitic carbon and iron oxide to produce iron and carbon dioxide [167]. The fact that there is a decomposition of graphitic carbon under nitrogen atmosphere due to the presence of the IONPs makes it possible that the same reaction could occur with MWCNTs when the IONP-10nmMWCNT hybrids are analysed, which would introduce uncertainty about the ligand/MWCNT composition in the hybrids.

Considering the impediments set by redox reaction between iron oxide and carbon at high temperatures under inert atmosphere, the TGA of the samples was performed under air with two heating profiles that aimed to decouple the oxidation of the organic ligands and the 10nmMWCNTs. Figure 5.10A and B show the TGA time profiles for the analysis of the OAIONP-10nmMWCNTs composites. A first

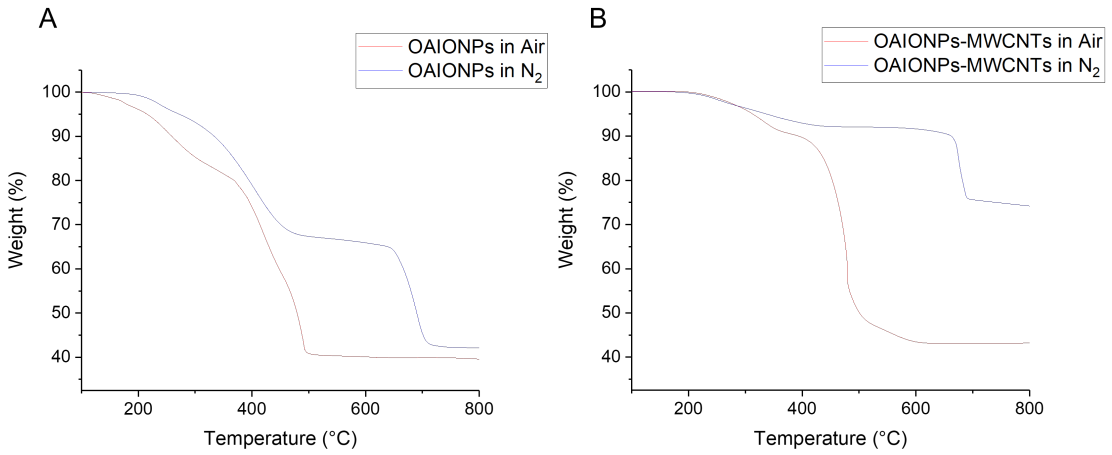


Figure 5.9: *TGA analysis of the samples OAIONPs in nitrogen and air atmosphere.*

heating step from 100 to 340 °C was performed, the temperature was held at 340 °C to fully decompose the OA ligands present in the sample. Afterwards a second heating step to 800 °C was used to oxidize the remaining MWCNTs. The same TGA profile was used for the analysis of PSIONP-10nmMWCNT hybrids (Figure 5.10C and D). The determination of the weight content of ligands, MWCNTs and iron oxide in the samples is described in Figure 5.10B and D. The first observed weight loss corresponds to the organic ligands in the nanoparticles (OA or PS), the second weight loss correspond to the 10nmMWCNT content in the sample and the remaining weight corresponds to iron oxide. In addition, we could calculate the nanoparticle composition by adding the compositions corresponding to the organic ligands and iron oxide.

The summary of the TGA results is presented in Table 5.1. The TGA provided us a detailed examination of the composition of ligands, MWCNTs and iron oxide content of the IONP-10nmMWCNTs hybrids. In addition to the values directly obtained from the TGA profiles, we estimated the IONP weight composition in the samples (by adding the weight percentage of the ligands and IO), the IO to MWCNT ratio (IO:MWCNT) and the IONP to MWCNT ratio (IONP:MWCNT). The results show that there is a strong dependency between the solvent medium used during the synthesis and the amount of IONPs found in the hybrids. Moreover, the relatively

small standard deviation (i.e. $\leq$20%) observed in the experiments strongly indicates that the solvent medium has a characteristic degree of functionalisation that can be clearly observed in the change of IO:MWCNTs ratio between samples.

For the functionalisation of MWCNTs with OAIONPs, we can observe that the amount of IO in each sample changes significantly when the solvent medium is modified. It would be expected that an increase of IO content in each sample would be accompanied by an increase of the amount of oleylamine in the sample but this was not observed, the OA content remained somewhat constant disregard of the solvent used during the functionalisation. When the ratio between the composition of ligand in the TGA of OAIONPs and OAIONP-10nmMWCNT hybrids is compared, it is observed that the nanoparticles present a higher amount of OA which is likely

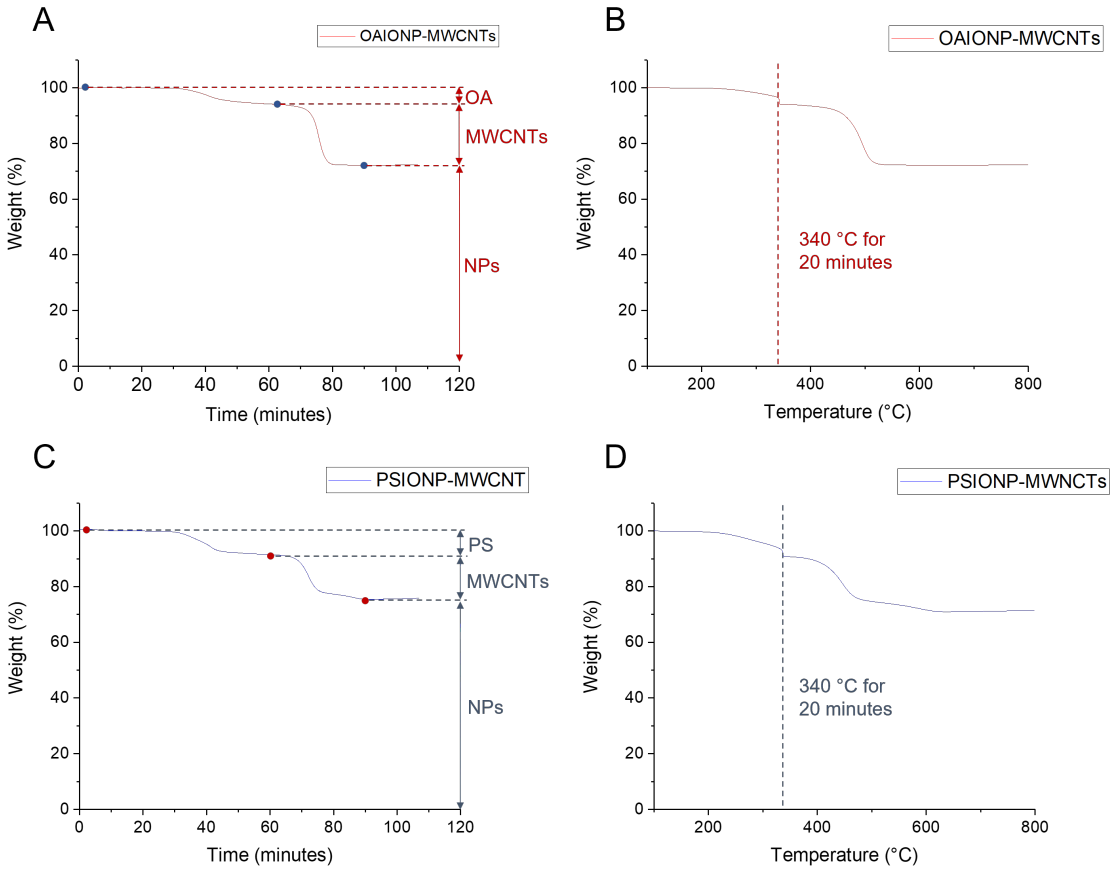


Figure 5.10: *TGA analysis of the samples. A) OAIONP-MWCNT hybrid TGA time profile. B) OAIONP-MWCNT hybrid TGA temperature profile. C) PSIONP-MWCNT hybrid TGA time profile. D) PSIONP-MWCNT hybrid TGA temperature profile.*

to be unbound from the nanoparticle surface. The excess OA might be interacting through non-covalent interactions with the MWCNTs that might have the effect of saturating the OAIONP-10nmMWCNT hybrid composition to a fixed amount. Nonetheless, the TGA results show that the amount of oleylamine present in all samples is similar and the increase on the degree of functionalisation is independent of the oleylamine content in the hybrid. Although the functionalisation of MWCNTs with oleylamine might be present in our samples and might have an important impact on the mechanisms of functionalisation, the solvent role in increasing the degree of functionalisation is clear and independent of the amounts of OA in the OAIONP-MWCNT hybrids.

Similar observations are found for the functionalisation of MWCNTs with PSIONPs where the degree of PSIONP functionalisation changed significantly depending on the solvent used during synthesis. The amount of PS ligand present in the hybrids varied depending on the solvent used during synthesis, where toluene and DCM presented similar PS composition while in THF a decreased amount was observed. However, this trend is not proportional with the IO composition since THF presented the highest amount of IO mass while presenting the smallest PS ligand content. My results demonstrate the complexity of the system, where there are four components: solvent, ligands, IONPS and MWCNTs in an equilibria where interactions between the components can happen independently form each other. The experiments performed during this study cannot provide information on the spatial

Table 5.1: *Composition of OAIONP-10nmMWCNT and PSIONP-10nmMWCNT hybrids.*

Sample	Solvent	Average ligand weight [%]	Average MWCNT weight [%]	Average IO weight [%]	Average IONP weight [%]	Average IO:MWCNT ratio	Average IONP:MWCNT ratio
OAIONP-10nmMWCNT	THF	7.5± 1.5	19.4±2.2	71.1±1.0	78.6±2.5	3.7±0.5	4.1±0.6
PSIONP-10nmMWCNT	THF	8.9± 0.3	17.8±2.0	71.5±2.4	80.4±2.45	4.1±0.6	4.6±0.6
OAIONP-10nmMWCNT	Toluene	7.5± 1.4	27.7±0.5	62.1±1.1	69.6±0.5	2.3±0.1	2.5±0.1
PSIONP-10nmMWCNT	Toluene	14.1± 1.5	25.5±1.3	57.8±1.5	71.9±1.4	2.3±0.2	2.8±0.2
OAIONP-10nmMWCNT	DCM	7.0± 0.3	22.8±2.1	67.9±2.1	74.9±2.3	3.0±0.4	3.3±0.4
PSIONP-10nmMWCNT	DCM	13.8± 0.2	28.3±2.3	55.1±2.7	68.9±2.6	2.0±0.3	2.5±0.3

conformation that the organic ligands have on the surface of the 10nmMWCNT. I expect that the organic molecules are located between the IONP core and the 10nmMWCNTs surface. However, further studies are required to evaluate how the ligands of both OAIONPs and PSIONPs are interacting with the surface of the 10nmMWCNTs. Our previous calculation of the height of the polymer ligands for PSIONPs demonstrated that the polymer chains are not fully extended, which would allow for different spatial arrangements of the polymer chains on the surface of the 10nmMWCNTs. In addition, it can be expected that the conformation of the oleylamine and polymer molecules on the surface of the MWCNTs might be different depending on the solvent media. Understanding these interactions might help to explain the variation in the composition of the ligands observed for these hybrids. Nonetheless, the solvent dependency on the degree of functionalisation is evident when we compare the IO content of the IONP-MWCNT hybrids.

The variation between ligand composition across samples seems not to be correlated with the final IO content of the composites. For this reason the IO:MWCNT ratio provides the best value for comparison of the degree of nanoparticle functionalisation of the MWCNT across all samples, since the increase in IO will always be evidence for the inclusion of more nanoparticles into the hybrid. By using the IO:MWCNT ratio to compare how the degree of functionalisation varied between PSIONPs and OAIONPs we can observe that in the case for THF and toluene there was a similar degree of functionalisation when OAIONPS or PSIONPs were used. Only in DCM there was a relevant difference, where OAIONPs displayed a larger degree of functionalisation than PSIONPs.

An interesting parameter to compare between PSIONPs and OAIONPS functionalisation was the distance between the nanoparticle core and the 10nmMWCNTs since PSIONPS had a considerably larger hydrodynamic diameter in comparison to OAIONPS. The similarity in functionalisation between OAIONPS and PSIONPs when THF and toluene where used as solvent suggest that the length of the organic

capping layer has smaller impact on the amount of nanoparticles functionalising the 10nmMWCNTs than the solvent used during the synthesis. This observation is not consistent with the reports of Sainsbury *et al.* [147] that observed a dependence on the degree of functionalisation that decreased when long alkyl-chains were present in between the MWCNT surface and AuNPs. In their report they explained that the electron-exchange interactions between the MWCNTs and the AuNPs decreased rapidly with increased distance between them, which caused a decrease in functionalisation. The fact that we still observe functionalisation of CNTs when the distance between the IONP core and the MWCNTs is large suggests that the interactions are not likely caused by direct MWCNT-IONP interaction, but through a different mechanism such as a solvophobic effect caused by the solvent-MWCNT interactions. This would explain the discrepancy between our study and Sainsbury *et al.* report, since they controlled the length of separation between the gold nanoparticle core and MWCNT by attaching alkyl chains into the surface of the MWNCTs. By changing the surface chemistry of the MWCNTs would also cause a change in the solvent-MWCNT interactions, which could hinder the solvophobic functionalisation of the MWCNTs with the AuNPs.

In the best of my knowledge the study from Rance *et al.* [158] is the only other report that has explored the role of the solvent in the interactions between nanoparticles and CNTs. As mentioned in Section 5.1.3 they explained that increasing the dielectric constant of the solvent caused an increase of the localised negative surface charge of the AuNPs that in turn increased the electrostatic repulsion with the negative charged surface of MWCNTs. I will show in the next section that my results do not correlate with this explanation since the degree of IONP functionalisation does not present any trend in relation to the dielectric constant of the solvent. Although the dielectric constant of the solvent might have an influence in the interactions between nanoparticles and MWCNT, I believe that the MWCNT-solvent interface might have a important contribution in the degree of nanoparticle functionalisation

of the MWCNTs in similar fashion to what was described in Chapter 3 and 4 for the PS-MWCNT system.

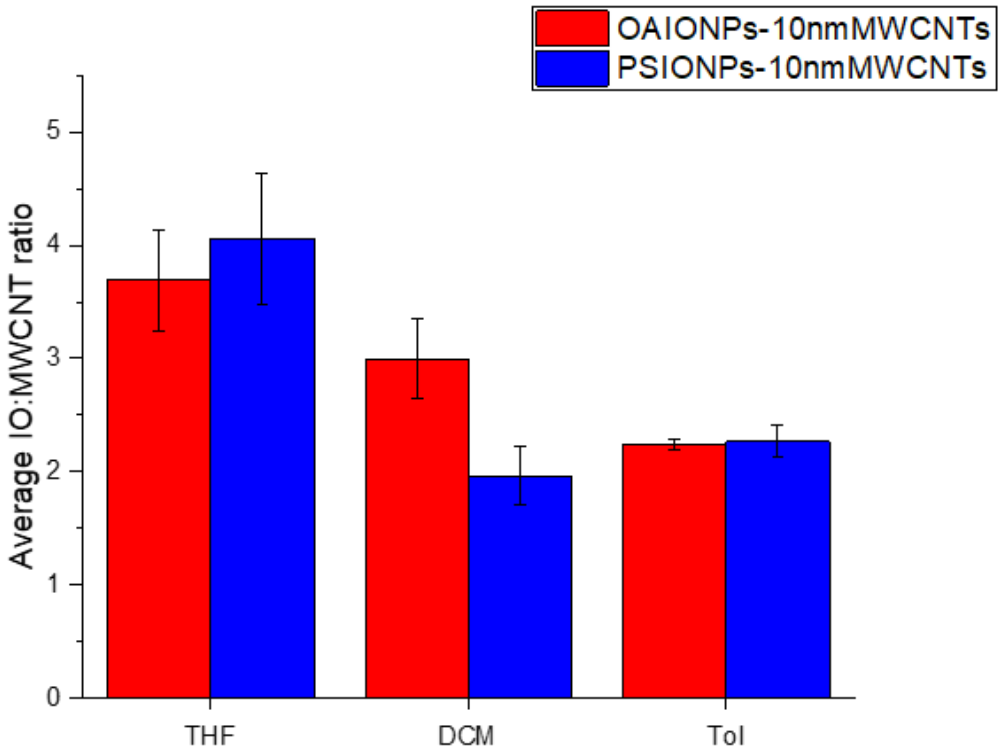


Figure 5.11: *Comparison of IO:MWCNT ratio of OAIONP-10nmMWCNT and PSIONP-10nmMWCNT hybrids prepared in THF, DCM and toluene.*

5.3.3 SEBSP for nanoparticle functionalisation

The strong dependence of the solvent medium in the functionalisation of MWCNTs with the IONPS strongly suggest that solvophobic effects play an important role mediating the interactions. Similarly to Chapter 4 the results were analysed by estimating the solvent-10nmMWCNTs interactions using the SEBSP theory. In Figure 5.12A and C the plot of IO:MWCNT weight ratio against the Hansen SEBSP distance of each solvent used for the synthesis of PSIONP-10nmMWCNT and OAIONP-10nmMWCNT hybrids is presented. It can be observed that in the case of the PSIONP-MWCNT hybrid the amount of IONPs in the hybrid increased

linearly when the Hansen SEBSP distance increased. This observations are consistent to the behaviour observed for the functionalisation of 10nmMWCNTs with polystyrene.

On the other hand, the composition of the OAIONP-10nmMWCNT hybrid was not predicted by the Hansen SEBSP distance. While the experiments performed in THF and toluene presented a correlation with the Hansen SEBSP distance, the composition of the OAIONP-MWCNT hybrid in DCM was found to have a larger amount of IONPs than what would be predicted with the Hansen SEBSP distance. The observation that the experiments made in DCM were going to be an outlier from the SEBSP distance prediction was expected since it was already demonstrated that only in DCM there was difference between the composition of the PSIONP-10nmMWCNT and OAIONP-10nmMWCNT hybrids. Therefore, there must be some unaccounted interaction occurring when DCM is used as a solvent for the synthesis of OAIONP-10nmMWCNT hybrid that should explain this behaviour.

From the substances involved in the synthesis, two unaccounted interactions could be playing a role. First, it could be that the interactions between the OAIONPs and 10nmMWCNTs are enhanced when DCM is used as a solvent. Otherwise, the DCM-OAIONP interaction is causing the increased functionalisation with the MWCNTs. The latter option seems to be more likely for several reasons. First, we can eliminate the hypothesis that the interactions between the core of the OAIONPs and the 10nmMWCNTs are increased when DCM is used as a solvent since the same observation should be expected from the synthesis with PSIONPs. The reason behind this is that the core of the PSIONPs is identical to the OAIONPs, so an interaction between the inorganic core mediated by the solvent similar to what was reported by Rance *et al.* is unlikely [158]. Another possibility is that the surface interactions between the OA ligands at the surface of the OAIONPs and the 10nmMWCNTs are improved by the presence of DCM. This hypothesis is more difficult to rebuke from the experimental evidence presented in this study. The interactions between

OA and the 10nmMWCNTs are likely to be through non-dispersive forces and there are no reasons to believe that DCM should have an effect on the ligand-MWCNT interactions that would not be also expected for PS ligands. For these reasons I am inclined to believe that the ligand-10nmMWCNT interactions are unlikely to contribute in the difference in composition of the hybrids when OAIONPs or PSIONPs are used.

On the other hand, there are experimental reasons to believe that the OAIONP-DCM interaction is responsible for the difference observed in the composition of the hybrid. As described in Section 5.3.1 the DLS and TEM characterisation of

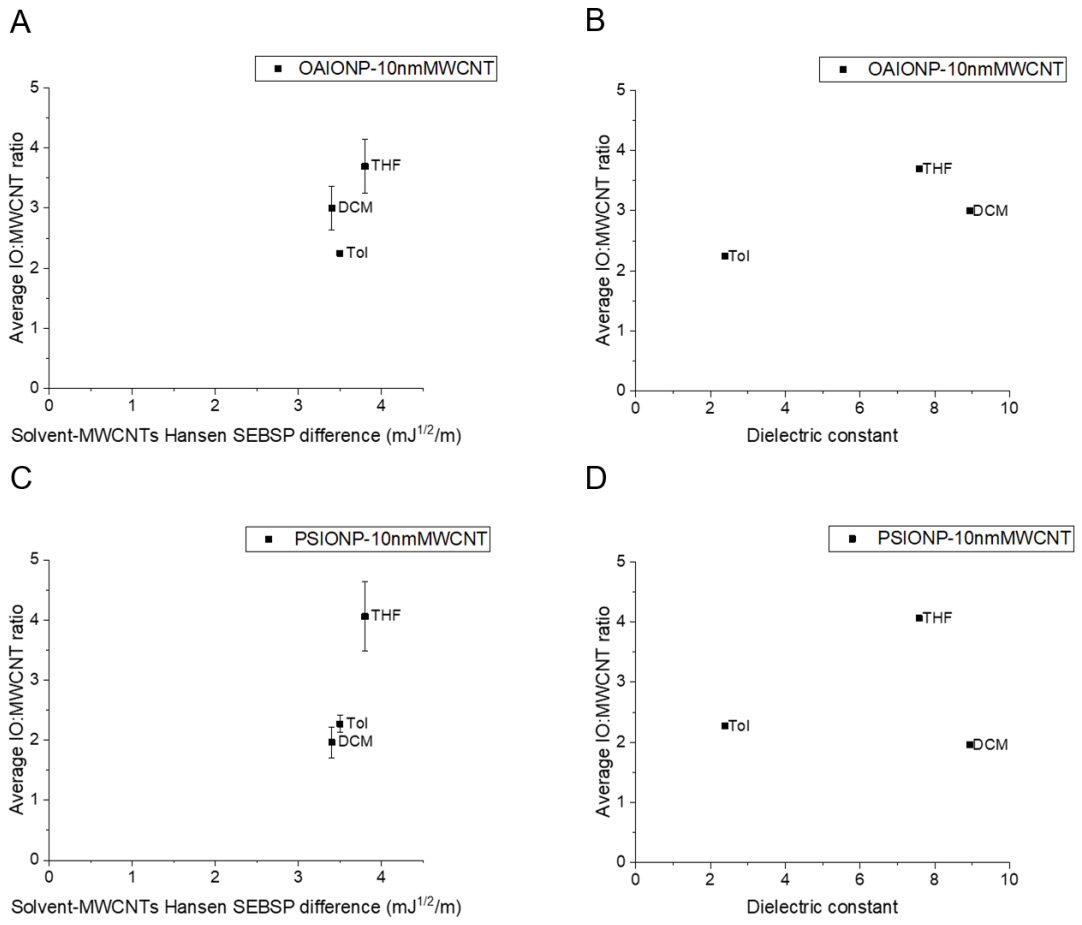


Figure 5.12: *Plots of A) Hansen SEBSP difference between solvents and MWCNTs against IO:MWCNT ratio for OAIONP-10nmMWCNT hybrid. B) Dielectric constant against the IO:MWCNT ratio for OAIONP-10nmMWCNT hybrid. Plots of C) Hansen SEBSP difference between solvents and MWCNTs against IO:MWCNT ratio for PSIONP-10nmMWCNT hybrid. D) Dielectric constant against the IO:MWCNT ratio for PSIONP-10nmMWCNT hybrid.*

OAIONPs in DCM showed a stable dispersion of nanoparticles. However, months after the synthesis of the OAIONP-10nmMWCNT hybrids the solution of OAIONPs in DCM formed aggregates that could be observed by simple sight and were confirmed by TEM characterisation (Figure 5.13). The aggregates where only observed in OAIONPs in DCM, while the rest of the OAIONP and PSIONP dispersions remained stable. This was confirmed using DLS where a new peak was observed confirming the presence of large aggregates with an average size of 440 ± 50 nm. These observations suggest that the OAIONP-DCM interaction is not thermodynamically favoured as originally believed. I propose two possible explanations for the observed phenomenon. First, that the OA-IONPs interactions are not thermodynamically favourable causing the aggregation of the OAIONPs due to solvophobic effects. This in turn means that the OAIONPs are more available to functionalise the surface of the 10nmMWCNTs as a way of minimising their interphase with DCM. This phenomenon would be analogous to the polymer wrapping mechanism proposed by O'Connel *et al.* but now applied to the DCM-OAIONP interactions. Another possibility is that DCM disrupts the coordination bond between the IONP core and the amine group of OA, this disruptions could be result of the formation of a hydrogen bond between the lone pair of the amine functionality of OA and the hydrogen atoms of DCM. This argument is sustained by previous reports that the coordination between OA and IONPs is not as robust as the one observed for carboxylate ions coordinated to the surface of IONPs [163]. In addition, DCM has the largest H-donor character among the solvents used in this study [138], which could explain why the disruption of the coordination bond of the OA with the IONP is only observed in DCM. Further experimentation is required to understand this phenomenon, which will be commented on Chapter 6.

Finally, in Figure 5.12 B and D the values of the IO:MWCNT ratio was plotted against values of the dielectric constant of the solvents used during the synthesis. Rance *et al.* [158] attributed the difference in the amount of functionalisation of

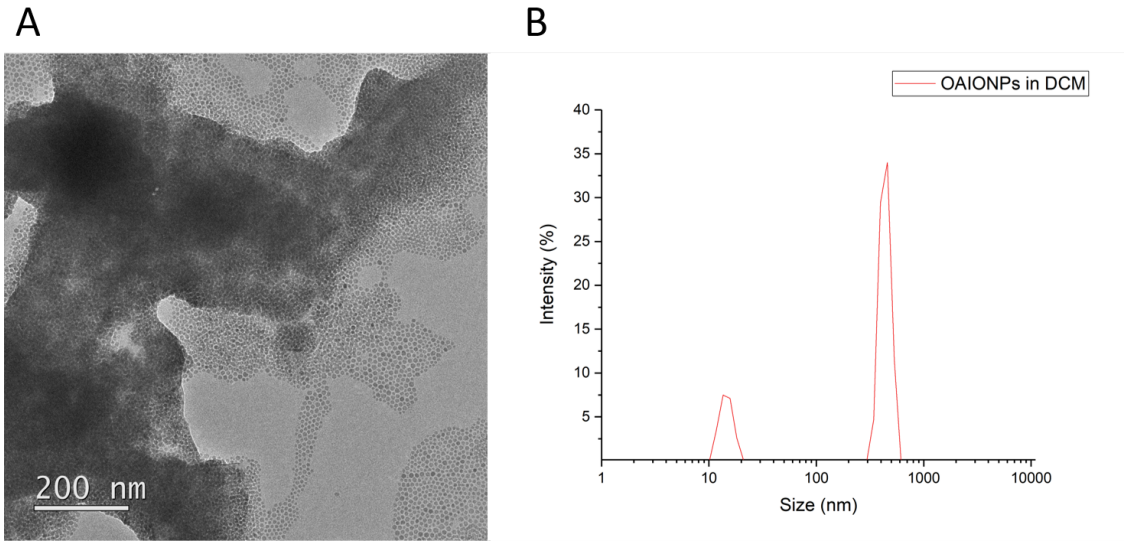


Figure 5.13: *A) TEM micrograph of OAIONPs and B) DLS particle size distribution showing the emergence of aggregates when DCM is used as the solvent.*

MWCNTs with AuNPs to the increase of localised negative surface charge in the nanomaterials when the dielectric constant of the solvent increased. However, in this case the dielectric constant of the solvent seems to have no correlation with the amount of nanoparticles found in the hybrid. On the other hand, the SEBSP seems to provide a more accurate descriptive model in this instance. While this observation does not discredit the observations reported by Rance *et al.*[158] it does suggest that the surface charge of the MWCNTs and nanoparticles do not play a crucial role in the final composition of the hybrids. Is important to note that the dodecanethiol ligands stabilising the gold nanoparticles in Rance *et al.* study are shorter in length in comparison to the polystyrene ligands used in our experiments. The electrostatic forces decrease quadratically with distance, which would explain why these forces might play a less important role in our system.

5.3.4 Effect of the concentration of starting solutions in the PSIONP-10nmMWCNT hybrid

In addition to studying the role that the solvent has during the functionalisation of MWCNTs, the impact of other variables such as the concentration of the start-

ing MWCNT and PSIONPs solutions, the PSIONP to MWCNT weight ratio and the effect of using MWCNTs with different diameters were explored. The mechanism of functionalisation of MWCNTs with nanoparticles includes the adsorption of nanoparticles onto the surface of MWCNTs in dispersions. For this reason one might expect that MWCNT dispersions where the MWCNT bundles have exfoliated might present a larger degree of nanoparticle functionalisation in comparison to solutions with a higher degree of MWCNT aggregation. A potential method to evaluate the role that the dispersion of the MWCNT starting solution might have in the process of nanoparticle functionalisation is by preparing PSIONP-10nmMWCNT hybrid using solutions with different concentrations. We would expect that PSIONP-10nmMWCNT hybrid prepared with starting solutions with low concentration would present a more effective degree of functionalisation since it would be less likely for MWCNT-MWCNT interactions to occur.

To study the effect of concentration of starting material on the fabrication of PSIONP-MWCNT hybrids, I synthesised a series of hybrids using starting PSIONPs and 10nmMWCNT solutions with concentrations that ranged from 0.2-0.025 mg/mL. Throughout the experiments the PSIONP to MWCNT ratio was maintained to a 1:1 weight ratio to probe only the effect on the dilution of the starting solutions. In Figure 5.14 the TEM micrographs of the different PSIONP-MWCNT hybrids is presented, it can be observed that the PSIONP-MWCNT hybrids present a morphology where the PSIONPs are found coating the external walls of the 10nmMWCNTs. Although a large amount of PSIONPS seem to be interacting with the 10nmMWCNTs, the coating layer of PSIONPS is not uniform through the MWCNT axis. In addition, the PSIONPs seem to create aggregates in between the structures of 10nmMWCNTs, which suggest that the interaction between the PSIONPs and MWCNTs occurs not at the level of single MWCNT units with PSIONPs but as MWCNT bundles and aggregates. Decreasing the concentration of the starting materials did not seem to have an obvious impact on the overall morphology of the PSIONP-MWCNT

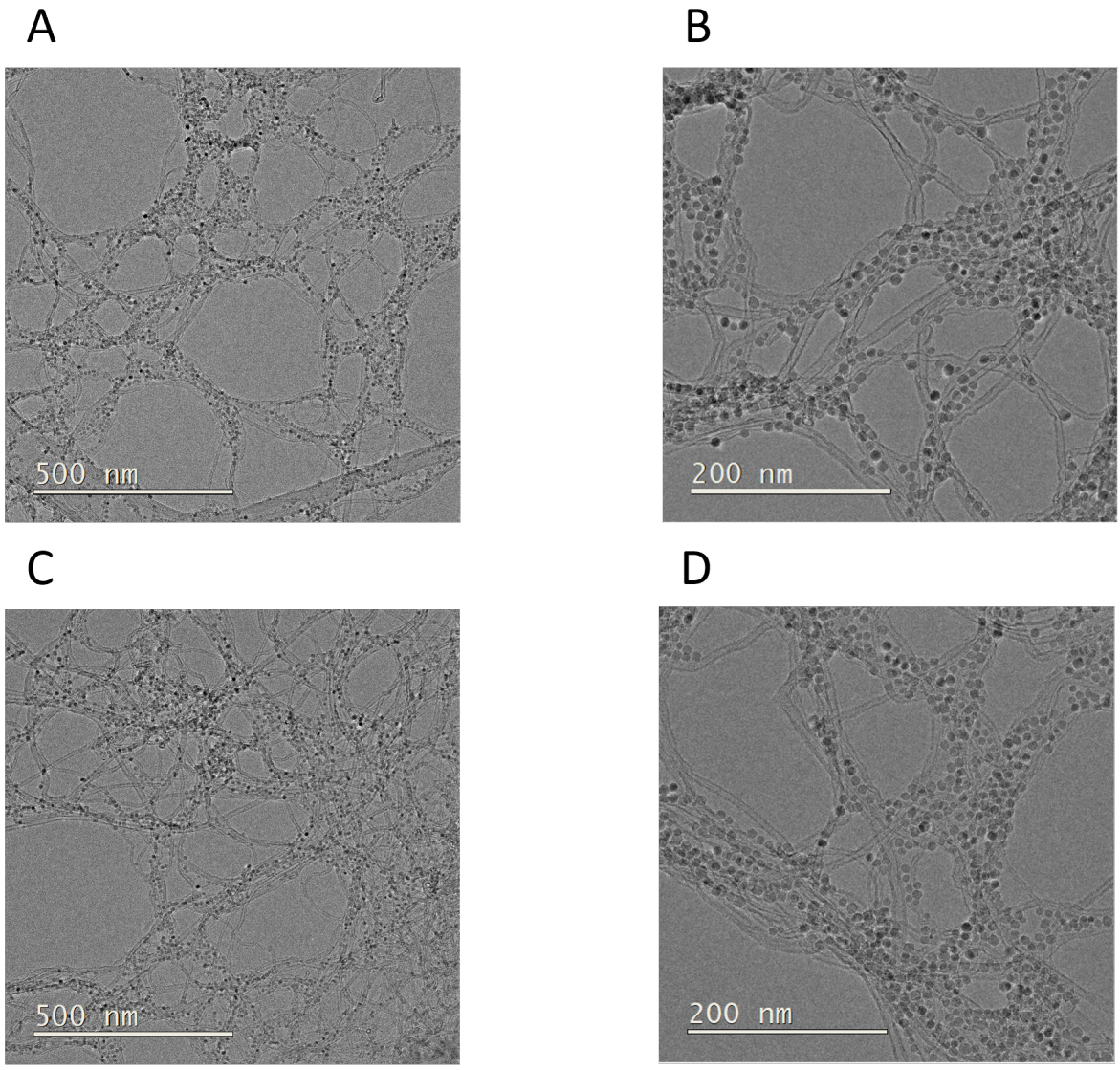


Figure 5.14: *TEM micrographs of PSIONP-MWCNT hybrids synthesised in a 1:1 PSIONP to MWCNT weight ratio. A-B) TEM micrograph of PSIONP-MWCNT hybrid with a concentration of 0.2 mg/mL of MWCNTs. C-D) TEM micrograph of PSIONP-MWCNT hybrid with a concentration of 0.1 mg/mL of MWCNTs. E-F) TEM micrograph of PSIONP-MWCNT hybrid with a concentration of 0.05 mg/mL of MWCNTs. G-H) TEM micrograph of PSIONP-MWCNT hybrid with a concentration of 0.1 mg/mL of MWCNTs. The micrographs show a non-uniform distribution of PSIONPs on the surface of MWCNTs regardless of the concentration of the sample.*

hybrids.

To understand if the observation of aggregates of PSIONPs between the MWCNT bundles are due to the cumulative aggregation of individual PSIONPs in solution or the interaction between MWCNT bundles and aggregated PSIONPs clusters in solution a series of experiments were performed where the concentration of 10nmMWC-

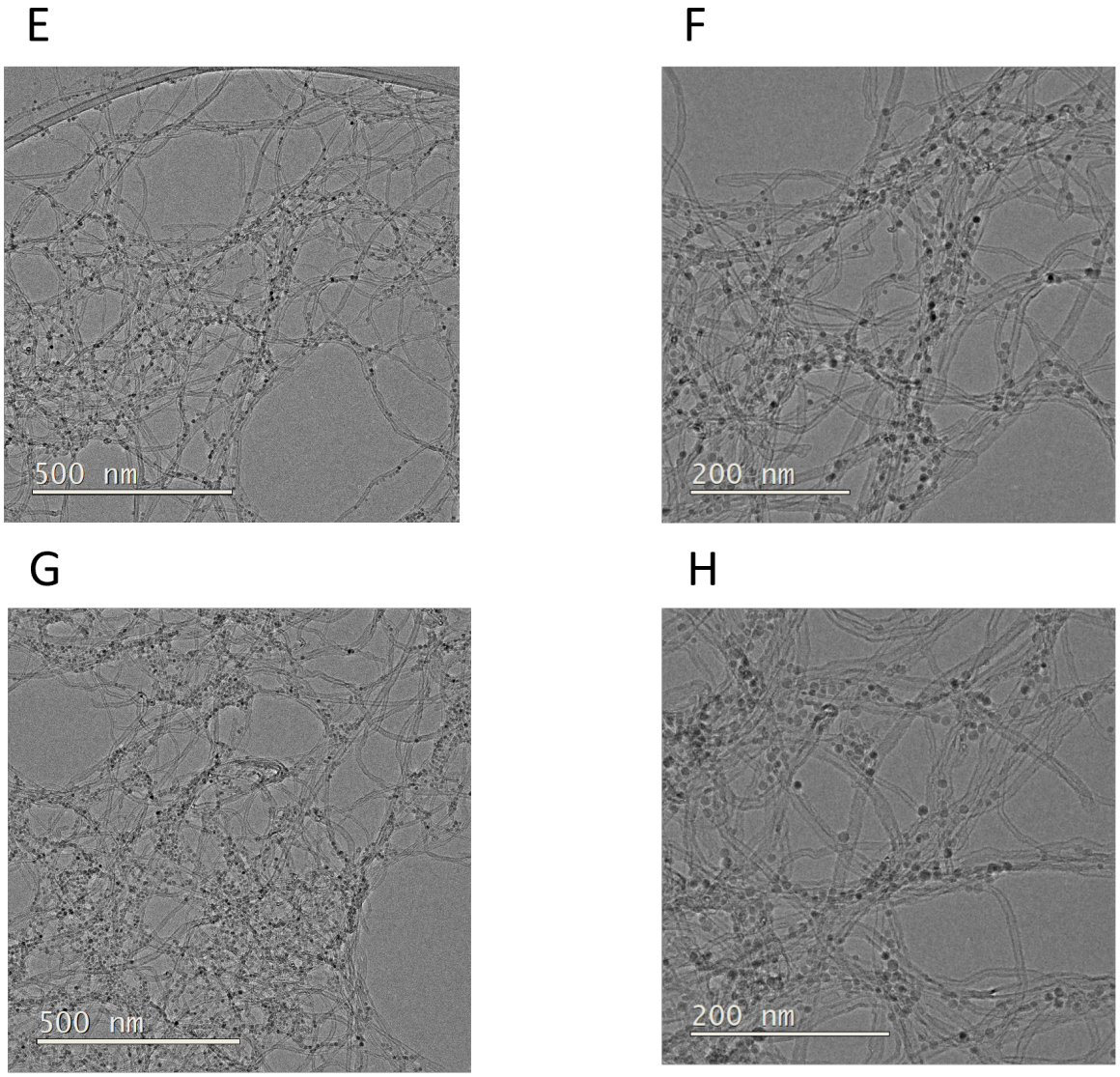


Figure 5.14: *TEM micrographs of PSIONP-MWCNT hybrids synthesised in a 1:1 PSIONP to MWCNT weight ratio. A-B) TEM micrograph of PSIONP-MWCNT hybrid with a concentration of 0.2 mg/mL of MWCNTs. C-D) TEM micrograph of PSIONP-MWCNT hybrid with a concentration of 0.1 mg/mL of MWCNTs. E-F) TEM micrograph of PSIONP-MWCNT hybrid with a concentration of 0.05 mg/mL of MWCNTs. G-H) TEM micrograph of PSIONP-MWCNT hybrid with a concentration of 0.1 mg/mL of MWCNTs. The micrographs show a non-uniform distribution of PSIONPs on the surface of MWCNTs regardless of the concentration of the sample.*

NTs was fixed while different concentration of PSIONPs were utilised. For the synthesis of the PSIONP-10nmMWCNTs hybrids the weight ratios of PSIONPs to MWCNTs were varied from 0.33:1 to 3:1 while maintaining a concentration of 10nmMWCNTs at 0.05 mg/mL.

The TEM micrographs of the synthesised PSIONP-10nmMWCNTs hybrids are presented in Figure 5.15. It can be observed that as the ratio between PSIONP to 10nmMWCNT is decreased the amount of PSIONPs aggregates between 10nmMWCNTs bundles decreases significantly. When the ratio between PSIONPS to MWCNTs is 0.33:1 an intermittent coating of PSIONPs on the surface of the MWCNTs is observed and there are no evidence of larger aggregates of PSIONPs in between the 10nmMWCNT bundles. When the ratio between PSIONPS to 10nmMWCNTs is increased to 1:1 there is no evidence of a more uniform coating of the 10nmMWCNT with the PSIONPs, but in fact the amount of aggregates of PSIONPs in between 10nmMWCNTs increases. A similar observation can be obtained from the TEM micrographs of the PSIONP-10nmMWCNTs hybrids synthesised in a 3:1 ratio where the PSIONPs aggregates can be clearly seen. The observation of no aggregates at low PSIONP to 10nmMWCNT ratio may suggest that the aggregates occur via the the cumulative aggregation of individual PSIONPs in solution rather than the presence of pre-existing PSIONPs aggregates since the aggregates are only observed as the concentration of PSIONPs is increased.

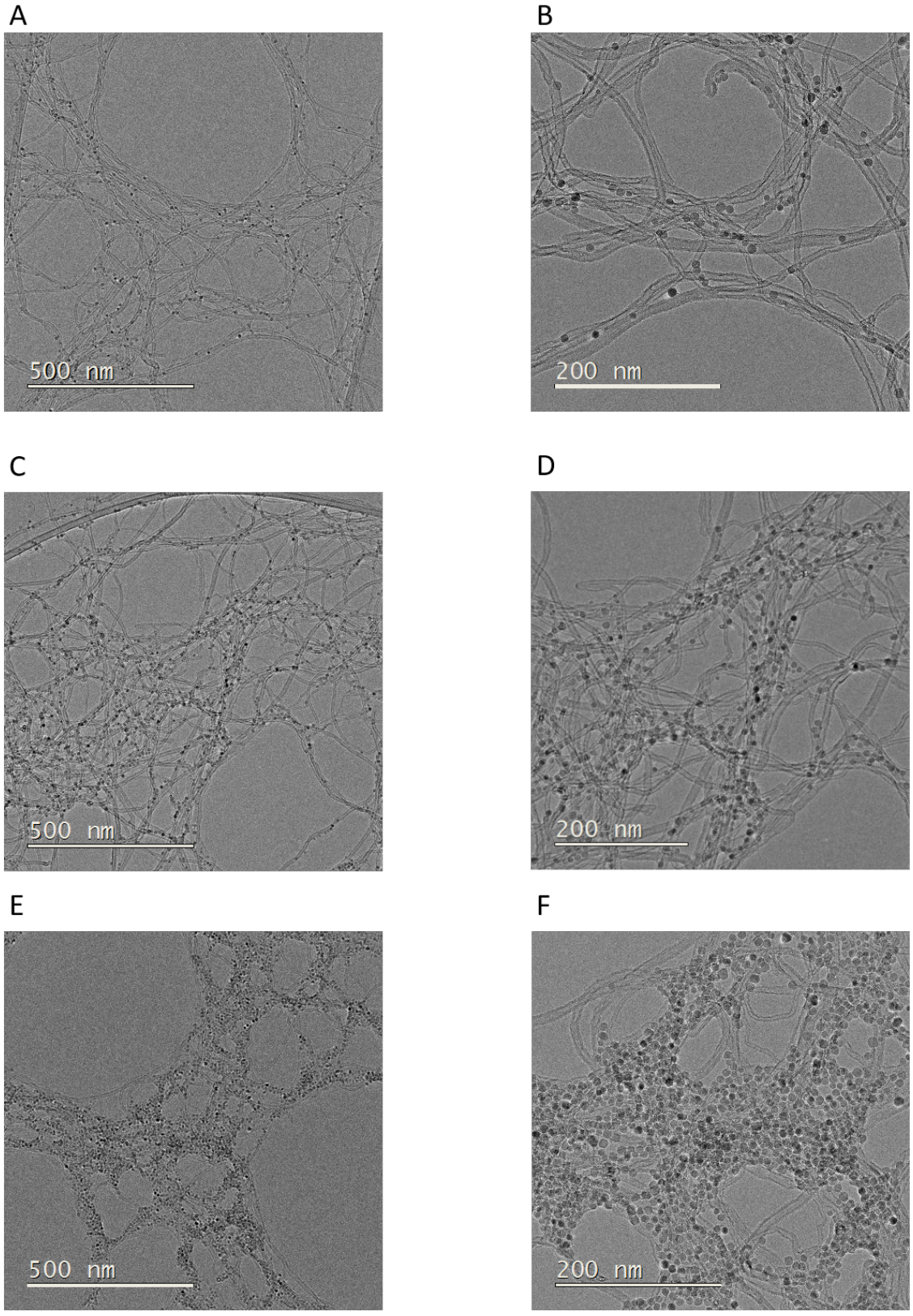


Figure 5.15: *TEM micrograph of PSIONP-MWCNT hybrids synthesised at different PSIONP to MWCNT weight ratios. The concentration of MWCNTs during all synthesis was 0.05 mg/mL. A) TEM micrograph of PSIONP-MWCNT hybrid with a 0.33:1 weight ratio. B) TEM micrograph of PSIONP-MWCNT hybrid with a 1:1 weight ratio. C) TEM micrograph of PSIONP-MWCNT hybrid with a 3:1 weight ratio. The results show that increasing the ratio between PSIONPs to MWCNTs increased the size of the aggregates observed in the products.*

5.3.5 Effect of the MWCNT diameter on the morphology of PSIONP-MWCNT hybrids

Another factor that might have an important impact in the morphology of PSIONP-MWCNT hybrids is the diameter ratio between MWCNTs and PSIONPs. The diameter of the MWCNT circumference will determine the amount of PSIONPs that can coat the MWCNT, since the circumference of the MWCNT will only be able to accommodate a limited number of PSIONPs. This is exemplified in Figure 5.16A and B. The diagram shows that five PSIONPs with a 13 nm hydrodynamic diameter are the maximum IONPs that can be in contact in a cross-section of a 10nmMWCNT. On the other hand fifteen PSIONPS can in theory be coating a 50nmMWCNT in a specific cross-section. In the previous experiments where PSIONP-10nmMWCNT hybrid were synthesised it was observed that the coating of the particles through the 10nmMWCNT surface was not uniform and the particles tended to create aggregates in between bundles of 10nmMWNCTs as depicted in Figure 5.16 C. To understand if the diameter of the MWCNTs could have an important impact in the observed morphology of the hybrids we synthesised PSIONP-50nmMWCNT hybrids using as AACVD MWCNTs with a an average diameter of 53 $\pm$ 25 nm.

In Figure 5.16E and F we can observe some of the differences in morphology between PSIONP-10nmMWCNT and PSIONP-50nmMWCNT hybrids. The latter seem to present a morphology where the particles are in a larger proportion coating the surface of the MWCNTs instead of forming clusters in between MWCNT bundles. The morphology observed for 50nmMWCNTs seems to be a mixture of concentrically coated PSIONPs around the nanotube surface (Figure 5.16)B and small PSIONP aggregates in between 50nmMWCNTs bundles. On the other hand, 10nmMWCNTs seem to lack concentric PSIONPs coatings on the MWCNT surface and tend to present more aggregates between the 10nmMWCNT bundles.

In a similar fashion to the studies made for PSIONP-10nmMWCNT hybrids

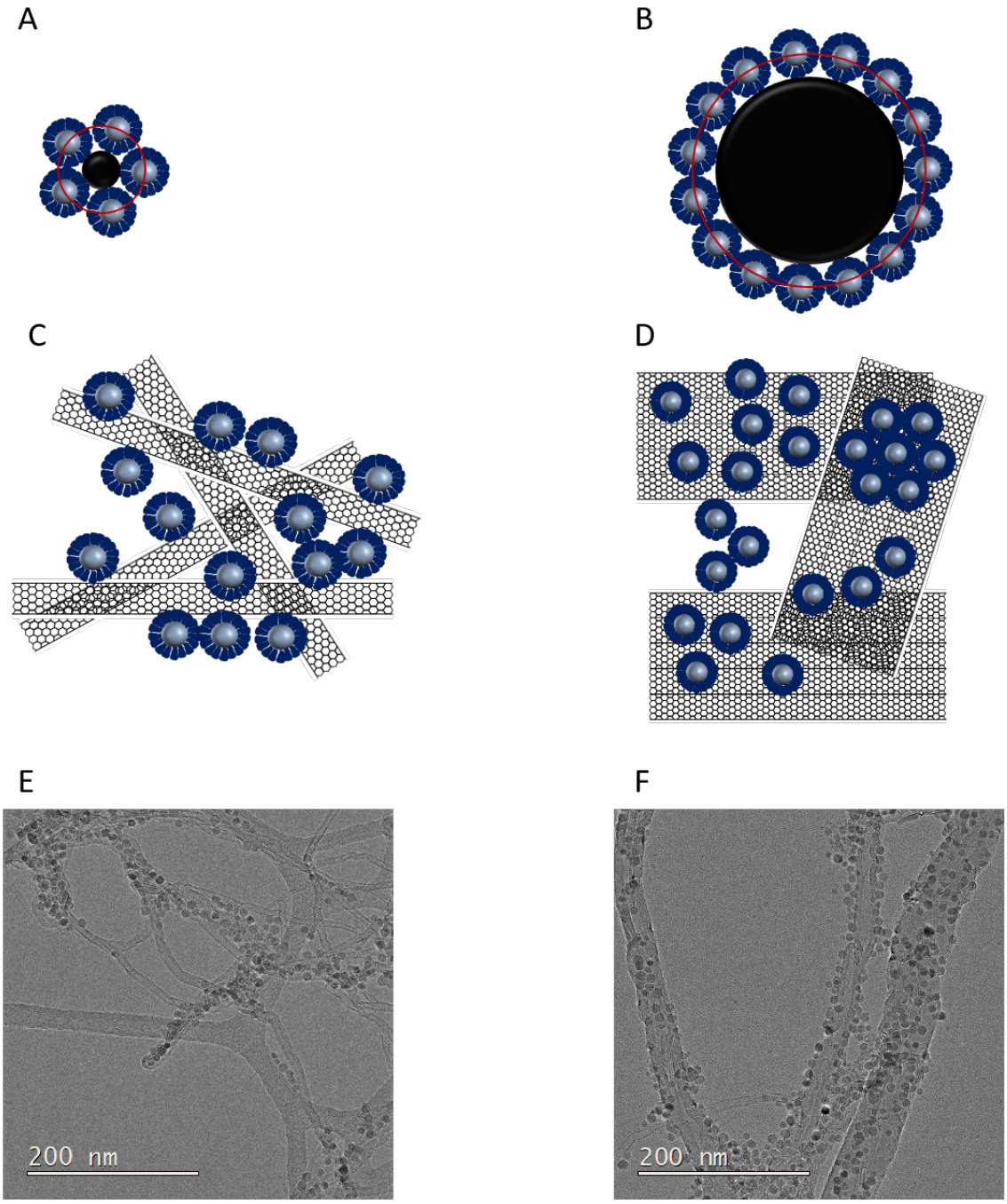


Figure 5.16: *Representation of different possible arrangements of PSIONPs coating the surface of MWCNTs. A) Representation of the maximum number of PSIONPs coating the surface of a 10nmMWCNT. B) Representation of the maximum number of PSIONPs coating the surface of a 50nmMWCNT. C) Representation of PSIONPs coating bundles or aggregates of 10nmMWCNTs. The particles are creating aggregates surrounding the bundles of 10nmMWCNTs. D) Representation of PSIONPs coating bundles or aggregates of 50nmMWCNTs. The particles are observed to coat the surface of the 50 nmMWCNTs and creating aggregates surrounding the bundles of 50nmMWCNTs. E) TEM micrograph of 10nmMWCNTs, the particles are observed to coat the surface of 10nmMWCNT with a low degree of uniformity. Most PSIONPs are observed in aggregates as exemplified in C). F) TEM micrograph of 50nmMWCNTs, the particles are observed to coat the surface of 50nmMWCNT with a larger degree of uniformity in comparison to 10nmMWCNTs. PSIONPs are also observed in aggregates, displaying a combination of the cases described in B) and D).*

we evaluated how the starting concentration of PSIONP and 50nmMWCNTs solutions impacted the morphology of the PSIONP-50nmMWCNT hybrids. To study the effect of concentration of the starting solutions on the morphology of PSIONP-50nmMWCNT hybrids, a series of hybrids were synthesised using starting PSIONPs and 50nmMWCNT solutions with concentrations that ranged from 0.2-0.025 mg/mL. The weight ratio between the PSIONPs and 50nmMWCNTs was kept at 1:1 across the whole range of the experiments. As it can be observed from the TEM micrographs in Figure 5.17, the morphology of the hybrids was similar throughout the experiments and the PSIONPs tended to cover the 50nmMWCNTs in a more uniform morphology in comparison to 10nmMWCNTs.

Since the coating of PSIONPs through the 50nmMWCNT surface had a higher level of uniformity it was possible to study the fraction of the 50nmMWCNT area of coverage by the PSIONPs. To obtain the area coverage I performed an image analysis on the TEM micrographs obtained from the PSIONP-50nmMWCNT samples (see Section 5.2.9 for details on the image analysis procedure). The results are summarised in Table 5.2. The first observation to make is that for each experiment the average area coverage for the PSIONP-50nmMWCNT hybrids presented large standard deviations demonstrating that the coating of PSIONPs through the 50nmMWCNT surfaces has a high level of variability and low uniformity. In addition, the average and median area coverage have similar values across the experiments and all within the standard deviation of the average values. These values support our observation that the morphology of the PSIONP-50nmMWCNT is not sensitive to this range of concentration of the PSIONP and 50nmMWCNT starting solutions.

In addition, we studied the role that the weight ratio between the PSIONP and 50nmMWCNT starting solutions had on the morphology of the hybrids. For this purpose PSIONP-50nmMWCNT were prepared by mixing solutions of PSIONP and 50nmMWCNT with weight ratios that ranged from 0.2:1 to 5:1. The TEM

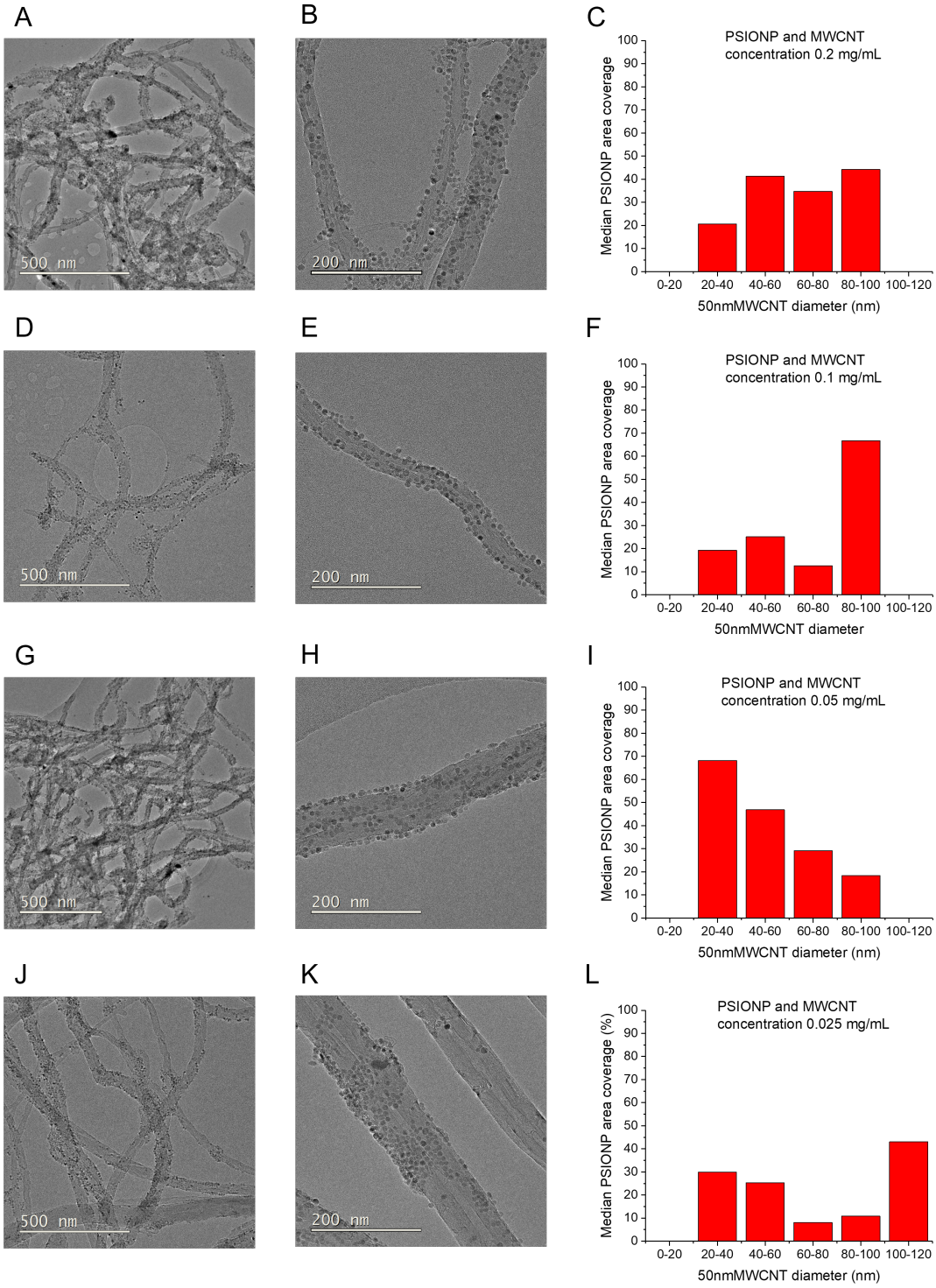


Figure 5.17: *TEM micrographs of PSIONP-MWCNT hybrids synthesised at a 1:1 PSIONP to MWCNT weight ratio and median area coverage distribution for MWCNTs with different diameters. A-C) PSIONP-MWCNT hybrids with a concentration of 0.2 mg/mL of MWCNTs D-F) PSIONP-MWCNT hybrids with a concentration of 0.1 mg/mL of MWCNTs. G-I) PSIONP-MWCNT hybrids with a concentration of 0.05 mg/mL. of MWCNTs. J-L) PSIONP-MWCNT hybrids with a concentration of 0.025 mg/mL of MWCNTs. The micrographs display a non-uniform distribution of PSIONPs on the surface of MWCNTs. Both TEM evidence and the median area coverage distribution suggest that MWCNTs with larger diameters presented a more uniform coverage of PSIONPs throughout their surface.*

Table 5.2: *Composition of OAIONP-10nmMWCNT and PSIONP-10nmMWCNT hybrids.*

PSIONP to MWCNT ratio	Concentration 50nmMWCNTs [mg/mL]	Concentration PSIONPs [mg/mL]	PSIONP average area coverage [%]	PSIONP median area coverage [%]
1:1	0.2	0.2	34±12	33
1:1	0.1	0.1	35±23	28
1:1	0.05	0.05	42±20	35

micrographs of the PSIONP-50nmMWCNT hybrids are presented in Figure 5.18. The TEM micrographs show a similar change in morphology to what it was observed for 10nmMWCNTs. When the ratio between PSIONPs to 50nmMWCNTs is low (Figure 5.18A-B) the PSIONPs are observed to be scattered on the surface of the 50nmMWCNT. As the PSIONP concentration increases (Figure 5.18D-E) a more uniform coverage of PSIONPs on the surface of the 50nmMWCNT is observed. Finally, at high weight ratios between PSIONPs and 50nmMWCNTs the formation of PSIONP aggregates bridging between 50nmMWCNTs is observed.

Increasing the PSIONP to 50nmMWCNT ratio resulted in an increase of area coverage as observed in Table 5.3. The median average area coverage increased from 3% when the PSIONP to 50nmMWCNT ratio was 0.2:1 to 37% when the ratio was increased to 5:1. The average area coverage for all samples still displays a large standard deviation confirming that the PSIONP-50nmMWCNT also presented a high degree of variability on the degree of PSIONP surface coverage. The observation of an increased amount of nanoparticle aggregates at high PSIONP to 50nmMWCNT weight ratios supports our previous claim that the PSIONP aggregates seem to occur by a successive adsorption of single PSIONPs into the surface of the PSIONP-50nmMWCNT hybrids.

The synthesis of PSIONP-50nmMWCNT permitted the study of the relationship between the average PSIONP area coverage and the diameter of the MWCNTs, since the 50nmMWCNT sample presents a wide distribution of MWCNT diameters. In Figure 5.17 and 5.18 C,F,I and L the distribution of the median area coverage of

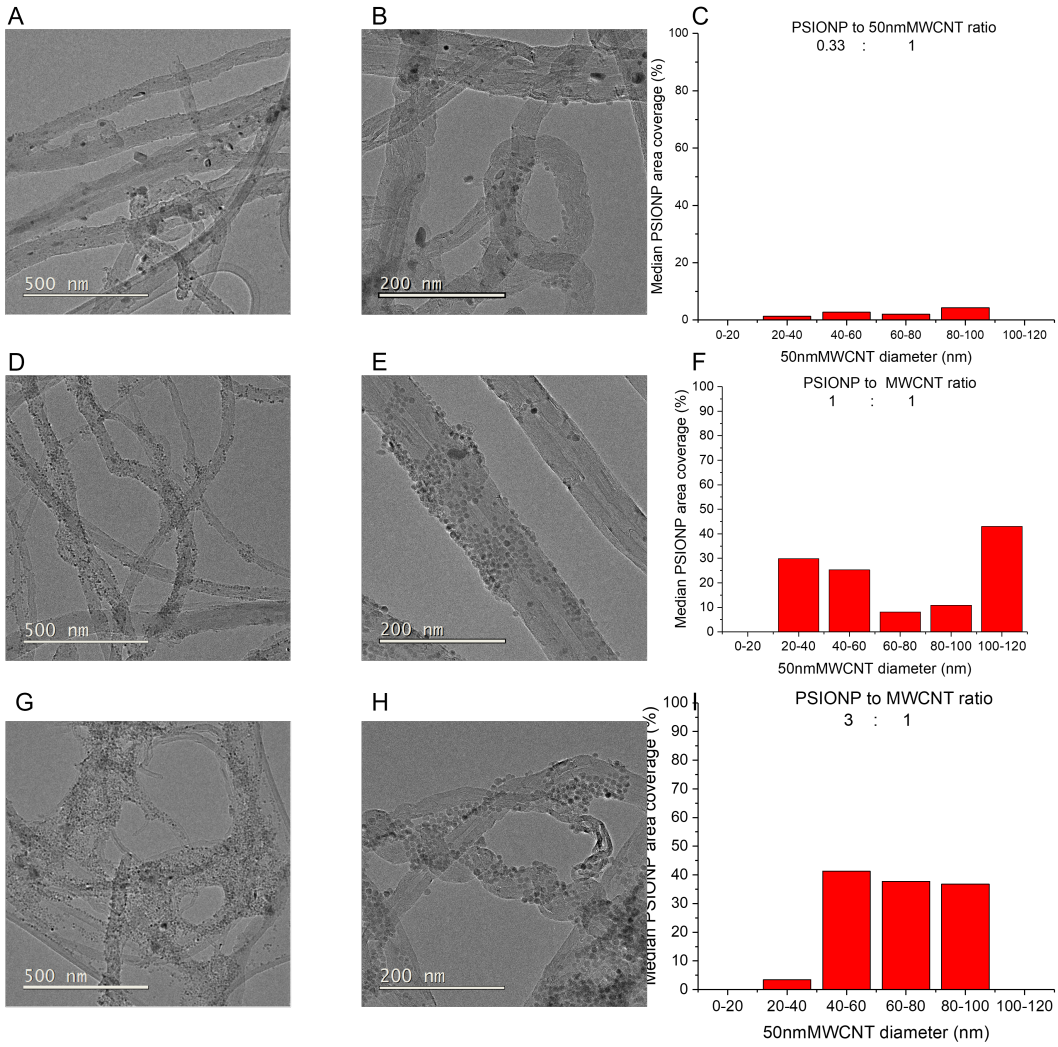


Figure 5.18: *TEM micrographs of PSIONP-MWCNT hybrids synthesised at different PSIONP to MWCNT weight ratios and median area coverage distribution for MWCNTs with different diameters. The concentration of MWCNTs during all synthesis was 0.05 mg/mL. A-C) PSIONP-MWCNT hybrid with a 0.33:1 weight ratio. D-F) PSIONP-MWCNT hybrid with a 1:1 weight ratio. G-I) PSIONP-MWCNT hybrid with a 3:1 weight ratio. The results show that increasing the ratio between PSIONPs to MWCNTs increased the area coverage of PSIONPs on the surface of the MWCNTs. Both TEM evidence and the median area coverage distribution suggest that MWCNTs with larger diameters presented a more uniform coverage of PSIONPs throughout their surface.*

Table 5.3: *Composition of OAIONP-10nmMWCNT and PSIONP-10nmMWCNT hybrids.*

PSIONP to MWCNT ratio	Concentration 50nmMWCNTs [mg/mL]	Concentration PSIONPs [mg/mL]	PSIONP average area coverage [%]	PSIONP median area coverage [%]
5:1	0.025	0.125	37±22	37
1:1	0.025	0.025	25±23	20
0.2:1	0.025	0.005	3±2	3

PSIONP in relation to the MWCNT diameter is plotted. Although the distribution varies for all samples it can be observed that the median area coverage of PSIONPs observed for 50nmMWCNT with a diameter between 20-40 nm tended to present the lowest median area coverage in most cases. This result suggests that smaller diameter MWCNTs do tend to have a smaller area coverage in comparison to MWCNTs with large diameters. Our current results are consistent with the observations of Rance *et al.* [159] where they observed that MWCNT with larger diameters are more efficiently functionalised by AuNPs. They argued that an increase in the diameter of MWNCTs increased their polarisability, thus increasing the strength of the Van der Waals interactions between AuNPs and MWCNTs. My results suggest a similar behaviour to the observations from Rance *et al.*, although they do not confirm whether the increase of area coverage is due to steric effects or due to an increase in the polarisability of the MWCNTs.

5.4 Conclusions

The main objective of this Chapter was to apply the knowledge obtained for the non-covalent functionalisation of MWCNTs in Chapter 3 and 4 to the synthesis of IONP-MWCNTs hybrids. In particular, if the solvent media had a considerable impact on the amount of IONP found in the hybrids. The results outlined in this Chapter showed that the solvent plays a crucial role in the synthesis of nanoparticle-MWCNT hybrids. The observation of a similar composition of the OAIONP-10nmMWCNT

and PSIONP-10nmMWCNT hybrids in THF and toluene, suggests that the effect that the solvent has on the amount of IONP found in the hybrids seems to be more impactful than other parameters such as the chemical nature or the height of the brush of the organic ligands coating the surface of the IONPs as previously reported by Sainsbury *et al.* [147]. The SEBSP theory provided a good prediction for the amount of IONP found in the hybrids when PS was the ligand stabilising the IONPs. In addition the SEBSP theory was found to be a better predictor than the dielectric constant of the solvent, which has been reported previously to be linked with the functionalisation of MWCNTs with AuNPs [158]. In the case of OAIONPs a discrepancy with the Hansen SEBSP predictions was found when DCM was used as a solvent during synthesis, which is attributed to the instability of OAIONPs in DCM observed overtime.

During my functionalisation experiments I found that IONPs tended to form aggregates between bundles of 10nmMWCNTs that seem to be formed by the successive absorption of IONPs into the surface of the MWCNTs. The morphology of the hybrids was independent of the overall concentration of the starting materials. However, the size of the aggregates could be controlled by decreasing the IONP:10nmMWCNT weight ratio. Finally, the effect of the MWCNT diameter on the morphology of PSION-MWCNT hybrids was studied. MWCNT with larger diameters displayed a higher amount of surface area coverage in comparison to smaller diameter MWCNTs. This observation is consistent with previous reports from Rance *et al.* [159], in which the authors attributed this behaviour to the higher polarisability of MWCNTs with large diameters. However, I believe that a combination of enhanced steric interference by the organic ligands in small diameter MWCNTs must also have effect on the morphology of the hybrids.

The experiments and results reported in this Chapter demonstrate how the bottom-up synthesis of nanostructures rapidly increases in complexity from the simple polymer-MWCNT interaction when another nanomaterial is included in the sys-

tem. The solvent-nanoparticle interaction and the ligand-nanoparticle interaction have to be taken into account to create models and guidelines that allow for the rational design of synthetic procedures for nanoparticle-CNT hybrids. More studies such as the reports by Sainsbury *et al.*, Rance *et al.* and the one presented herein are required to expand our capability of the bottom-up synthesis of hierarchical nanostructures.

Chapter 6

Summary, Conclusions and Outlook

The objective of this Thesis was to study the interactions between MWCNTs and polymers for their application in the synthesis of hierarchical nanostructures such as inorganic nanoparticles and MWCNTs hybrids. The approach taken throughout this work was to focus on the interactions between the materials from a bottom-up perspective, with the aim to obtain a holistic understanding of the system at different levels of structural hierarchy. To achieve this I first focused on the MWCNT-polymer interactions as a case study that represented the lowest level of hierarchy. The studies discussed in Chapter 3 compared covalent and non-covalent functionalisation of MWCNTs with polystyrene, showing that the latter was the most efficient method for MWCNT functionalisation. The enhanced efficiency of the non-covalent approach was judged by the observation of a similar degree of functionalisation and irreversibility in comparison to the covalent methodologies used during the study, while the non-covalent method offered a less complicated synthetic methodology. In fact, the characterisation suggested that even when covalent functionalisation was attempted there was no evidence for the formation of direct chemical bonds between

the MWCNTs and polymer chains, and the presence of polystyrene in the products of covalent methodologies were more likely due to non-covalent forces. While the evidence discussed in this Chapter should not be taken as evidence against previous reports of covalent functionalisation for other CNTs and small organic molecules, it does highlight the importance of taking into account non-covalent interactions between CNTs and polymers even when covalent functionalisation methodologies are attempted. In addition, this study strongly supports that the reporting of control experiments similar to the ones described in this studies should become a requisite practice to be reported in studies where the covalent functionalisation methodologies of CNTs are attempted in order to assess the presence of covalent bonds formation in the functionalised CNTs.

Additionally, the evidence presented in Chapter 3 showed that the solvent was found to be the parameter that had a larger impact on the degree of functionalisation when both covalent and non-covalent methodologies were attempted. Future work should focus in testing this solvent dependent behaviour on different types of polymers. While polystyrene represents the case of a hydrophobic polymer, there are still a wide range of polymers that are routinely used to functionalise CNTs that have a different chemical structures and properties. For example, water soluble polymers such as polyvinyl pyridine and polyacrylic acid are widely used to create CNT dispersions and they could be used to mediate the interactions between CNTs and other nanomaterials. Other types of polymers that should be tested are π-conjugated polymer due to their reported affinity to CNT structures [52]. Finally, shifting from intuitive experimental designs (based on the chemical structure of the polymers) is required to fully exploit the plethora of CNT-polymer interactions that could be used for the bottom-up synthesis of nanostructures. To achieve this further studies should focus on characterising the final composition of polymer functionalised CNTs through non-covalent interactions as it was presented in this work, instead of relying on the quality of CNT dispersions as is normally reported. By having an accurate

picture of the amount of polymer present in the functionalised samples, we could start creating effective guidelines to maximise CNT-polymer interactions.

In Chapter 4 I proposed to apply the SEBSP theory to understand the differences in the amount of polystyrene functionalisation of MWCNTs observed in different solvents. To achieve this I measured the surface energy and HSP of MWCNTs to calculate the Hildebrand and Hansen SEBSP solvent distance. Our findings showed that the predictions from the Hansen SEBSP theory displayed a high correlation with the amount of polystyrene found in the MWCNTs. This is the first time that a model has been proposed for the prediction of the degree of functionalisation of MWCNTs with any organic polymer via non-covalent interactions, and its application should be of great assistance for future research that aim to maximise polymer-MWCNT interactions. Moreover, the implications of this results have an important impact in our understanding of the mechanism of polymer wrapping for CNTs, since it provides experimental evidence for the hypothesis proposed by O'Connel *et al.* decades ago.

Further work should be carried to test the ability of the SEBSP theory as a model to predict the polymer functionalisation of CNTs. In particular, characterising through IGC of the surface energy and HSP of different CNTs and studying how their surface properties affect their polymer functionalisation would be desirable to provide robustness to the SEBSP theory. An interesting material to study would be nitrogen doped CNTs since they are widely known to present different surface energy values in comparison to CNTs and reports have shown that different qualities of dispersion are observed for CNTs in comparison to N-CNTs in different solvents [168].

In Chapter 5 the interactions between MWCNTs and IONPs mediated by either polystyrene or oleylamine was discussed. This system represented a progression in the level of hierarchy from the molecular level to the nanostructural level in our studies. Inspired by the knowledge that was obtained from the previous Chapters I studied the effect that the solvent media has on the synthesis of PSIONP-

10nmMWCNT and OAIONP-10nmMWCNT hybrids. Once again, the solvent used during the synthesis had an important impact on the amount of nanoparticles observed in the products, in which each experiment presented a characteristic amount of IONPs depending of the solvent used during synthesis. In addition, when the PSIONP and OAIONP were compared it was found that in toluene and THF there was no quantitative difference between the final composition of the hybrids when oleylamine or polystyrene was coating the nanoparticles. From this evidence I can recommend that when the non-covalent functionalisation of CNTs with IONPs is attempted, the main parameter that should be taken into account is the solvent used during the synthesis of the hybrid.

Is important to highlight that in DCM there were differences in the amount of IONPs present in the hybrid when polystyrene or oleylamine where used to coat the surface of the particles. The potential explanations behind this behaviour were discussed in Section 5.3.3, where it was suggested that the difference of functionalisation was potentially due to unfavourable interactions between the OAIONPs and DCM. Preliminary studies on the surface properties of the OAIONPs through IGC were carried out in collaboration with Dr. Vikram Karde from Imperial College. However, the HSP parameters obtained through this experiments resulted in negative values which are not consistent with the SEBSP theories. In addition, the surface energy of the OAIONPS and PSIONPs were calculated. The OAIONPs presented a surface energy value of 56.8 mJ/m^2, which was higher in comparison to the 45.6 mJ/m^2 observed for PSIONPs. This might suggest that the OAIONPs would have indeed a higher surface energy in comparison to PSIONP and potentially could explain the aggregation in DCM. However, this result is not conclusive and further investigation is required. In particular, it should also be analysed if the DCM molecules are disrupting the coordination bond of the amine group of oleylamine with the surface of the IONPs. A potential way to explore this experimentally would be by performing the same synthesis of IONP-MWCNT hybrids

using oleic acid coated IONPS. Oleic acid is chemically analogous to oleylamine with the difference of having a carboxylic acid group instead of an amine. This system would be more suitable for comparison with the PSIONPs used in this study since they also have carboxylic acid groups anchoring the ligands to the IONPs.

The Hansen SEBSP theory was used to model the amount of IONP characterisation present in OAIONP-10nmMWCNT and PSIONP-10nmMWCNT hybrids. The Hansen SEBSP theory was found to provide a good prediction of the differences observed in the composition of the PSIONP-10nmMWCNT hybrids synthesised in different solvents. However, the Hansen SEBSP theory failed to predict the composition of the OAIONP-10nmMWCNT hybrids in DCM. We believe that this is due to the unfavourable interactions between OAIONPs and DCM, discussed in the paragraph above. In addition, we compared the predictions made by the Hansen SEBSP theory with the previous studies of Sainsbury *et al.* [147] and Rance *et al.* [158] that had proposed the nanoparticle-MWCNT distance and the dielectric constant of the solvent as determinant parameters for the functionalisation of MWCNTs with inorganic nanoparticles. I concluded that our reports are not in conflict and can be considered as complementary models. Further research should focus in bridging between these reports to have a comprehensive understanding of the different forces that affect the non-covalent interactions between MWCNTs and inorganic nanoparticles.

In Chapter 5 I studied how other parameters such as the relative concentration of PSIONPs to MWCNTs affected the morphology of the hybrids. Our results show that the at low nanoparticle concentrations the morphology of the hybrids displayed a intermittent coating of the surface of the 10nmMWCNTs with no nanoparticle aggregates observed. As the concentration of the IONPs relative to MWCNTs increased the emergence of particle aggregates between MWCNT bundles was observed. Finally, the effect of the nanoparticle diameter on the morphology of PSIONP-MWCNT hybrids was analysed. Our results showed that MWCNTs

that presented larger diameters presented higher degree of surface area coverage, which agree with previous results that have explored the functionalisation of MWCNTs with AuNPs. While previous studies have explained that this affinity of large diameter MWCNT is due to their higher dispersability, I also believe that this phenomena might also be explained to be result of steric interference caused by the organic ligand coating the CNTs.

The bottom-up synthesis of nanostructures is an exciting field of research for anyone interested in the controlled assembly of inorganic materials mediated by chemical interactions with organic molecules. However, the field still presents many challenges due to the wide variety of interactions that can occur within these systems, which was well exemplified by the addition of a second nanomaterial in Chapter 5. To achieve progress in this field more nuanced studies that take a holistic approach to understand and predict this interactions is required, and the field should shift from the simple hypothetical explanations that are commonly used in research articles within the field. Experimental based models such as Rance *et al.*, Salisbury *et al.*, and the work published herein should be encouraged, and should be tested with other theoretical and modelling work. It is my hope that the studies presented throughout this Thesis will shed light in aspects that previously were not taken into account and provide useful synthetic guidelines for future research.

Bibliography

[1] Deep Jariwala, Vinod K. Sangwan, Lincoln J. Lauhon, Tobin J. Marks, and Mark C. Hersam. Carbon nanomaterials for electronics, optoelectronics, photovoltaics, and sensing. *Chemical Society Reviews*, 42(7):2824–2860, mar 2013.

[2] Agnieszka Lekawa-Raus, Jeff Patmore, Lukasz Kurzepa, John Bulmer, and Krzysztof Koziol. Electrical properties of carbon nanotube based fibers and their future use in electrical wiring. *Advanced Functional Materials*, 24(24):3661–3682, jun 2014.

[3] Yuan Li, Junchi Wu, and Nitin Chopra. Nano-carbon-based hybrids and heterostructures: progress in growth and application for lithium-ion batteries. *Journal of Materials Science*, 50(24):7843–7865, dec 2015.

[4] Kowsik Sambath Kumar, Nitin Choudhary, Yeonwoong Jung, and Jayan Thomas. Recent Advances in Two-Dimensional Nanomaterials for Supercapacitor Electrode Applications. *ACS Energy Letters*, 3(2):482–495, feb 2018.

[5] Qiang Zhang, Jia-Qi Huang, Wei-Zhong Qian, Ying-Ying Zhang, and Fei Wei. The Road for Nanomaterials Industry: A Review of Carbon Nanotube Production, Post-Treatment, and Bulk Applications for Composites and Energy Storage. *Small*, 9(8):1237–1265, apr 2013.

[6] S. C. Tjong. Novel Nanoparticle-Reinforced Metal Matrix Composites with Enhanced Mechanical Properties. *Advanced Engineering Materials*, 9(8):639–652, aug 2007.

[7] Guohai Yang, Chengzhou Zhu, Dan Du, Junjie Zhu, and Yuehe Lin. Graphene-like two-dimensional layered nanomaterials: Applications in biosensors and nanomedicine. *Nanoscale*, 7(34):14217–14231, sep 2015.

[8] Silvia Marchesan and Maurizio Prato. Nanomaterials for (Nano)medicine, feb 2013.

[9] Peter J. F. Harris. *Carbon Nanotube Science*. Cambridge University Press, Cambridge, 2009.

[10] Ado Jorio, Riichiro Saito, Gene Dresselhaus, and Mildred S. Dresselhaus. *Raman Spectroscopy in Graphene Related Systems*. 2011.

[11] Philip G Collins. *Defects and disorder in carbon nanotubes*, volume 1. Oxford University Press, jul 2017.

[12] Alan M Cassell, Jeffrey A Raymakers, Jing Kong, and Hongjie Dai. Large Scale CVD Synthesis of Single-Walled Carbon Nanotubes. *The Journal of Physical Chemistry B*, 103(31):6484–6492, aug 1999.

[13] Seyyed Shayan Meysami, Panagiotis Dallas, Jude Britton, Juan G. Lozano, Adrian T. Murdock, Claudio Ferraro, Eduardo Saiz Gutierrez, Niek Rijnveld, Philip Holdway, Kyriakos Porfyrakis, and Nicole Grobert. Ultra-stiff large-area carpets of carbon nanotubes. *Nanoscale*, 8(23):11993–12001, jun 2016.

[14] Qiaohuan Cheng, Sourabhi Debnath, Elizabeth Gregan, and Hugh J Byrne. Ultrasound-Assisted SWNTs Dispersion: Effects of Sonication Parameters and Solvent Properties. *The Journal of Physical Chemistry C*, 114(19):8821–8827, may 2010.

[15] Shane D Bergin, Zhenyu Sun, David Rickard, Philip V Streich, James P Hamilton, and Jonathan N Coleman. Multicomponent Solubility Parameters for Single-Walled Carbon Nanotube−Solvent Mixtures. *ACS Nano*, 3(8):2340–2350, aug 2009.

[16] M. F. Lin and Kenneth W. K. Shung. Magnetoconductance of carbon nanotubes. *Physical Review B*, 51(12):7592–7597, mar 1995.

[17] Sander J Tans, Michel H. Devoret, Hongjie Dai, Andreas Thess, Richard E. Smalley, L. J. Geerligs, and Cees Dekker. Individual single-wall carbon nanotubes as quantum wires. *Nature*, 386(6624):474–477, apr 1997.

[18] Stefan Frank. Carbon Nanotube Quantum Resistors. *Science*, 280(5370):1744–1746, jun 1998.

[19] Eric Pop, David Mann, Qian Wang, Kenneth Goodson, and Hongjie Dai. Thermal Conductance of an Individual Single-Wall Carbon Nanotube above Room Temperature. *Nano Letters*, 6(1):96–100, jan 2006.

[20] P Kim, L Shi, A Majumdar, and P. L. McEuen. Thermal Transport Measurements of Individual Multiwalled Nanotubes. *Physical Review Letters*, 87(21):215502, oct 2001.

[21] Jean-Paul Salvetat-Delmotte and Angel Rubio. Mechanical properties of carbon nanotubes: a fiber digest for beginners. *Carbon*, 40(10):1729–1734, aug 2002.

[22] Jean-Paul Salvetat, G. Briggs, Jean-Marc Bonard, Revathi Bacsa, Andrzej Kulik, Thomas Stöckli, Nancy Burnham, and László Forró. Elastic and Shear Moduli of Single-Walled Carbon Nanotube Ropes. *Physical Review Letters*, 82(5):944–947, feb 1999.

[23] Jean-Paul Salvetat, Andrzej J. Kulik, Jean-Marc Bonard, G. Andrew D. Briggs, Thomas Stöckli, Karine Méténier, Sylvie Bonnamy, François Béguin, Nancy A. Burnham, and Lásló Forró. Elastic Modulus of Ordered and Disordered Multiwalled Carbon Nanotubes. *Advanced Materials*, 11(2):161–165, feb 1999.

[24] Noriaki Hamada, Shin-Ichi Sawada, and Atsushi Oshiyama. New one-dimensional conductors: Graphitic microtubules. *Physical Review Letters*, 68(10):1579–1581, mar 1992.

[25] Nikolaos Karousis, Nikos Tagmatarchis, and Dimitrios Tasis. Current Progress on the Chemical Modification of Carbon Nanotubes. *Chemical Reviews*, 110(9):5366–5397, sep 2010.

[26] T. W. Ebbesen, H. J. Lezec, H. Hiura, J. W. Bennett, H. F. Ghaemi, and T. Thio. Electrical conductivity of individual carbon nanotubes. *Nature*, 382(6586):54–56, jul 1996.

[27] Takeshi Nakanishi, Masatsura Igami, and Tsuneya Ando. Conductance quantization in the presence of huge and short-range potential in carbon nanotubes. *Physica E: Low-dimensional Systems and Nanostructures*, 6(1-4):872–875, feb 2000.

[28] Leonor Chico, Lorin X Benedict, Steven G Louie, and Marvin L Cohen. Quantum conductance of carbon nanotubes with defects. *Physical Review B*, 54(4):2600–2606, jul 1996.

[29] E.T. Mickelson, C.B. Huffman, A.G. Rinzler, R.E. Smalley, R.H. Hauge, and J.L. Margrave. Fluorination of single-wall carbon nanotubes. *Chemical Physics Letters*, 296(1-2):188–194, oct 1998.

[30] Takahiro Yamamoto, Satoshi Watanabe, and Kazuyuki Watanabe. Universal Features of Quantized Thermal Conductance of Carbon Nanotubes. *Physical Review Letters*, 92(7):075502, feb 2004.

[31] Michael T. Pettes and Li Shi. Thermal and Structural Characterizations of Individual Single-, Double-, and Multi-Walled Carbon Nanotubes. *Advanced Functional Materials*, 19(24):3918–3925, dec 2009.

[32] Cem Sevik, Hâldun Sevinçli, Gianaurelio Cuniberti, and Tahir Çağın. Phonon Engineering in Carbon Nanotubes by Controlling Defect Concentration. *Nano Letters*, 11(11):4971–4977, nov 2011.

[33] Jean-Paul Salvetat, G. Briggs, Jean-Marc Bonard, Revathi Bacsa, Andrzej Kulik, Thomas Stöckli, Nancy Burnham, and László Forró. Elastic and Shear Moduli of Single-Walled Carbon Nanotube Ropes. *Physical Review Letters*, 82(5):944–947, feb 1999.

[34] Amy M Marconnet, Matthew A Panzer, and Kenneth E Goodson. Thermal conduction phenomena in carbon nanotubes and related nanostructured materials. *Reviews of Modern Physics*, 85(3):1295–1326, aug 2013.

[35] Vito Sgobba and Dirk M Guldi. Carbon nanotubes–electronic/electrochemical properties and application for nanoelectronics and photonics. *Chemical Society reviews*, 38(1):165–184, 2009.

[36] Marko Burghard. Electronic and vibrational properties of chemically modified single-wall carbon nanotubes. *Surface Science Reports*, 58:1–109, 2005.

[37] Zhongfang Chen, Walter Thiel, and Andreas Hirsch. Reactivity of the Convex and Concave Surfaces of Single-Walled Carbon Nanotubes (SWCNTs) towards Addition Reactions: Dependence on the Carbon-Atom Pyramidalization. *ChemPhysChem*, 4(1):93–97, jan 2003.

[38] Giuliano Giambastiani, Stefano Cicchi, Alessandra Giannasi, Lapo Luconi, Andrea Rossin, Francesco Mercuri, Claudio Bianchini, Alberto Brandi, Manuela Melucci, Giacomo Ghini, Paola Stagnaro, Lucia Conzatti, Elisa Passaglia, Marco Zoppi, Tiziano Montini, and Paolo Fornasiero. Functionalization of Multiwalled Carbon Nanotubes with Cyclic Nitrones for Materials and Composites: Addressing the Role of CNT Sidewall Defects. *Chem. Mater*, 23:1923–1938, 2011.

[39] Mingwen Zhao, Yueyuan Xia, James P Lewis, and Liangmo Mei. Chemical Reactivity of Single-Walled Carbon Nanotubes to Amidogen from Density Functional Calculations. *The Journal of Physical Chemistry B*, 108(28):9599–9603, jul 2004.

[40] V. Datsyuk, M. Kalyva, K. Papagelis, J. Parthenios, D. Tasis, A. Siokou, I. Kallitsis, and C. Galiotis. Chemical oxidation of multiwalled carbon nanotubes. *Carbon*, 46(6):833–840, 2008.

[41] Kirk J Ziegler, Zhenning Gu, Haiqing Peng, Erica L Flor, Robert H Hauge, and Richard E Smalley. Controlled Oxidative Cutting of Single-Walled Carbon Nanotubes. *Journal of the American Chemical Society*, 127(5):1541–1547, feb 2005.

[42] John G. Coroneus, Brett R. Goldsmith, Jorge A. Lamboy, Alexander A. Kane, Philip G. Collins, and Gregory A. Weiss. Mechanism-guided improvements to the single molecule oxidation of carbon nanotube sidewalls. *ChemPhysChem*, 9(7):1053–1056, 2008.

[43] Hidefumi Hiura, Thomas W. Ebbesen, and Katsumi Tanigaki. Opening and purification of carbon nanotubes in high yields. *Advanced Materials*, 7(3):275–276, mar 1995.

[44] Jeffrey L Bahr, Jiping Yang, Dmitry V Kosynkin, Michael J Bronikowski, Richard E Smalley, and James M Tour. Functionalization of Carbon Nanotubes by Electrochemical Reduction of Aryl Diazonium Salts: A Bucky Paper Electrode. *Journal of the American Chemical Society*, 123(27):6536–6542, jul 2001.

[45] Dimitrios Tasis, Nikos Tagmatarchis, Alberto Bianco, and Maurizio Prato. Chemistry of Carbon Nanotubes. *Chemical Reviews*, 106(3):1105–1136, mar 2006.

[46] Jian Chen, Mark A Hamon, Hui Hu, Yongsheng Chen, Apparao M Rao, Peter C Eklund, and Robert C Haddon. Solution Properties of Single-Walled Carbon Nanotubes. *Science*, 282(5386):95–98, oct 1998.

[47] Karl S Coleman, Sam R Bailey, Siân Fogden, and Malcolm L H Green. Functionalization of Single-Walled Carbon Nanotubes via the Bingel Reaction. *Journal of the American Chemical Society*, 125(29):8722–8723, jul 2003.

[48] Nikos Tagmatarchis and Maurizio Prato. Functionalization of carbon nanotubes via 1,3-dipolar cycloadditions. *Journal of Materials Chemistry*, 14(4):437, feb 2004.

[49] Mustafa K Bayazit and Karl S Coleman. Fluorescent Single-Walled Carbon Nanotubes Following the 1,3-Dipolar Cycloaddition of Pyridinium Ylides. *Journal of the American Chemical Society*, 131(30):10670–10676, 2009.

[50] A P Herman and S Boncel. Nitrile N-oxides in programmable one-pot functionalization of multi-wall carbon nanotubes via 1,3-dipolar cycloaddition. *RSC Adv.*, 6(68):64129–64132, 2016.

[51] Mercedes Alvaro, Pedro Atienzar, Pilar De La Cruz, Juan L Delgado, Hermenegildo Garcia, and Fernando Langa. Sidewall Functionalization of Single-Walled Carbon Nanotubes with Nitrile Imines. Electron Transfer from the Substituent to the Carbon Nanotube. *Journal of the American Chemical Society*, 108(34):12691–12697, 2004.

[52] Yan-Li Zhao and J. Fraser Stoddart. Noncovalent Functionalization of Single-Walled Carbon Nanotubes. *Accounts of Chemical Research*, 42(8):1161–1171, aug 2009.

[53] O. S. Zueva, O. N. Makshakova, B. Z. Idiyatullin, D. A. Faizullin, N. N. Benevolenskaya, A. O. Borovskaya, E. A. Sharipova, Yu N. Osin, V. V. Salnikov, and Yu F. Zuev. Structure and properties of aqueous dispersions of sodium dodecyl sulfate with carbon nanotubes. *Russian Chemical Bulletin*, 65(5):1208–1215, may 2016.

[54] Yutaka Maeda, Takeshi Akasaka, Jing Lu, and Shigeru Nagase. Dispersion and Separation of Single-Walled Carbon Nanotubes. In *Chemistry of Nanocarbons*, pages 365–383. John Wiley & Sons, Ltd, Chichester, UK, jun 2010.

[55] Claudia Backes and Andreas. Hirsch. Noncovalent Functionalization of Carbon Nanotubes. In *Chemistry of Nanocarbons*, pages 1–48. John Wiley & Sons, Ltd, Chichester, UK, jun 2010.

[56] Michael J. O'Connell, Peter Boul, Lars M. Ericson, Chad Huffman, Yuhuang Wang, Erik Haroz, Cynthia Kuper, Jim Tour, Kevin D. Ausman, and Richard E. Smalley. Reversible water-solubilization of single-walled carbon nanotubes by polymer wrapping. *Chemical Physics Letters*, 342(3-4):265–271, jul 2001.

[57] Robert J. Chen, Yuegang Zhang, Dunwei Wang, and Hongjie Dai. Noncovalent Sidewall Functionalization of Single-Walled Carbon Nanotubes for Protein Immobilization. *Journal of the American Chemical Society*, 123(16):3838–3839, apr 2001.

[58] Naotoshi Nakashima, Yasuhiko Tomonari, and Hiroto Murakami. Water-Soluble Single-Walled Carbon Nanotubes via Noncovalent Sidewall-Functionalization with a Pyrene-Carrying Ammonium Ion. *Chemistry Letters*, 31(6):638–639, jun 2002.

[59] Christian Ehli, G M Aminur Rahman, Norbert Jux, Domenico Balbinot, Dirk M Guldi, Francesco Paolucci, Massimo Marcaccio, Demis Paolucci, Manuel Melle-Franco, Francesco Zerbetto, Stéphane Campidelli, and Maurizio Prato. Interactions in Single Wall Carbon Nanotubes/Pyrene/Porphyrin Nanohybrids. *Journal of the American Chemical Society*, 128(34):11222–11231, aug 2006.

[60] Hiroto Murakami, Takuro Nomura, and Naotoshi Nakashima. Noncovalent porphyrin-functionalized single-walled carbon nanotubes in solution and the formation of porphyrin–nanotube nanocomposites. *Chemical Physics Letters*, 378(5-6):481–485, sep 2003.

[61] Yasuhiko Tomonari, Hiroto Murakami, and Naotoshi Nakashima. Solubilization of Single-Walled Carbon Nanotubes by using Polycyclic Aromatic Ammonium Amphiphiles in Water—Strategy for the Design of High-Performance Solubilizers. *Chemistry - A European Journal*, 12(15):4027–4034, may 2006.

[62] Panayiotis Bilalis, Dimitrios Katsigiannopoulos, Apostolos Avgeropoulos, and Georgios Sakellariou. Non-covalent functionalization of carbon nanotubes with polymers. *RSC Adv.*, 4(6):2911–2934, 2014.

[63] Chelsea R. Martinez and Brent L. Iverson. Rethinking the term "pi-stacking". *Chemical Science*, 3(7):2191, 2012.

[64] S. Meuer, L. Braun, T. Schilling, and R. Zentel. α-Pyrene polymer functionalized multiwalled carbon nanotubes: Solubility, stability and depletion phenomena. *Polymer*, 50(1):154–160, jan 2009.

[65] Jianhua Zou, Jianhua Liu, Binh Tran, Qun Huo, and Lei Zhai. Modification of Nanotubes with Conjugated Block Copolymers. In *Surface Modification of Nanotube Fillers*, pages 67–89. Wiley-VCH Verlag GmbH & Co. KGaA, Weinheim, Germany, apr 2011.

[66] Shuhui Qin, Dongqi Qin, Warren T Ford, Daniel E Resasco, and Jose E Herrera. Functionalization of Single-Walled Carbon Nanotubes with Polystyrene via Grafting to and Grafting from Methods. *Macromolecules*, 37(3):752–757, feb 2004.

[67] Matthew J. Shea, Jialiang Wang, Jessica T. Flach, Martin T. Zanni, and Michael S. Arnold. Less severe processing improves carbon nanotube photovoltaic performance. *APL Materials*, 6(5):056104, may 2018.

[68] K.L. Lu, R.M. Lago, Y.K. Chen, M.L.H. Green, P.J.F. Harris, and S.C. Tsang. Mechanical damage of carbon nanotubes by ultrasound. *Carbon*, 34(6):814–816, jan 1996.

[69] Woo Ram Jung, Jin Hyuk Choi, Naesung Lee, Kwanwoo Shin, Jun-Hyuk Moon, and Young-Soo Seo. Reduced damage to carbon nanotubes during ultrasound-assisted dispersion as a result of supercritical-fluid treatment. *Carbon*, 50(2):633–636, feb 2012.

[70] Sun Hwa Lee, Duck Hyun Lee, Won Jun Lee, and Sang Ouk Kim. Tailored assembly of carbon nanotubes and graphene. *Advanced Functional Materials*, 21(8):1338–1354, 2011.

[71] Feixiang Wu and Gleb Yushin. Conversion cathodes for rechargeable lithium and lithium-ion batteries. *Energy Environ. Sci.*, 10(2):435–459, 2017.

[72] Hailiang Wang and Hongjie Dai. Strongly coupled inorganic–nano-carbon hybrid materials for energy storage. *Chemical Society Reviews*, 42(7):3088, feb 2013.

[73] Yang Li, Huicai Wang, Yousi Chen, and Mujie Yang. A multi-walled carbon nanotube/palladium nanocomposite prepared by a facile method for the detection of methane at room temperature. *Sensors and Actuators, B: Chemical*, 132(1):155–158, 2008.

[74] Andrea Masotti, Andrea Caporali, Andrea Masotti, and Andrea Caporali. Preparation of Magnetic Carbon Nanotubes (Mag-CNTs) for Biomedical and Biotechnological Applications. *International Journal of Molecular Sciences*, 14(12):24619–24642, dec 2013.

[75] Yongye Liang, Yanguang Li, Hailiang Wang, and Hongjie Dai. Strongly Coupled Inorganic/Nanocarbon Hybrid Materials for Advanced Electrocatalysis. *Journal of the American Chemical Society*, 135(6):2013–2036, feb 2013.

[76] Krzysztof Matyjaszewski and Nicolay V. Tsarevsky. Nanostructured functional materials prepared by atom transfer radical polymerization. *Nature Chemistry*, 1(4):276–288, jul 2009.

[77] Peter J. Hore. *Nuclear magnetic resonance*. Oxford University Press, New York, 2nd editio edition, 2015.

[78] Renato Zenobi. *Ionization Processes and Detection in MALDI-MS of Polymers*, chapter 2, pages 9–26. John Wiley & Sons, Ltd, 2009.

[79] André M. Striegel, Wallace W. Yau, Joseph J. Kirkland, and Donald D. Bly. *Modern Size-Exclusion Liquid Chromatography: Practice of Gel Permeation and Gel Filtration Chromatography: Second Edition*. 2009.

[80] Gregoriou Aldred A. Christy, Yukihiro Ozaki, Vasilis G. Modern Fourier Transform Infrared Spectroscopy. In *Volume 35 of Comprehensive analytical chemistry*, page 356. Elsevier Science, 2001.

[81] Paul van der Heide. *X-Ray Photoelectron Spectroscopy: An Introduction to Principles and Practices*. 2011.

[82] Benjamin Dietzek, Dana Cialla, Michael Schmitt, and Jürgen Popp. *Introduction to the Fundamentals of Raman Spectroscopy*, pages 47–68. Springer International Publishing, Cham, 2018.

[83] Riichiro Saito, Cristiano Fantini, and Jie Jiang. *Excitonic States and Resonance Raman Spectroscopy of Single-Wall Carbon Nanotubes*, pages 251–286. Springer Berlin Heidelberg, Berlin, Heidelberg, 2008.

[84] R. Graupner. Raman spectroscopy of covalently functionalized single-wall carbon nanotubes. *Journal of Raman Spectroscopy*, 38(6):673–683, jun 2007.

[85] Peter Haines, editor. *Principles of Thermal Analysis and Calorimetry*. Royal Society of Chemistry, Cambridge, 2002.

[86] Andr M. Striegel, Wallace W. Yau, Joseph J. Kirkland, and Donald D. Bly. Frontmatter. In *Modern Size-Exclusion Liquid Chromatography*, pages i–xvi. John Wiley & Sons, Inc., Hoboken, NJ, USA, nov 2009.

[87] David B. Williams and C. Barry Carter. *Transmission electron microscopy: A textbook for materials science*. 2009.

[88] C B Murray, C R Kagan, and M G Bawendi. Synthesis and Characterization of Monodisperse Nanocrystals and Close-Packed Nanocrystal Assemblies. *Annual Review of Materials Science*, 30(1):545–610, aug 2000.

[89] Jörg Polte. Fundamental growth principles of colloidal metal nanoparticles – a new perspective. *CrystEngComm*, 17(36):6809–6830, sep 2015.

[90] R E Dinnebier and S J L Billinge, editors. *Powder Diffraction*. Royal Society of Chemistry, Cambridge, mar 2008.

[91] Malvern Instruments. *Zetasizer Nano User Manual MAN0485 Issue 1.1 April 2013 English*. 2007.

[92] Durairaj Baskaran, Jimmy W Mays, and Matthew S Bratcher. Noncovalent and Nonspecific Molecular Interactions of Polymers with Multiwalled Carbon Nanotubes. *Chemistry of Materials*, 17(13):3389–3397, jun 2005.

[93] Wenhui Yi, Andrey Malkovskiy, Qinghui Chu, Alexei P. Sokolov, Marisabel Lebron Colon, Michael Meador, and Yi Pang. Wrapping of Single-Walled Carbon Nanotubes by a π-Conjugated Polymer: The Role of Polymer Conformation-Controlled Size Selectivity. *The Journal of Physical Chemistry B*, 112(39):12263–12269, oct 2008.

[94] Shingo Tamesue, Munenori Numata, Kenji Kaneko, Tony D. James, and Seiji Shinkai. Hierarchical carbon nanotube assemblies created by sugar–boric or boronic acid interactions. *Chemical Communications*, 0(37):4478, sep 2008.

[95] Hiromi Kitano, Kazutaka Tachimoto, Tadashi Nakaji-Hirabayashi, and Hiroaki Shinohara. Wrapping of single-walled carbon nanotubes with A-B-A block telomers. *Macromolecular Chemistry and Physics*, 205(15):2064–2071, 2004.

[96] Syamal S. Tallury and Melissa A. Pasquinelli. Molecular Dynamics Simulations of Flexible Polymer Chains Wrapping Single-Walled Carbon Nanotubes. *The Journal of Physical Chemistry B*, 114(12):4122–4129, apr 2010.

[97] Wei Liu, Chuan-Lu Yang, Ying-Tao Zhu, and Mei-shan Wang. Interactions between Single-Walled Carbon Nanotubes and Polyethylene/Polypropylene/Polystyrene/Poly(phenylacetylene)/Poly(p - phenylenevinylene) Considering Repeat Unit Arrangements and Conformations: A Molecular Dynamics Simulation Study. *The Journal of Physical Chemistry C*, 112(6):1803–1811, feb 2008.

[98] Peter May, Umar Khan, J Marguerite Hughes, and Jonathan N Coleman. Role of Solubility Parameters in Understanding the Steric Stabilization of Exfoliated Two-Dimensional Nanosheets by Adsorbed Polymers. *The Journal of Physical Chemistry C*, 116(20):11393–11400, may 2012.

[99] Cuiping Yuan, Jianjun Wang, Guangming Chen, Jinhao Zhang, and Jiping Yang. Orientation studies of uniaxial drawn syndiotactic polystyrene/carbon nanotube nanocomposite films. *Soft Matter*, 7(8):4039, 2011.

[100] Zhinan Zhang, Jun Zhang, Peng Chen, Baoqing Zhang, Jiasong He, and Guo-Hua Hu. Enhanced interactions between multi-walled carbon nanotubes and polystyrene induced by melt mixing. *Carbon*, 44(4):692–698, apr 2006.

[101] Hernan Garate, Mirta L. Fascio, Iñaki Mondragon, Norma B. D'Accorso, and Silvia Goyanes. Surfactant-aided dispersion of polystyrene-functionalized carbon nanotubes in a nanostructured poly(styrene-b-isoprene-b-styrene) block copolymer. *Polymer*, 52(10):2214–2220, may 2011.

[102] Greg J. Bahun, Clair Wang, and Alex Adronov. Solubilizing single-walled carbon nanotubes with pyrene-functionalized block copolymers. *Journal of Polymer Science Part A: Polymer Chemistry*, 44(6):1941–1951, mar 2006.

[103] Stefan Meuer, Lydia Braun, and Rudolf Zentel. Solubilisation of multi walled carbon nanotubes by α-pyrene functionalised PMMA and their liquid crystalline self-organisation. *Chemical Communications*, (27):3166, 2008.

[104] Darron E. Hill, Yi Lin, Apparao M. Rao, Lawrence F. Allard, and Ya-Ping Sun. Functionalization of Carbon Nanotubes with Polystyrene. *Macromolecules*, 35(25):9466–9471, dec 2002.

[105] Darron E. Hill, Yi Lin, Lawrence F. Allard, and Ya-Ping Sun. Solubilization of carbon nanotubes via polymer Attachment. *International Journal of Nanoscience*, 01(03n04):213–221, jun 2002.

[106] Nina I. Kovtyukhova, Thomas E. Mallouk, Ling Pan, and Elizabeth C. Dickey. Individual Single-Walled Nanotubes and Hydrogels Made by Oxidative Exfoliation of Carbon Nanotube Ropes. *Journal of the American Chemical Society*, 125(32):9761–9769, aug 2003.

[107] Albert W. Xiao, Koen Evers, Marzena Tkaczyk, Ruth S. Jones, Claire Saxby, Kalin Dragnevski, and Nicole Grobert. Electrophoretic Fabrication of Robust Carbon Nanotube "Buckyfilms" for Flexible Electronics. *ACS Applied Nano Materials*, 2(8):5190–5199, aug 2019.

[108] Guodong Xu, Bo Zhu, Yang Han, and Zhishan Bo. Covalent functionalization of multi-walled carbon nanotube surfaces by conjugated polyfluorenes. *Polymer*, 48(26):7510–7515, dec 2007.

[109] Shiyun Li, Hui Chen, Wuguo Bi, Jianjun Zhou, Yanhui Wang, Jianzhong Li, Wenxi Cheng, Meiye Li, Lin Li, and Tao Tang. Synthesis and characterization of polyethylene chains grafted onto the sidewalls of single-walled carbon nanotubes via copolymerization. *Journal of Polymer Science Part A: Polymer Chemistry*, 45(23):5459–5469, dec 2007.

[110] Manoko S. Maubane, Messai A. Mamo, Edward N. Nxumalo, Willem A.L. van Otterlo, and Neil J. Coville. Tubular shaped composites made from polythiophene covalently linked to Prato functionalized N-doped carbon nanotubes. *Synthetic Metals*, 162(24):2307–2315, dec 2012.

[111] Amit Mandal and Arun K. Nandi. Physical properties of poly(vinylidene fluoride) composites with polymer functionalized multiwalled carbon nanotubes using nitrene chemistry. *Journal of Materials Chemistry*, 21(39):15752–15763, oct 2011.

[112] Wei Wu, Shuang Zhang, Yong Li, Junxin Li, Luqi Liu, Yujun Qin, Zhi-Xin Guo, Liming Dai, Cheng Ye, and Daoben Zhu. PVK-Modified Single-Walled Carbon Nanotubes with Effective Photoinduced Electron Transfer. *Macromolecules*, 36(17):6286–6288, aug 2003.

[113] Yuanqin Liu, Zhaoling Yao, and Alex Adronov. Functionalization of Single-Walled Carbon Nanotubes with Well-Defined Polymers by Radical Coupling. *Macromolecules*, 38(4):1172–1179, feb 2005.

[114] Christa M. Homenick, Gregor Lawson, and Alex Adronov. Polymer Grafting of Carbon Nanotubes Using Living Free-Radical Polymerization. *Polymer Reviews*, 47(2):265–290, apr 2007.

[115] Seyyed Shayan Meysami, Antal A. Koós, Frank Dillon, and Nicole Grobert. Aerosol-assisted chemical vapour deposition synthesis of multi-wall carbon nanotubes: II. An analytical study. *Carbon*, 58:159–169, jul 2013.

[116] Aura Tintaru, Christophe Chendo, Trang N T Phan, Marion Rollet, Laurent Giordano, Stéphane Viel, Didier Gigmes, and Laurence Charles. End-Group Cleavage in MALDI of ATRP-Made Polystyrene: A Silver-Catalyzed Reaction during Sample Preparation. *Analytical Chemistry*, 85(11):5454–5462, jun 2013.

[117] Pei Yuin Keng, Inbo Shim, Bryan D. Korth, Jack F. Douglas, and Jeffrey Pyun. Synthesis and Self-Assembly of Polymer-Coated Ferromagnetic Nanoparticles. *ACS Nano*, 1(4):279–292, nov 2007.

[118] Raoul Blume, Dirk Rosenthal, Jean-Philippe Tessonnier, Henan Li, Axel Knop-Gericke, and Robert Schlögl. Characterizing Graphitic Carbon with X-ray Photoelectron Spectroscopy: A Step-by-Step Approach. *ChemCatChem*, 7(18):2871–2881, sep 2015.

[119] Gilad Zorn, Li-Hong Liu, Líney Árnadóttir, Hui Wang, Lara J Gamble, David G Castner, and Mingdi Yan. X-ray Photoelectron Spectroscopy Investigation of the Nitrogen Species in Photoactive Perfluorophenylazide-Modified Surfaces. *The Journal of Physical Chemistry C*, 118(1):376–383, jan 2014.

[120] Christopher A Dyke and James M Tour. Covalent Functionalization of Single-Walled Carbon Nanotubes for Materials Applications. *The Journal of Physical Chemistry A*, 108(51):11151–11159, dec 2004.

[121] Jeffrey L. Bahr, Edward T. Mickelson, Michael J. Bronikowski, Richard E. Smalley, and James M. Tour. Dissolution of small diameter single-wall carbon nanotubes in organic solvents? *Chemical Communications*, 0(2):193–194, jan 2001.

[122] Kevin D Ausman, Richard Piner, Oleg Lourie, Rodney S Ruoff, and Mikhail Korobov. Organic Solvent Dispersions of Single-Walled Carbon Nanotubes: Toward Solutions of Pristine Nanotubes. *The Journal of Physical Chemistry B*, 104(38):8911–8915, sep 2000.

[123] Attila Imre and W. Alexander Van Hook. Liquid–Liquid Demixing from Solutions of Polystyrene. 1. A Review. 2. Improved Correlation with Solvent Properties. *Journal of Physical and Chemical Reference Data*, 25(2):637–661, mar 1996.

[124] J. V. Dawkins. Thermodynamic interpretation of polystyrene retention on crosslinked polystyrene gels in GPC with poor and theta solvents. *Journal of Polymer Science: Polymer Physics Edition*, 14(3):569–571, mar 1976.

[125] Hyeong Jun Lim, Kunsil Lee, Young Shik Cho, Yern Seung Kim, Taehoon Kim, and Chong Rae Park. Experimental consideration of the Hansen solubility parameters of as-produced multi-walled carbon nanotubes by inverse gas chromatography. *Physical Chemistry Chemical Physics*, 16(33):17466, jul 2014.

[126] S. Detriche, J. B. Nagy, Z. Mekhalif, and J. Delhalle. Surface State of Carbon Nanotubes and Hansen Solubility Parameters. *Journal of Nanoscience and Nanotechnology*, 9(10):6015–6025, 2009.

[127] S. Detriche, G. Zorzini, J.-F. Colomer, A. Fonseca, and J. B. Nagy. Application of the Hansen Solubility Parameters Theory to Carbon Nanotubes. *Journal of Nanoscience and Nanotechnology*, 8(11):6082–6092, nov 2008.

[128] Robert Menzel, Adam Lee, Alexander Bismarck, and Milo S P Shaffer. Inverse Gas Chromatography of As-Received and Modified Carbon Nanotubes. *Langmuir*, 25(14):8340–8348, jul 2009.

[129] Charles M. Hansen. *Hansen Solubility Parameters A User's Handbook*. CRC Press, Boca Raton FL, second edi edition, 2007.

[130] A. Beerbower. Surface free energy: A new relationship to bulk energies. *Journal of Colloid and Interface Science*, 35(1):126–132, jan 1971.

[131] D M Koenhen and C. A. Smolders. The determination of solubility parameters of solvents and polymers by means of correlations with other physical quantities. *Journal of Applied Polymer Science*, 19(4):1163–1179, apr 1975.

[132] J. Lyklema. The surface tension of pure liquids. *Colloids and Surfaces A: Physicochemical and Engineering Aspects*, 156(1-3):413–421, oct 1999.

[133] Manuel J Louwerse, Ana Maldonado, Simon Rousseau, Chloe Moreau-Masselon, Bernard Roux, and Gadi Rothenberg. Revisiting Hansen Solubility Parameters by Including Thermodynamics. *ChemPhysChem*, 18(21):2999–3006, nov 2017.

[134] A Hardy and H Bock. Toward High-Throughput Computational Screening of Carbon Nanotube Solvents. *Langmuir*, 33(43):12267–12275, oct 2017.

[135] Pirre P. Ylä-Mäihäniemi, Jerry Y Y Heng, Frank Thielmann, and Daryl R Williams. Inverse Gas Chromatographic Method for Measuring the Dispersive Surface Energy Distribution for Particulates. *Langmuir*, 24(17):9551–9557, sep 2008.

[136] J. Schultz, L. Lavielle, and C. Martin. The Role of the Interface in Carbon Fibre-Epoxy Composites. *The Journal of Adhesion*, 23(1):45–60, sep 1987.

[137] Carl L. Yaws. *Thermophysical Properties of Chemicals and Hydrocarbons*. Elsevier, second edi edition, 2014.

[138] Christopher A. Hunter. Quantifying Intermolecular Interactions: Guidelines for the Molecular Recognition Toolbox. *Angewandte Chemie International Edition*, 43(40):5310–5324, oct 2004.

[139] Stryer L. Berg JM, Tymoczko JL. Section 1.3 Chemical Bonds in Biochemistry. In *Biochemistry*. 2002.

[140] Pablo Quijano Velasco, Kyriakos Porfyrakis, and Nicole Grobert. The application of the surface energy based solubility parameter theory for the rational design of polymer-functionalized MWCNTs. *Physical Chemistry Chemical Physics*, 21(10):5331–5334, 2019.

[141] Wei Wei Liu, Jian Nong Wang, and Xiao Xia Wang. Charging of unfunctionalized graphene in organic solvents. *Nanoscale*, 4(2):425–428, jan 2012.

[142] Dominique Piché, Isabella Tavernaro, Jana Fleddermann, Juan G. Lozano, Aakash Varambhia, Mahon L. Maguire, Marcus Koch, Tomofumi Ukai, Armando J. Hernández Rodríguez, Lewys Jones, Frank Dillon, Israel Reyes Molina, Mai Mitzutani, Evelio R. González Dalmau, Toru Maekawa, Peter D. Nellist, Annette Kraegeloh, and Nicole Grobert. Targeted T 1 Magnetic Resonance Imaging Contrast Enhancement with Extraordinarily Small CoFe 2 O 4 Nanoparticles. *ACS Applied Materials & Interfaces*, 11(7):6724–6740, feb 2019.

[143] Graham A. Rance and Andrei N. Khlobystov. Interactions Between Nanoparticles and Carbon Nanotubes: Directing the Self-Assembly of One-Dimensional Superstructures. In *Comprehensive Nanoscience and Nanotechnology*, volume 1-5, pages 219–236. Elsevier, jan 2019.

[144] Xianglong Li, Joe D. Thompson, Yingying Zhang, Christina I. Brady, Guifu Zou, Nathan H. Mack, Darrick Williams, Juan G. Duque, Quanxi Jia, and Stephen K. Doorn. Efficient synthesis of tailored magnetic carbon nanotubesvia a noncovalent chemical route. *Nanoscale*, 3(2):668–673, 2011.

[145] Xianglong Li, Yi Jia, and Anyuan Cao. Tailored Single-Walled Carbon Nanotube−CdS Nanoparticle Hybrids for Tunable Optoelectronic Devices. *ACS Nano*, 4(1):506–512, jan 2010.

[146] Ju Feng, Yongye Liang, Hailiang Wang, Yanguang Li, Bo Zhang, Jigang Zhou, Jian Wang, Tom Regier, and Hongjie Dai. Engineering manganese oxide/nanocarbon hybrid materials for oxygen reduction electrocatalysis. *Nano Research*, 5(10):718–725, oct 2012.

[147] Toby Sainsbury, Jacek Stolarczyk, and Donald Fitzmaurice. An Experimental and Theoretical Study of the Self-Assembly of Gold Nanoparticles at the Surface of Functionalized Multiwalled Carbon Nanotubes. *The Journal of Physical Chemistry B*, 109(34):16310–16325, sep 2005.

[148] Dominik Eder. Carbon Nanotube−Inorganic Hybrids. *Chemical Reviews*, 110(3):1348–1385, mar 2010.

[149] Xiaohui Peng, Jingyi Chen, James A. Misewich, and Stanislaus S. Wong. Carbon nanotube–nanocrystal heterostructures. *Chemical Society Reviews*, 38(4):1076, mar 2009.

[150] Xiaohui Peng and Stanislaus S. Wong. Controlling Nanocrystal Density and Location on Carbon Nanotube Templates. *Chemistry of Materials*, 21(4):682–694, feb 2009.

[151] N. Chopra, M. Majumder, and B. J. Hinds. Bifunctional Carbon Nanotubes by Sidewall Protection. *Advanced Functional Materials*, 15(5):858–864, may 2005.

[152] Lei Wang, Jinkyu Han, Jessica Hoy, Fang Hu, Haiqing Liu, Molly M. Gentleman, Matthew Y. Sfeir, James A. Misewich, and Stanislaus S. Wong. Probing differential optical and coverage behavior in nanotube–nanocrystal heterostructures synthesized by covalent versus non-covalent approaches. *Dalton Transactions*, 43(20):7480, may 2014.

[153] Toby Sainsbury and Donald Fitzmaurice. Carbon-Nanotube-Templated and Pseudorotaxane-Formation-Driven Gold Nanowire Self-Assembly. *Chemistry of Materials*, 16(11):2174–2179, jun 2004.

[154] Li Han, Wendy Wu, F. Louis Kirk, Jin Luo, Mathew M. Maye, Nancy N. Kariuki, Yuehe Lin, Chongmin Wang, and Chuan-Jian Zhong. A Direct Route toward Assembly of Nanoparticle−Carbon Nanotube Composite Materials. *Langmuir*, 20(14):6019–6025, jul 2004.

[155] Vasilios Georgakilas, Vasilios Tzitzios, Dimitrios Gournis, and Dimitrios Petridis. Attachment of Magnetic Nanoparticles on Carbon Nanotubes and Their Soluble Derivatives. *Chemistry of Materials*, 17(7):1613–1617, apr 2005.

[156] A. V. Ellis, K. Vijayamohanan, R. Goswami, N. Chakrapani, L. S. Ramanathan, P. M. Ajayan, and G. Ramanath. Hydrophobic Anchoring of Monolayer-Protected Gold Nanoclusters to Carbon Nanotubes. *Nano Letters*, 3(3):279–282, mar 2003.

[157] G.M. Aminur Rahman, Dirk M. Guldi, Elena Zambon, Lucia Pasquato, Nikos Tagmatarchis, and Maurizio Prato. Dispersable Carbon Nanotube/Gold Nanohybrids: Evidence for Strong Electronic Interactions. *Small*, 1(5):527–530, may 2005.

[158] G. A. Rance and A. N. Khlobystov. Interactions of carbon nanotubes and gold nanoparticles: the effects of solvent dielectric constant and temperature on controlled assembly of superstructures. *Dalton Transactions*, 43(20):7400, may 2014.

[159] Graham A. Rance, Dan H. Marsh, Stephen J. Bourne, Thomas J. Reade, and Andrei N. Khlobystov. van der Waals Interactions between Nanotubes and Nanoparticles for Controlled Assembly of Composite Nanostructures. *ACS Nano*, 4(8):4920–4928, aug 2010.

[160] Zhichuan Xu, Chengmin Shen, Yanglong Hou, Hongjun Gao, and Shouheng Sun. Oleylamine as Both Reducing Agent and Stabilizer in a Facile Synthesis of Magnetite Nanoparticles. *Chemistry of Materials*, 21(9):1778–1780, may 2009.

[161] Wonbaek Kim, Chang-Yul Suh, Sung-Wook Cho, Ki-Min Roh, Hanjung Kwon, Kyungsun Song, and In-Jin Shon. A new method for the identification and quantification of magnetite–maghemite mixture using conventional X-ray diffraction technique. *Talanta*, 94:348–352, may 2012.

[162] Jitkang Lim, Swee Pin Yeap, Hui Xin Che, and Siew Chun Low. Characterization of magnetic nanoparticle by dynamic light scattering. *Nanoscale Research Letters*, 8(1):381, dec 2013.

[163] Richard Anthony Harris, Poslet Morgan Shumbula, and Hendriëtte van der Walt. Analysis of the Interaction of Surfactants Oleic Acid and Oleylamine with Iron Oxide Nanoparticles through Molecular Mechanics Modeling. *Langmuir*, 31(13):3934–3943, apr 2015.

[164] Xingchen Ye, Chenhui Zhu, Peter Ercius, Shilpa N. Raja, Bo He, Matthew R. Jones, Matthew R. Hauwiller, Yi Liu, Ting Xu, and A. Paul Alivisatos. Structural diversity in binary superlattices self-assembled from polymer-grafted nanocrystals. *Nature Communications*, 6(1):10052, dec 2015.

[165] Richard A.L. Jones. *Soft Condensed Matter*. Oxford University Press, New York, 1st edition, 2002.

[166] V. Pérez-Dieste, O. M. Castellini, J. N. Crain, M. A. Eriksson, A. Kirakosian, J.-L. Lin, J. L. McChesney, F. J. Himpsel, C. T. Black, and C. B. Murray. Thermal decomposition of surfactant coatings on Co and Ni nanocrystals. *Applied Physics Letters*, 83(24):5053–5055, dec 2003.

[167] M. Bystrzejewski. Synthesis of carbon-encapsulated iron nanoparticles via solid state reduction of iron oxide nanoparticles. *Journal of Solid State Chemistry*, 184(6):1492–1498, jun 2011.

[168] Madhuri Dutta, Valeria Nicolosi, Ekaterina Obratzsova, Antal A. Koós, Alison Crossley, and Nicole Grobert. Stable Dispersions of Nitrogen Containing Multi-Walled Carbon Nanotubes. *Materials Express*, 1(3):201–209, sep 2011.

Appendix A

List of Common Abbreviations

0D	Zero-dimensional
1D	One-dimensional
2D	Two-dimensional
ATR	Attenuated total reflection
ATRP	Atom transfer radical polymerisation
AuNP	Gold nanoparticle
CNT	Carbon nanotube
CVD	Chemical vapor deposition
DMF	Dimethylformamide
DWCNT	Double-wall carbon nanotube
FTIR	Fourier transform infrared spectroscopy
GPC	Gel permeation chromatography
HSP	Hansen solubility parameter

IGC	Inverse gas chromatography
SWCNT	Single-wall carbon nanotube
MWCNT	Multi-wall carbon nanotube
NMP	N-Methyl-2-pyrrolidone
IONP	Iron oxide nanoparticle
XPS	X-ray photoelectron spectroscopy
TGA	Thermogravimetric analysis
NMR	Nuclear magnetic resonance
MALDI	Matrix-assisted laser desorption/ionisation
PXRD	Powder X-ray diffraction
TEM	Transmission electron microscopy
DLS	Dynamic light scattering
PS	Polystyrene
THF	Tetrahydrofuran
DMF	Dimethylformamide
NMP	N-methyl-2-pyrrolidone
DCM	Dichloromethane
o-DCB	Orto-dichlorobenzene
10nmMWCNT	NC700 MWCNT
50nmMWCNT	Aerosol assisted chemical vapor deposition MWCNT

PS-N_3	Polystyrene with an azide end-group
PS-Al	Polystyrene with an aldehyde end-group
PS-Py	Polystyrene with a pyrene end-group
PS-Br	Polystyrene as synthetised by ATRP
SEBSP	Surface energy based solubility parameter theory
IONP	Iron oxide nanoparticle
OAIONP	Oleylamine coated iron oxide nanoparticle
OA	Oleylamine
PSIONP	Polystyrene coated iron oxide nanoparticle

Appendix B

List of Common Symbols

D/G	Intensity ratio between the Raman D-peak and G-peak of a CNT
V_g	Specific retention volume
ΔG_{ads}	Gibbs free energy of adsorption
ΔG_{mix}	Gibbs free energy of mixing
ΔH_{ads}	Enthalpy of adsorption
ΔH_{mix}	Enthalpy of mixing
ΔS_{mix}	Entropy of mixing
δ	Solubility parameter
∂	Surface energy based solubility parameter
E_{sur}	Surface energy
γ	Surface tension

Appendix C

Supplementary Characterisation Data

The following appendix includes figures relevant to the characterisation of the experiments performed throughout this thesis that were not included in the main text due to their supplementary role in supporting the findings of these studies. A section for each experimental chapter has been included within this appendix and the supplementary characterisation data are classified by the characterisation technique used for the measurements.

C.1 Functionalisation of MWCNTs with polystyrene through covalent and non-covalent methodologies

C.1.1 NMR

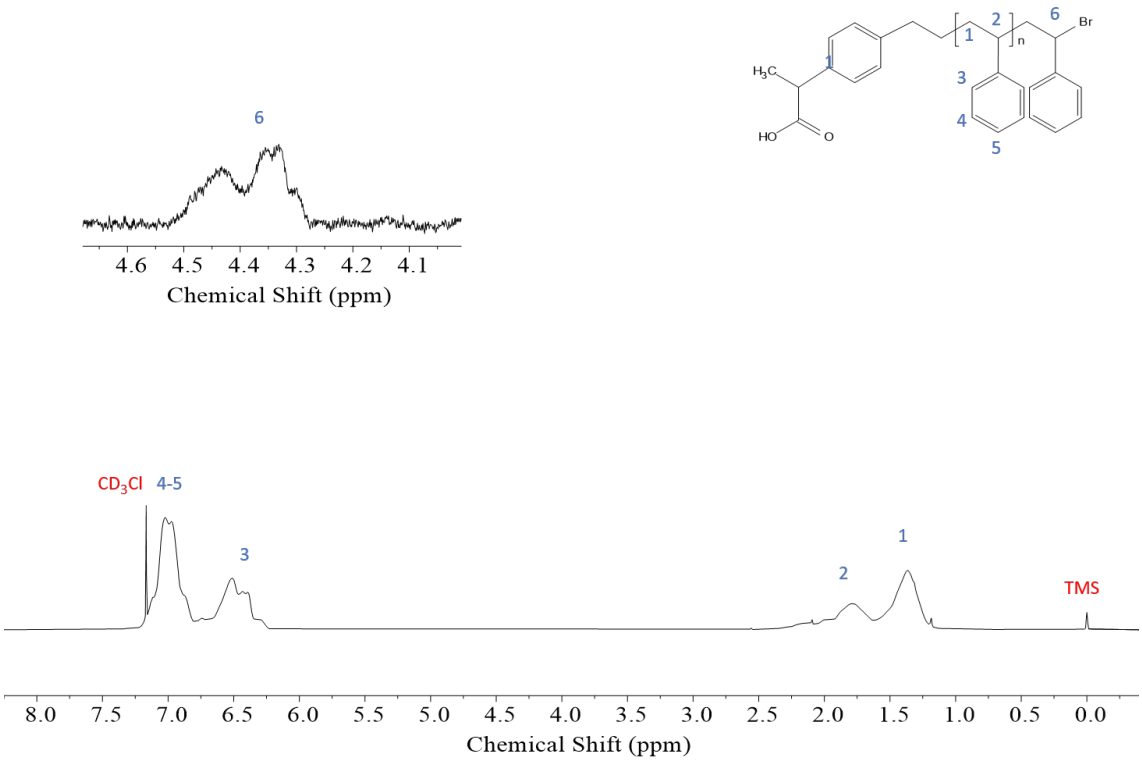


Figure C.1: *NMR spectrum of PS-Br.* ^1H *NMR (450MHz,* $CDCl_3$*):* δ 7.1-6.5 *ppm (broad, aromatic H),* 4.5-4.2 *(broad,* CH_2*-Br)* 2.5-1.1 *ppm (broad,* $CH+CH_2$*).*

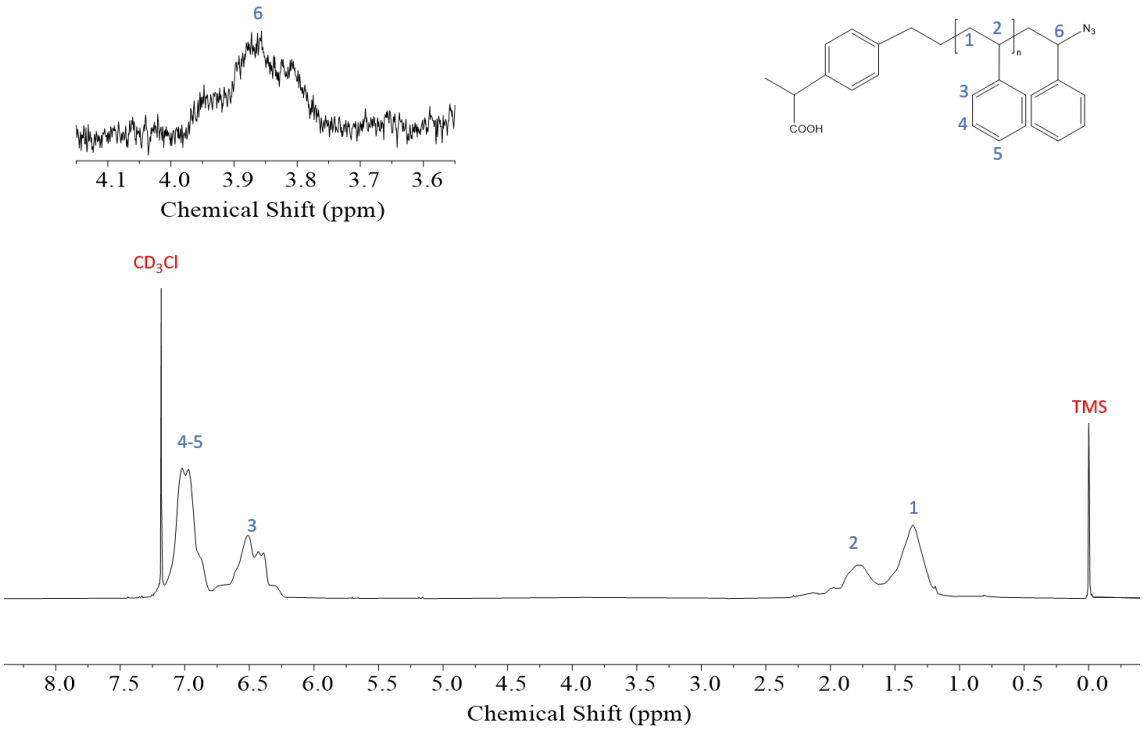


Figure C.2: *NMR spectrum of PS-N_3.* ^{1}*H NMR (450MHz, $CDCl_3$):* δ 7.1-6.5 *ppm (broad, aromatic H),* 2.5-1.1 *ppm (broad, CH+CH_2),* 3.9 *(singlet, CH_2-N_3).*

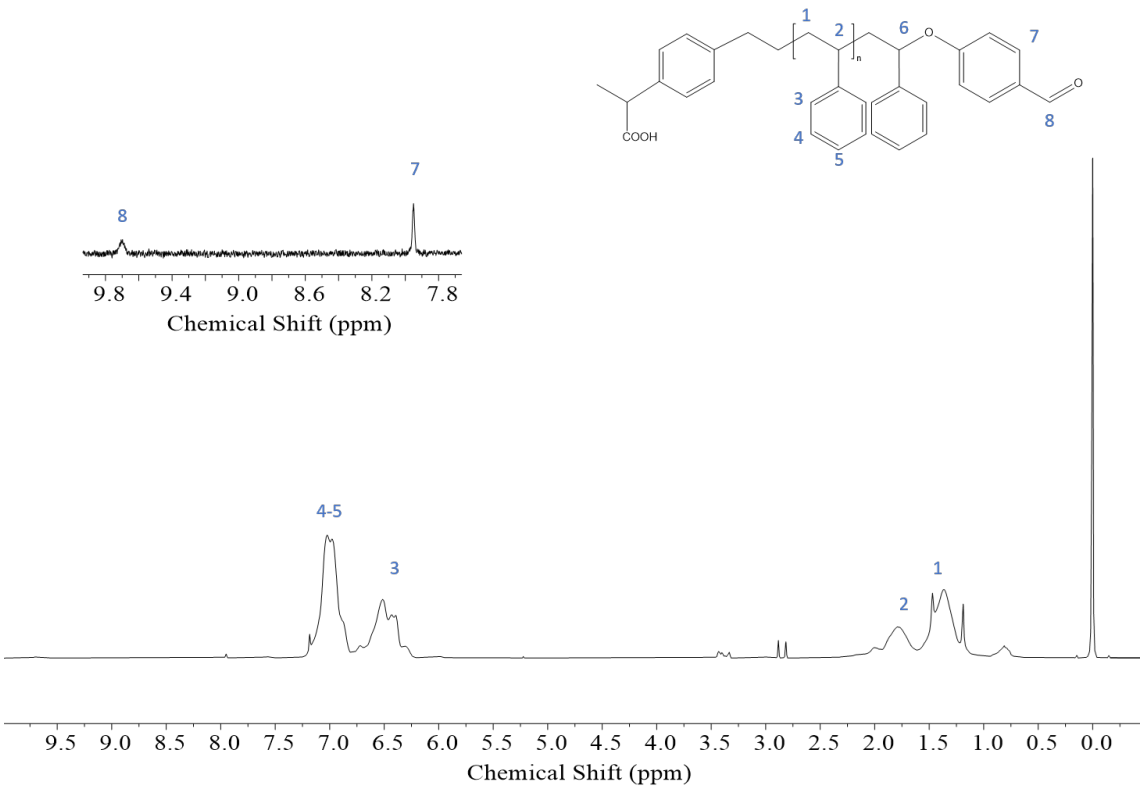


Figure C.3: *NMR spectrum of PS-Al.* ^{1}*H NMR (450MHz, $CDCl_3$):* δ 7.1-6.5 *ppm (broad, aromatic H),* 2.5-1.1 ppm *(broad, CH+CH_2),* 9.7 *ppm (s, CH=O),* 7.6 *ppm (broad, aromatic aldehyde).*

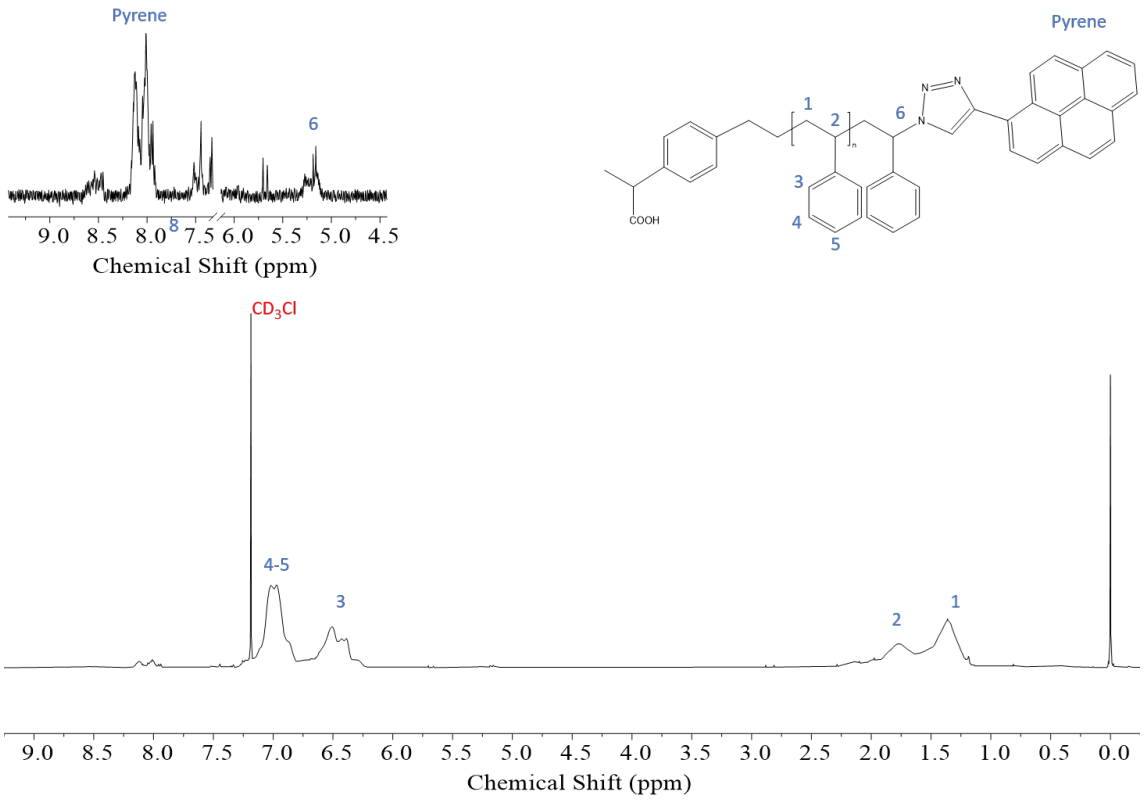


Figure C.4: *NMR spectrum of PS-Py.* ^1H *NMR (450MHz, CDCl3):* δ 7.1-6.5 *ppm (broad, benzene aromatic H),* 4.5-4.2 *(duplet,* CH_2*-Br)* 2.5-1.1 *ppm (broad,* $CH+CH_2$*),* 7.9-8.5 *ppm (broad, pyrene aromatic H),* 5.2 *(broad, CH-N).*

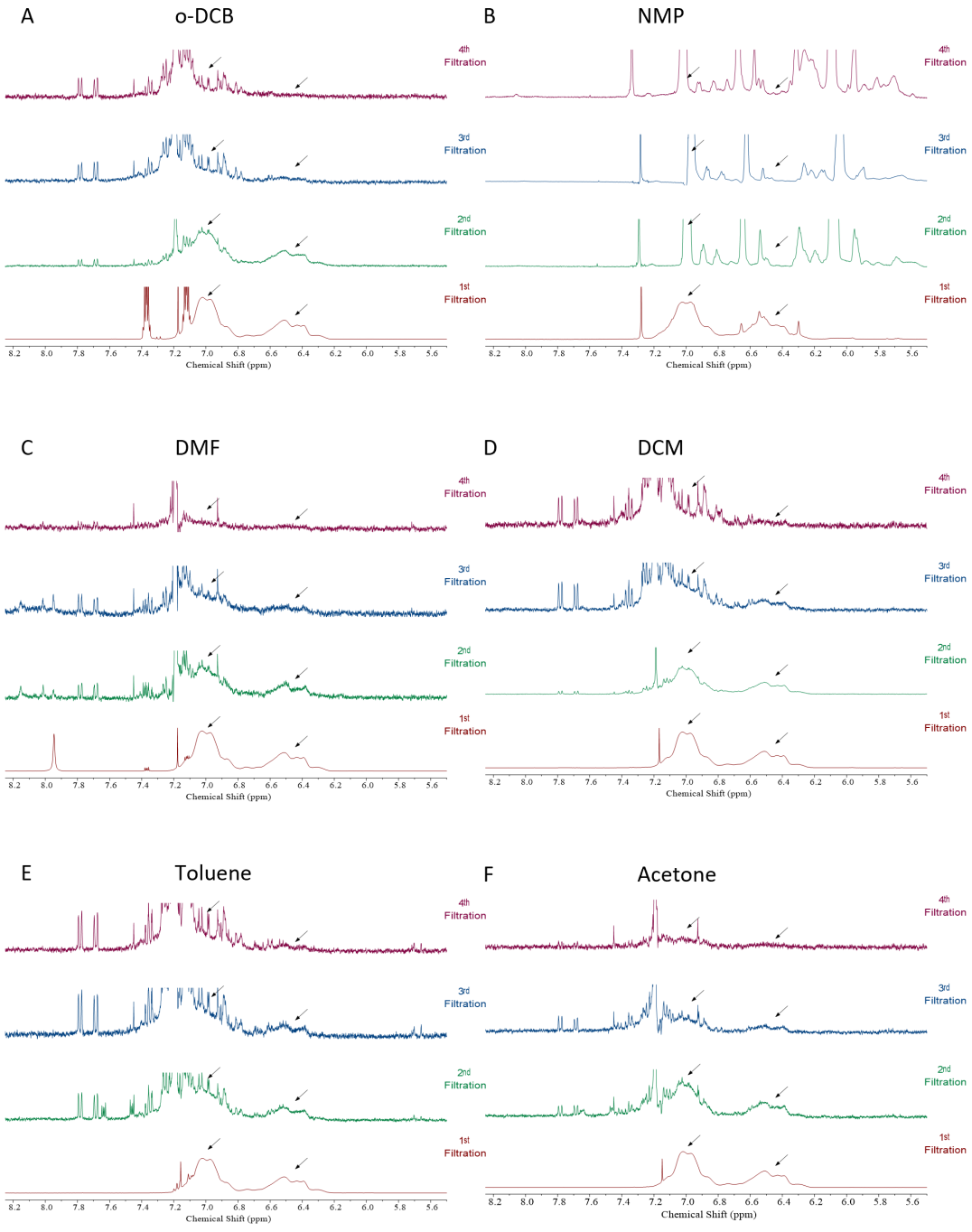


Figure C.5: *NMR spectra of the filtrates after each washing step of the functionalisation procedure for the six different solvents used in the study. The arrows point to the position of polystyrene aromatic protons. No polymer can be observed after the fourth redispersion*

C.1.2 Mass spectrometry

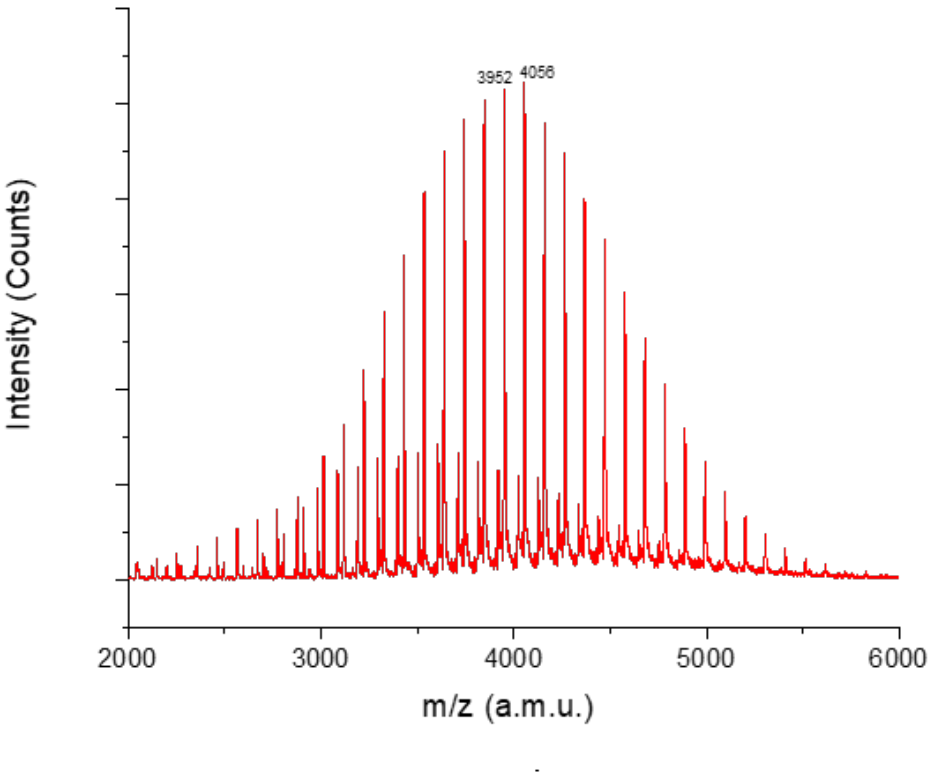


Figure C.6: *MALDI-TOF mass spectrum of PS synthesised by ATRP. It can be observed that each molecular peak differs by* 104 *amu, this is the equivalent mass of an ionised styrene monomer.*

C.1.3 XPS

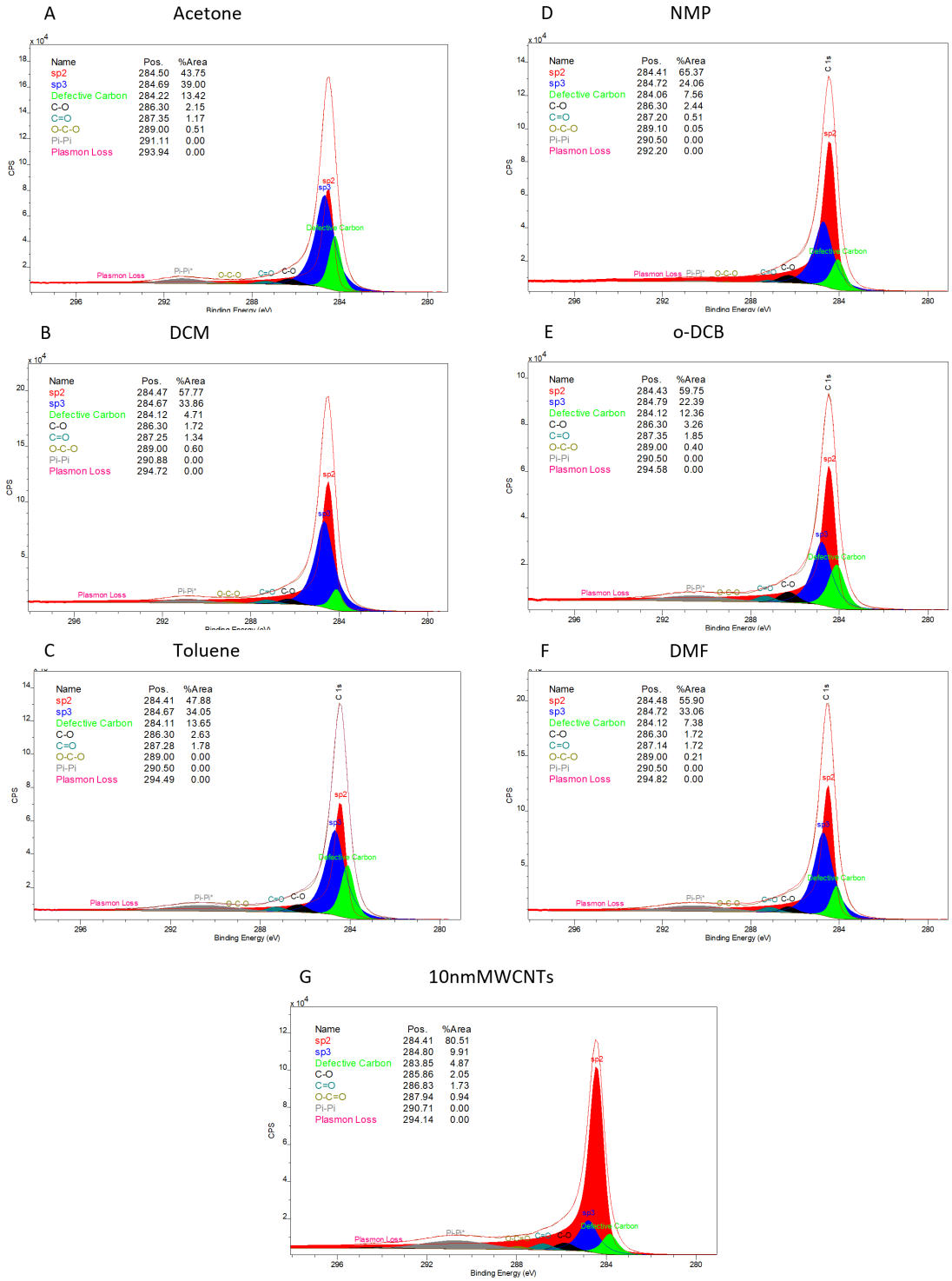


Figure C.7: *XPS spectra of PS-MWCNTs funcionalised via non-covalent functionalisation in different solvents.*

C.2 Synthesis of IONP-MWCNT hybrids

C.2.1 Surface coverage analysis

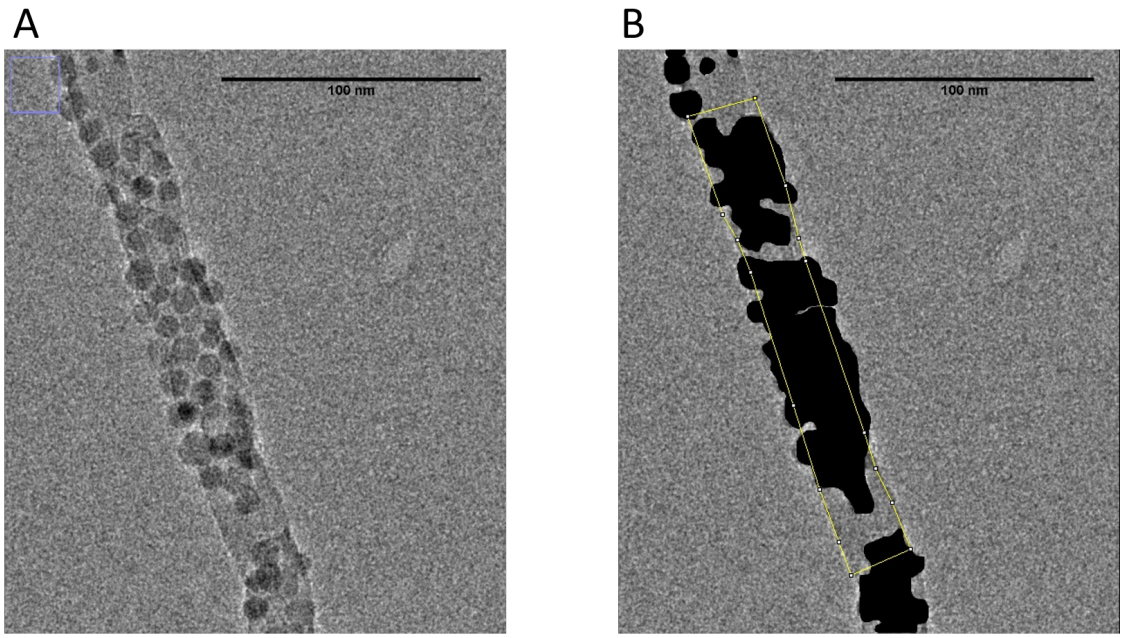


Figure C.8: *A) Original TEM micrograph of a PSIONP-50nmMWCNT hybrid. B) Processed TEM image where the PSIONPs have been removed from the micrograph. The yellow box represents the section of the surface of the 50nmMWNCTs that was analysed.*

C.2.2 FTIR

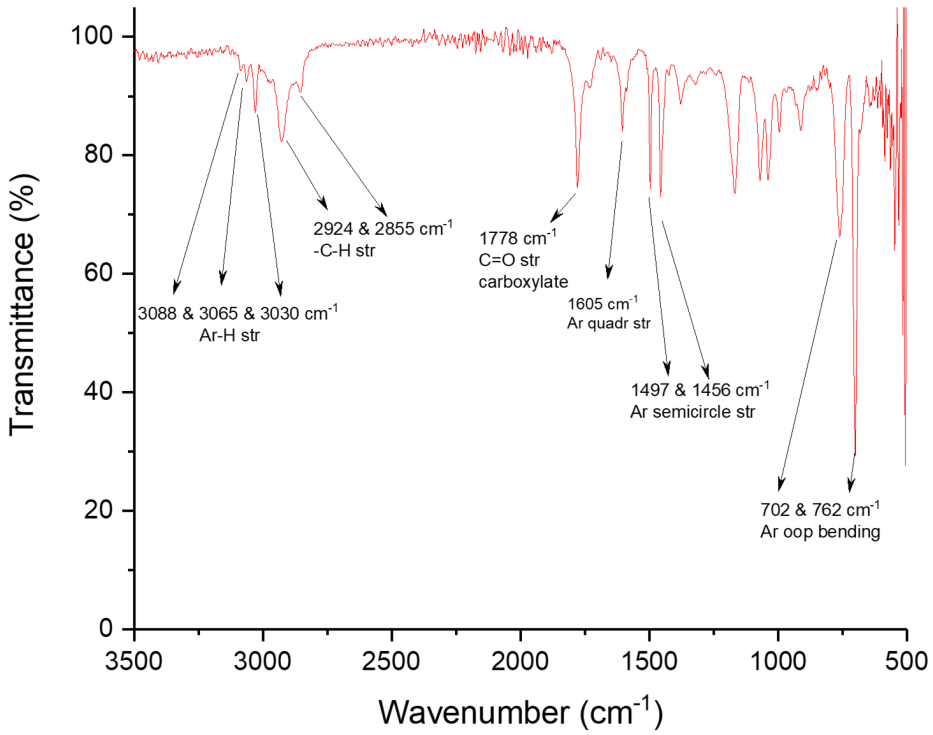


Figure C.9: *FTIR spectrum of polystyrene. Vibration modes: carbon-aromatic hydrogen bond stretching (three peaks,* 3088-3030 cm^{-1}*). Carbon-aliphatic hydrogen bond stretching (two peaks,* 2930-2855 cm^{-1}*). Carbon-oxygen double bond stretch (one peak,* 1778 cm^{-1}*). Carbon-carbon aromatic bond stretch (three peaks,* 1605-1455 cm^{-1}*). Carbon-aromatic hydrogen out of plane bond bending (two peaks,* 762-702 cm^{-1}*).*